Supplementary material to the EMEP Status Report 1/2020
Date: August 2020

METEOROLOGISK INSTITUTT
Norwegian Meteorological Institute

EMEP MSC-W model performance for acidifying and eutrophying components, photo-oxidants and particulate matter in 2018

EMEP/MSC-W:
Michael Gauss, Svetlana Tsyro and Anna Benedictow

EMEP/CCC:
Anne-Gunn Hjellbrekke, Wenche Aas and Sverre Solberg

Supplementary material to EMEP Status Report 1/2020

Contents

CHAPTER 1

Introduction

1.1 The contents of this report

This report is a supplement to the EMEP Status Report 1/2020 and presents a detailed evaluation of the EMEP MSC-W model. The report is publicly available from the EMEP website: (https://emep.int/emep_publications.html).

The EMEP MSC-W model is evaluated with respect to acidifying and eutrophying components, photo-oxidants and particulate matter. Model results for 2018 are validated against measurements that have been collected from the EMEP monitoring network for 2018.
This year we present results from EMEP MSC-W model version rv4.35, which is slightly different from model version rv4.33 used for last year's evaluation (Gauss et al. 2019a,b, Tsyro et al. 2019). Recent changes in the EMEP MSC-W model code are described in Simpson et al. (2020). As usual, the meteorological input is based on data from the ECMWF-IFS model. The model has been run on a 0.1 x 0.1 degree regular longitude-latitude grid. For a more detailed description of this year's model setup see the status chapter of the EMEP Status Report 1/2020 (section *Setup for EMEP MSC-W model runs*).

Tables of model skill and time series plots are presented in this report for different chemical species at individual EMEP measurement stations, along with scatter plots and maps covering the EMEP domain.

As in previous evaluation reports, data from some measurement stations have been excluded from this evaluation for either of the following reasons:

- Problems have been identified in regard to the measurements (during Quality Control by EMEP-CCC).
- The measurement site is located in a mountain area, and the difference between its height above sea level and the mean elevation in the respective EMEP MSC-W model grid cell is larger than 500m.

The agreement between model results and observations depends on a combination of several factors - the measurement accuracy (sampling and analysis), the representativeness of the measurement sites, the adequacy of emissions, and the model performance. Thus, any model underestimation or overestimation in the evaluation presented in the following chapters only implies that the modelled values are different from the observations, but is not necessarily an indication of model deficiency.

Chapter 2 of this report deals with acidifiying and eutrophying components (sulphur and nitrogen species), Chapter 3 with photo-oxidants (ozone and nitrogen dioxide), and Chapter 4 with particulate matter.

1.2 Comparison with observations from EEA

A major effort this year has been put into the development of a web interface that presents a detailed evaluation against measurements from the European Environment Agency's (EEA) Air Quality e-Reporting Database:
https://aerocom-evaluation.met.no/main.php?project=emep
On that page the user can select the classification of measurement data (rural, urban, non-traffic, or all stations) and view a large number of statistical parameters (bias, correlation, root mean square error, etc.).

The web interface displays the co-located observational and model data sets and contains:

- daily and monthly time series for each station, or averaged per country (or the full domain);
- hourly time series representing an average week for the whole year and for each season;
- statistics and scatter plots calculated for each station and country;
- an overall evaluation of the results using statistics calculated for each country and for the full model domain.

In all cases the statistics are calculated using monthly resolution data by default. Daily statistics are available by adding &stats=daily to the site URL given above.

Evaluation is made for the following chemical species and indicators: NO_2, O_3, $PM_{2.5}$ and PM_{10}, and O_3max (maximum daily ozone). Different types of visualization (bar charts, line charts, tables, etc.) are available for viewing and for download. The measurement data have been retrieved from the validated *E1a* stream of EEA and further harmonized and quality controlled by the GHOST tool (Globally Harmonised Observational Surface Treatment) developed at the Barcelona Supercomputing Center (BSC).

For supplemental evaluation of Elemental Carbon (EC), the modelled absorption coefficient (mainly due to EC) is compared to surface in-situ observations of the aerosol light absorption coefficient, accessed through the Global Atmospheric Watch - WDCA database EBAS (http://ebas.nilu.no/). More details about this can be found in the chapter on Elemental Carbon in the EMEP Status Report 1/2020.

References

M. Gauss, A.-G. Hjellbrekke, W. Aas, and S. Solberg. Ozone. Supplementary material to EMEP Status Report 1/2019, available online at www.emep.int, The Norwegian Meteorological Institute, Oslo, Norway, 2019a.

M. Gauss, S. Tsyro, H. Fagerli, A.-G. Hjellbrekke, and W. Aas. Acidifying and eutrophying components. Supplementary material to EMEP Status Report 1/2019, available online at www.emep.int, The Norwegian Meteorological Institute, Oslo, Norway, 2019b.

D. Simpson, R. Bergström, and P. Wind. Updates to the emep msc-w model, 2019-2020. In *Transboundary particulate matter, photo-oxidants, acidifying and eutrophying components. EMEP Status Report 1/2020*. The Norwegian Meteorological Institute, Oslo, Norway, 2020.

S. Tsyro, M. Gauss, A.-G. Hjellbrekke, and W. Aas. Pm10, pm2.5 and individual aerosol components. Supplementary material to EMEP Status Report 1/2019, available online at www.emep.int, The Norwegian Meteorological Institute, Oslo, Norway, 2019.

CHAPTER 2

Acidifying and eutrophying components

In this chapter the EMEP MSC-W model is evaluated with respect to acidifying and eutrophying components. Section 2.1 includes an overview table of the model performance and scatter plots for acidifying and eutrophying components. In Section 2.2 we present time series plots for all EMEP stations with measurements in year 2018, while Section 2.3 contains combined maps of modelled and measured air concentrations and of concentrations in precipitation for selected species in 2018.

2.1 Scatter plots and tables

Evaluations of the EMEP MSC-W model performance for acidifying and eutrophying components have been presented earlier in numerous EMEP publications (e.g. Gauss et al. 2019).

In addition, an overview study of how the model performance has changed over the years was presented in Chapter 3 of EMEP Status Report 1/2013 (Simpson et al. 2013). The main conclusions of that study still hold:

- Year-to-year variations in evaluations of model performance can be large when all EMEP mearusements available are used. This is mainly caused by the varying number of measurement sites available from year to year. Futhermore, changes in instrumentation, protocols and personnel may influence the quality of measurements.
- Model performance varies strongly among pollutants.
- Model performance is (as expected) generally better for secondary than for primary pollutants;
- Systematic evaluations, where all inputs and observations are held constant while only the model version is changed, are useful. In this way key factors behind changes in model performance can be identified (benchmarking).

Component	N_{stat}	Obs.	Mod.	Bias (%)	RMSE	Corr.	IOA
NO_2 (μg(N) m^{-3})	73	1.71	1.49	-13	0.68	0.87	0.92
SO_2 (μg(S) m^{-3})	57	0.30	0.26	-13	0.21	0.63	0.78
SO_4^{2-}, sea salt corrected (μg(S) m^{-3})	24	0.38	0.21	-44	0.24	0.87	0.69
SO_4^{2-}, including sea salt (μg(S) m^{-3})	32	0.48	0.29	-39	0.24	0.87	0.71
NO_3^- (μg(N) m^{-3})	25	0.27	0.31	15	0.12	0.78	0.87
HNO_3 (μg(N) m^{-3})	17	0.12	0.10	-17	0.08	0.54	0.68
NO_3^-+HNO_3 (μg(N) m^{-3})	34	0.42	0.43	1	0.08	0.94	0.97
NH_3 (μg(N) m^{-3})	20	0.64	0.68	7	0.28	0.91	0.95
NH_4^+ (μg(N) m^{-3})	26	0.50	0.42	-16	0.20	0.78	0.86
NH_3+NH_4^+ (μg(N) m^{-3})	31	1.28	1.59	24	1.47	0.70	0.69
SO_4^{2-} wd (mg(S)m^{-2})	43	9587	6149	-36	253	0.76	0.61
SO_4^{2-} cp (mg(S)l^{-1})	43	0.30	0.19	-38	0.27	0.60	0.55
NH_4^+ wd (mg(N)m^{-2})	42	11065	11625	5	185	0.62	0.78
NH_4^+ cp (mg(N)l^{-1})	42	0.38	0.38	0	0.20	0.62	0.78
NO_3^- wd (mg(N)m^{-2})	43	9003	8348	-7	156	0.58	0.73
NO_3^- cp (mg(N)l^{-1})	43	0.30	0.27	-12	0.24	0.46	0.58
Precipitation (mm)	43	33815	37004	9	259	0.84	0.90

Table 2.1: Comparison of model results and observations for 2018. Annual averages over all EMEP sites with measurements. N_{stat}= number of stations, wd=wet deposition (integrated over the year and stations), cp= concentration in precipitation, Corr. = spatial correlation coefficient, RMSE = root mean square error, IOA = index of agreement.

Table 2.1 shows for each component the number of stations where measurements were available and data coverage criteria were satisfied in 2018 (N_{stat}), along with measured yearly average over all stations (Obs), modelled yearly average over all stations (Mod), bias ($\frac{Mod-Obs}{Obs} \times 100\%$), spatial correlation between observation and model for station yearly averages (Corr), root mean square error, Rmse ($\sqrt{\frac{1}{n}\sum_{i=1}^{n}(m_i - o_i)^2}$ where m_i and o_i are modelled and measured concentration at monitoring station *i*), and index of agreement (Willmott 1981, 1982). The index of agreement is calculated as follows: IOA= $1 - \frac{\sum_{i=1}^{N_{stat}}(m_i - o_i)^2}{\sum_{i=1}^{N_{stat}}(|m_i - Obs| + |o_i - Obs|)^2}$). It varies between 0 (theoretical minimum) and 1 (perfect agreement between observed and predicted values) and gives the degree to which model predictions are error free.

The scatter plots in Figures 2.1–2.3 are based on yearly averages of observed data at EMEP stations that have provided measurements for 2018. The lines on the scatter plots display deviations in the scatter of 30% ('30% line') and 50% ('50% line') relative bias, respectively. Relative bias is defined here as $\frac{Mod-Obs}{0.5\,(Mod+Obs)} \times 100\%$, where 'Mod' refers to yearly averaged modelled concentrations, while 'Obs' refers to yearly averaged measured concentrations.

Sulphur dioxide in air

SO_2 has, on annual average, a negative bias (-13%) compared to measurements in 2018, up from -19% last year. Figure 2.1(a) shows largest overestimations for SO_2 occurring at stations IS0002, ES0006 and ES0008, and large underestimations at NO0015, SE0005, FI0036, AT0005, ES0009 and ES0012.

Sulphate in air

Figures 2.1(b) and 2.1(c) show EMEP model results compared to measurements for, respectively, sea salt-corrected sulphate and sulphate including sea salt. For comparisons with measurements including sea salt, 7% of the modelled sea salt[1] have been added to modelled sulphate. The modelled and observed sulphate levels are in somewhat better agreement when sea salt sulphate is included (except for correlation). In particular the bias is smaller for sulphate including sea salt. The IOA is slightly better for sea salt including sulphate than for sulphate without sea salt (0.71 vs. 0.69).

In 2012 a change in the scheme for the oxidation of SO_2 to SO_4^{2-} was implemented in the EMEP model (Fagerli et al. 2012, Simpson et al. 2012) resulting in higher oxidation rate and, consequently, less underestimation of sulphate concentrations in air. But the underestimation remains, as visible from the bias, but also from the scatter plots.

Time series for sulphate in air are shown in Figures 2.14–2.22.

Nitrate and nitric acid in air

Measurements of airborne nitrate are expected to have a rather large uncertainty due to the very different physical characteristics of the compounds making up total nitrate. Whilst nitric acid is a spatially variable volatile gas with fast dry deposition, particulate nitrate dry deposits only slowly and hence concentrations are more determined by long range transport.

In Figure 2.2 we show scatter plots for total nitrate, particulate nitrate and nitric acid in air. Time series for total nitrate in air are shown in Figures 2.25–2.29.

Normally, the results for nitrate aerosol and nitric acid are somewhat worse than for total nitrate, because the monitoring data quality for these components are in general not as good as for total nitrate. The reason for this is that the individual concentrations of nitrate and nitric acid are biased when using the common filter-pack method.

In this year's model results, HNO_3 is underestimated by 17%, while NO_3^- is overestimated by 15%. The sum of NO_3^-+HNO_3 is almost unbiased (1%), an improvement since last year. The spatial correlation is 0.78 for nitrate aerosol, but much better for the sum of aerosol and gas (Corr = 0.94), while being worse for nitric acid (Corr = 0.54).

Ammonia and ammonium aerosol in air

In order to evaluate the model performance for NH_x (NH_3+NH_4^+) properly, ammonia and ammonium should be studied separately. However, the number of measurements for 2018 where the gaseous and particle phase were analyzed both separately and at the same time is limited, e.g. NH_3 measurements are available only from 20 sites (2 less than last year).

In earlier evaluations, individual results for NH_3 and NH_4^+ used to be somewhat worse than for total reduced nitrogen (NH_x), because the monitoring data quantity and quality for

[1] Sea salt is assumed to consist of approximately 7% sulphate.

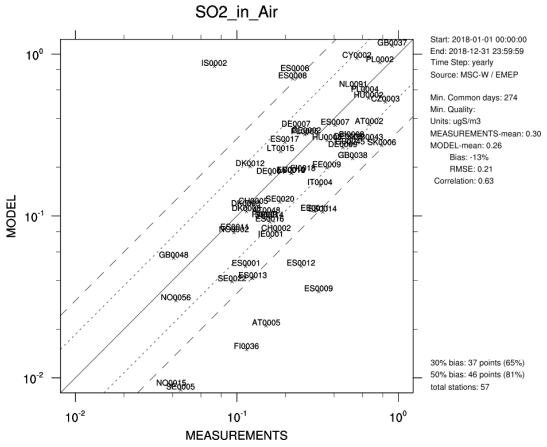

(a) SO_2

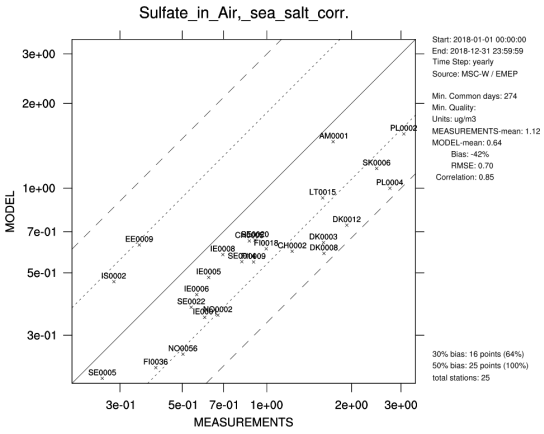

(b) SO_4^{2-}, measurements corrected for sea salt

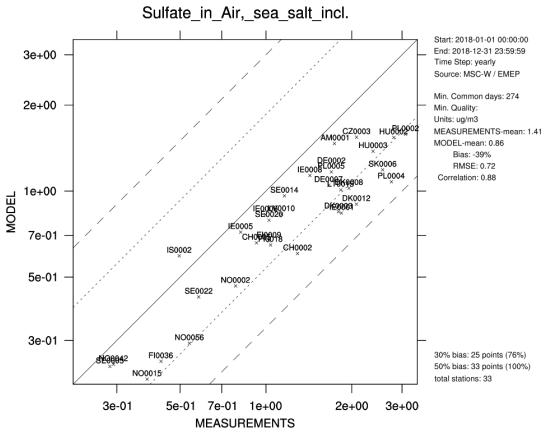

(c) SO_4^{2-}, including sea salt SO_4^{2-}

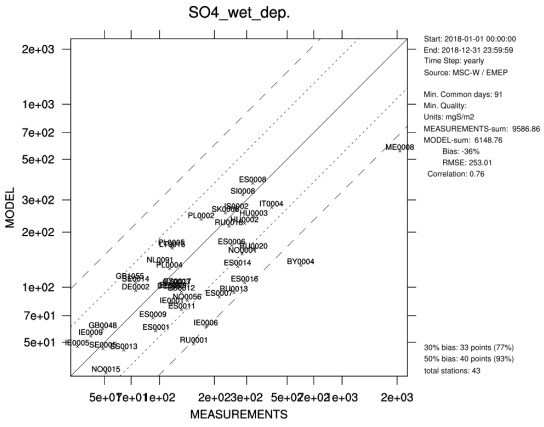

(d) SO_4^{2-} wet dep.

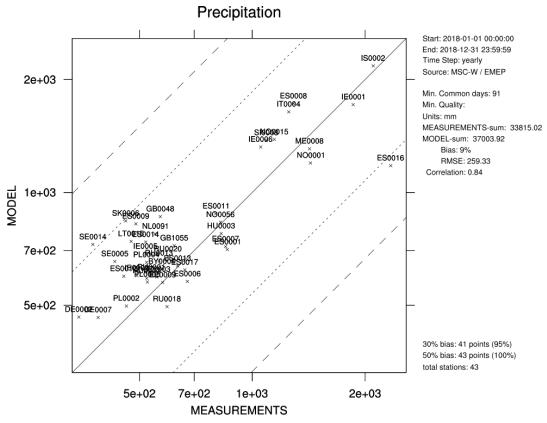

(e) Precipitation

Figure 2.1: Scatter plots of model results versus observations of a) sulphur dioxide [μg(S) m^{-3}], b+c) sulphate [μg(S) m^{-3}], d) wet deposition of sulphur [mg(S)m^{-2}], and e) precipitation [mm]. For sulphate concentrations, panel (b) shows a comparison of model results to sea salt corrected sulphate measurements, while panel (c) shows model results of sulphate plus 7 % sea salt in comparison to non-corrected measurement data.

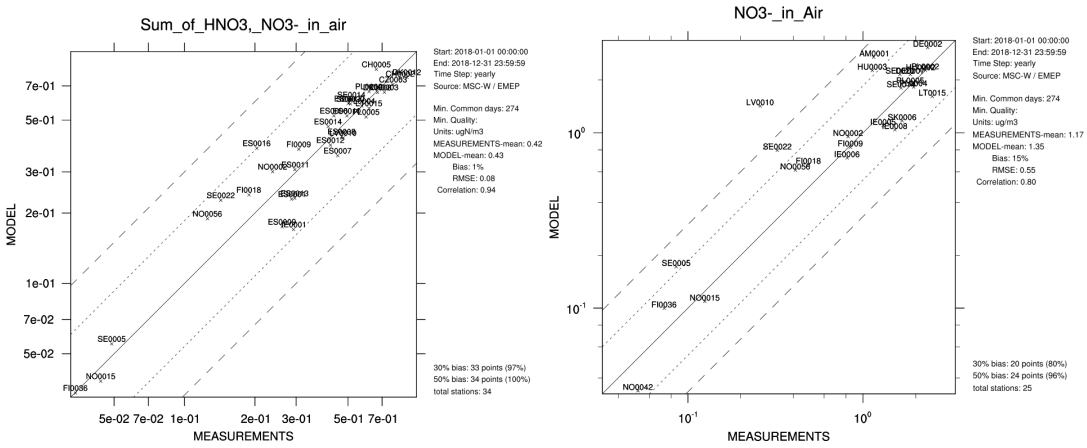

(a) NO_3^-+HNO_3 (b) NO_3^-

(c) HNO_3 (d) NO_3^- wet dep.

Figure 2.2: Scatter plots of modelled versus observed concentrations of total nitrate, nitrate aerosol, nitric acid [μg(N) m^{-3}] and wet deposition of oxidized nitrogen [mg(N)m^{-2}].

these components are in general not as good as for the sum of NH_3+NH_4^+.

Since 2017, however, the RMSE and spatial correlations for the sum are worse than for the individual components.

The modelled yearly averages of the concentrations of ammonia, ammonium and the sum of ammonia and ammonium have biases of 7%, -16% and 24%, respectively, compared to the monitoring data. The spatial correlations for NH_3 is very high (0.91), while the spatial correlations for NH_4^+ and the sum are lower (0.78 and 0.70, respectively). On a positive note, these values are clearly better than last year. Also, one has to keep in mind that the number of stations for the sum is higher than the number of stations measuring the individual components, and that the outlier ES0016 may explain part of the somewhat worse performance for the sum.

Scatter plots for modelled versus measured concentrations for total ammonium+ammonia, aerosol ammonium and ammonia in air in 2018 are presented in Figures 2.3(a), 2.3(b) and 2.3(c), respectively, while time series for NH_3+NH_4^+ are shown in Figures 2.31–2.34.

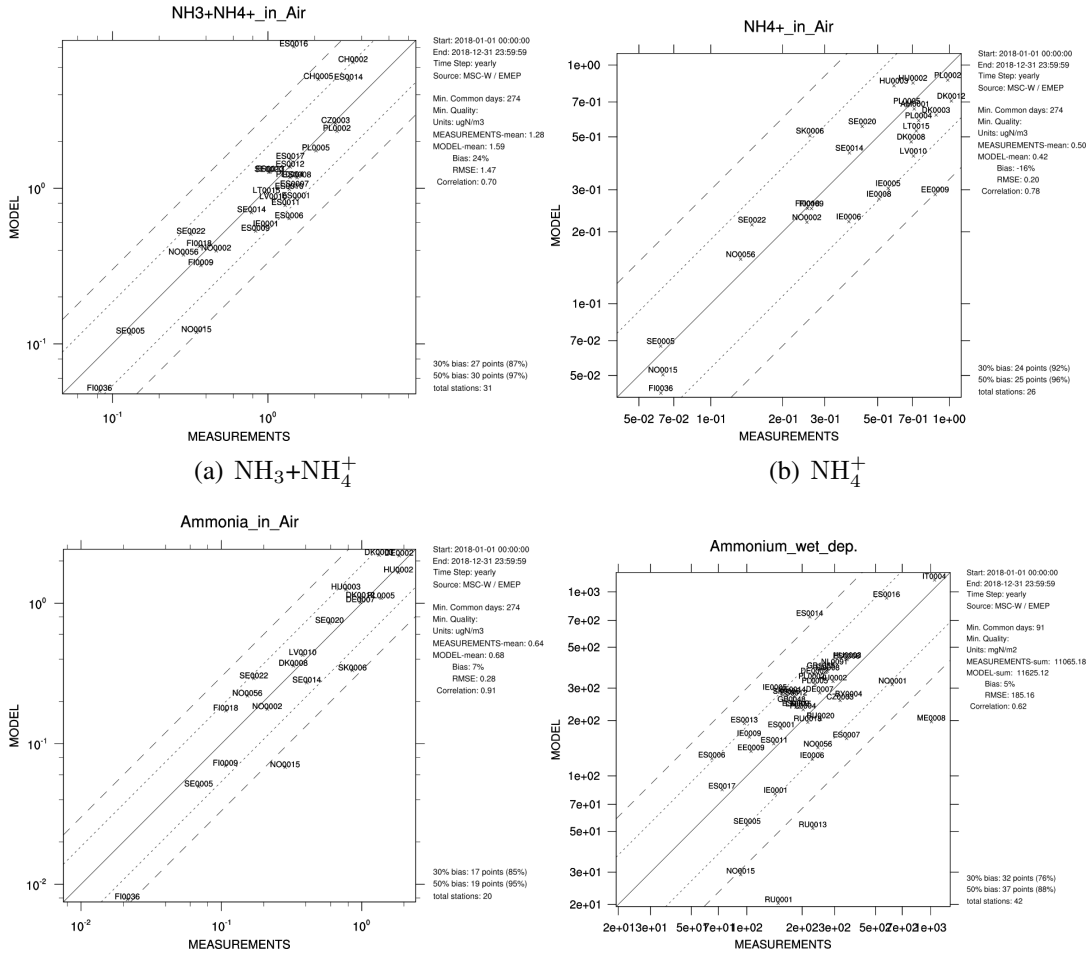

(a) NH_3+NH_4^+ (b) NH_4^+

(c) NH_3 (d) NH_4^+ wet dep.

Figure 2.3: Scatter plots of modelled versus observed concentrations of total ammonium+ammonia, aerosol ammonium and ammonia in air [μg(N) m^{-3}] and wet deposition of reduced nitrogen [mg(N)m^{-2}].

Concentrations in precipitation / wet depositions

The ability of the model to predict concentrations in precipitations and wet depositions is limited by the accuracy of the precipitation fields used in the model. The precipitation field pattern is very patchy (e.g. influenced by local topographic effects), and the regional scale model is unable to resolve this sub grid scale distribution. A typical problem arises with small scale showers. In reality precipitation is high in a small area of a given grid, but a large fraction of the grid should remain dry. Within the model, however, this precipitation is averaged out to cover the whole grid at a lower intensity. Thus, even though average precipitation amounts may be simulated well, the model experiences precipitation more often, but in lower amounts than in reality. On a shorter time scale, e.g on daily basis, this may lead to too high concentrations in precipitation for episodes when it rains only in a small part of the grid square. For a regional scale model it is more sensible to compare the bulk concentrations, i.e the sum of the wet deposited compounds divided by the sum of precipitation.

The spatial correlation between model and measurements for concentrations in precipitation and wet depositions will to a large extent depend on the model precipitation field.

A scatter plot for modelled versus observed precipitation is shown in Figure 2.1(e). On average, the observed and modelled precipitation is similar (bias=9%) and the spatial correlation is high (0.84). This also contributes to the relatively good model performance in terms of oxidized/reduced nitrogen in precipitation (low biases and good correlations). Sulphur in precipitation is clearly underestimated, but less so than sulphate itself. Two stations (BY0004/Vysokoe and ME0008/Zabljak) contribute strongly to the low performance, see Figure 2.1(d) and corresponding panels in Figures 2.36 and 2.39.

Scatter plots for modelled versus observed wet depositions of sulphur, oxidized nitrogen and reduced nitrogen are shown in Figures 2.1(d), 2.2(d) and 2.3(d), respectively. The overall performance is good, although some outliers are visible.

2.2 Time series

In this section we present time series plots for a selection of stations that have supplied data on acidifying and eutrophying components to EMEP/CCC for 2018. The plots show daily model results and measurements, where available. Time series for sulphur dioxide in air are shown in Figures 2.4–2.13, for sulphate in air in Figures 2.14–2.24, for total nitrate in air in Figures 2.25–2.30 and for ammonia+ammonium in air in Figures 2.31–2.35. In addition, time series are shown for wet deposition of sulphur, oxidized nitrogen and reduced nitrogen in Figures 2.36–2.42, Figures 2.43–2.49 and Figures 2.50–2.56, respectively.

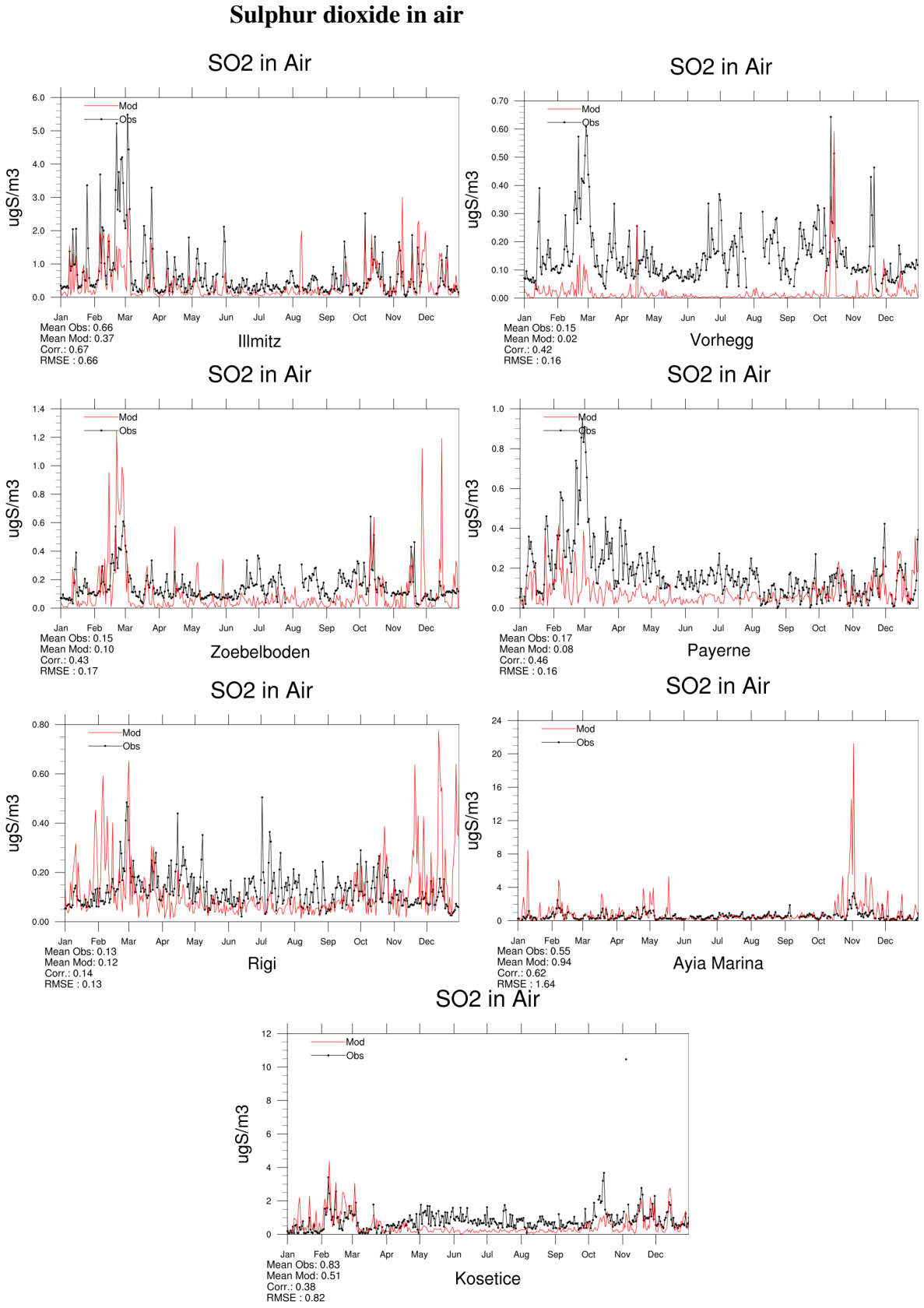

Figure 2.4: Comparison of model results and measurements (daily) for SO_2 in air [μg(S) m^{-3}] for stations that have measured SO_2 in 2018.

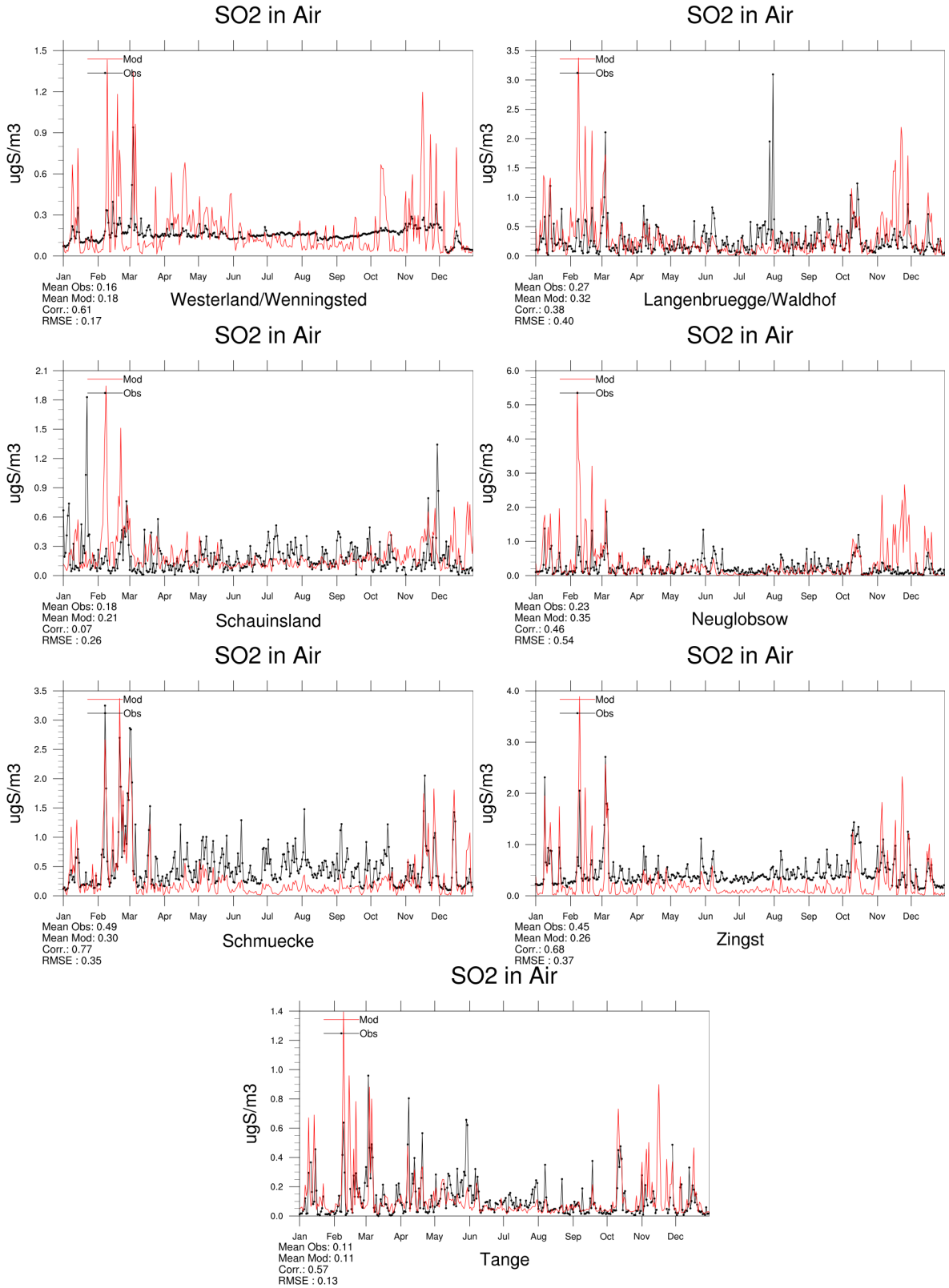

Figure 2.5: Comparison of model results and measurements (daily) for SO_2 in air [μg(S) m^{-3}] for stations that have measured SO_2 in 2018.

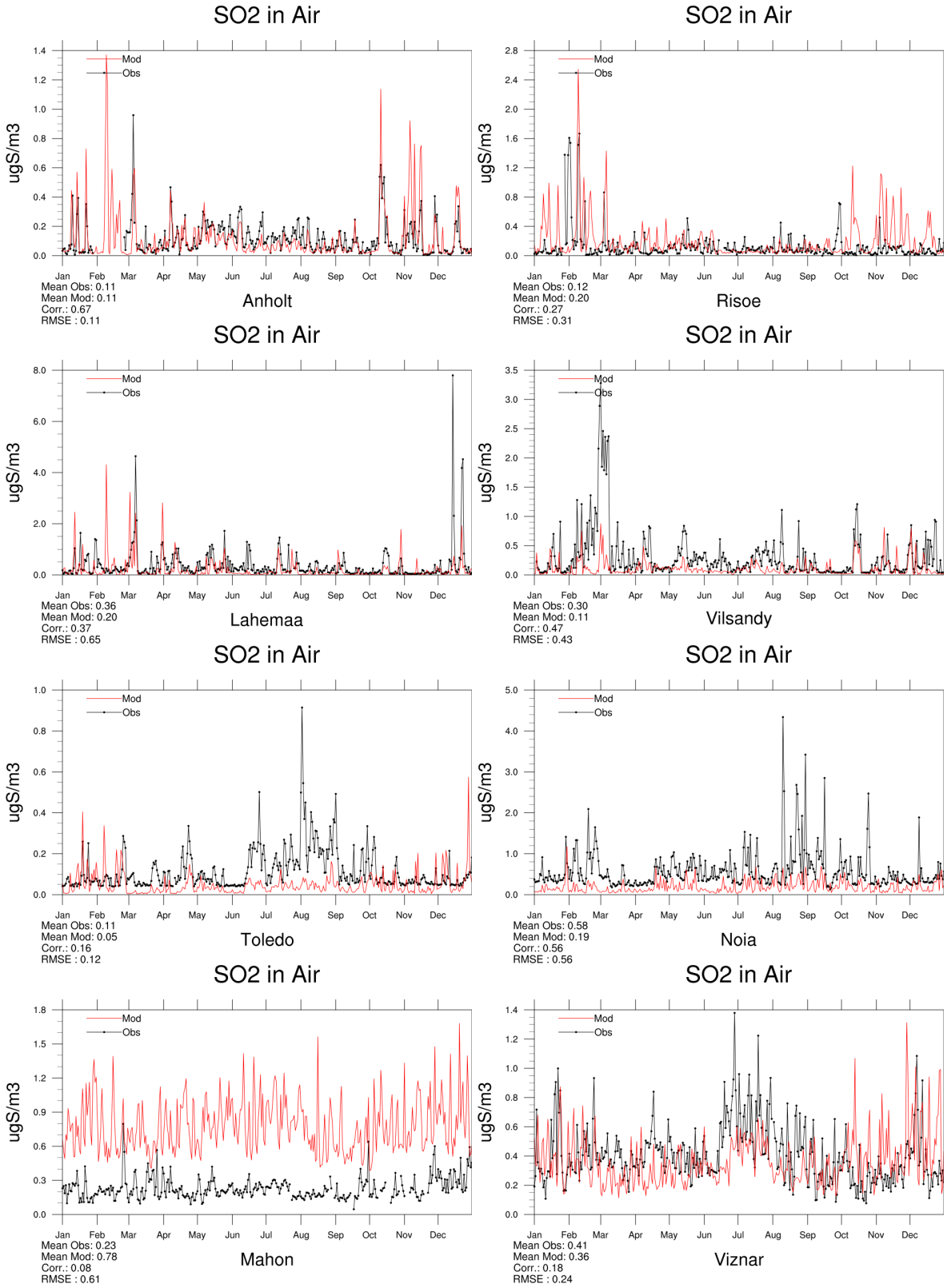

Figure 2.6: Comparison of model results and measurements (daily) for SO_2 in air [μg(S) m^{-3}] for stations that have measured SO_2 in 2018.

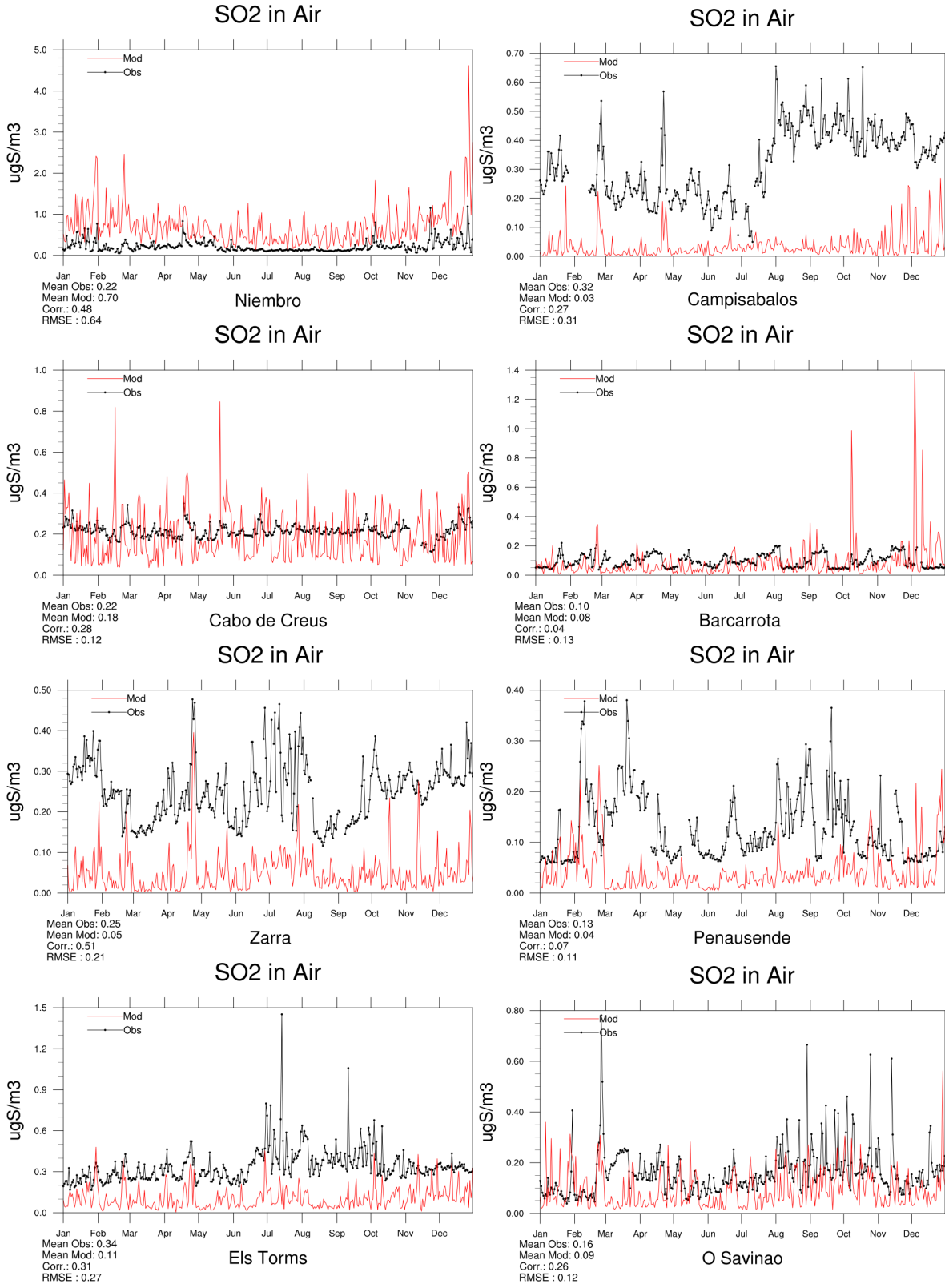

Figure 2.7: Comparison of model results and measurements (daily) for SO_2 in air [μg(S) m^{-3}] for stations that have measured SO_2 in 2018.

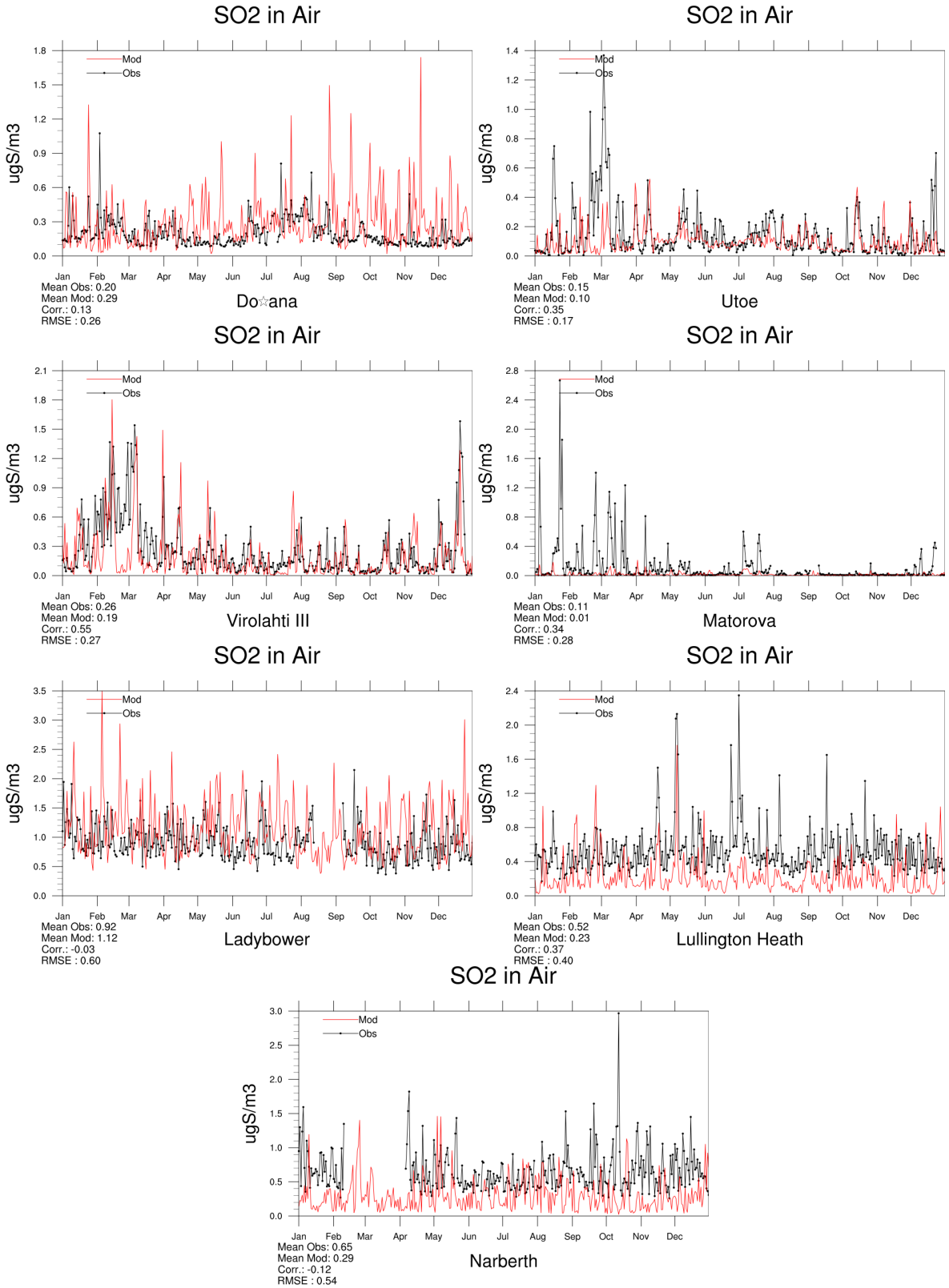

Figure 2.8: Comparison of model results and measurements (daily) for SO_2 in air [μg(S) m^{-3}] for stations that have measured SO_2 in 2018.

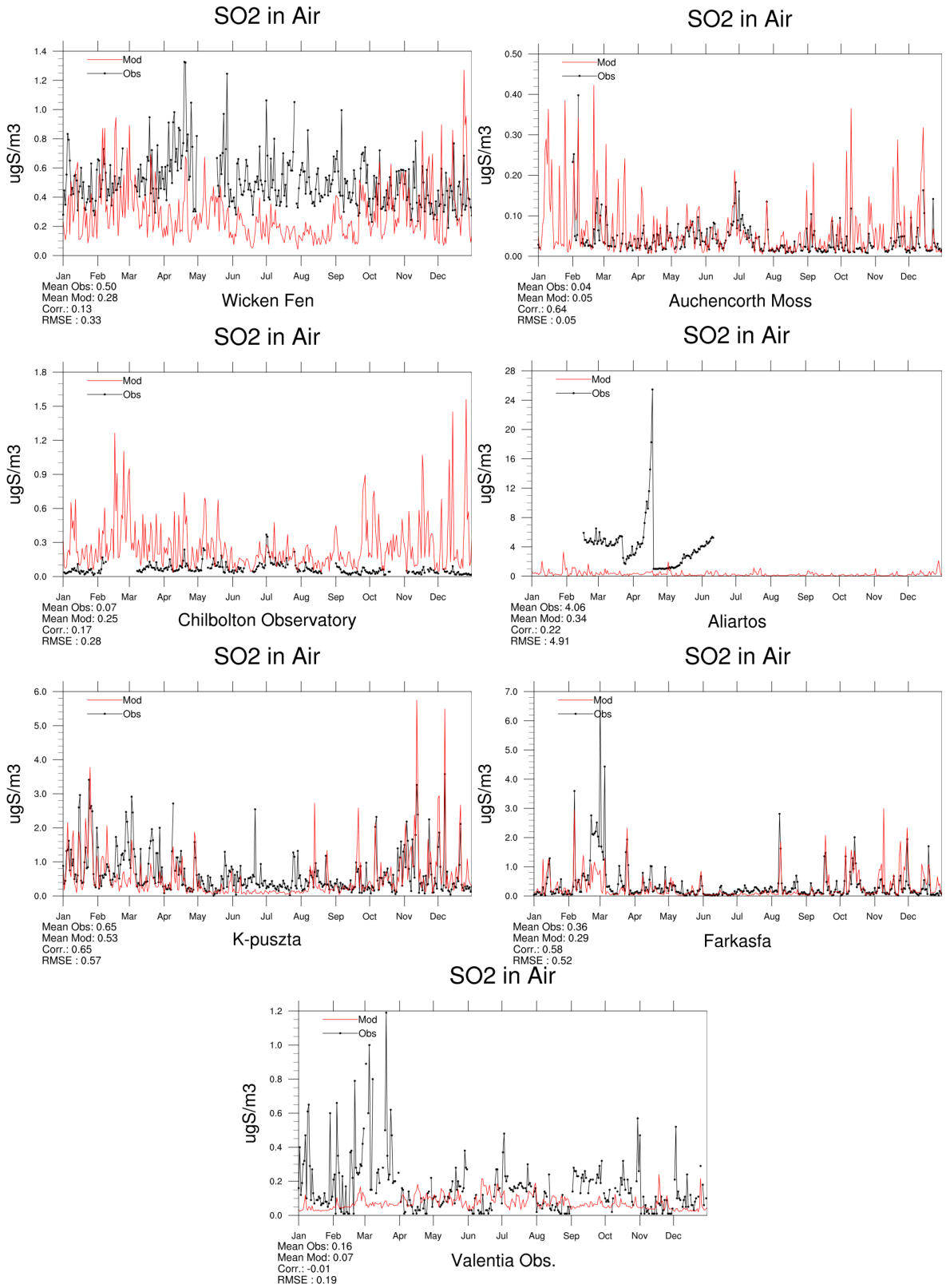

Figure 2.9: Comparison of model results and measurements (daily) for SO_2 in air [μg(S) m^{-3}] for stations that have measured SO_2 in 2018.

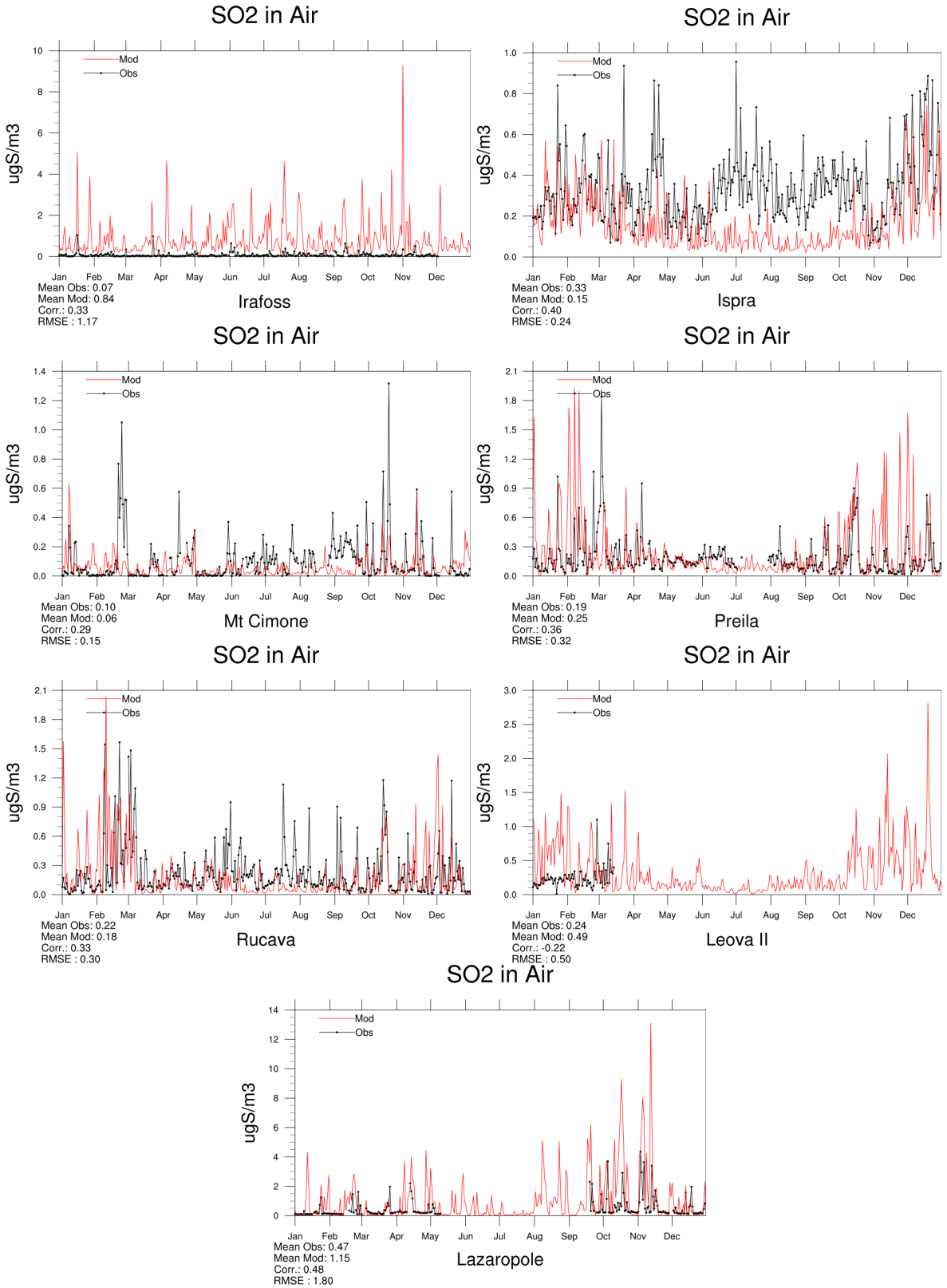

Figure 2.10: Comparison of model results and measurements (daily) for SO_2 in air [μg(S) m^{-3}] for stations that have measured SO_2 in 2018.

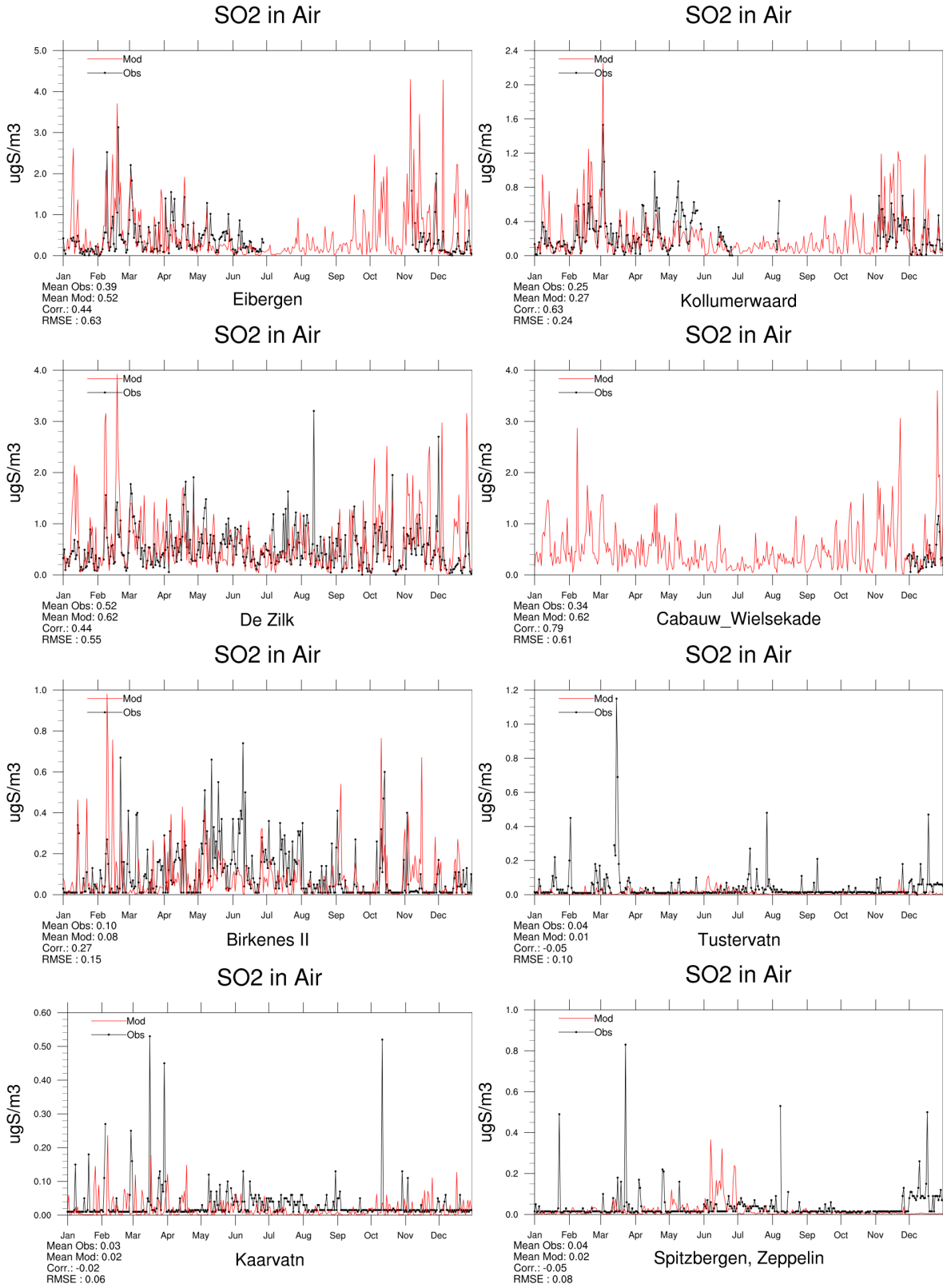

Figure 2.11: Comparison of model results and measurements (daily) for SO_2 in air [μg(S) m^{-3}] for stations that have measured SO_2 in 2018.

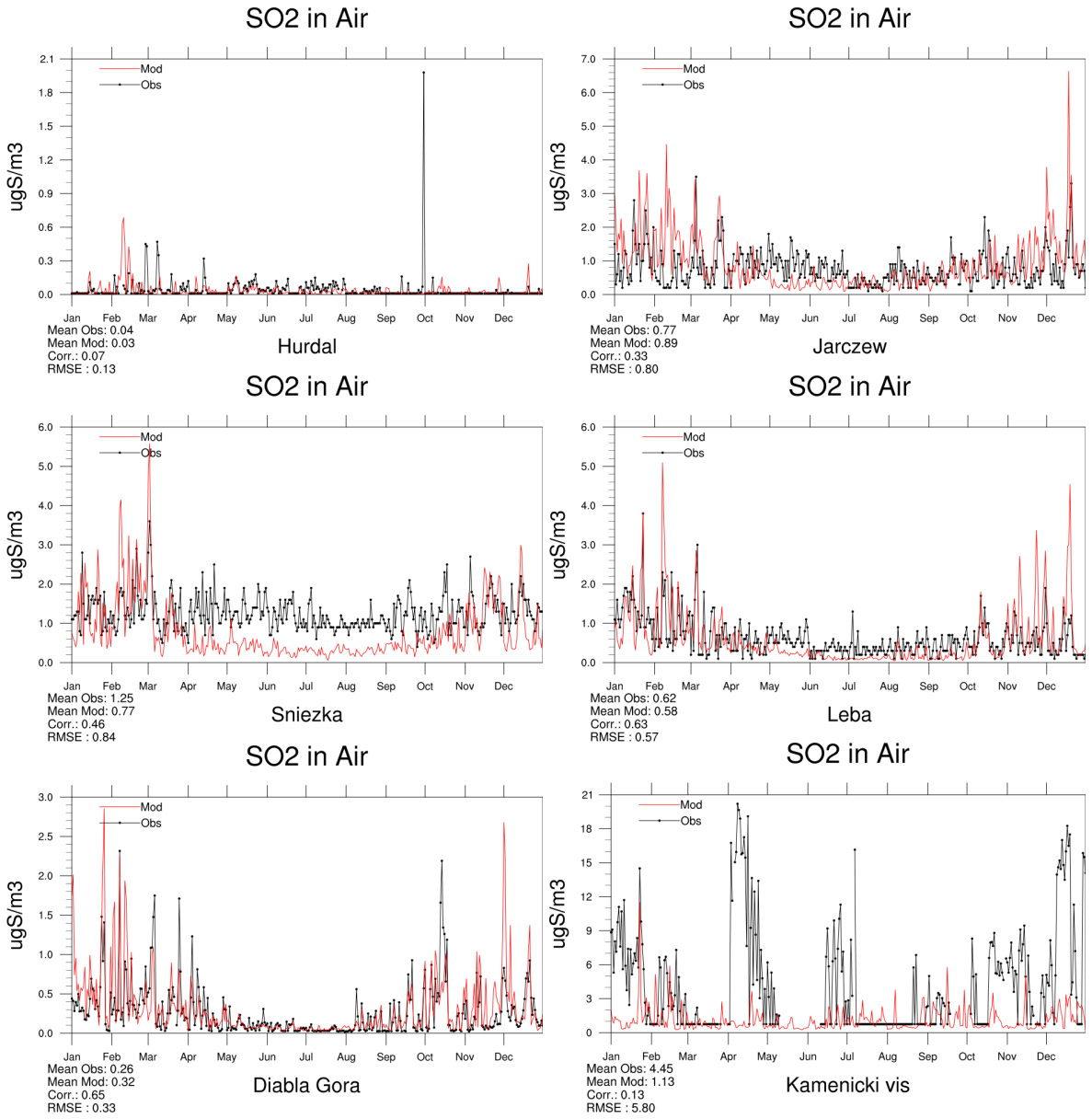

Figure 2.12: Comparison of model results and measurements (daily) for SO_2 in air [μg(S) m^{-3}] for stations that have measured SO_2 in 2018.

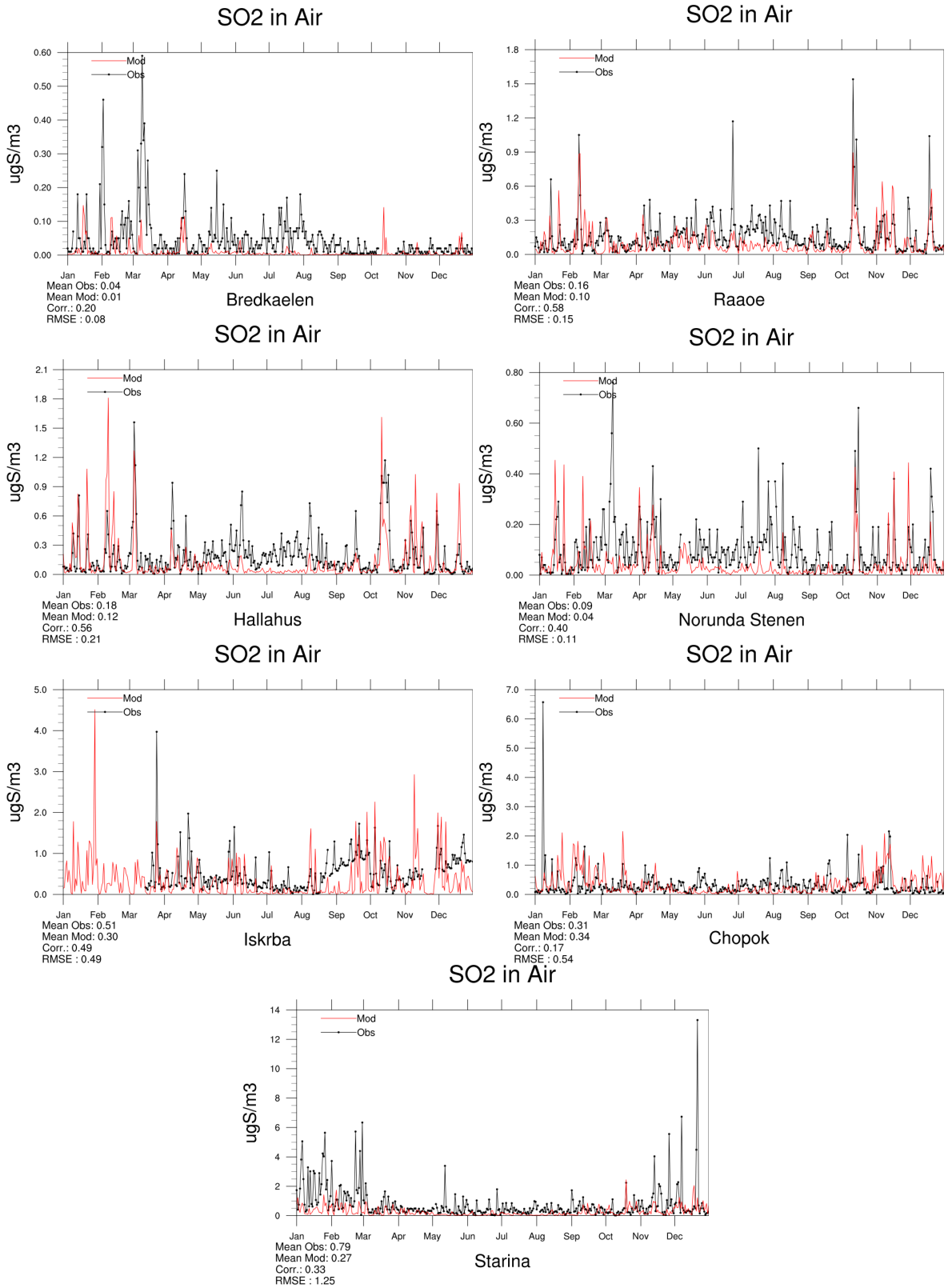

Figure 2.13: Comparison of model results and measurements (daily) for SO_2 in air [μg(S) m^{-3}] for stations that have measured SO_2 in 2018.

Sulphate in air – sea salt corrected

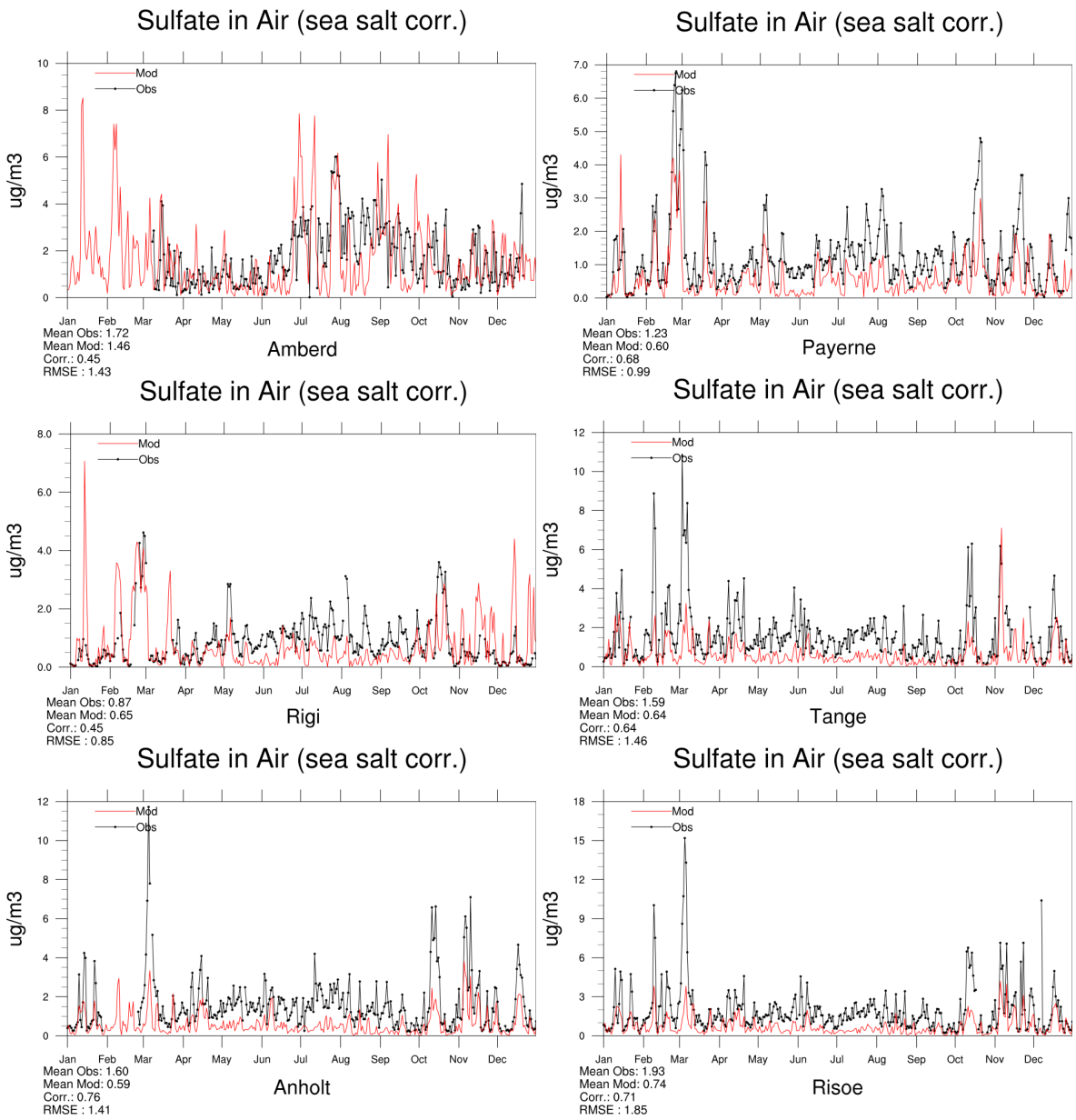

Figure 2.14: Comparison of model results and measurements (daily) for sea salt corrected sulphate in air [μg(S) m^{-3}] for stations that have measured sulphate in 2018.

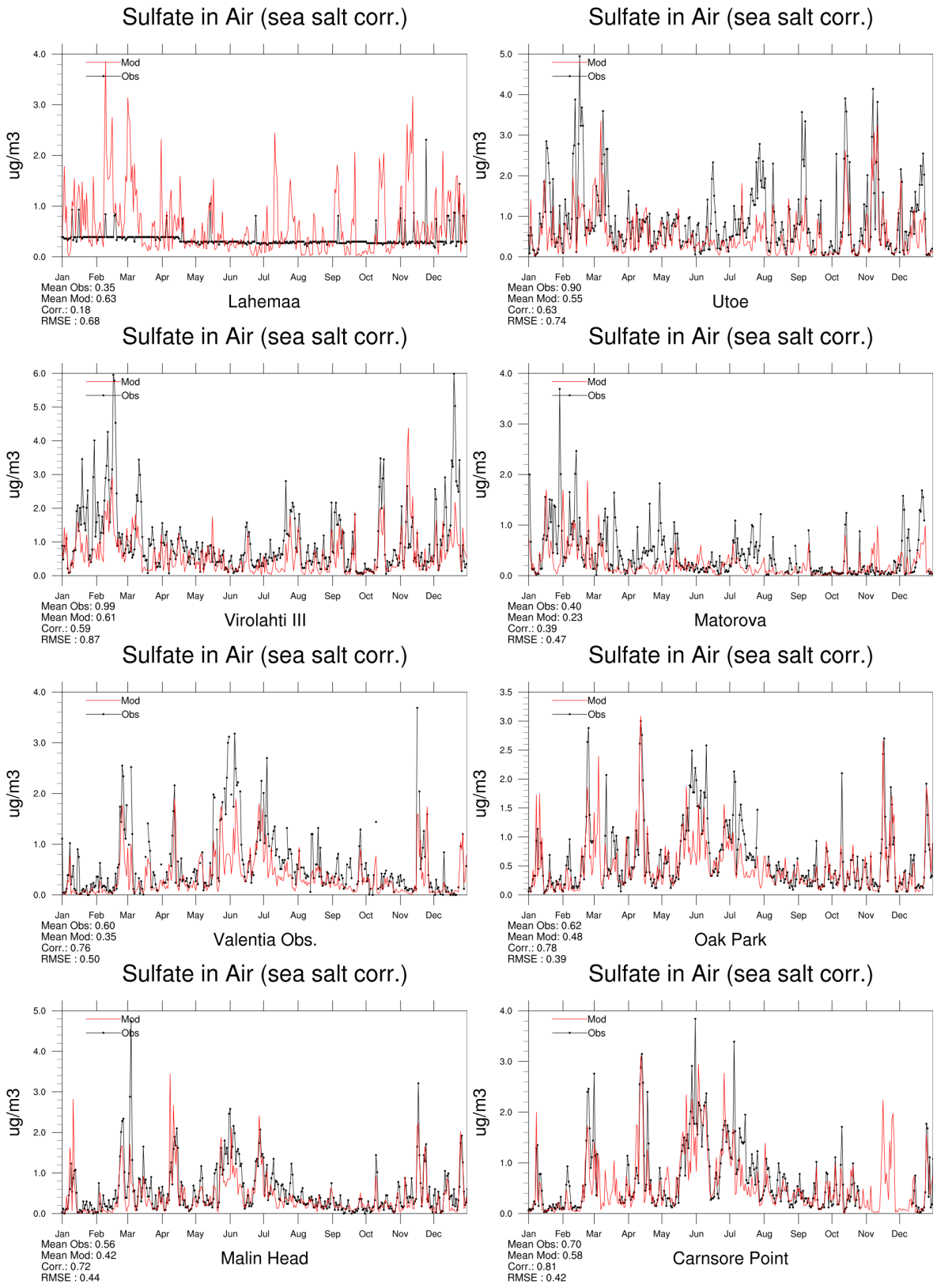

Figure 2.15: Comparison of model results and measurements (daily) for sea salt corrected sulphate in air [μg(S) m^{-3}] for stations that have measured sulphate in 2018.

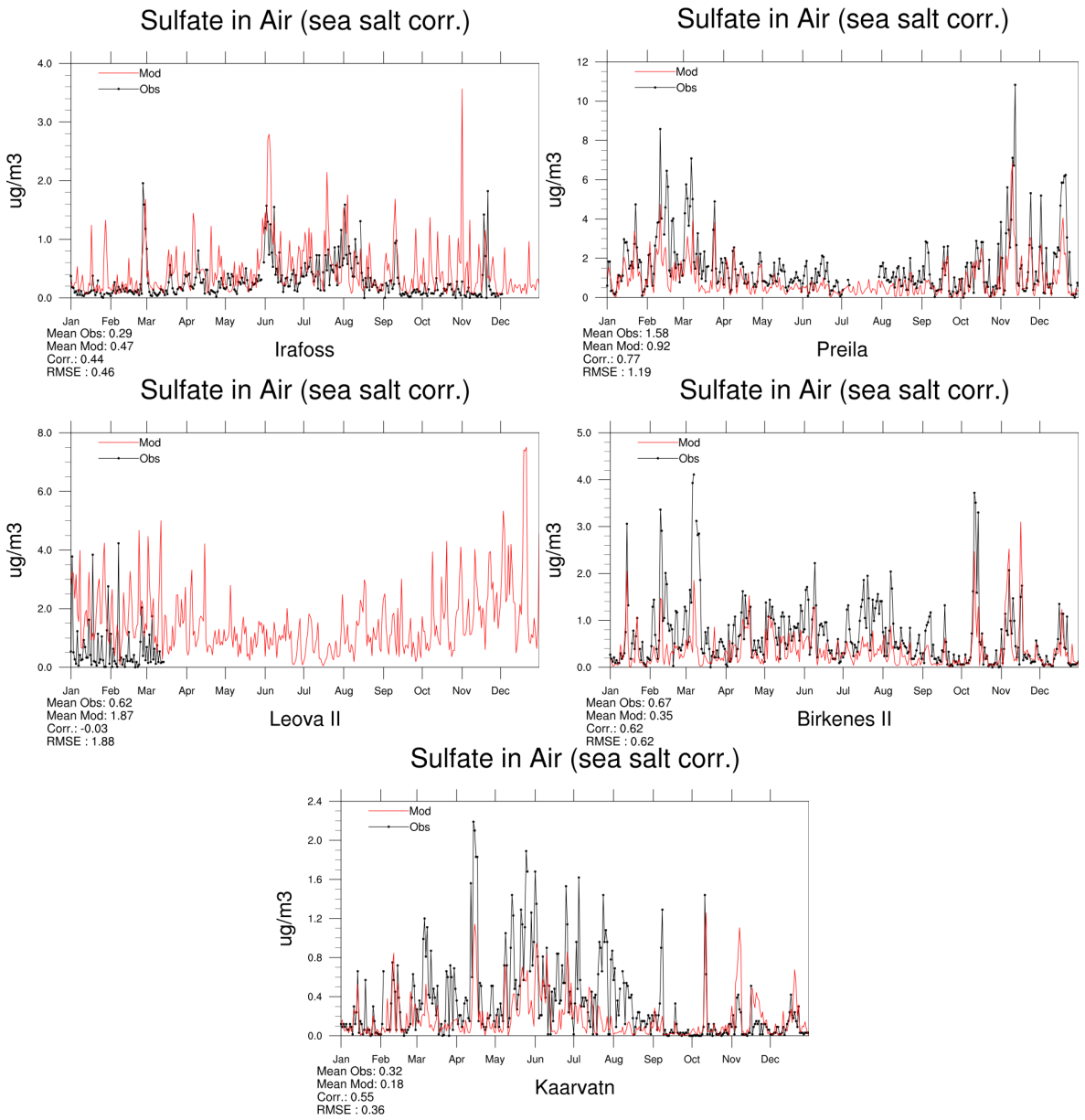

Figure 2.16: Comparison of model results and measurements (daily) for sea salt corrected sulphate in air [μg(S) m^{-3}] for stations that have measured sulphate in 2018.

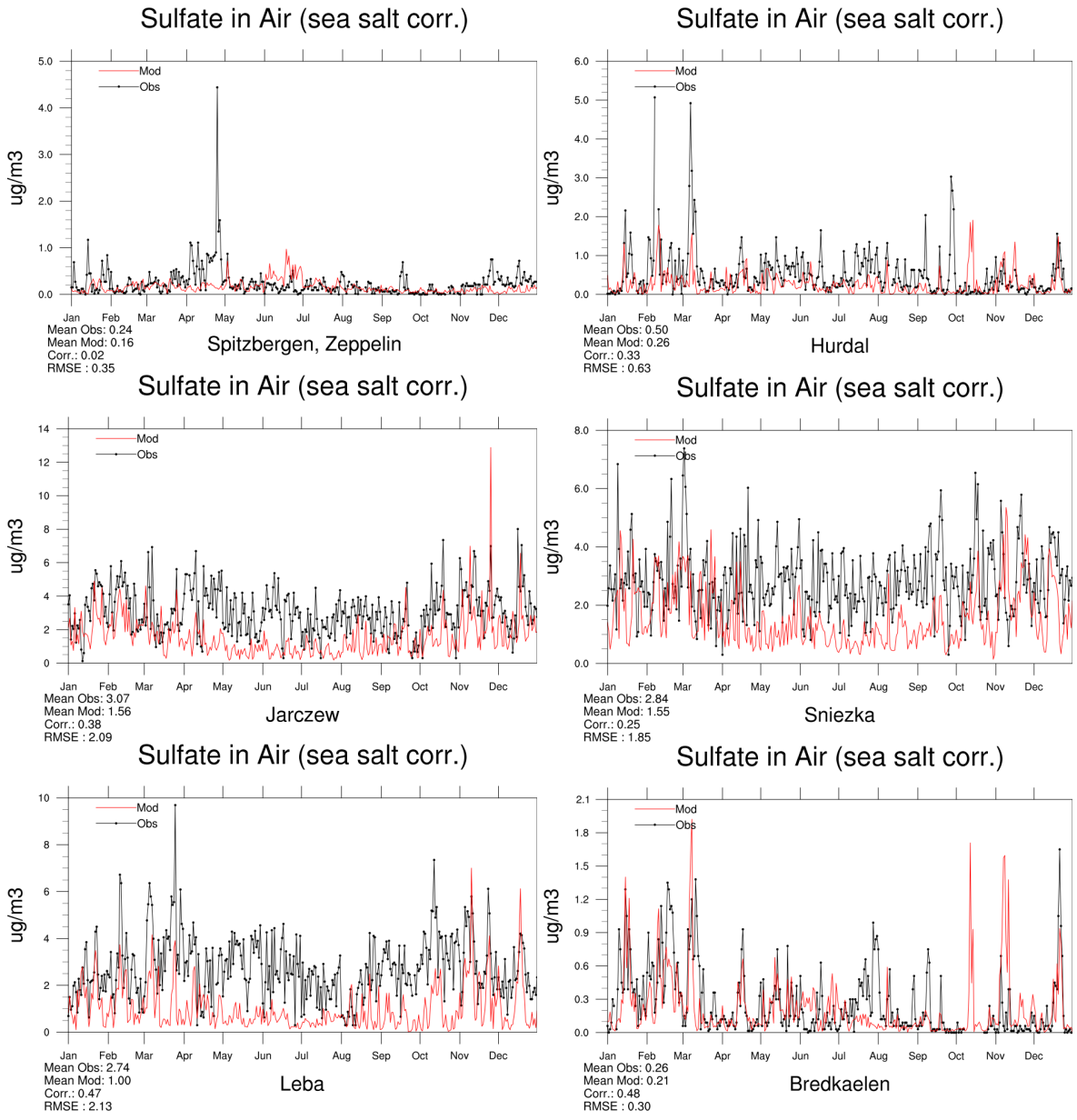

Figure 2.17: Comparison of model results and measurements (daily) for sea salt corrected sulphate in air [μg(S) m^{-3}] for stations that have measured sulphate in 2018.

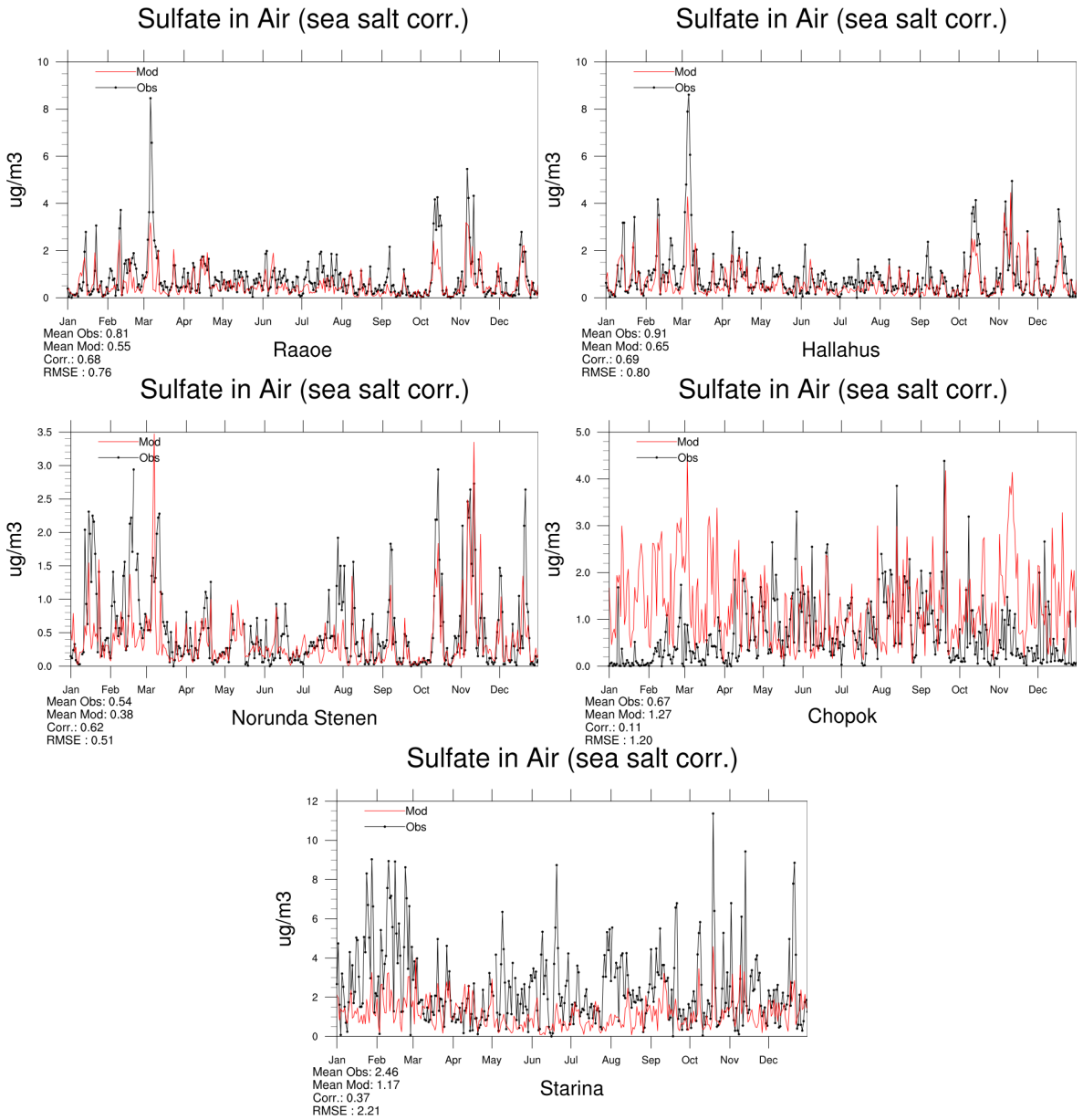

Figure 2.18: Comparison of model results and measurements (daily) for sea salt corrected sulphate in air [μg(S) m^{-3}] for stations that have measured sulphate in 2018.

Sulphate in air – sea salt included

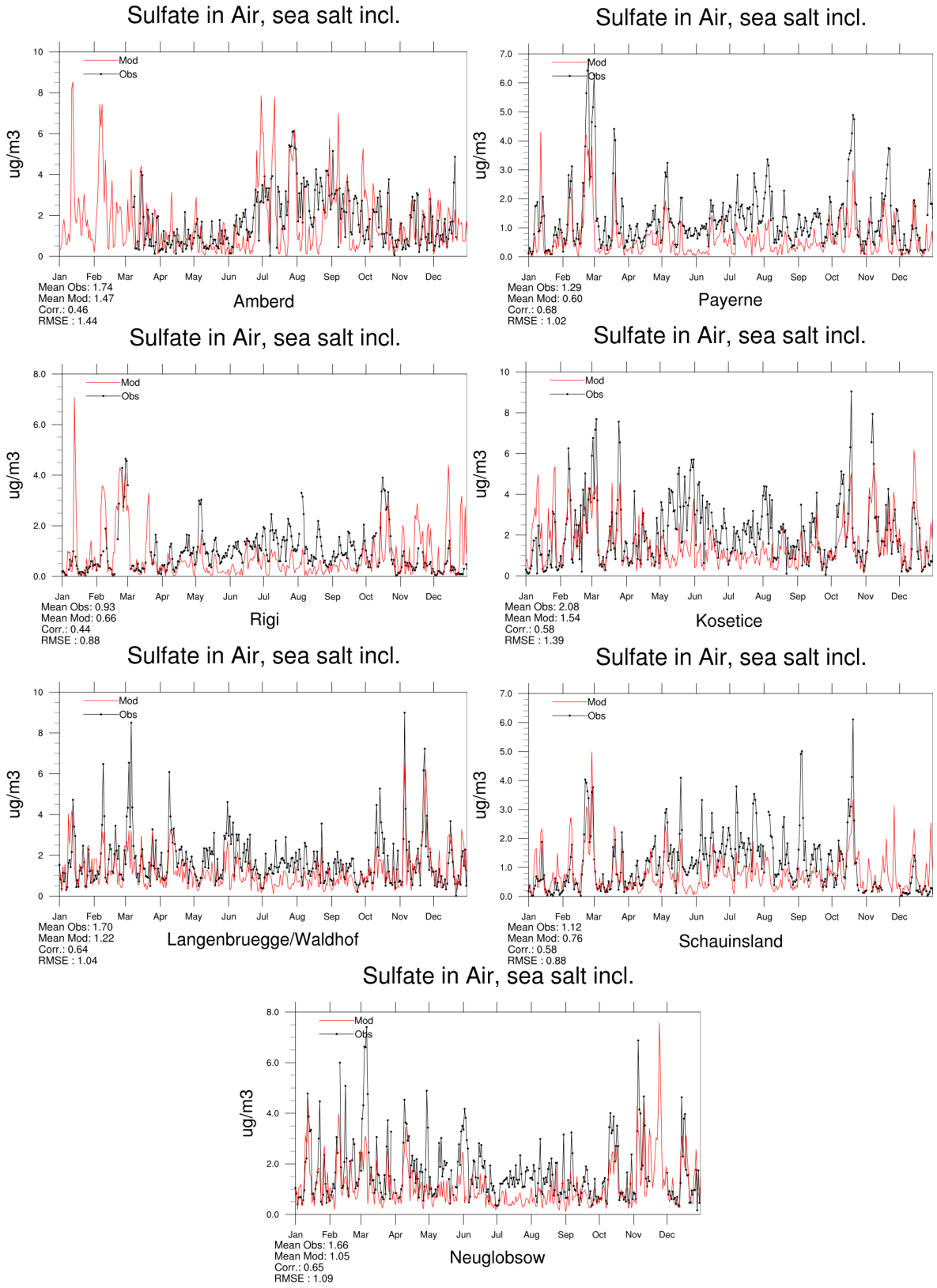

Figure 2.19: Comparison of model results and measurements (daily) for sulphate (including sea salt) in air [μg(S) m^{-3}] for stations that have measured sulphate in 2018.

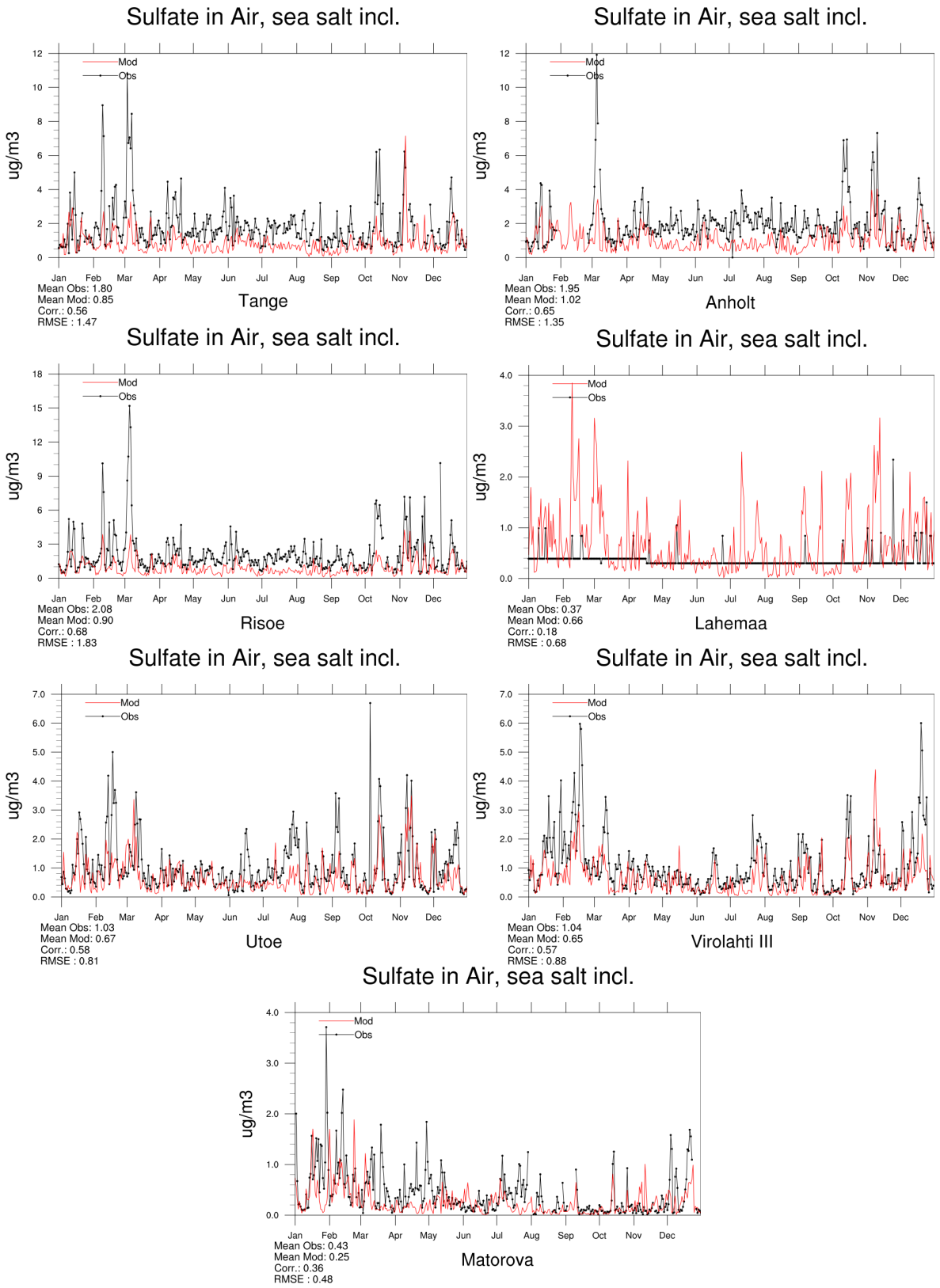

Figure 2.20: Comparison of model results and measurements (daily) for sulphate (including sea salt) in air [μg(S) m^{-3}] for stations that have measured sulphate in 2018.

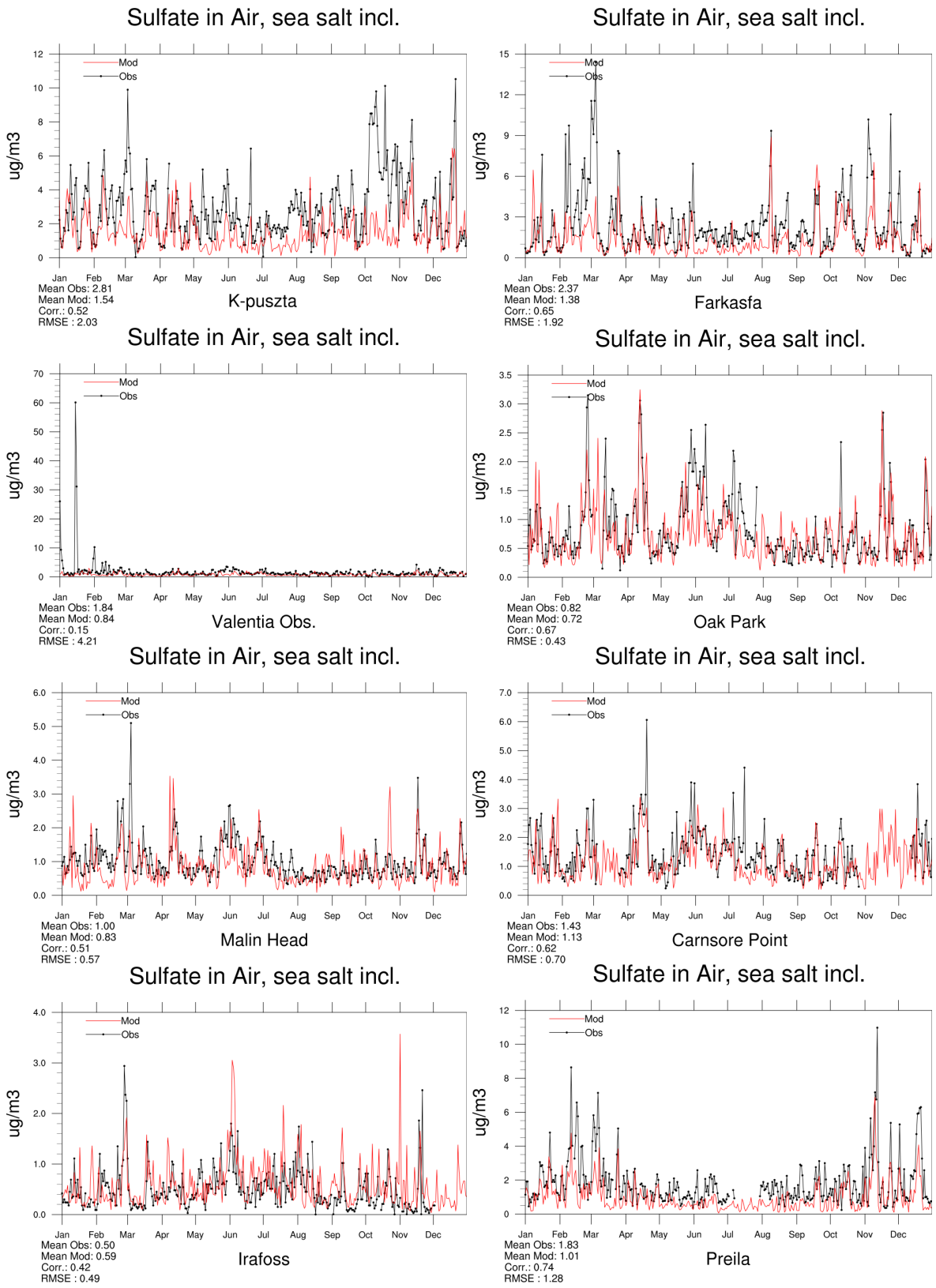

Figure 2.21: Comparison of model results and measurements (daily) for sulphate (including sea salt) in air [μg(S) m^{-3}] for stations that have measured sulphate in 2018.

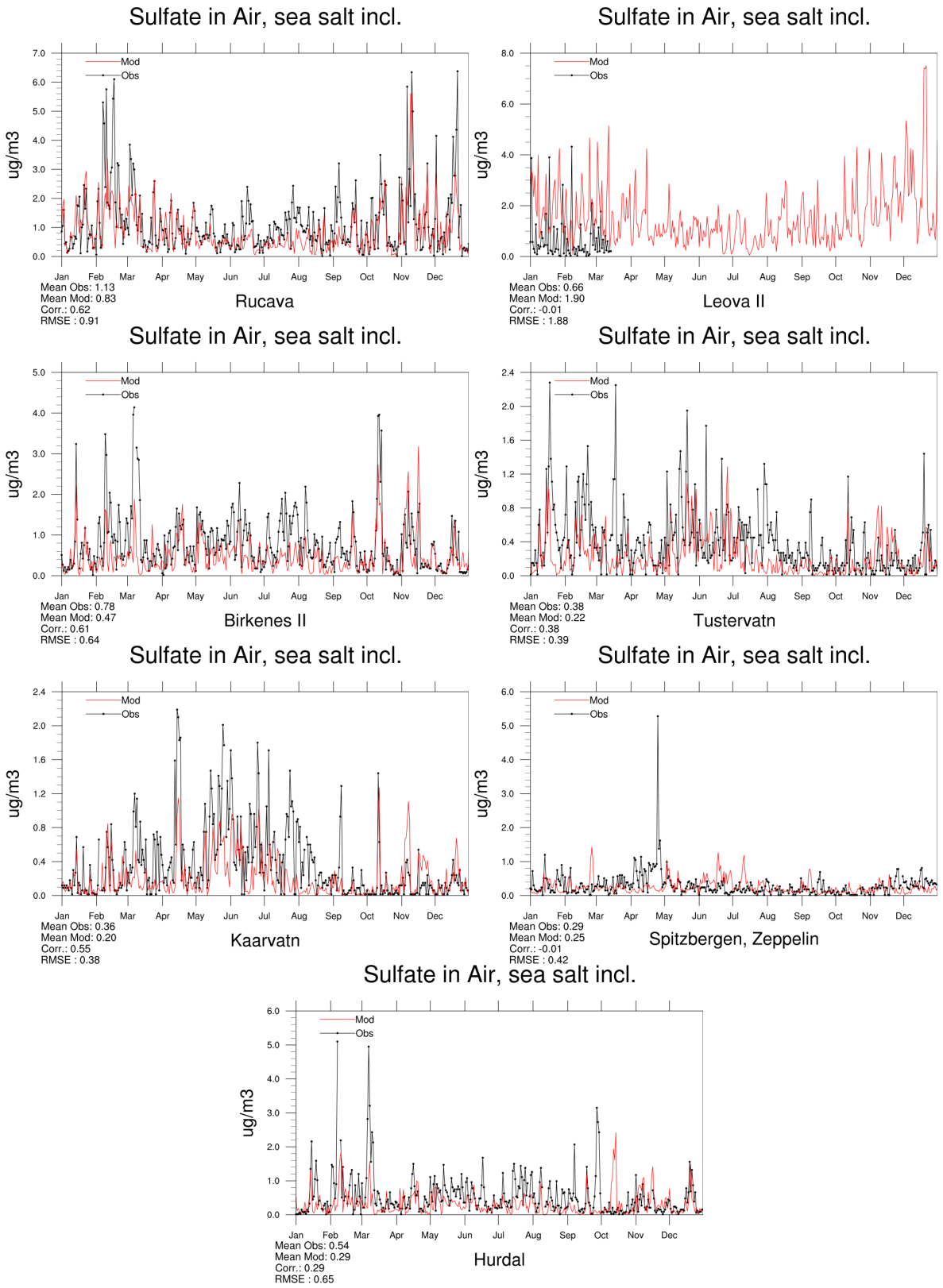

Figure 2.22: Comparison of model results and measurements (daily) for sulphate (including sea salt) in air [μg(S) m^{-3}] for stations that have measured sulphate in 2018.

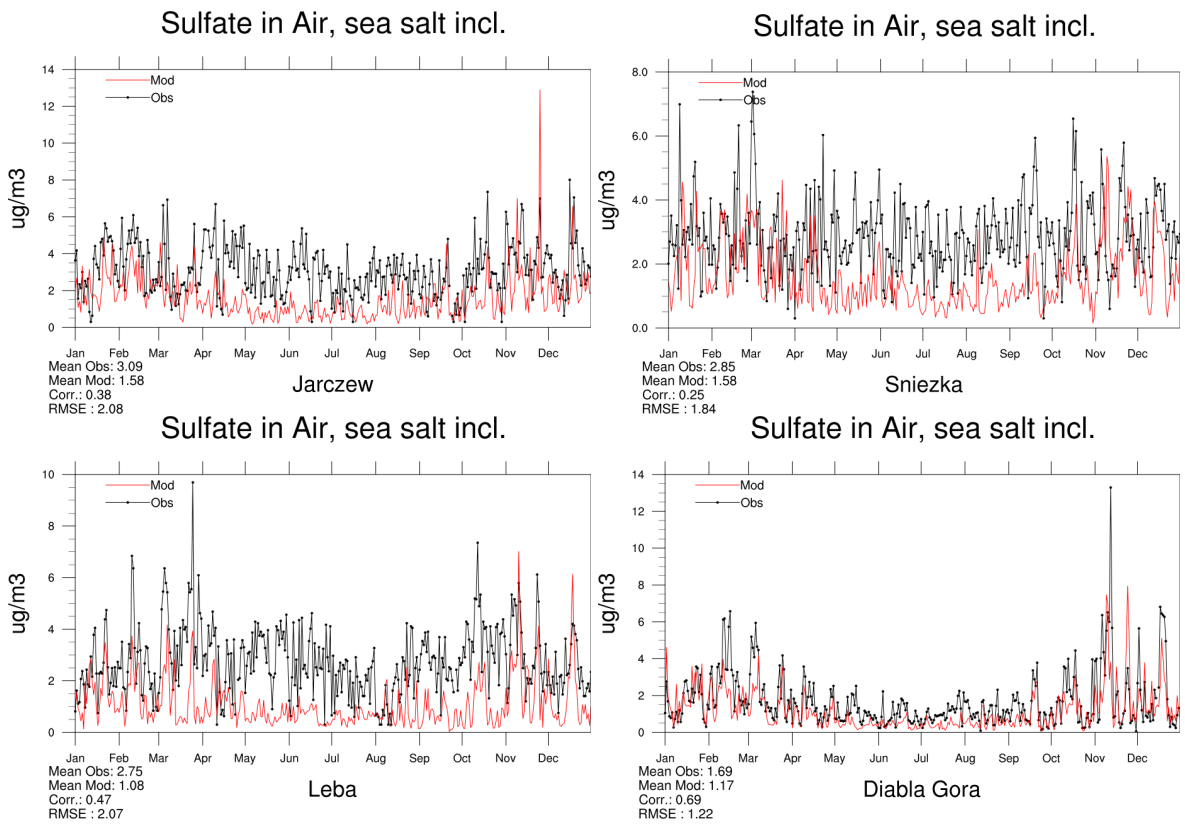

Figure 2.23: Comparison of model results and measurements (daily) for sulphate (including sea salt) in air [μg(S) m^{-3}] for stations that have measured sulphate in 2018.

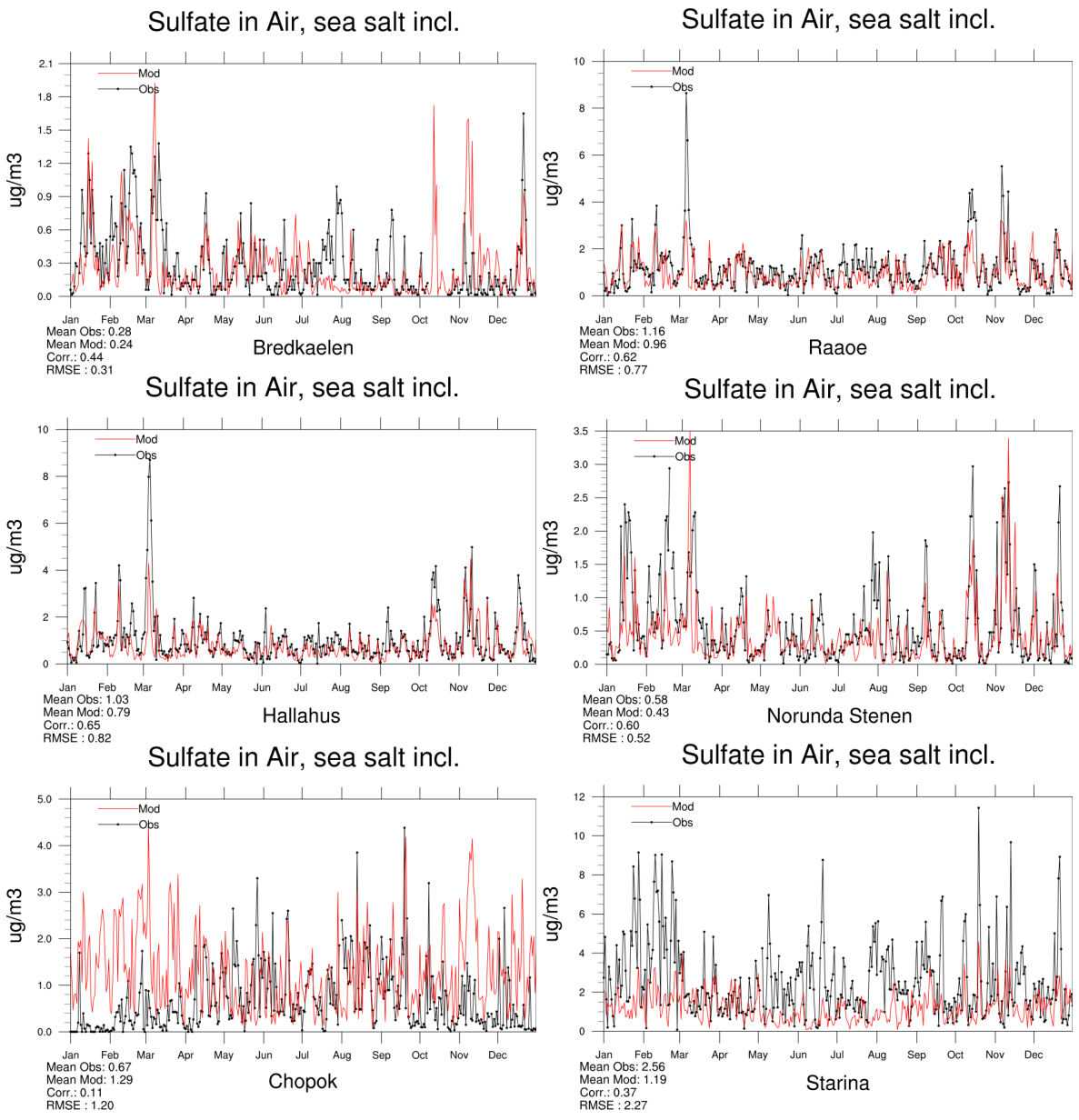

Figure 2.24: Comparison of model results and measurements (daily) for sulphate (including sea salt) in air [μg(S) m^{-3}] for stations that have measured sulphate in 2018.

Total nitrate in air

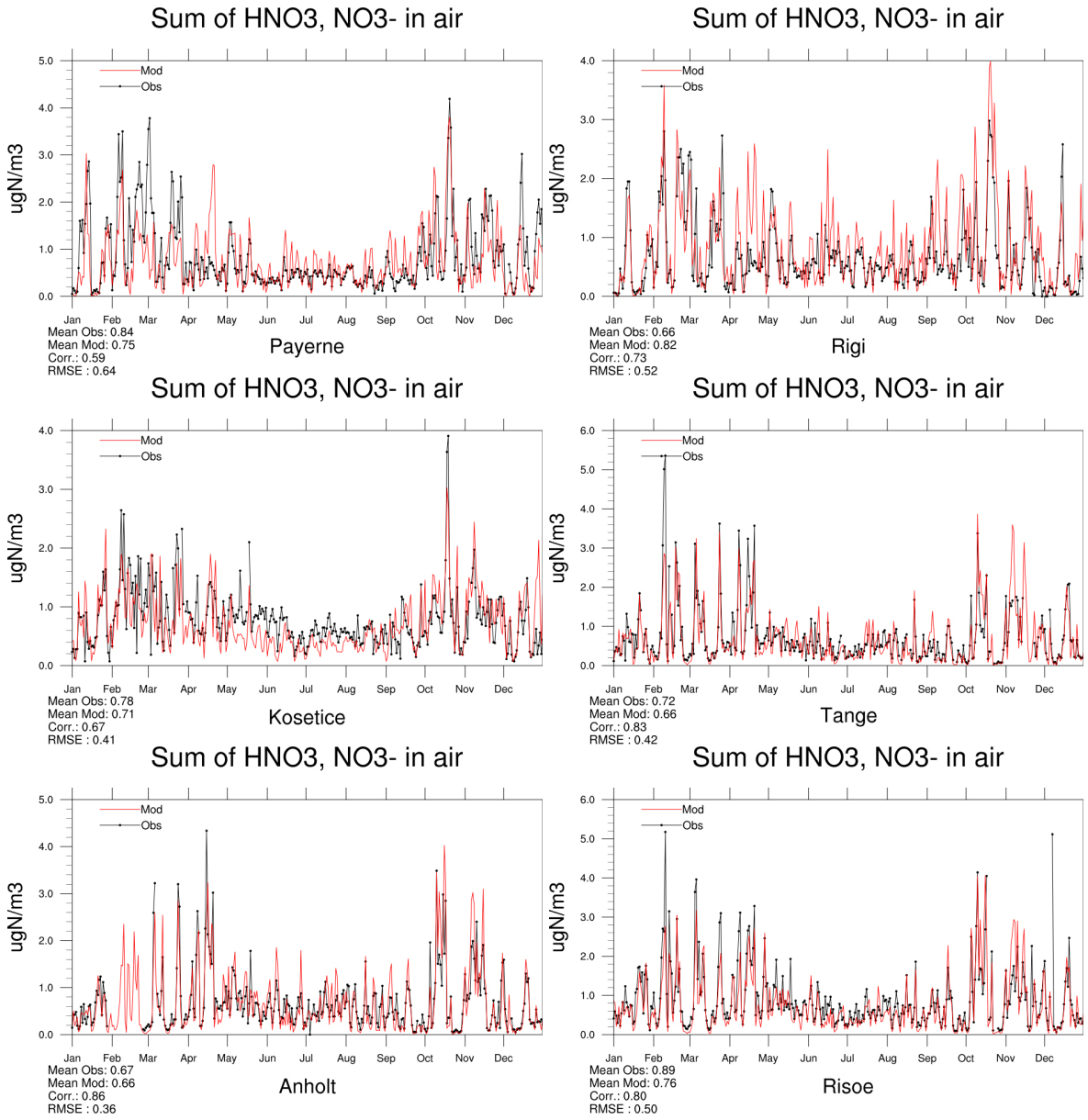

Figure 2.25: Comparison of model results and measurements (daily) total nitrate concentrations [μg(N) m^{-3}] for stations that have measured total nitrate in 2018.

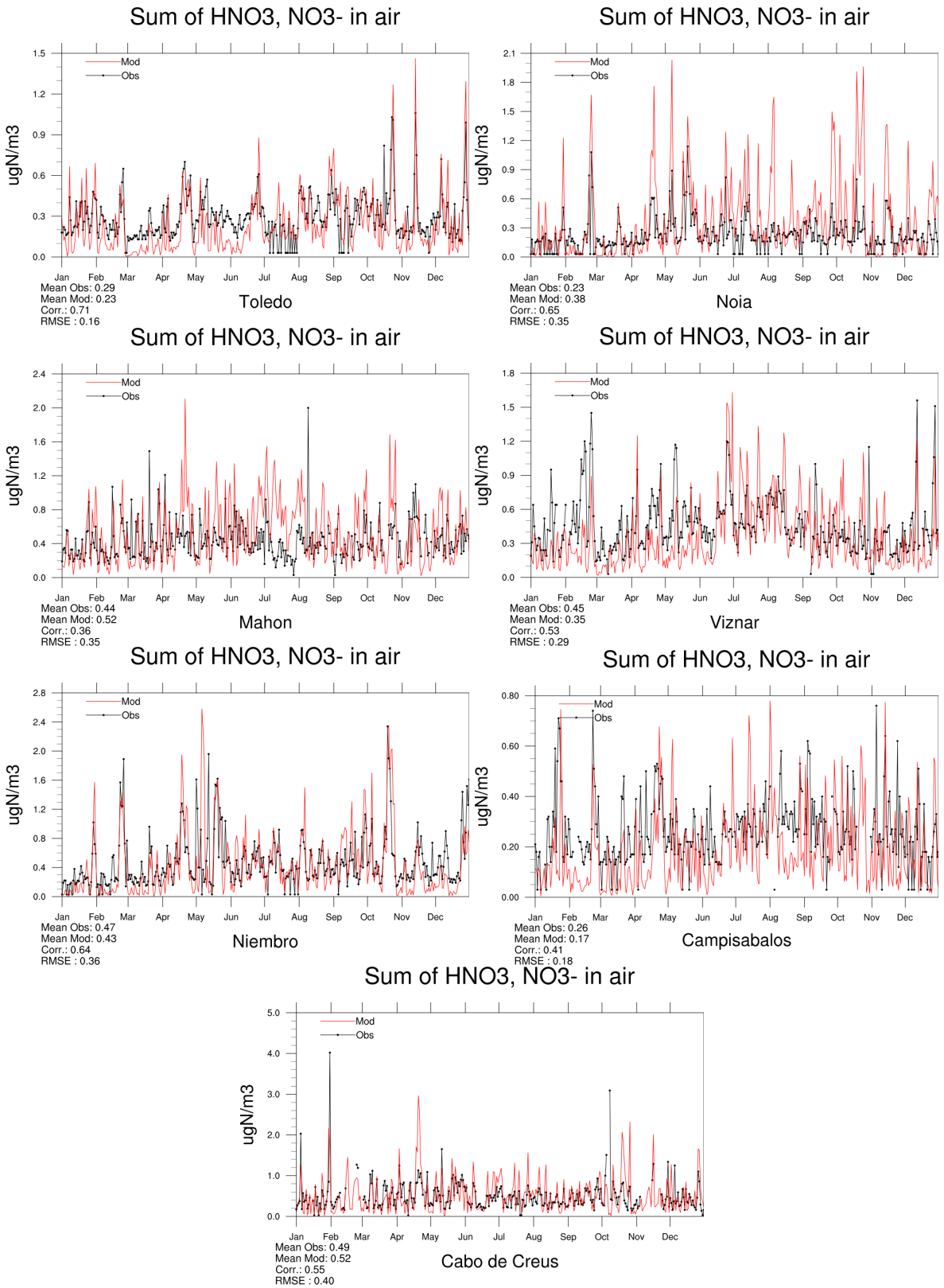

Figure 2.26: Comparison of model results and measurements (daily) total nitrate concentrations [μg(N) m^{-3}] for stations that have measured total nitrate in 2018.

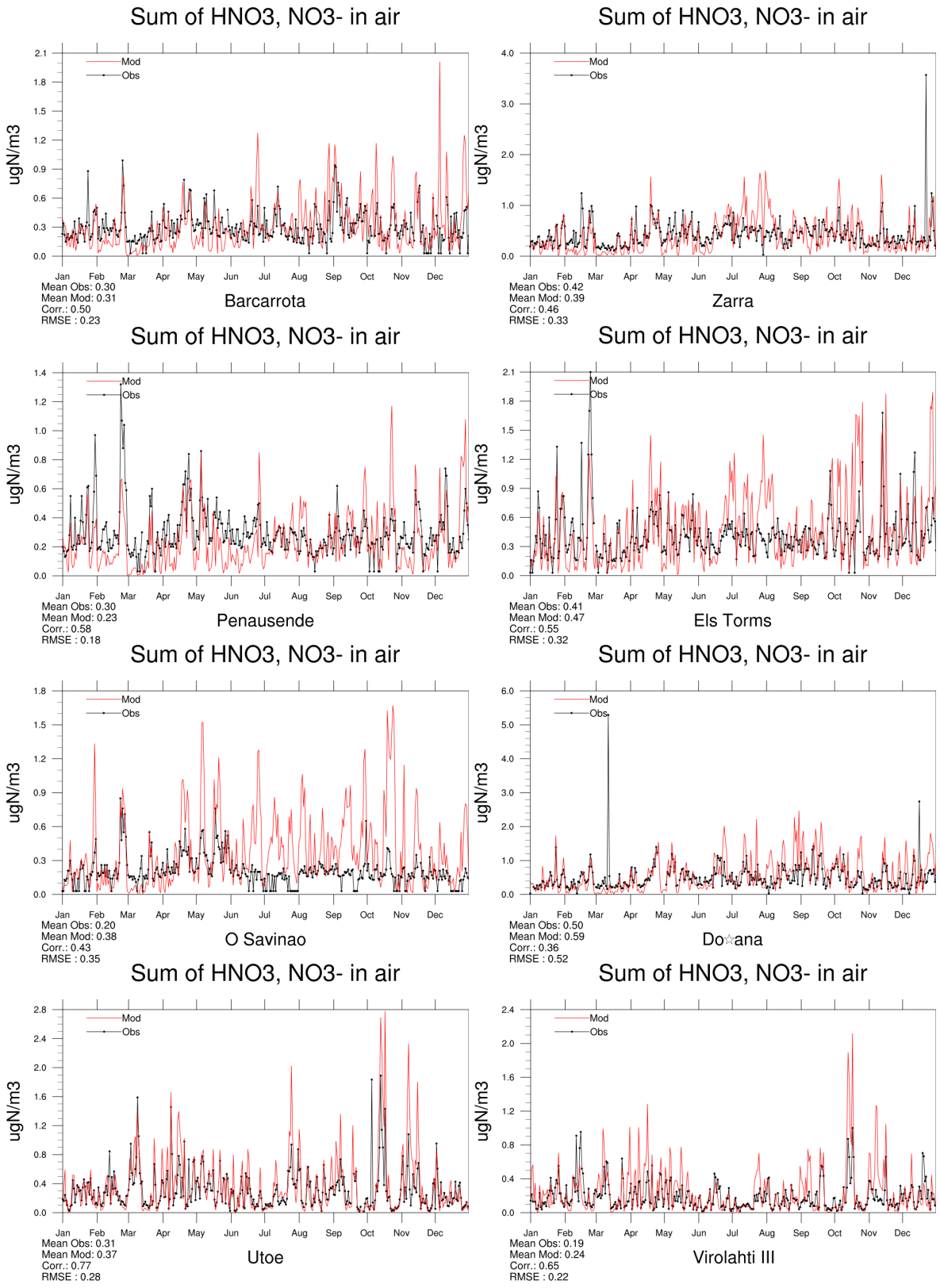

Figure 2.27: Comparison of model results and measurements (daily) total nitrate concentrations (μg(N) m^{-3}) for stations that have measured total nitrate in 2018.

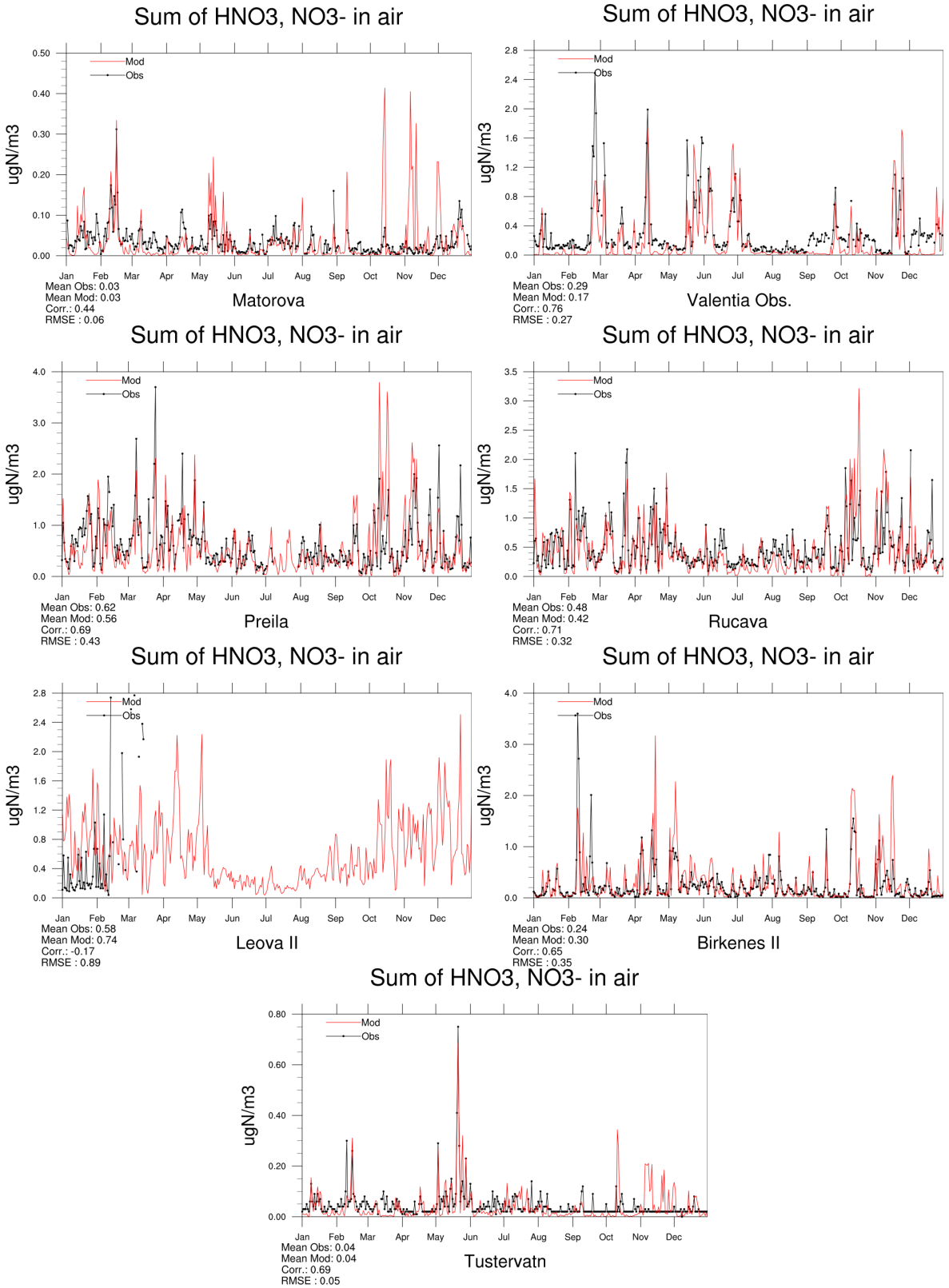

Figure 2.28: Comparison of model results and measurements (daily) total nitrate concentrations [μg(N) m^{-3}] for stations that have measured total nitrate in 2018.

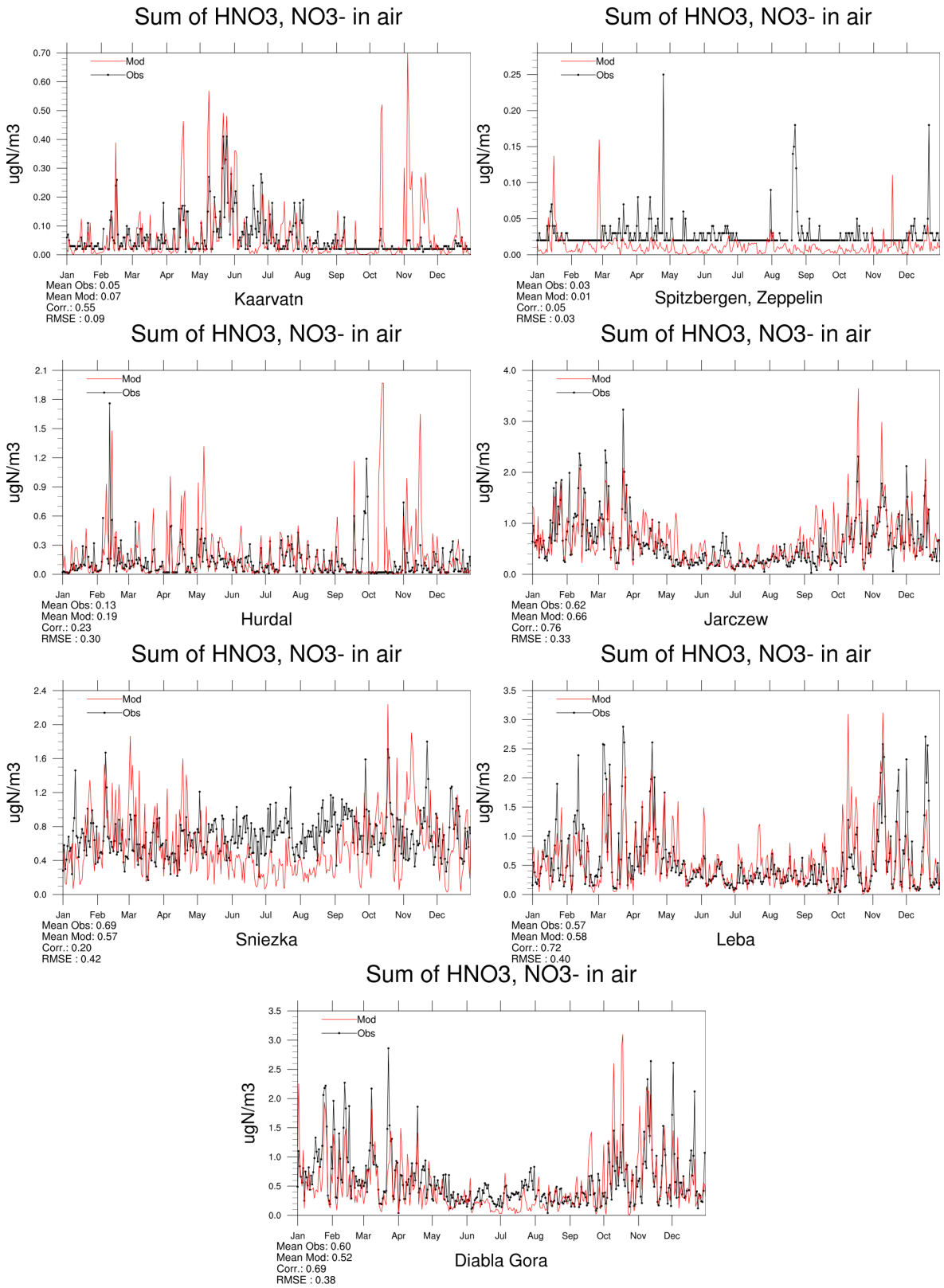

Figure 2.29: Comparison of model results and measurements (daily) total nitrate concentrations [μg(N) m^{-3}] for stations that have measured total nitrate in 2018.

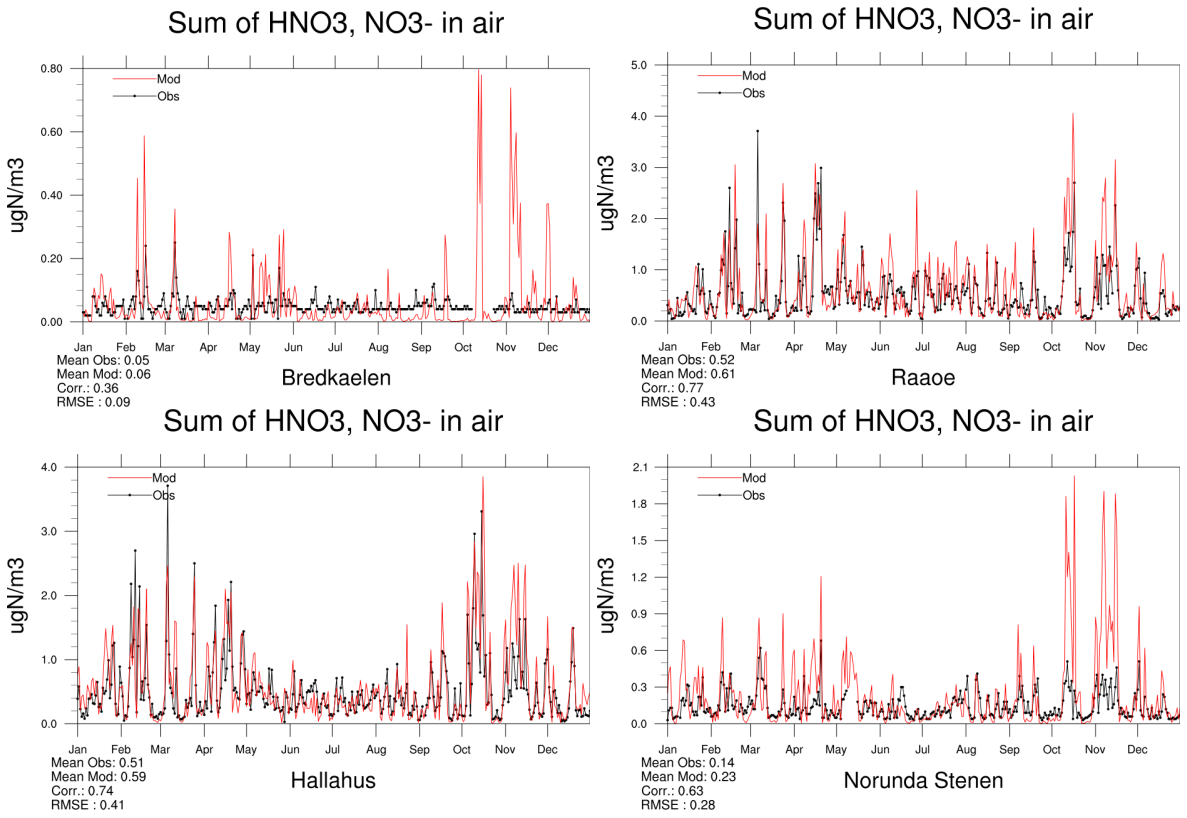

Figure 2.30: Comparison of model results and measurements (daily) total nitrate concentrations [μg(N) m^{-3}] for stations that have measured total nitrate in 2018.

Ammonia+ammonium in air

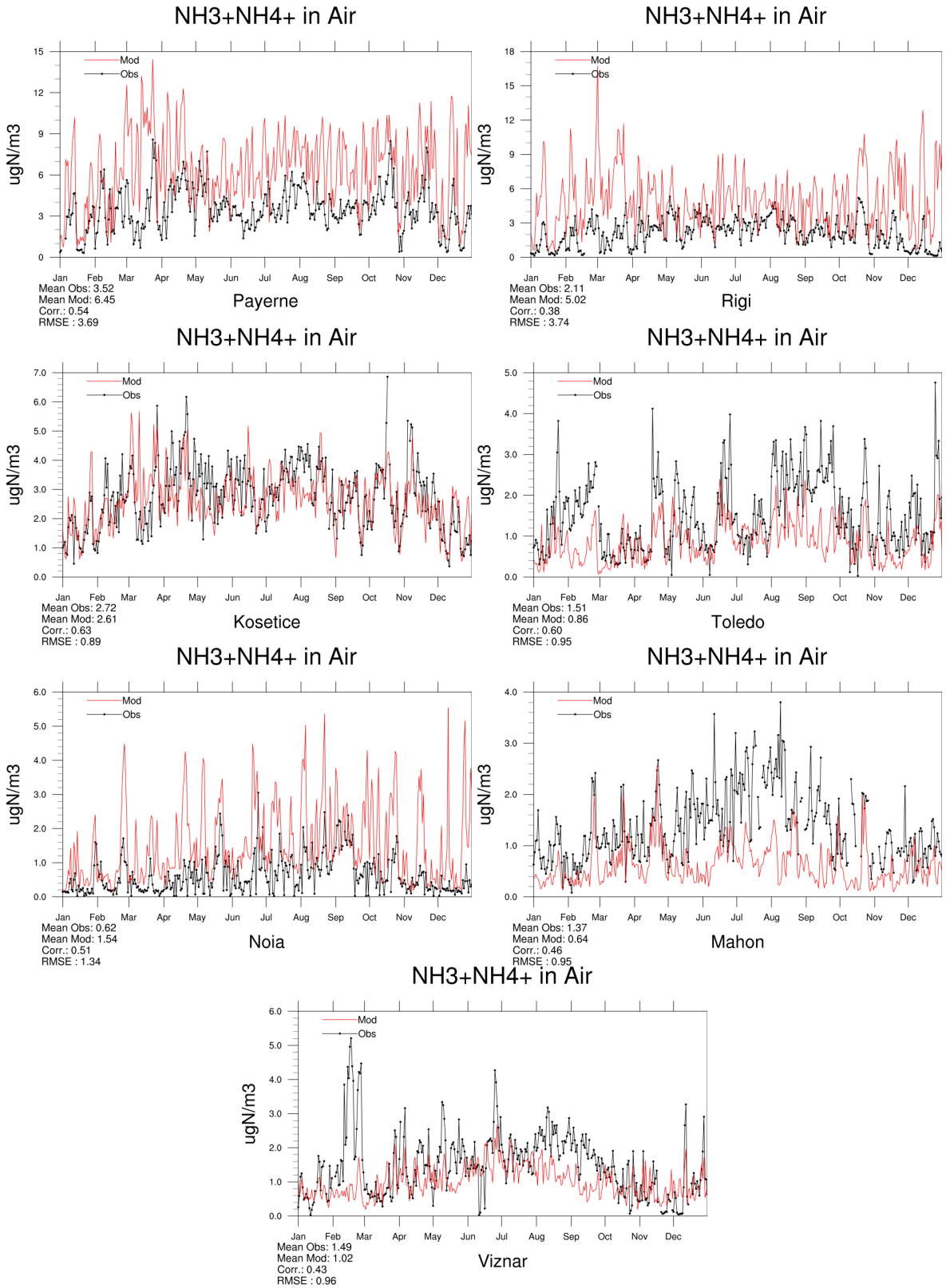

Figure 2.31: Comparison of model results and measurements (daily) total ammonium+ammonia concentrations [μg(N) m^{-3}] for stations that have measured total ammonium+ammonia in 2018.

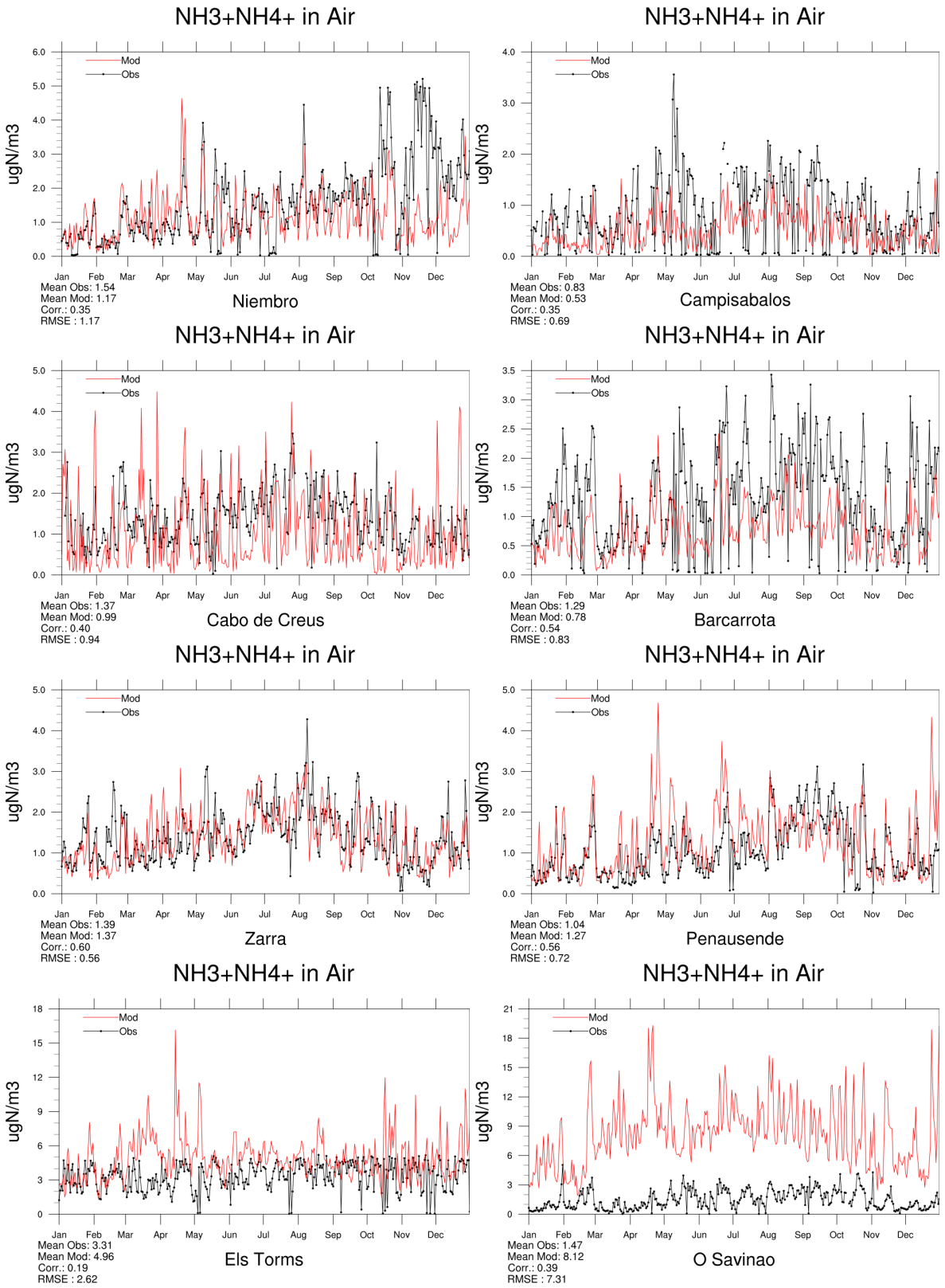

Figure 2.32: Comparison of model results and measurements (daily) total ammonium+ammonia concentrations [μg(N) m^{-3}] for stations that have measured total ammonium+ammonia in 2018.

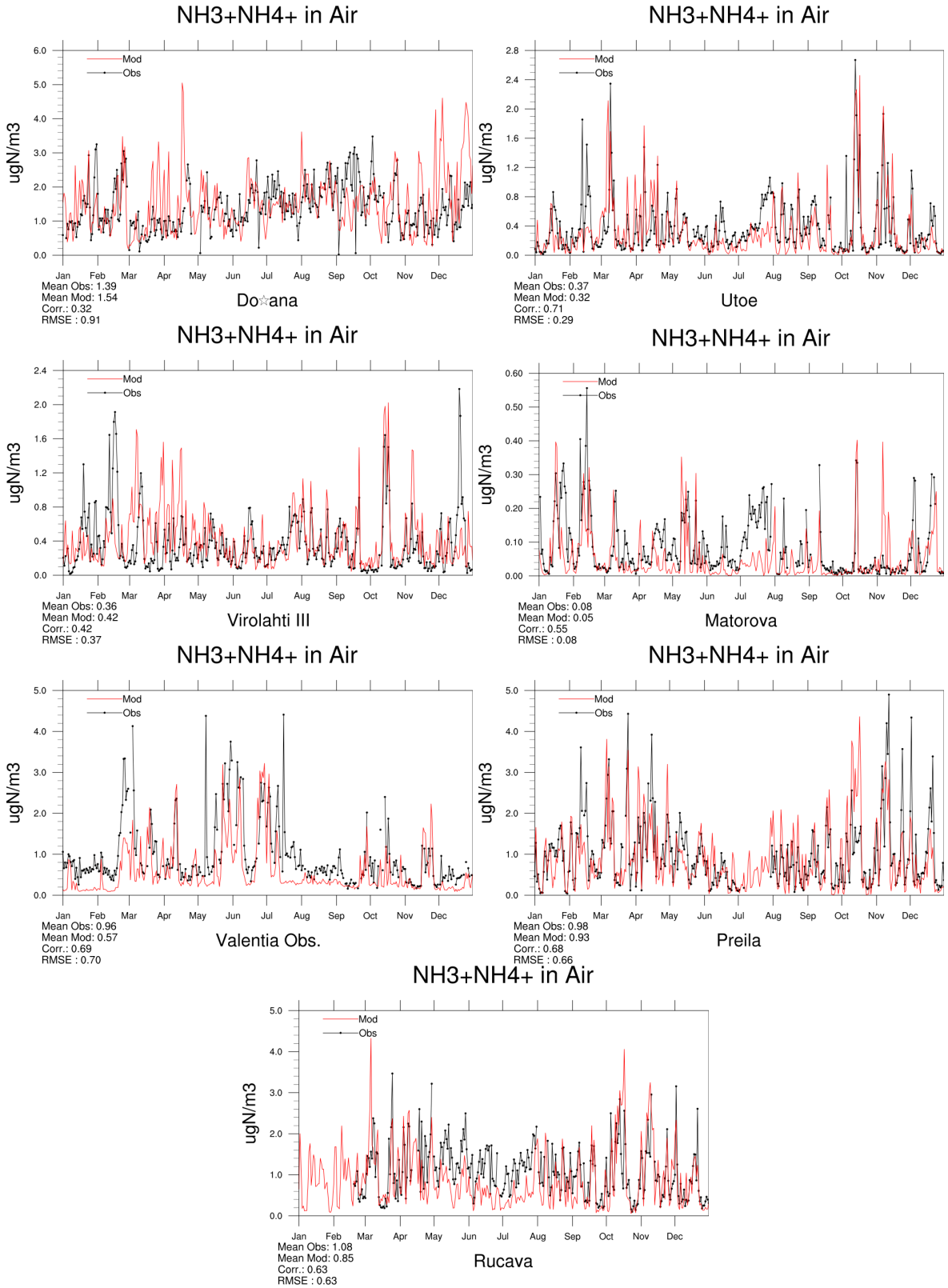

Figure 2.33: Comparison of model results and measurements (daily) total ammonium+ammonia concentrations [μg(N) m^{-3}] for stations that have measured total ammonium+ammonia in 2018.

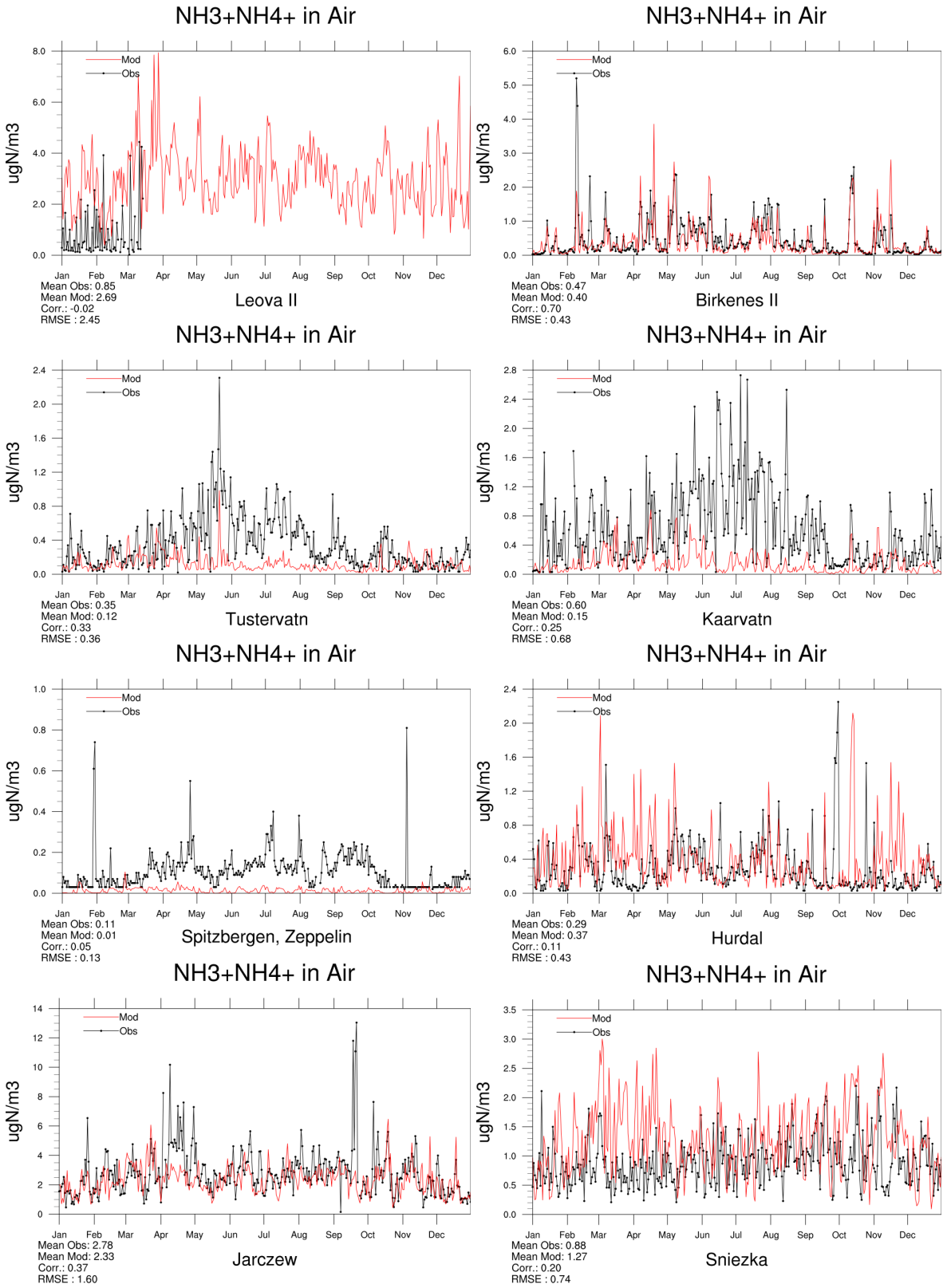

Figure 2.34: Comparison of model results and measurements (daily) total ammonium+ammonia concentrations [μg(N) m^{-3}] for stations that have measured total ammonium+ammonia in 2018.

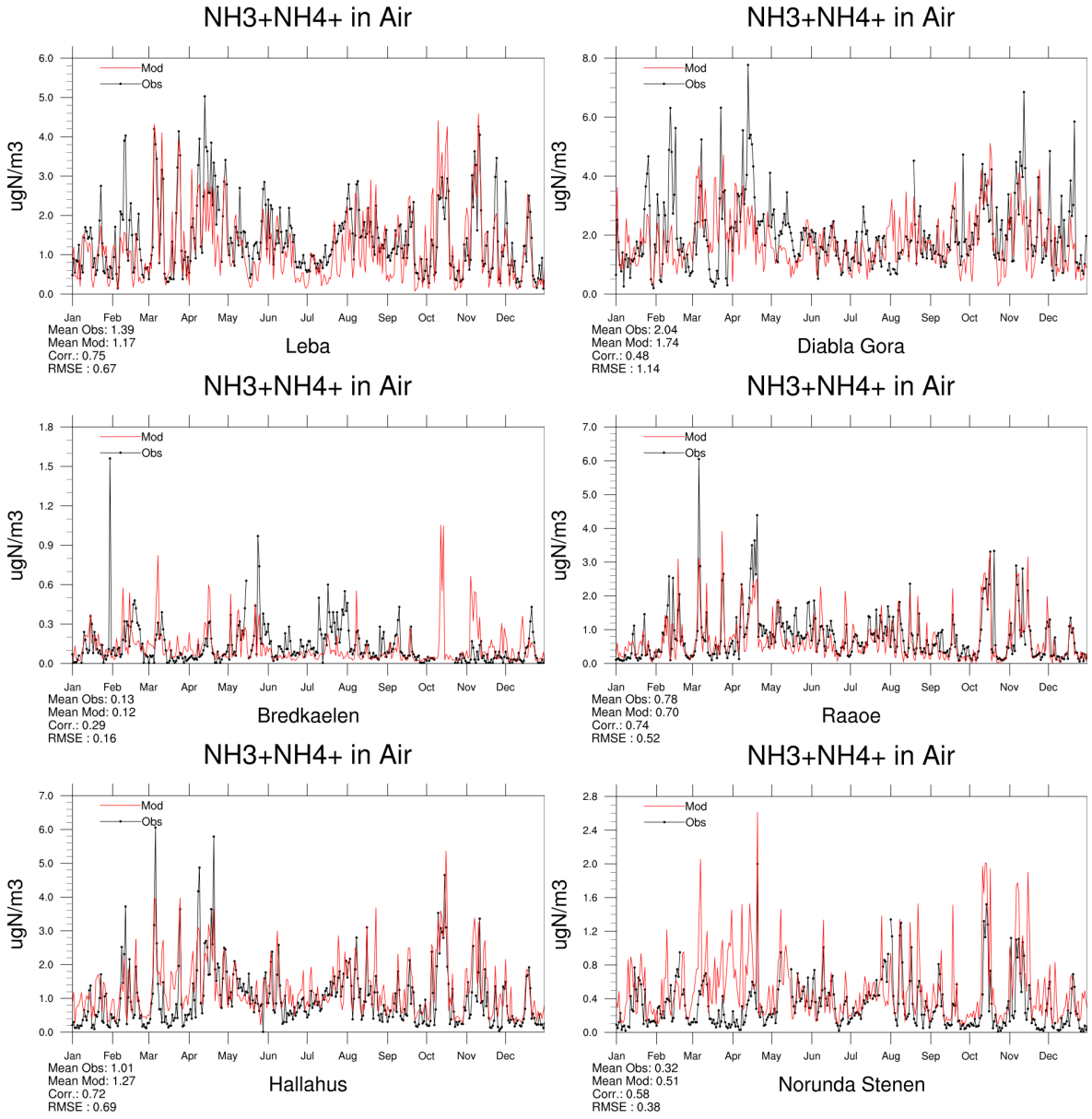

Figure 2.35: Comparison of model results and measurements (daily) total ammonium+ammonia concentrations [μg(N) m^{-3}] for stations that have measured total ammonium+ammonia in 2018.

Sulphur in precipitation

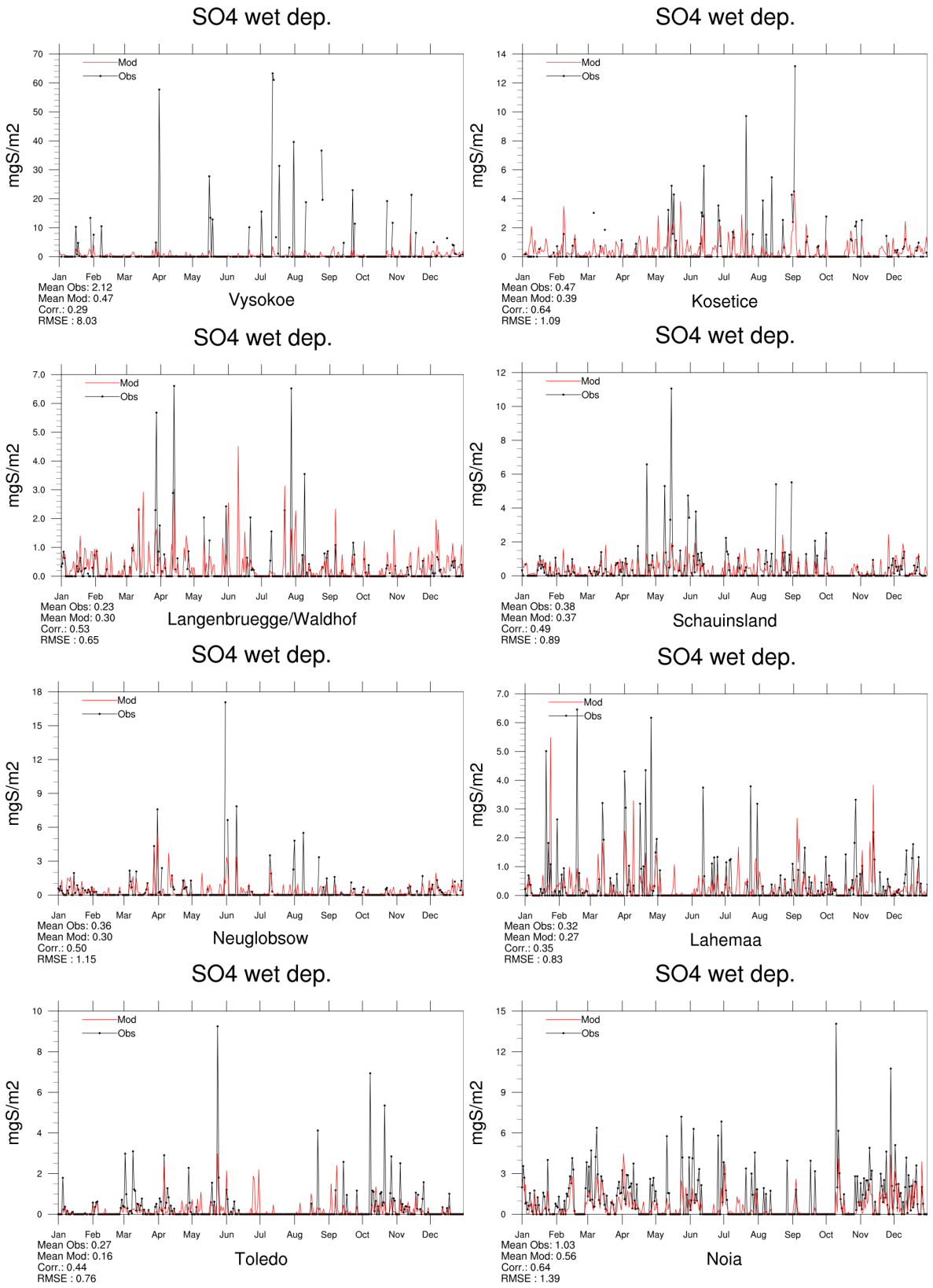

Figure 2.36: Comparison of model results and measurements (daily) for wet deposition of sulphur [mg(S)m^{-2}] in 2018.

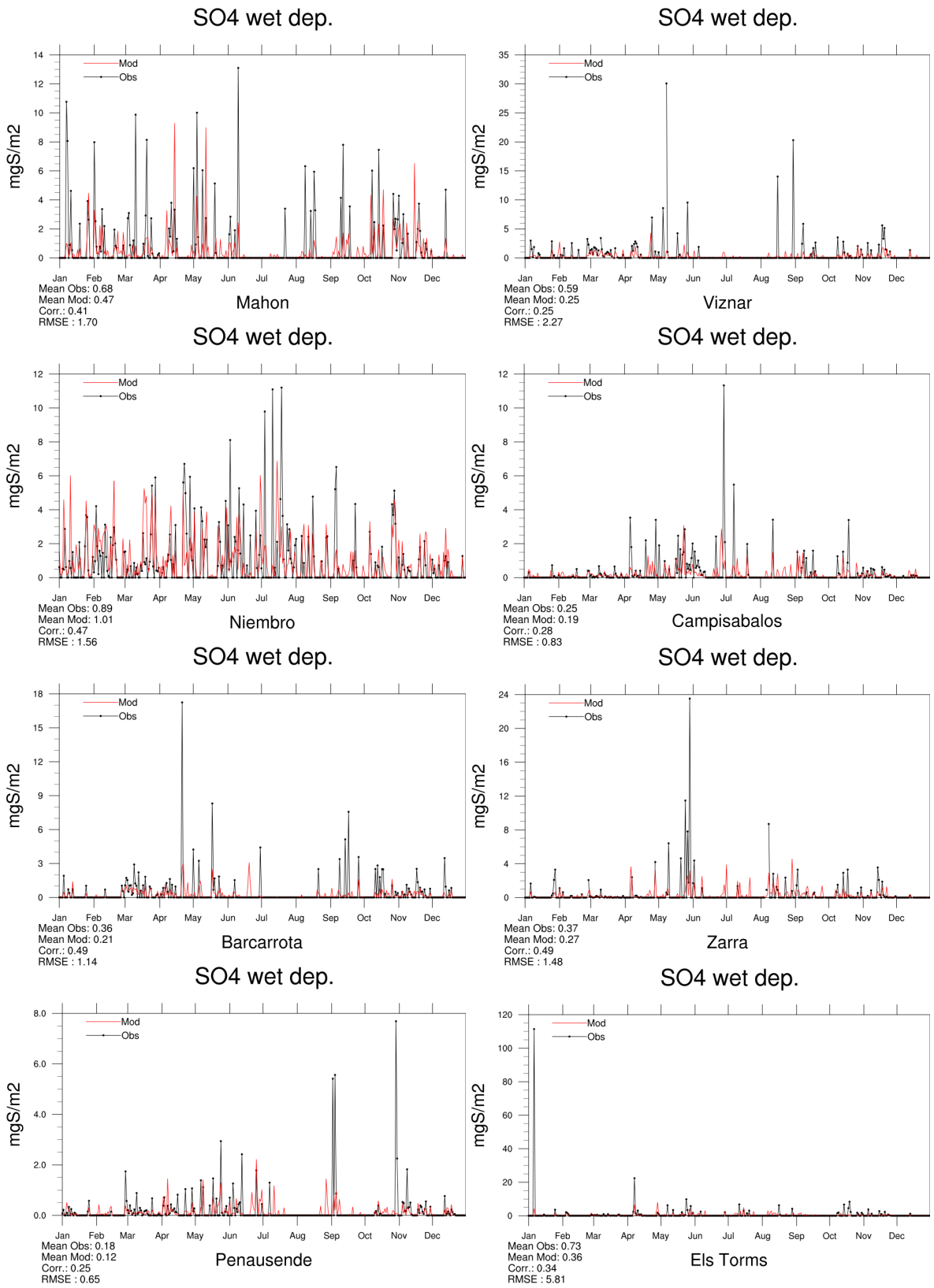

Figure 2.37: Comparison of model results and measurements (daily) for wet deposition of sulphur [mg(S)m^{-2}] in 2018.

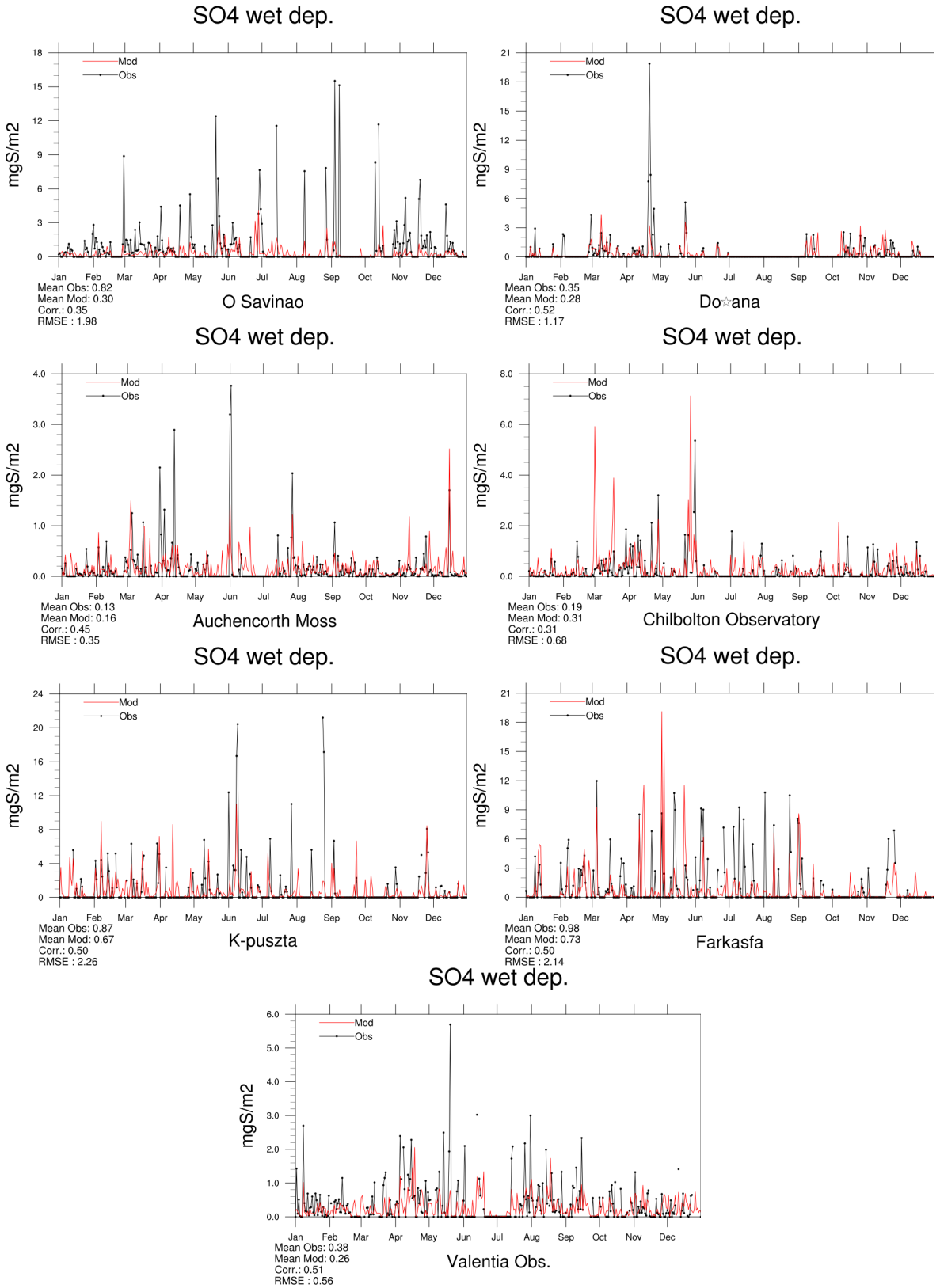

Figure 2.38: Comparison of model results and measurements (daily) for wet deposition of sulphur [mg(S)m^{-2}] in 2018.

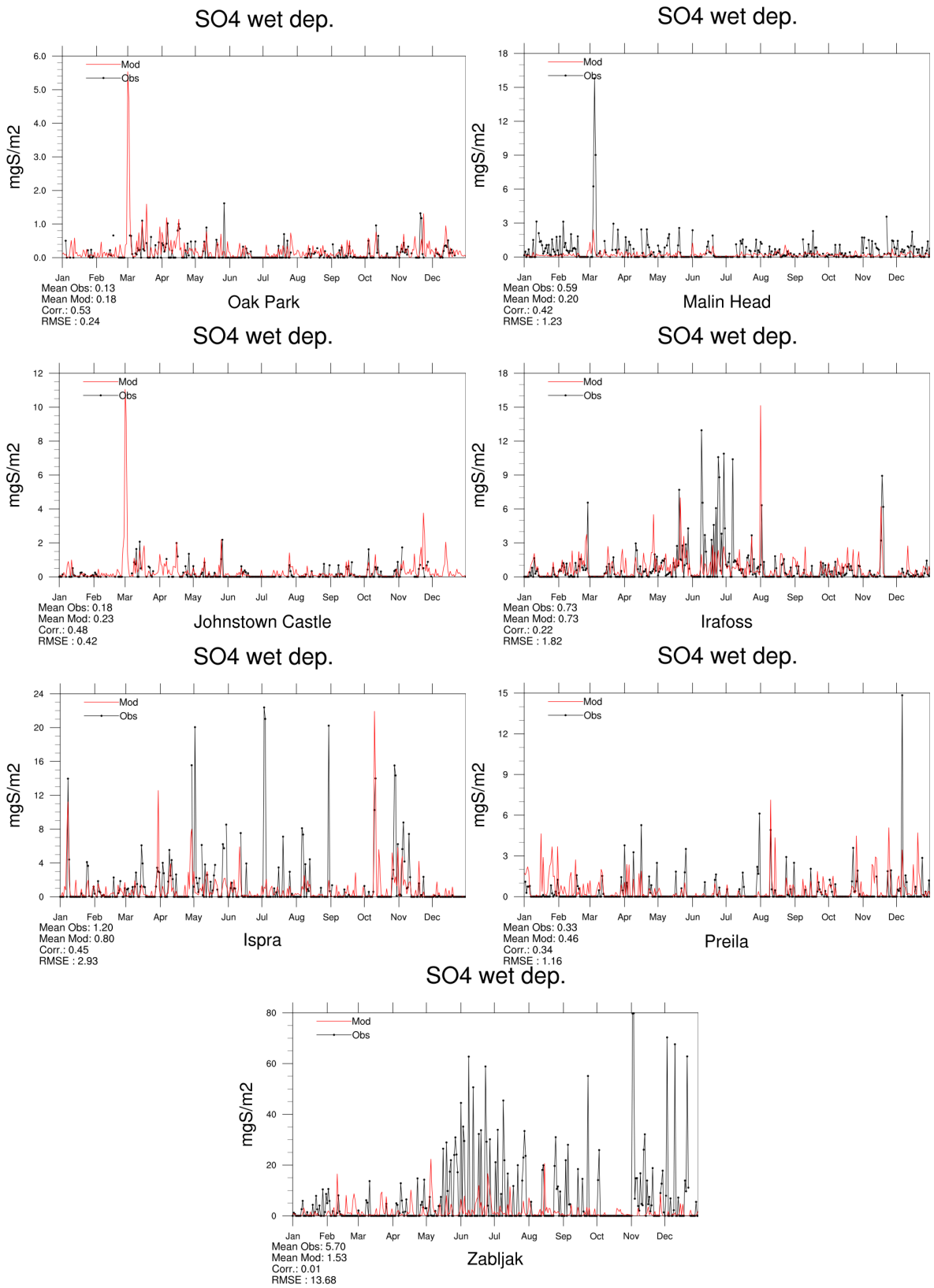

Figure 2.39: Comparison of model results and measurements (daily) for wet deposition of sulphur [mg(S)m^{-2}] in 2018.

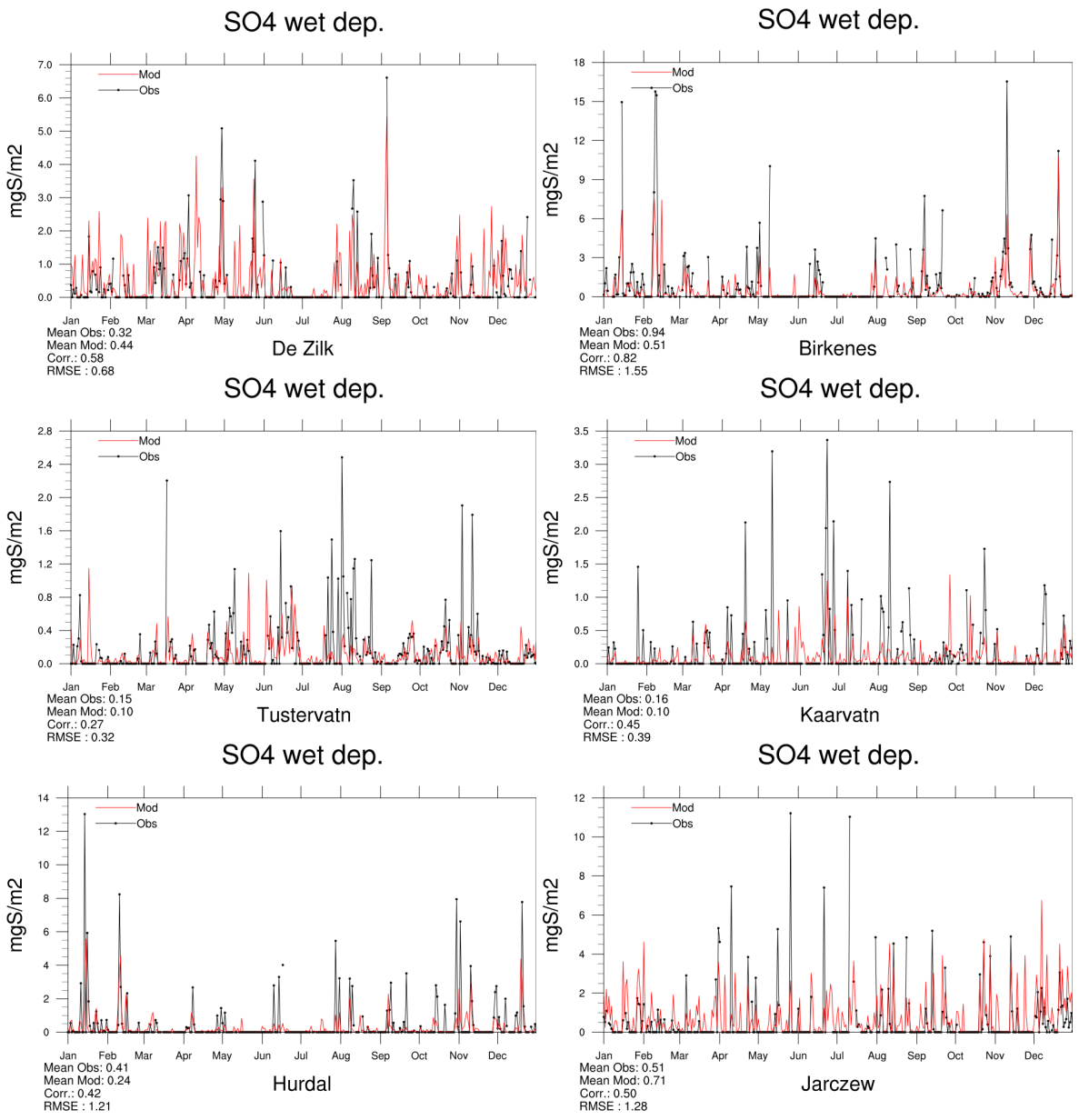

Figure 2.40: Comparison of model results and measurements (daily) for wet deposition of sulphur [mg(S)m^{-2}] in 2018.

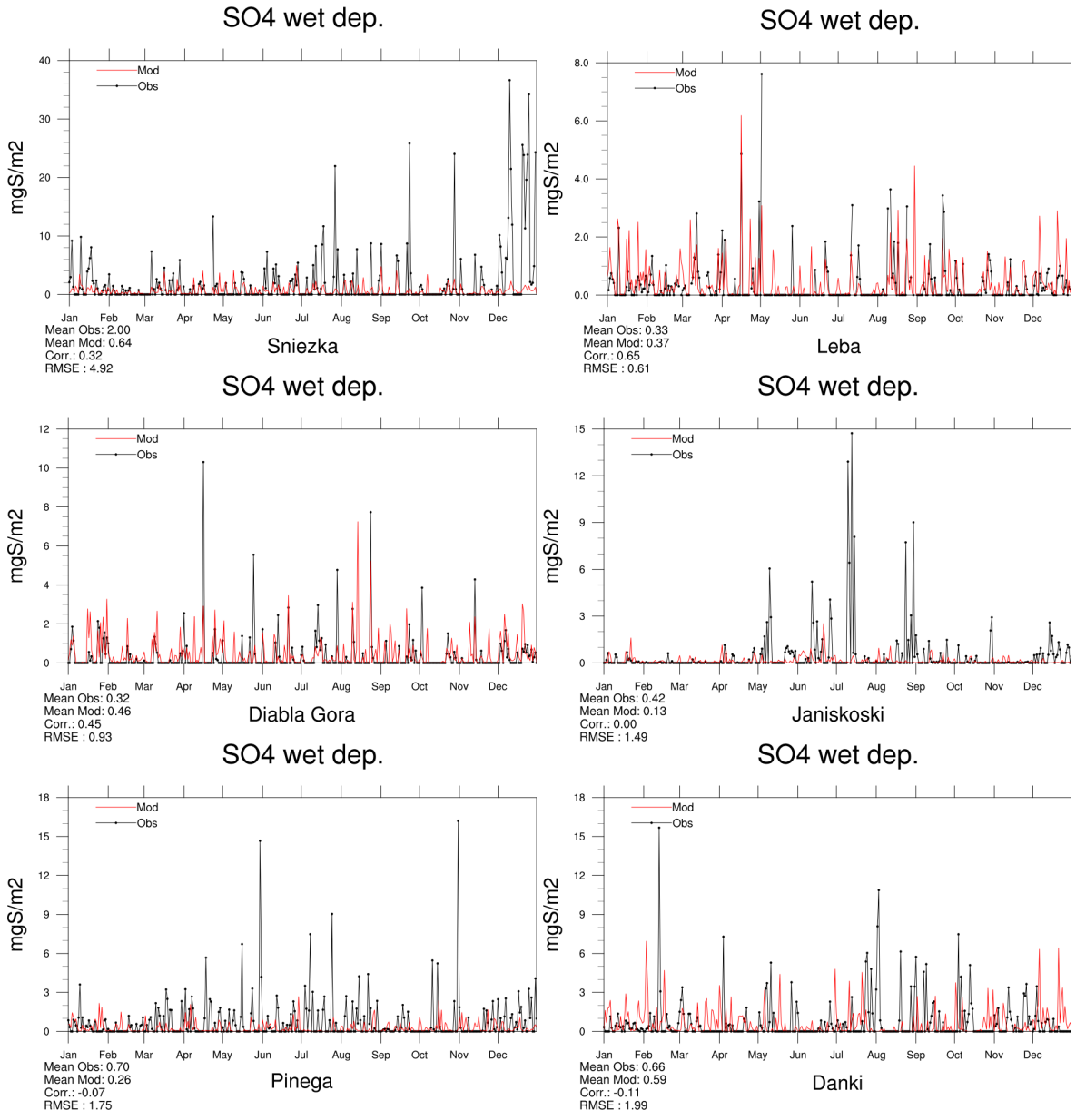

Figure 2.41: Comparison of model results and measurements (daily) for wet deposition of sulphur [mg(S)m^{-2}] in 2018.

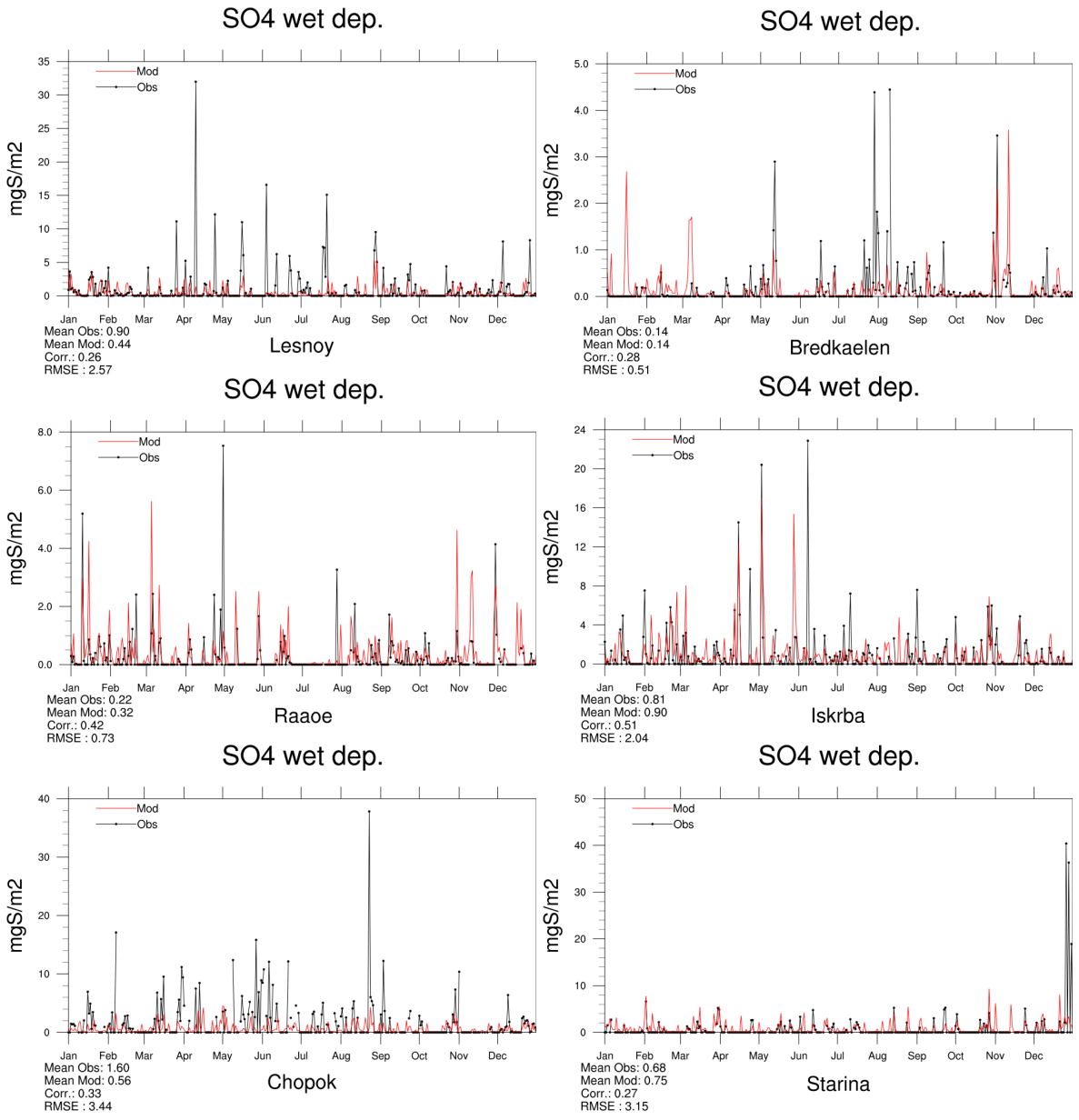

Figure 2.42: Comparison of model results and measurements (daily) for wet deposition of sulphur [mg(S)m^{-2}] in 2018.

Oxidized nitrogen in precipitation

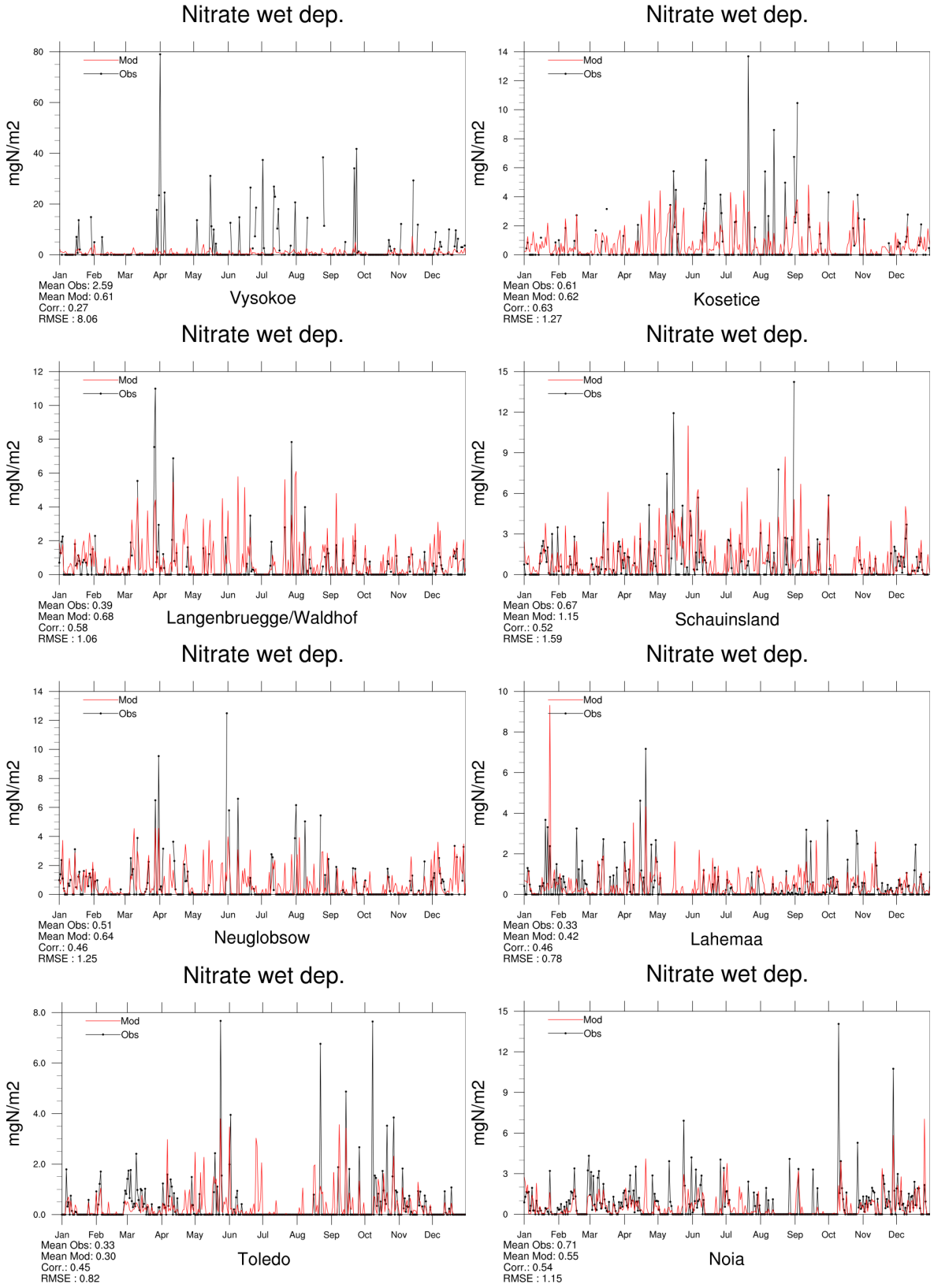

Figure 2.43: Comparison of model results and measurements (daily) for wet deposition of oxidized nitrogen [mg(N)m^{-2}] in 2018.

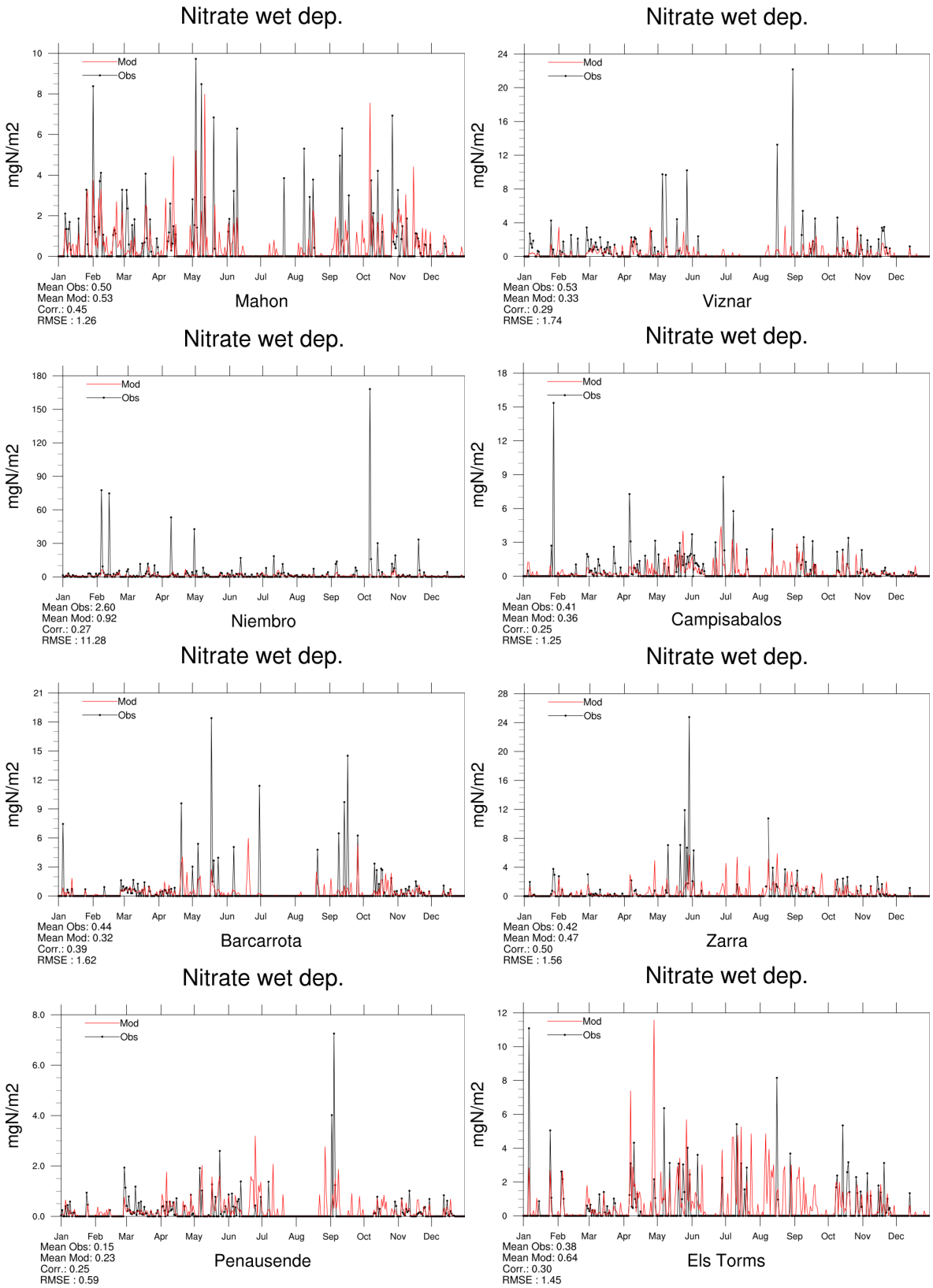

Figure 2.44: Comparison of model results and measurements (daily) for wet deposition of oxidized nitrogen [mg(N)m^{-2}] in 2018.

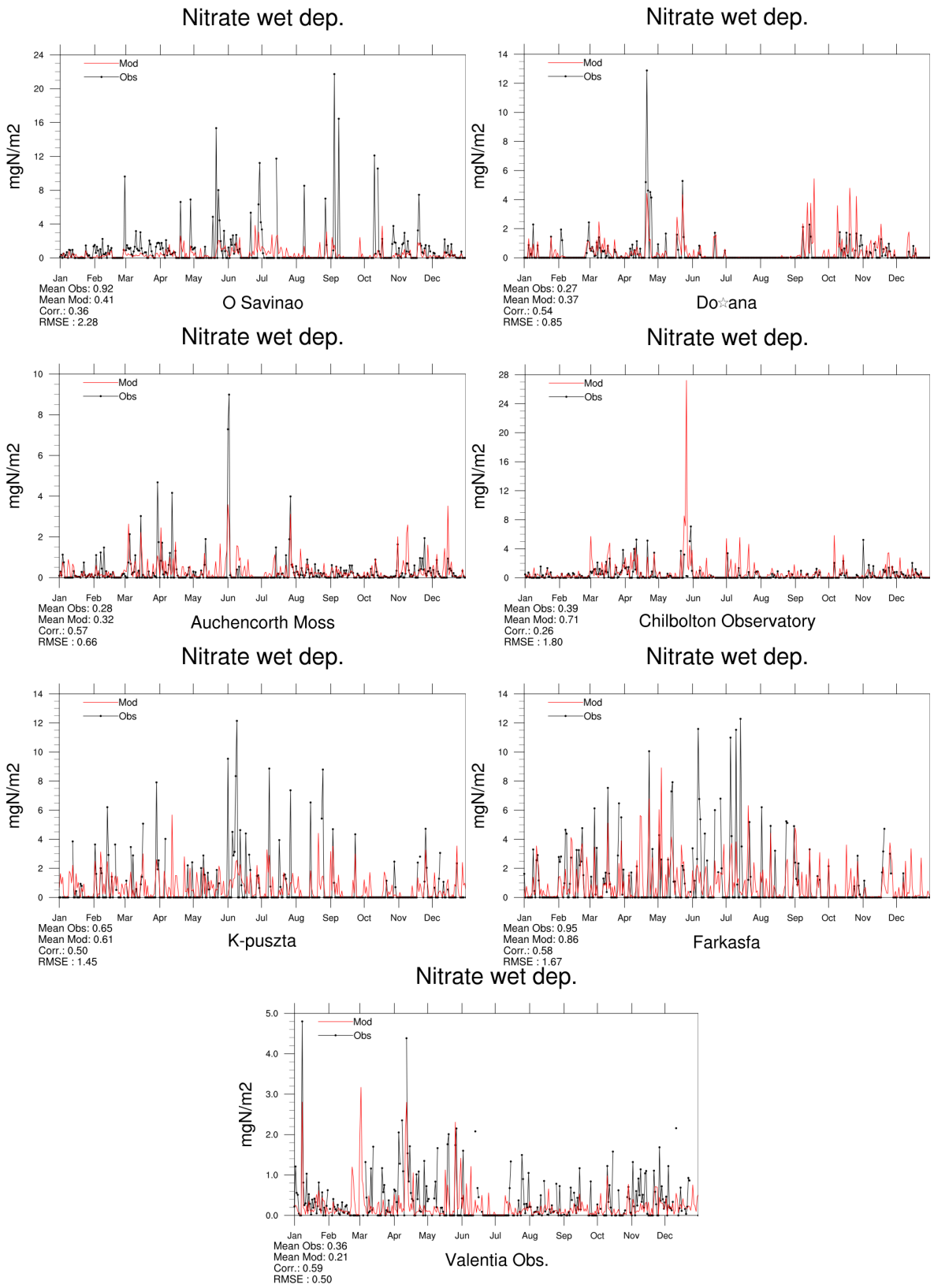

Figure 2.45: Comparison of model results and measurements (daily) for wet deposition of oxidized nitrogen [mg(N)m^{-2}] in 2018.

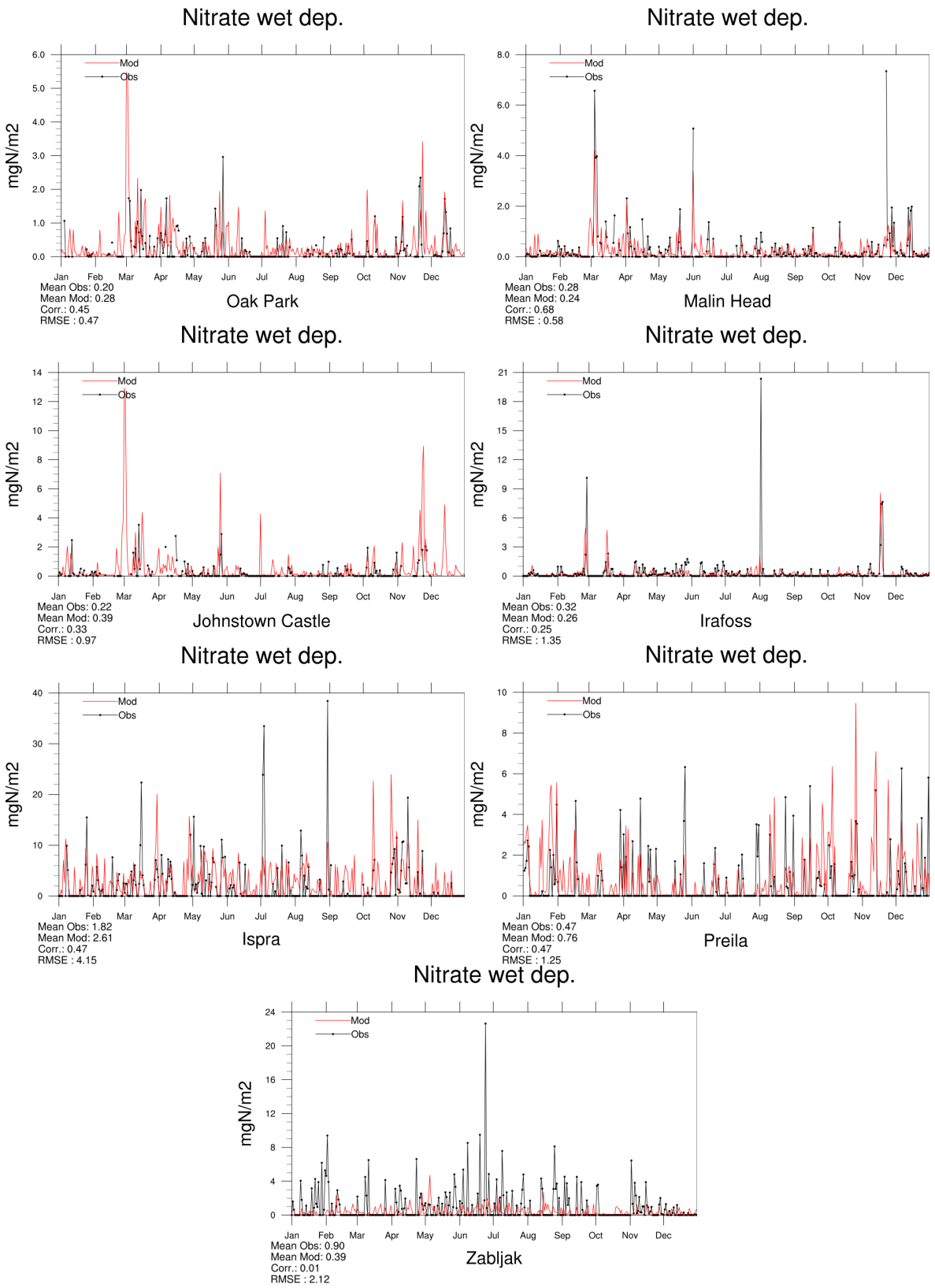

Figure 2.46: Comparison of model results and measurements (daily) for wet deposition of oxidized nitrogen [mg(N)m^{-2}] in 2018.

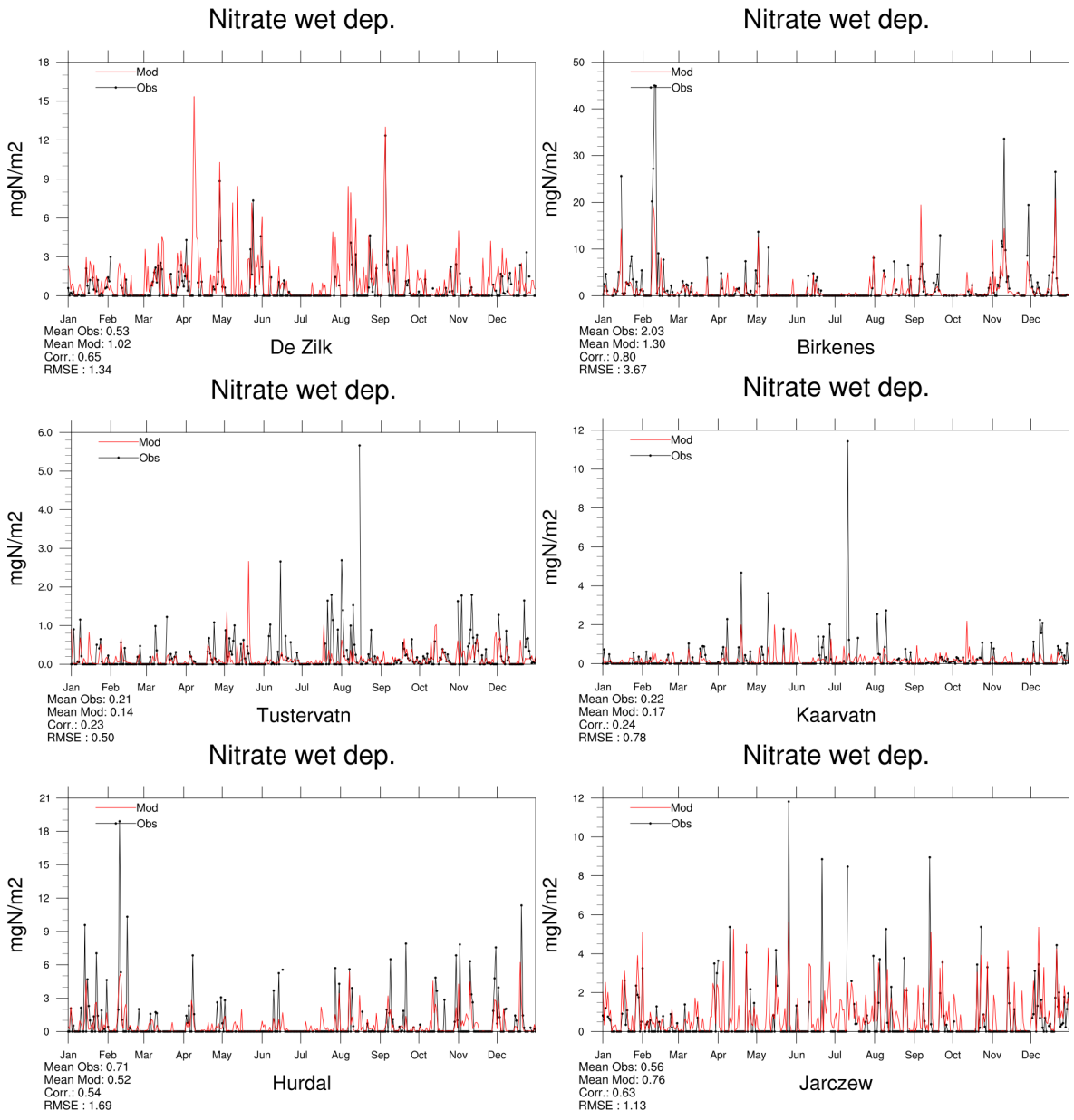

Figure 2.47: Comparison of model results and measurements (daily) for wet deposition of oxidized nitrogen [mg(N)m^{-2}] in 2018.

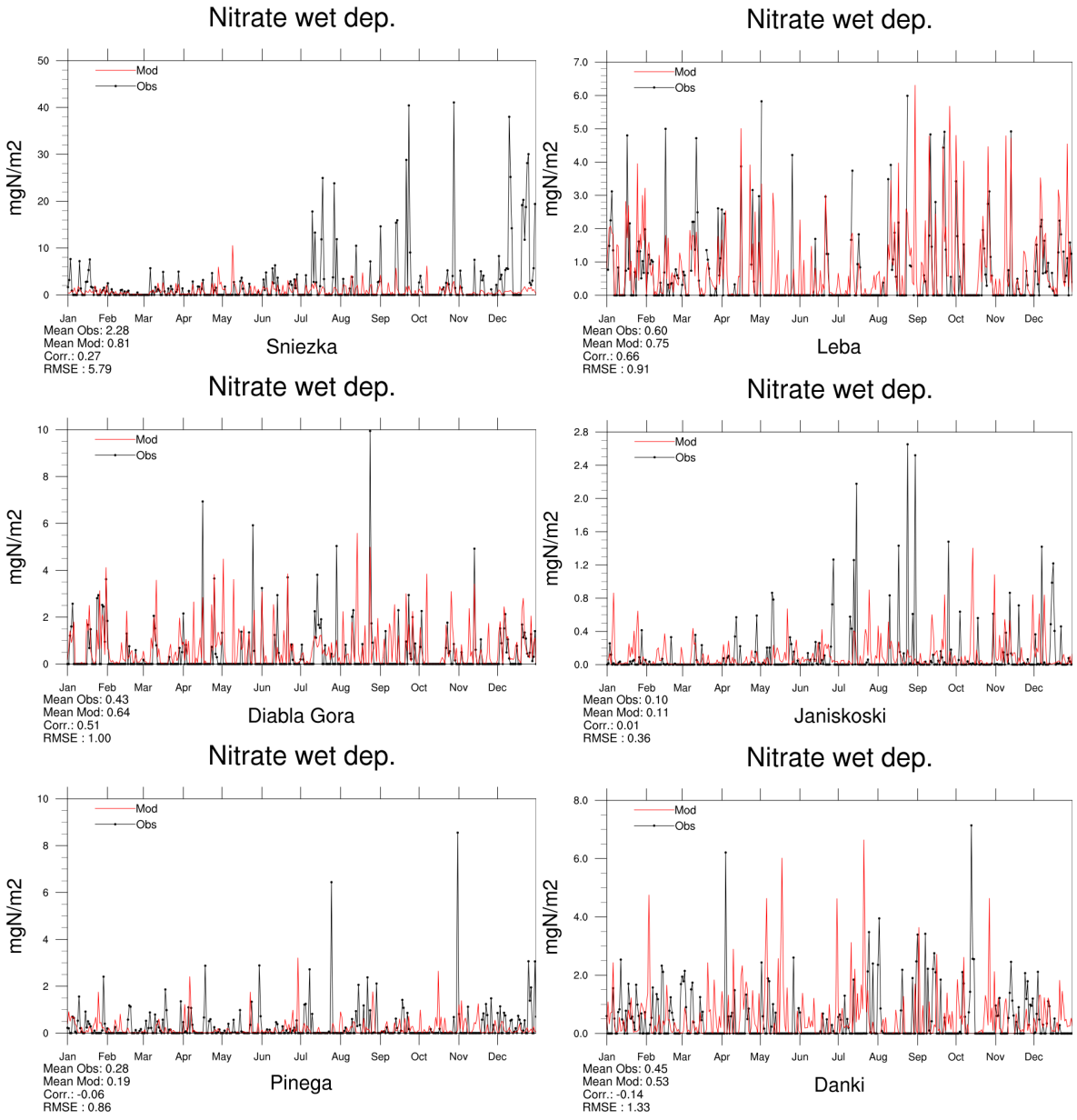

Figure 2.48: Comparison of model results and measurements (daily) for wet deposition of oxidized nitrogen [mg(N)m^{-2}] in 2018.

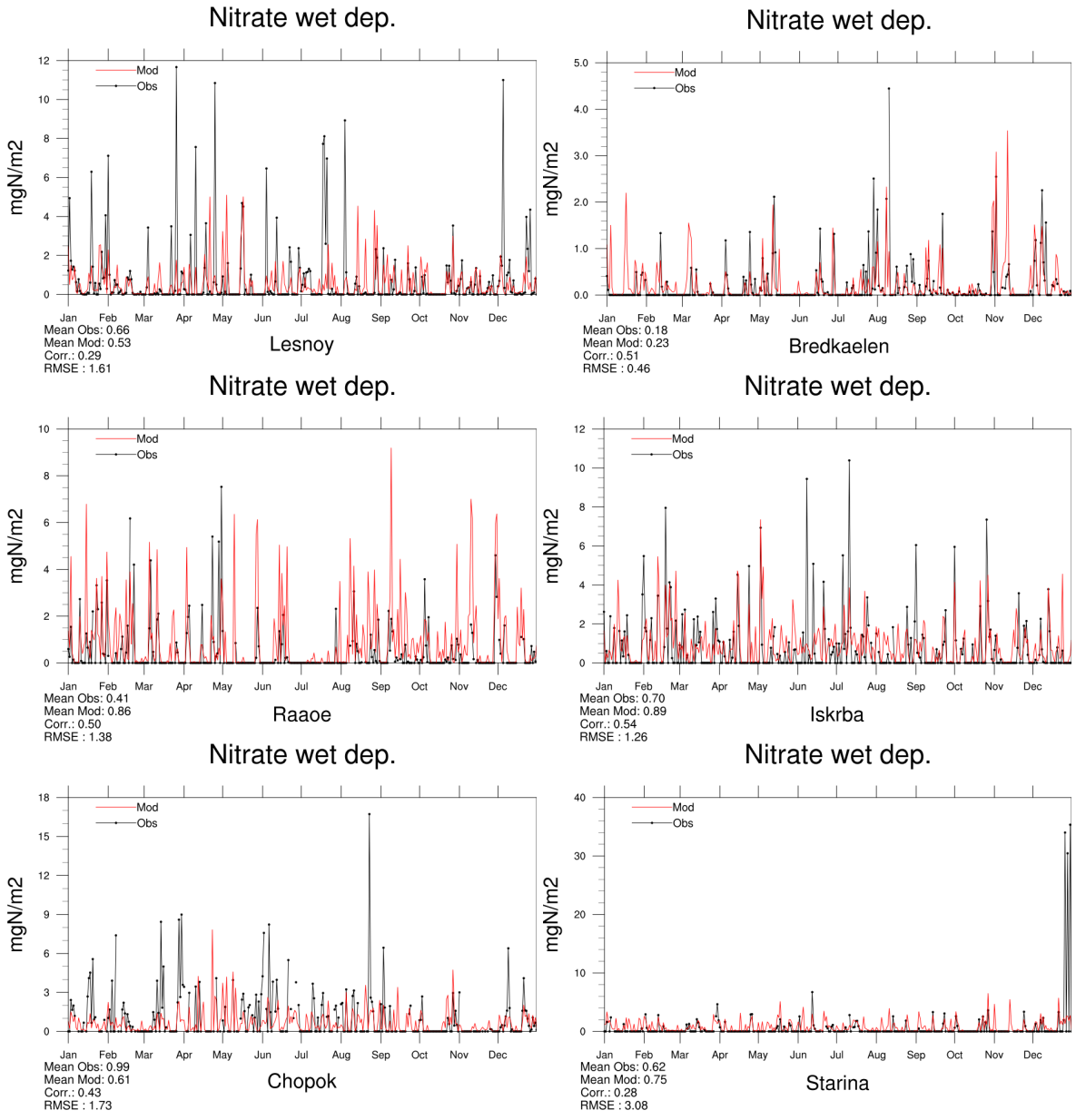

Figure 2.49: Comparison of model results and measurements (daily) for wet deposition of oxidized nitrogen [mg(N)m^{-2}] in 2018.

Reduced nitrogen in precipitation

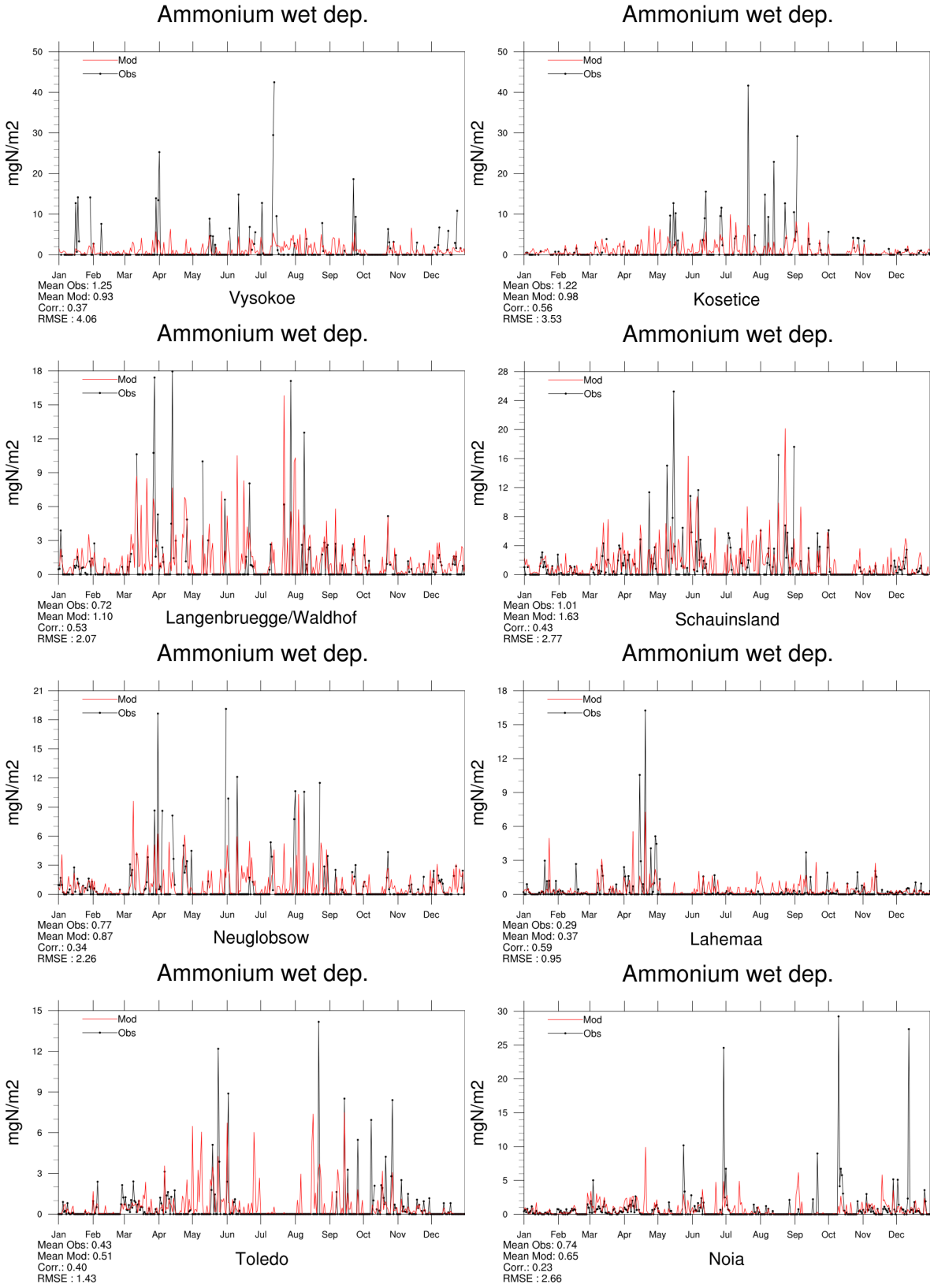

Figure 2.50: Comparison of model results and measurements (daily) for wet deposition of reduced nitrogen [mg(N)m^{-2}] in 2018.

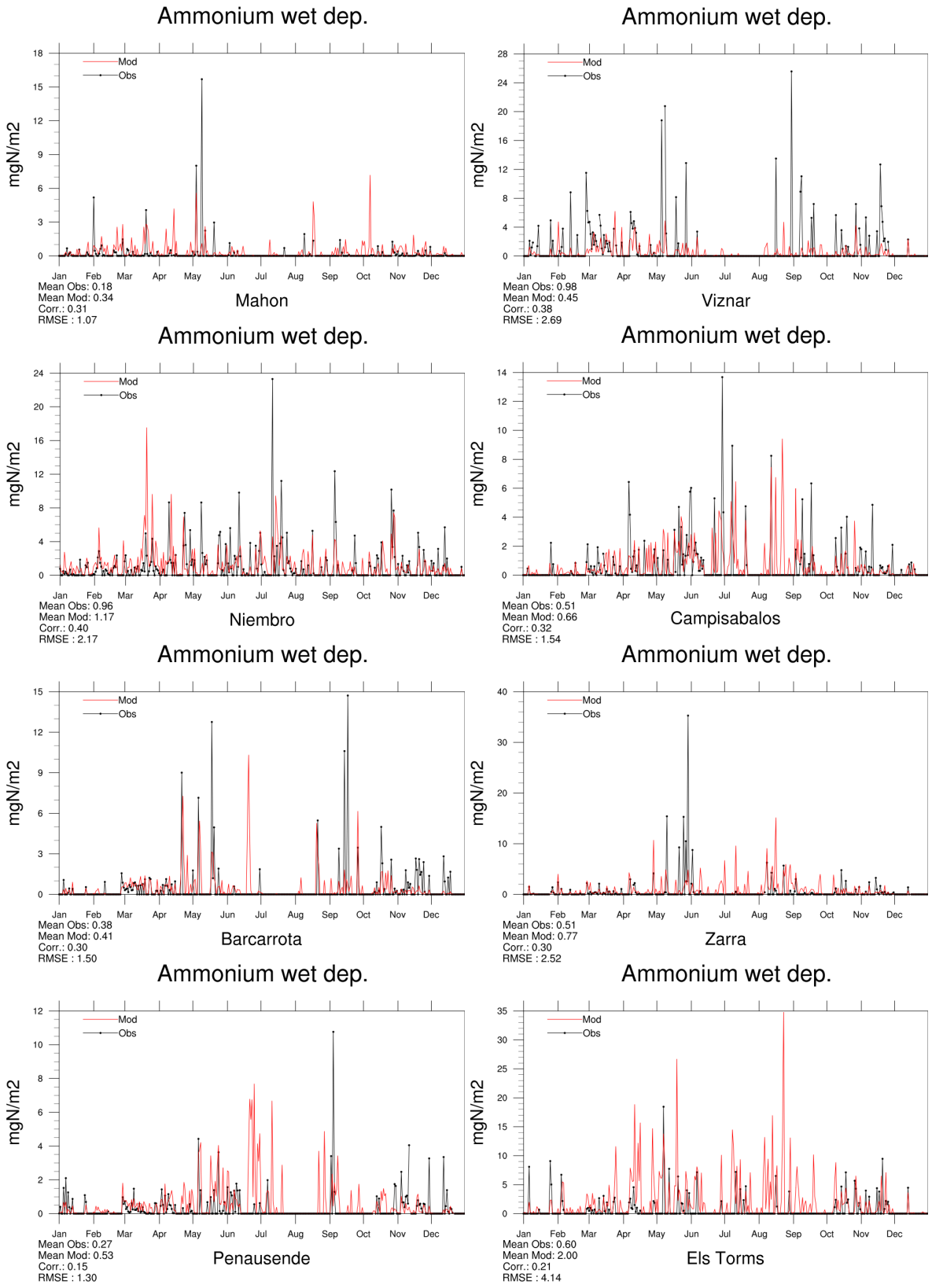

Figure 2.51: Comparison of model results and measurements (daily) for wet deposition of reduced nitrogen [mg(N)m^{-2}] in 2018.

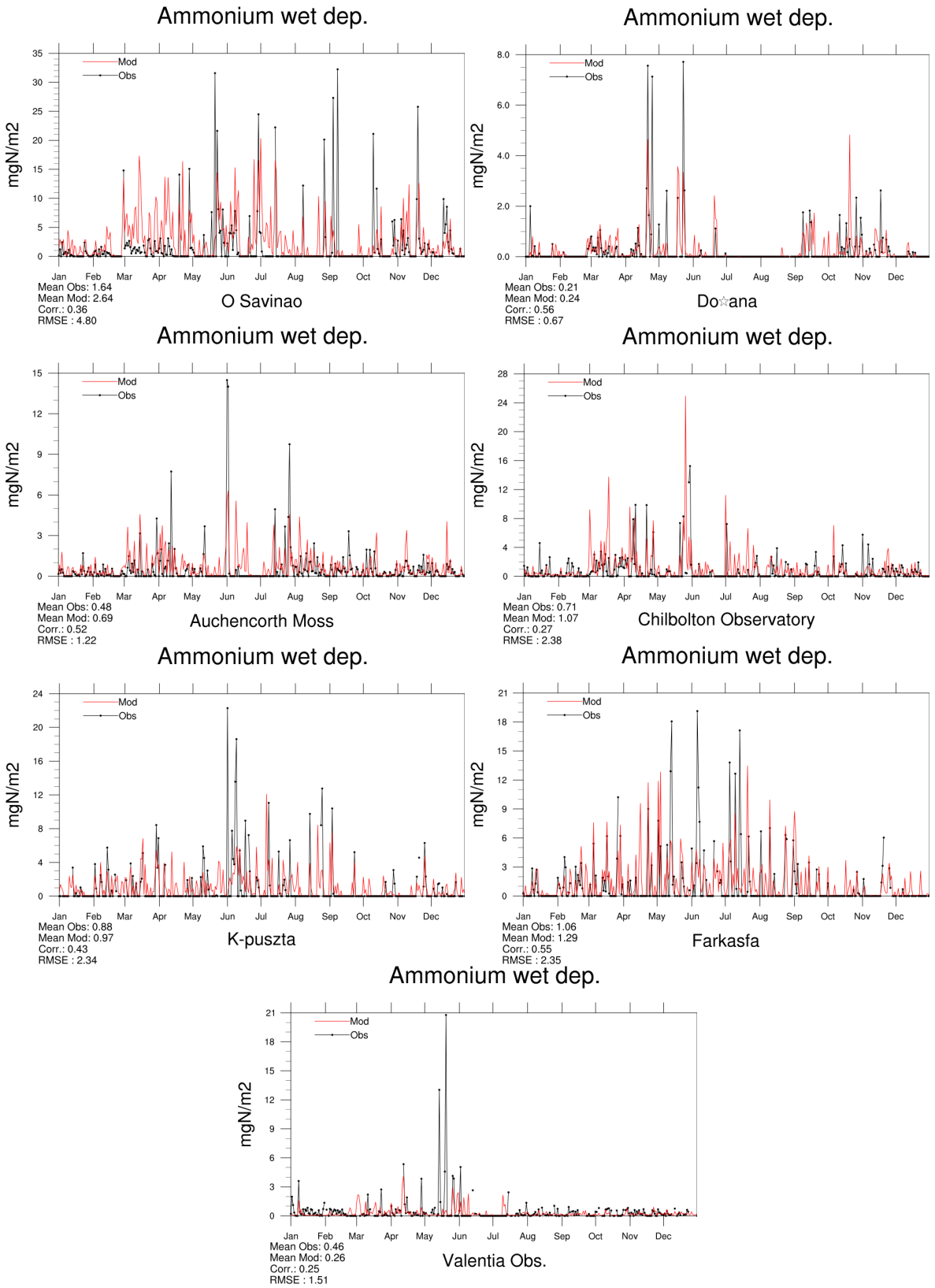

Figure 2.52: Comparison of model results and measurements (daily) for wet deposition of reduced nitrogen [mg(N)m^{-2}] in 2018.

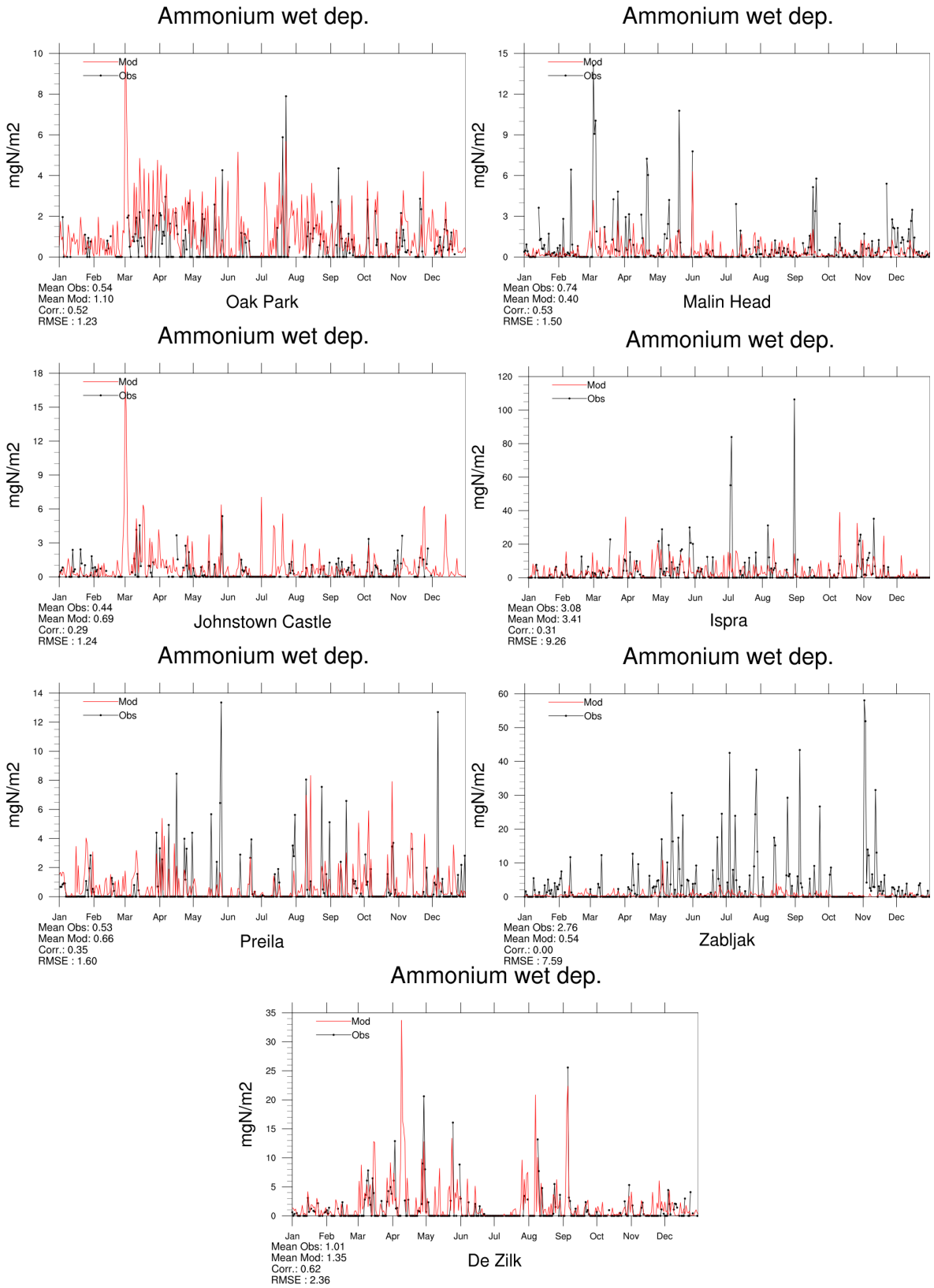

Figure 2.53: Comparison of model results and measurements (daily) for wet deposition of reduced nitrogen [mg(N)m^{-2}] in 2018.

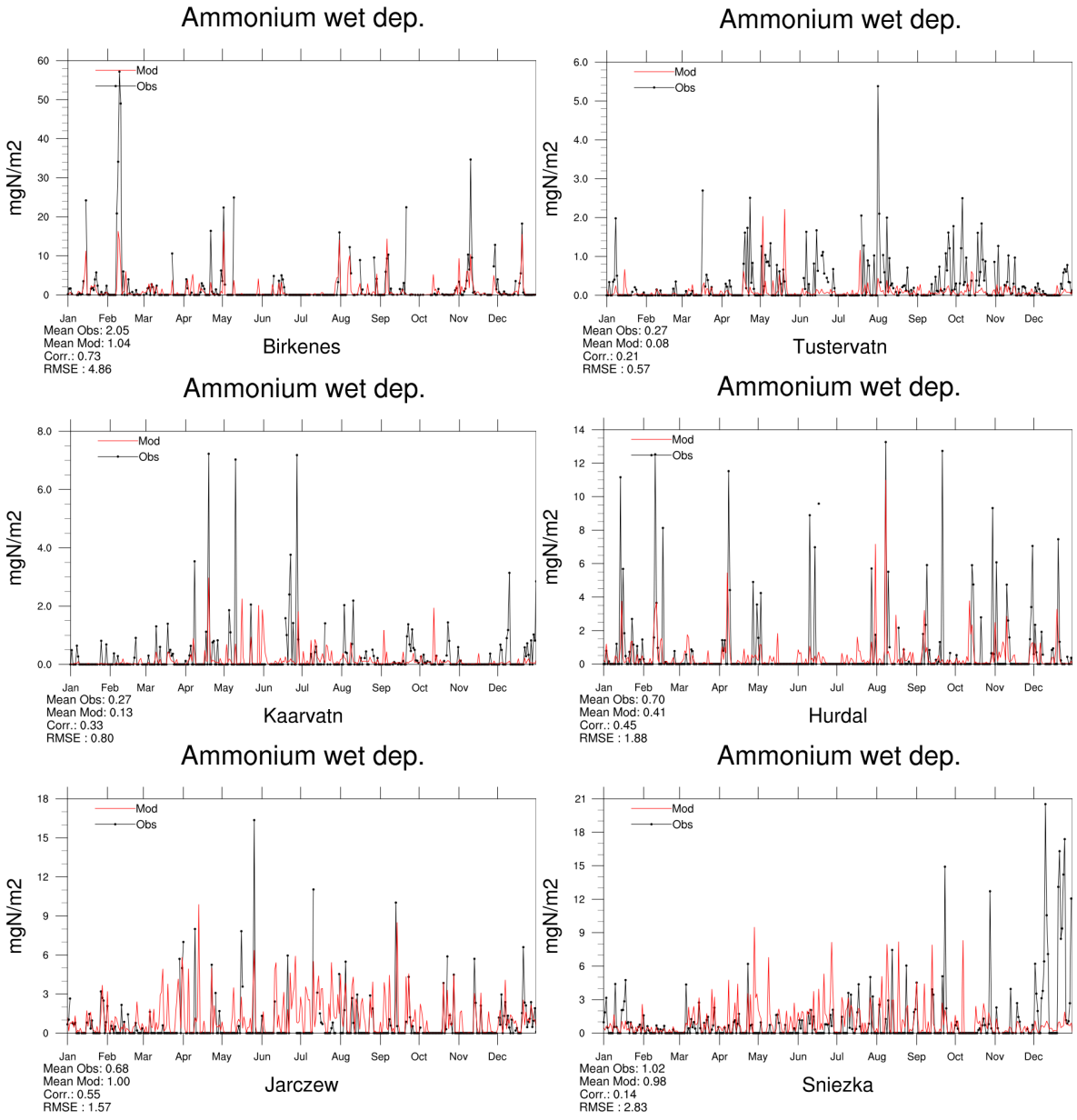

Figure 2.54: Comparison of model results and measurements (daily) for wet deposition of reduced nitrogen [mg(N)m^{-2}] in 2018.

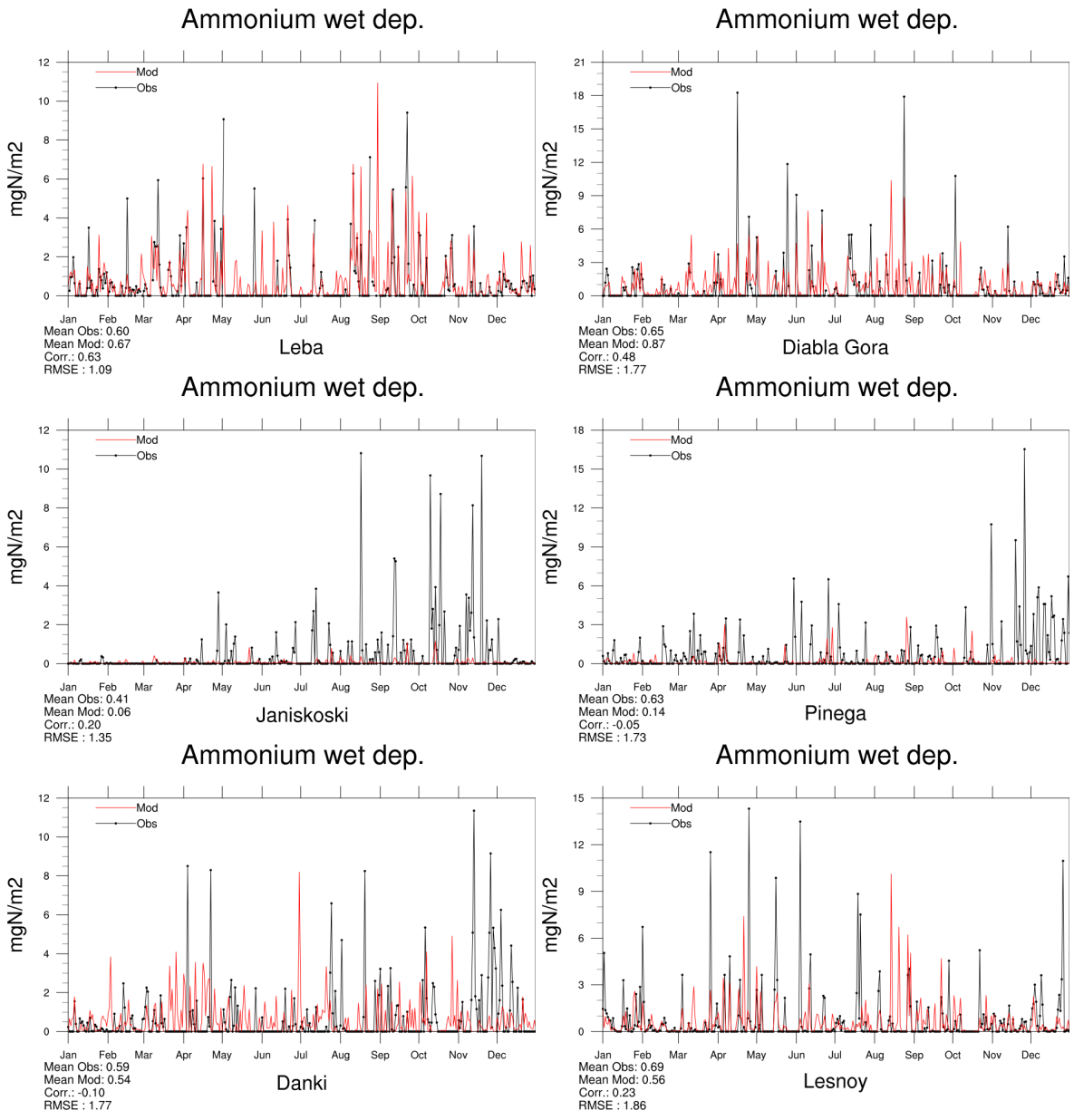

Figure 2.55: Comparison of model results and measurements (daily) for wet deposition of reduced nitrogen [mg(N)m^{-2}] in 2018.

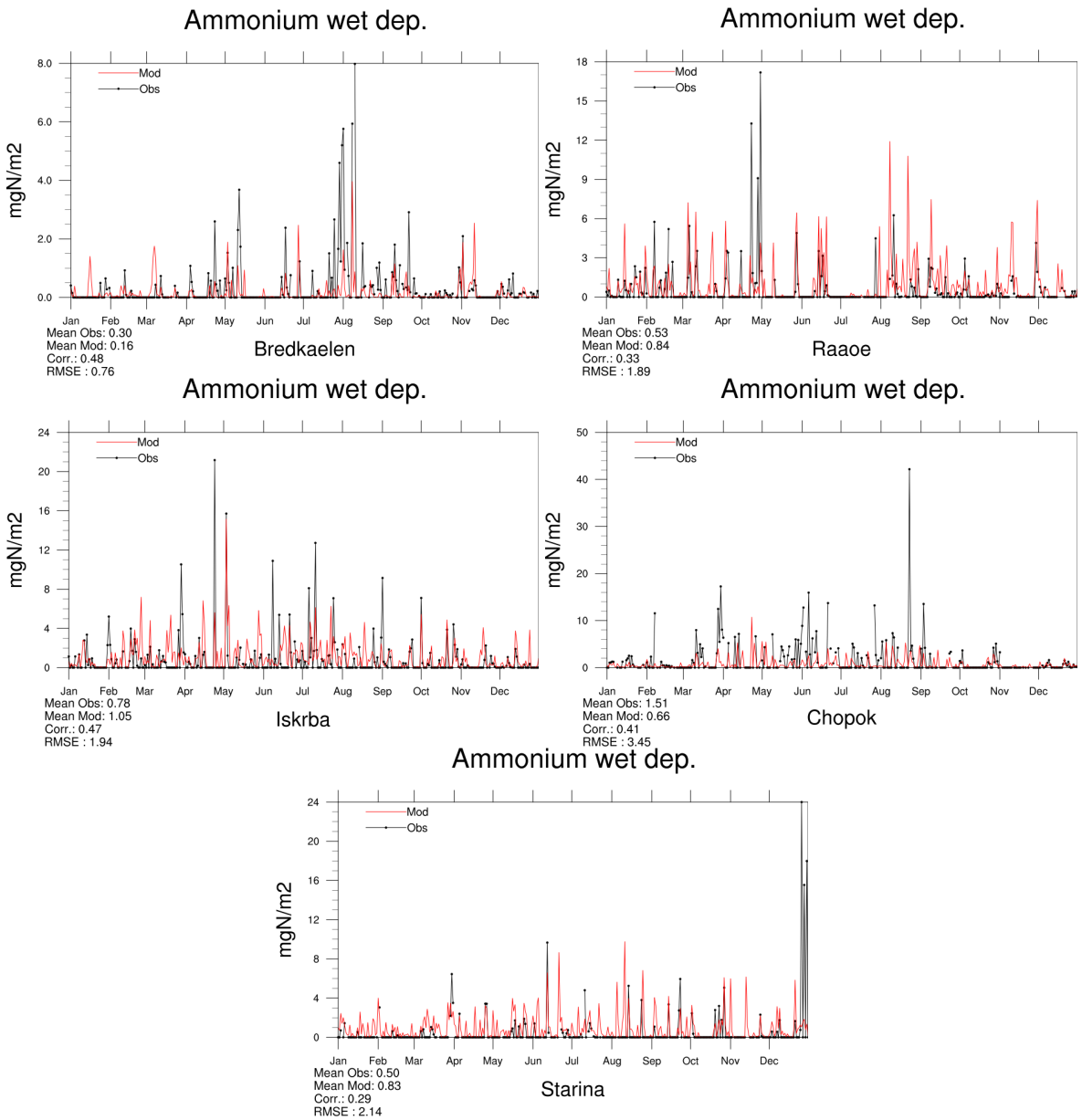

Figure 2.56: Comparison of model results and measurements (daily) for wet deposition of reduced nitrogen [mg(N)m^{-2}] in 2018.

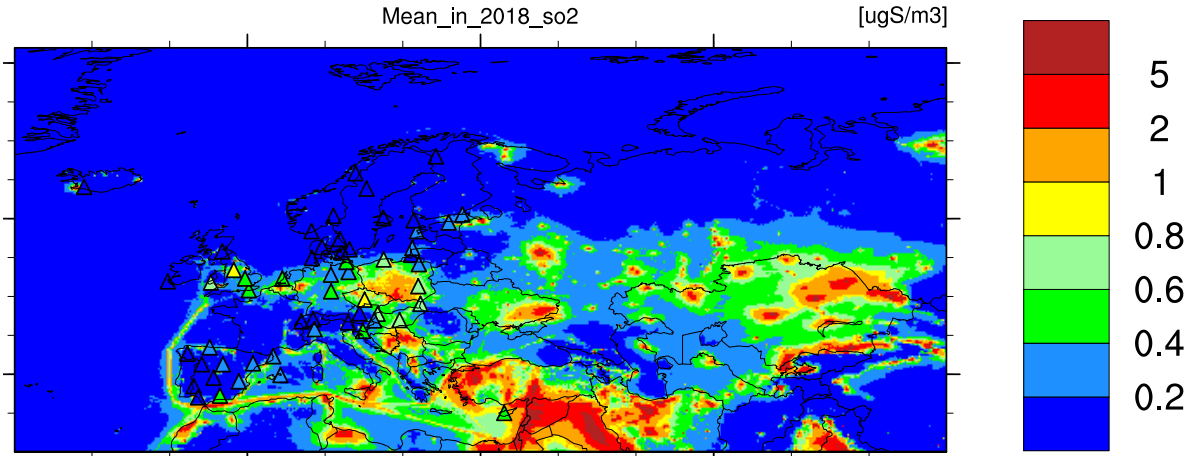

(a) SO_2

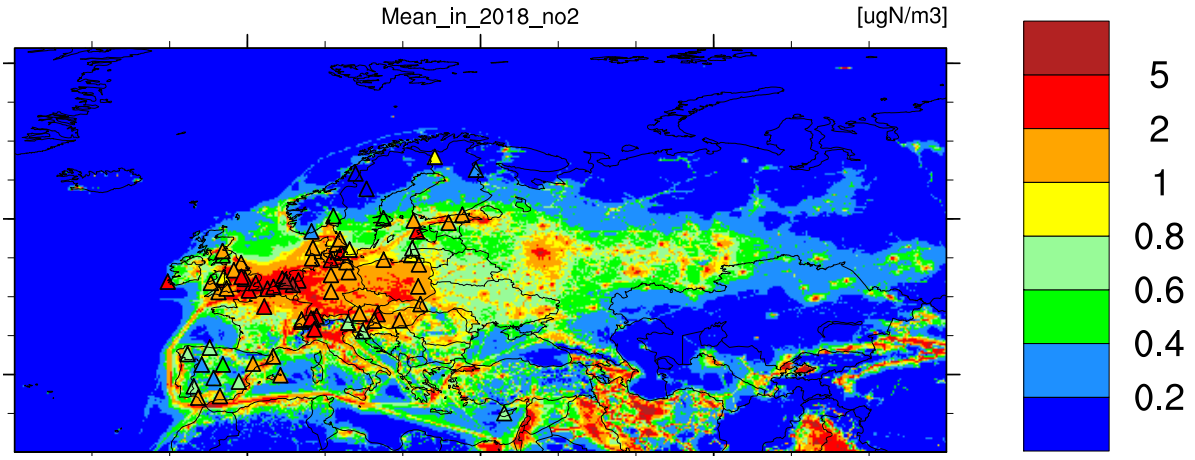

(b) NO_2

Figure 2.57: Yearly concentrations of SO_2 and NO_2 in 2018 [μg(S) m^{-3}or μg(N) m^{-3}]. The maps show model results, with observations superimposed by triangles.

2.3 Combined maps of model results and observations

In this section we present maps (Figures 2.57–2.59) showing both modelled and observed values concentrations in air and wet depositions in precipitation for a number of sulphur and nitrogen species. In general, there is good agreement between model results and observations in 2018.

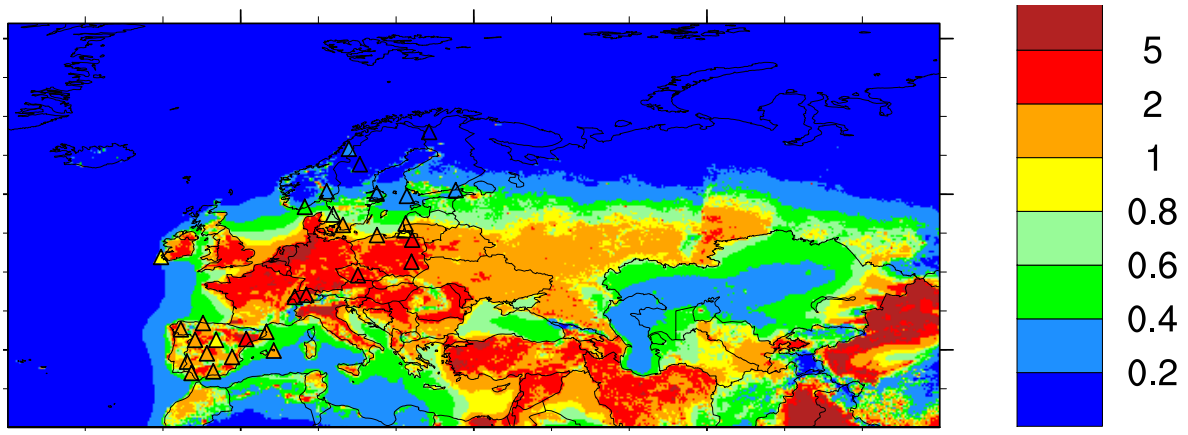

(a) NHx

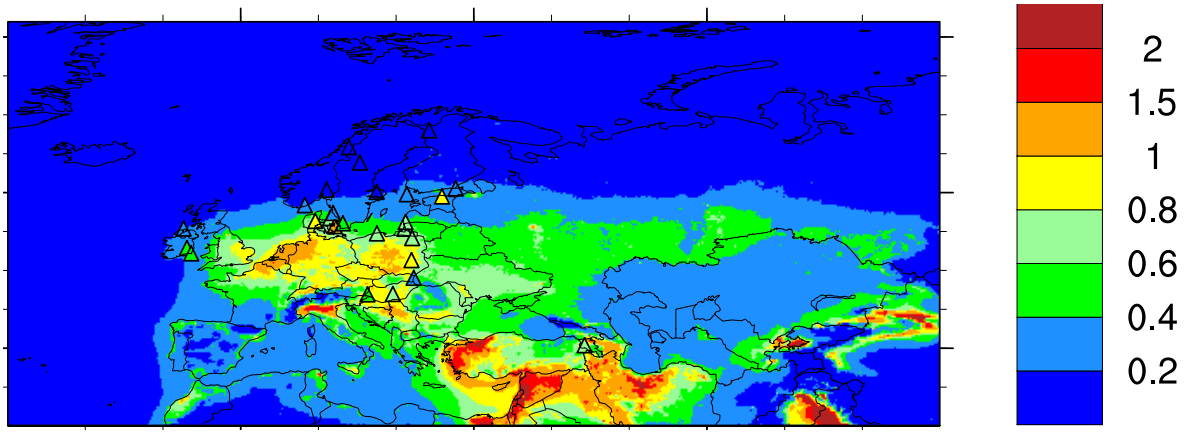

(b) NH_4^+

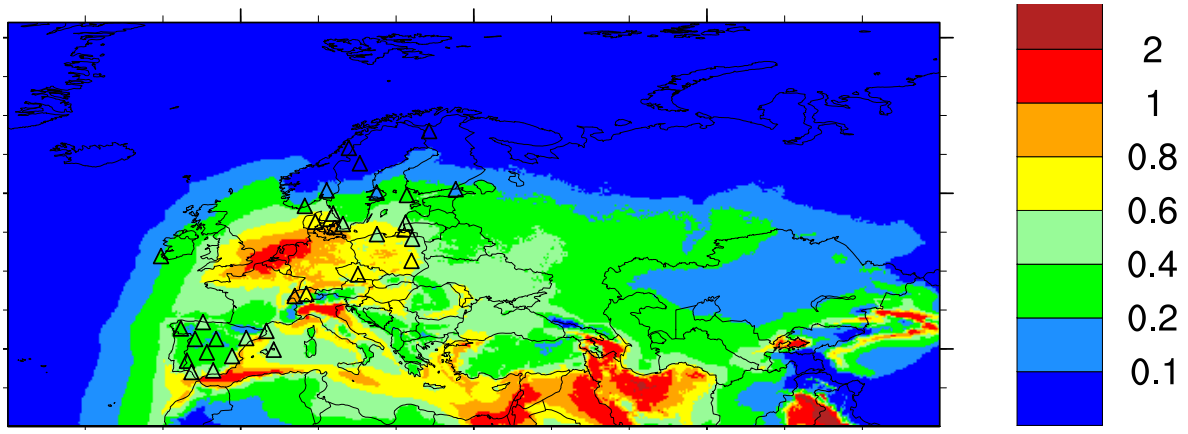

(c) tNO3

Figure 2.58: Yearly concentrations of reduced nitrogen (NHx), NH_4^+, and the sum HNO_3+NO_3^- (tNO3) in 2018 [μg(N) m^{-3}]. The maps show model results, with observations superimposed by triangles.

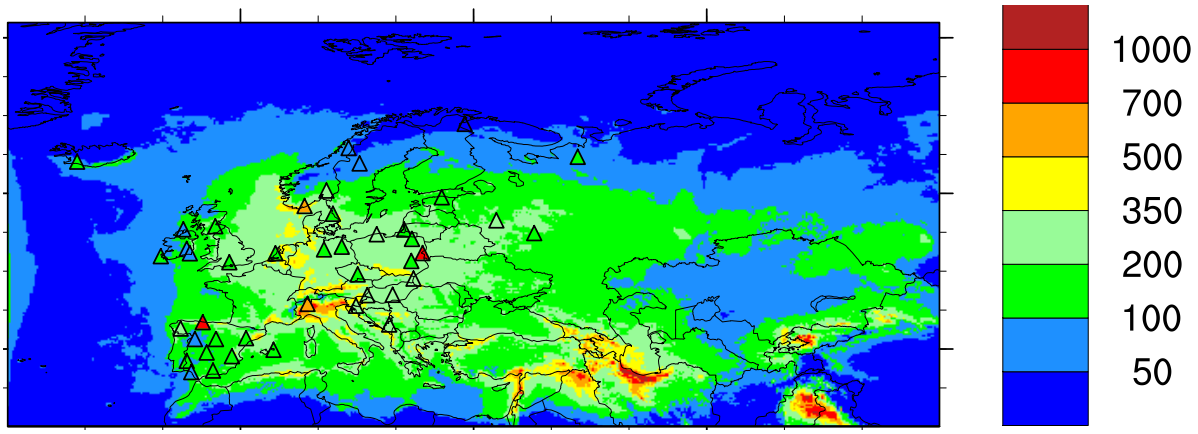

(a) WDEP OXN

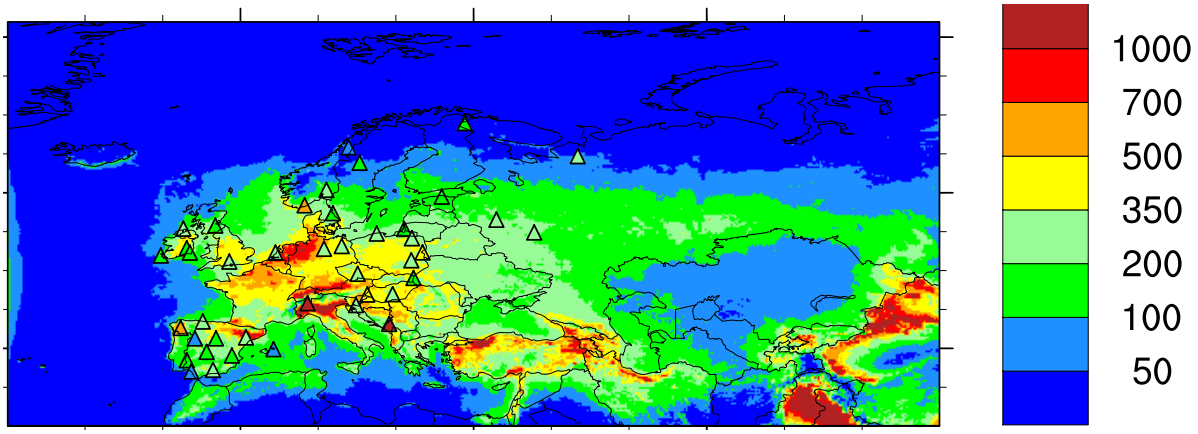

(b) WDEP RDN

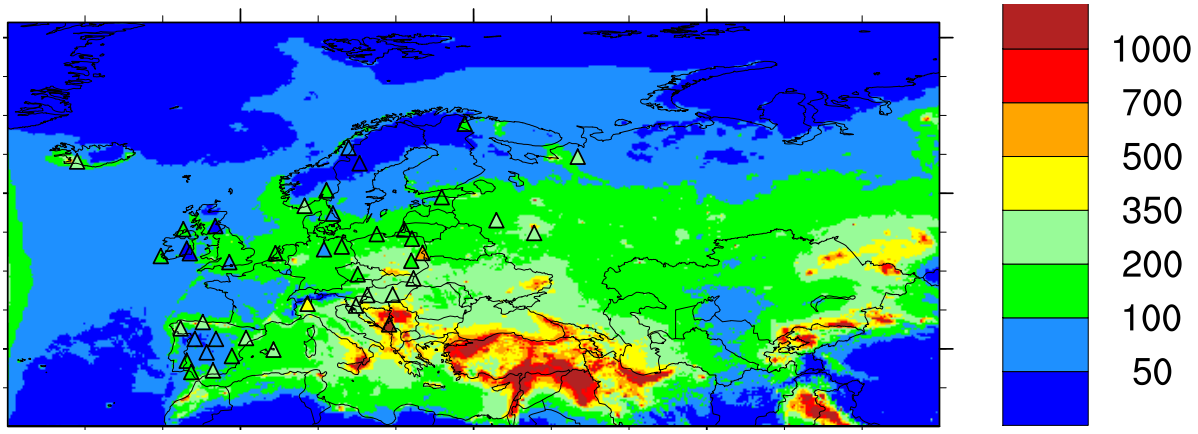

(c) WDEP SOX

Figure 2.59: Yearly wet deposition of oxidized nitrogen (OXN), reduced nitrogen (RDN), oxides of sulphur (SOX), in 2018 [mg(N)m^{-2}or mg(S)m^{-2}]. The maps show model results, with observations superimposed by triangles.

References

H. Fagerli, B. M. Steensen, and A.-G. Hjellbrekke. Acidifying and eutrophying components: validation and combined maps. Supplementary material to EMEP Status Report 1/2012, available online at www.emep.int, The Norwegian Meteorological Institute, Oslo, Norway, 2012.

M. Gauss, S. Tsyro, H. Fagerli, A.-G. Hjellbrekke, and W. Aas. Acidifying and eutrophying components. Supplementary material to EMEP Status Report 1/2019, available online at www.emep.int, The Norwegian Meteorological Institute, Oslo, Norway, 2019.

D. Simpson, A. Benedictow, H. Berge, R. Bergström, L. D. Emberson, H. Fagerli, G. D. Hayman, M. Gauss, J. E. Jonson, M. E. Jenkin, A. Nyíri, C. Richter, V. S. Semeena, S. Tsyro, J.-P. Tuovinen, Á. Valdebenito, and P. Wind. The EMEP MSC-W chemical transport model – technical description. *Atmos. Chem. Physics*, 12(16):7825–7865, 2012. doi:10.5194/acp-12-7825-2012.

D. Simpson, S. Tsyro, P. Wind, and B. M. Steensen. Emep model development. In *Transboundary acidification, eutrophication and ground level ozone in Europe in 2011. EMEP Status Report 1/2013*. The Norwegian Meteorological Institute, Oslo, Norway, 2013.

Cort J. Willmott. On the validation of models. *Physical Geography*, 2:184–194, 1981.

Cort J. Willmott. Some comments on the evaluation of model performance. *Bulletin American Meteorological Society*, 63(11):1309–1313, 1982. doi:10.1175/1520-0477(1982)063<1309:SCOTEO>2.0.CO;2.

CHAPTER 3

Ozone and NO_2

In this chapter the EMEP MSC-W model is evaluated with respect to surface ozone and NO_2 concentrations in air. In the following section we present tables of mean values and model performance indicators, and in Sections 3.2 and 3.3 time series are plotted for selected stations to illustrate the performance of the EMEP MSC-W model for the year 2018 with respect to ozone and NO_2. In Section 3.4 we present maps of ozone for 2018, created by combining measurements and model results.

3.1 Scatter plots and tables

Table 3.1 shows for daily maximum ozone, daily mean ozone and NO_2 the number of stations where measurements were available and data coverage criteria were satisfied (N_{stat}), measured yearly average over all stations (Obs), modelled yearly average over all stations (Mod), bias, spatial correlation between observation and model for station yearly averages, root mean square error, and index of agreement (IOA, as defined in Section 2.1).

Model performance for daily maximum ozone is usually better than for daily mean ozone, mainly due to the difficulty of reproducing night-time ozone correctly. This year the difference is only small, however, with the bias in daily mean ozone being +4% compared to -3% in the case of daily maximum ozone. The spatial correlation is slightly better than last year, and in the case of daily maximum ozone equals 0.82.

The scatter plots in Figure 3.1 are based on yearly averages of observed data at EMEP stations that have provided measurements for 2018. The lines on the scatter plots display deviations in the scatter of 30% ('30% line') and 50% ('50% line') relative bias, respectively. Relative bias is defined here as $\frac{Mod-Obs}{0.5\,(Mod+Obs)} \times 100\%$, where 'Mod' refers to yearly averaged modelled concentrations, while 'Obs' refers to yearly averaged measured concentrations.

Modelled daily maximum ozone values have been evaluated against measurements from all stations that supply data to EMEP CCC. Table 3.2 summarises these comparisons, and Fig-

Component	N_{stat}	Obs.	Mod.	Bias (%)	RMSE	Corr.	IOA
Ozone daily max (ppb)	117	42.60	41.46	-3	3.03	0.82	0.84
Ozone daily mean (ppb)	117	33.00	34.36	4	4.14	0.72	0.76
NO_2 (μg(N) m^{-3})	73	1.71	1.49	-13	0.68	0.87	0.92

Table 3.1: Comparison of model results and observations for 2018. Annual averages over all EMEP sites with measurements. N_{stat}= number of stations, wd=wet deposition, cp= concentration in precipitation, Corr. = spatial correlation coefficient, RMSE = root mean square error, IOA = index of agreement.

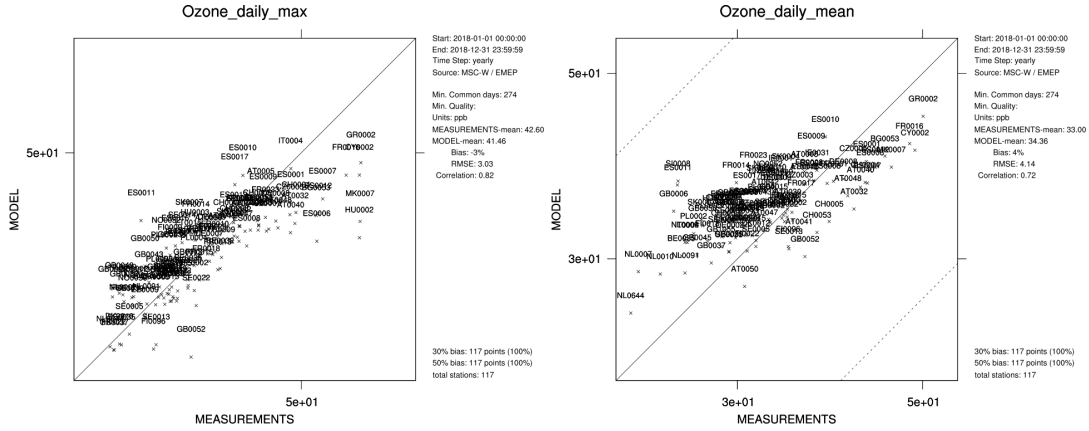

(a) Ozone max (b) Ozone mean

Figure 3.1: Scatter plots of model results versus observations of a) Daily maximum ozone [ppb], b) daily mean ozone [ppb].

ures 3.2 to 3.21 show time series plots for selected stations representing the different regions of Europe. To judge model performance, Table 3.2 shows the temporal correlations (daily measurements against daily model output at each station over the year), root mean square error (RMSE) and the *index of agreement* (IOA, defined in Section 2.1).

Similarly to last year (Gauss et al. 2019), the model performance is good for daily maximum ozone. At most of the stations, the index of agreement is between 0.7 and 0.9.

Some more detail is given in the next sections where different regions of the EMEP domain are addressed separately, along with time series plots of model results and observations.

As a supplement this year, an animation (mp4 format, 91 Mbyte) has been created showing horizontal distributions of ozone daily maximum values in a sequence for the entire year of 2018, with superimposed circles representing measurement data:
https://emep.int/publ/reports/2020/O3daymax_2018.mp4

Table 3.2: Comparison of modelled versus observed ozone for year 2018. Concentrations are given as means of daily maximum ozone values [ppb]. Correlation coefficients (r), root mean square error (RMSE), and index of agreement (IOA) are included to judge the agreement between model and observations.

Code	Station	Obs. [ppb]	Mod. [ppb]	r	RMSE	IOA
		Nordic countries				
DK0005	Keldsnor	38.82	38.42	0.73	8.21	0.83
DK0010	Nord, Greenland	36.45	35.88	0.74	4.85	0.85
DK0012	Risoe	40.05	38.85	0.87	6.17	0.92
DK0031	Ulborg	37.25	38.89	0.83	6.43	0.88
FI0009	Utoe	39.80	41.87	0.82	5.59	0.89
FI0018	Virolahti III	36.69	37.69	0.84	5.55	0.90
FI0022	Oulanka	36.09	35.53	0.81	5.60	0.88
FI0096	Pallas	38.67	35.57	0.74	6.38	0.82
NO0002	Birkenes II	40.26	38.66	0.82	6.04	0.88
NO0015	Tustervatn	39.44	38.44	0.75	5.57	0.86
NO0039	Kaarvatn	38.23	41.88	0.70	7.89	0.78
NO0042	Spitzbergen, Zeppelin	38.72	39.47	0.78	4.06	0.87
NO0043	Prestebakke	37.70	38.53	0.84	5.71	0.90
NO0052	Sandve	39.55	42.39	0.78	6.31	0.84
NO0056	Hurdal	37.30	38.35	0.86	5.74	0.91
SE0005	Bredkaelen	37.08	36.50	0.76	6.21	0.86
SE0013	Esrange	38.85	35.84	0.74	6.67	0.82
SE0014	Raaoe	40.65	42.78	0.80	6.89	0.88
SE0018	Asa	39.60	39.17	0.85	5.65	0.91
SE0019	Oestad	40.00	38.96	0.86	5.86	0.91
SE0020	Hallahus	41.05	39.54	0.87	6.30	0.90
SE0022	Norunda Stenen	41.65	38.36	0.63	9.70	0.75
SE0032	Norra-Kvill	40.31	38.84	0.87	5.56	0.91
SE0035	Vindeln	36.58	35.83	0.77	6.28	0.86
SE0039	Grimsoe	37.11	37.66	0.88	5.52	0.92
		Eastern European Countries				
BG0053	Rojen peak	51.32	44.86	0.69	9.06	0.70
CZ0001	Svratouch	47.07	43.66	0.86	8.53	0.88
CZ0003	Kosetice	46.39	43.73	0.84	8.95	0.87
CZ0005	Churanov	49.03	44.91	0.82	7.95	0.86
EE0009	Lahemaa	38.11	37.58	0.82	6.10	0.88
EE0011	Vilsandy	40.64	41.44	0.78	6.68	0.86
HU0002	K-puszta	55.33	43.15	0.80	17.04	0.74
HU0003	Farkasfa	41.58	42.98	0.87	6.95	0.91
LT0015	Preila	41.10	42.21	0.85	6.49	0.90
LV0010	Rucava	39.75	39.43	0.79	8.15	0.83
LV0016	Zoseni	38.24	38.47	0.83	4.98	0.91
MK0007	Lazaropole	55.39	44.39	0.48	13.45	0.53
PL0002	Jarczew	39.42	41.32	0.85	7.72	0.90
PL0003	Sniezka	47.91	43.25	0.74	8.92	0.81

continued on next page

Code	Station	Obs.	Mod.	r	RMSE	IOA
PL0004	Leba	41.51	41.12	0.83	6.63	0.89
PL0005	Diabla Gora	39.08	39.62	0.85	7.01	0.90
SK0002	Chopok	53.99	43.82	0.77	12.44	0.71
SK0004	Stara Lesna	47.26	43.80	0.81	8.96	0.82
SK0006	Starina	44.20	43.03	0.76	7.48	0.84
SK0007	Topolniky	41.16	43.73	0.83	8.78	0.88
	Central and NW European Countries					
AT0002	Illmitz	40.51	41.99	0.90	7.35	0.93
AT0005	Vorhegg	46.59	46.15	0.70	8.26	0.79
AT0030	Pillersdorf	45.77	43.72	0.85	9.28	0.88
AT0032	Sulzberg	49.45	44.23	0.81	9.36	0.85
AT0034	Sonnblick	58.07	51.45	0.74	9.10	0.75
AT0038	Gerlitzen	51.39	41.27	0.83	12.64	0.76
AT0040	Masenberg	49.08	43.53	0.83	8.87	0.84
AT0041	Haunsberg	44.37	42.86	0.84	8.04	0.90
AT0042	Heidenreichstein	44.75	43.20	0.87	8.15	0.89
AT0043	Forsthof	44.91	44.06	0.86	7.95	0.90
AT0045	Dunkelsteinerwald	43.55	42.72	0.88	8.53	0.90
AT0046	Gaenserndorf	45.35	43.64	0.86	9.35	0.89
AT0047	Stixneusiedl	44.87	42.89	0.87	8.89	0.90
AT0048	Zoebelboden	48.02	43.90	0.77	9.33	0.82
AT0049	Grebenzen	51.35	43.92	0.74	10.12	0.74
AT0050	Graz Lustbuehel	42.55	42.57	0.87	7.44	0.93
BE0001	Offagne	41.94	41.78	0.86	8.04	0.90
BE0032	Eupen	43.43	40.91	0.85	10.03	0.86
BE0035	Vezin	41.08	39.72	0.85	9.67	0.88
CH0002	Payerne	43.99	43.72	0.85	9.95	0.87
CH0003	Taenikon	44.49	43.27	0.87	9.57	0.90
CH0004	Chaumont	49.54	45.08	0.80	9.09	0.84
CH0005	Rigi	46.32	44.46	0.79	8.82	0.88
CH0053	Beromuenster	46.43	44.12	0.85	9.35	0.90
DE0001	Westerland/Wenningsted	41.10	41.60	0.83	6.92	0.89
DE0002	Langenbruegge/Waldhof	41.52	39.37	0.90	7.89	0.92
DE0003	Schauinsland	53.17	43.18	0.76	13.50	0.75
DE0007	Neuglobsow	42.63	41.43	0.88	7.80	0.91
DE0008	Schmuecke	47.84	44.42	0.86	8.56	0.90
DE0009	Zingst	42.80	42.63	0.84	7.28	0.89
FR0008	Donon	44.94	44.00	0.86	7.89	0.89
FR0009	Revin	43.52	41.70	0.83	8.70	0.88
FR0010	Morvan	43.05	42.12	0.77	6.22	0.86
FR0013	Peyrusse Vieille	43.25	40.82	0.69	7.88	0.80
FR0014	Montandon	41.65	43.59	0.73	10.74	0.77
FR0015	La Tardiere	41.89	40.11	0.70	8.21	0.82
FR0016	Le Casset	54.07	48.10	0.64	9.44	0.70
FR0017	Montfranc	41.78	41.73	0.81	5.38	0.89
FR0018	La Coulonche	42.40	40.35	0.73	7.99	0.80
FR0019	Pic du Midi	52.03	45.94	0.26	10.67	0.51

continued on next page

Code	Station	Obs.	Mod.	r	RMSE	IOA
FR0020	SIRTA Atm.Res.Obs	35.17	33.61	0.85	9.57	0.90
FR0023	Saint-Nazaire-le-Déser	46.99	44.70	0.78	9.61	0.79
FR0025	Verneuil	42.88	41.91	0.83	7.28	0.88
FR0030	Puy de Dôme	51.51	43.84	0.74	10.23	0.71
GB0002	Eskdalemuir	37.36	38.96	0.79	5.48	0.86
GB0006	Lough Navar	36.01	38.94	0.80	6.74	0.83
GB0013	Yarner Wood	41.05	40.11	0.71	7.46	0.80
GB0014	High Muffles	39.72	39.13	0.81	5.87	0.88
GB0015	Strath Vaich Dam	39.01	38.92	0.80	4.51	0.89
GB0031	Aston Hill	39.37	38.88	0.70	7.04	0.81
GB0033	Bush	36.75	38.62	0.79	5.74	0.86
GB0037	Ladybower	36.11	35.50	0.69	6.66	0.79
GB0038	Lullington Heath	39.94	41.36	0.63	8.54	0.75
GB0039	Sibton	39.81	38.65	0.69	8.57	0.79
GB0043	Narberth	38.37	39.94	0.73	6.67	0.82
GB0045	Wicken Fen	39.22	39.09	0.78	8.09	0.85
GB0048	Auchencorth Moss	36.44	39.19	0.81	5.38	0.86
GB0049	Weybourne	39.92	39.61	0.74	7.03	0.84
GB0050	St. Osyth	38.11	41.07	0.65	9.15	0.77
GB0052	Lerwick	41.28	35.08	0.78	7.94	0.73
GB1055	Chilbolton Observatory	40.34	39.35	0.70	8.94	0.80
IE0001	Valentia Obs.	40.31	41.58	0.71	6.20	0.81
IE0031	Mace Head	42.50	41.96	0.77	5.27	0.86
NL0007	Eibergen	36.68	37.74	0.86	9.12	0.88
NL0009	Kollumerwaard	36.67	39.08	0.85	7.13	0.89
NL0010	Vreedepeel	39.91	38.66	0.89	9.42	0.90
NL0091	De Zilk	38.16	37.79	0.80	8.88	0.86
NL0644	Cabauw Wielsekade	35.86	35.71	0.85	7.86	0.90
	Mediterranean Countries and Portugal					
CY0002	Ayia Marina	55.33	48.11	0.71	9.69	0.72
ES0001	Toledo	49.08	45.89	0.75	7.02	0.80
ES0005	Noia	39.83	43.35	0.71	6.88	0.79
ES0006	Mahon	51.38	42.89	0.61	11.54	0.62
ES0007	Viznar	51.90	46.16	0.68	9.97	0.71
ES0008	Niembro	45.48	42.54	0.70	6.45	0.79
ES0009	Campisabalos	46.80	45.71	0.75	7.76	0.77
ES0010	Cabo de Creus	45.17	48.08	0.76	7.17	0.83
ES0011	Barcarrota	37.84	44.46	0.65	9.72	0.67
ES0012	Zarra	51.50	45.01	0.79	9.46	0.74
ES0013	Penausende	44.46	44.30	0.78	6.20	0.82
ES0014	Els Torms	46.43	44.06	0.84	6.62	0.87
ES0016	O Savinao	40.17	42.55	0.81	5.76	0.86
ES0017	Doñana	44.55	47.32	0.81	5.85	0.87
GR0001	Aliartos	72.74	45.52	0.74	31.08	0.52
GR0002	Finokalia	55.46	49.16	0.72	9.06	0.71
IT0004	Ispra	49.10	48.65	0.88	10.55	0.93
IT0009	Mt Cimone	56.90	46.98	0.61	13.29	0.63

continued on next page

Code	Station	Obs.	Mod.	r	RMSE	IOA
IT0018	Lampedusa	51.80	47.08	0.43	8.35	0.61
IT0019	Monte Martano	47.71	45.58	0.66	8.17	0.78
SI0008	Iskrba	44.88	44.03	0.58	10.40	0.70
SI0031	Zarodnje	47.46	43.62	0.85	8.02	0.88
SI0032	Krvavec	52.95	44.23	0.77	10.99	0.74

3.2 Time series for ozone

In this section we present time series plots for a selection of stations that have supplied data on ozone levels to EMEP CCC for 2018. The plots show daily model results and measurements of ozone, where available.

Nordic sites

In addition to the statistics for the Nordic sites listed in Table 3.2, measured and modelled ozone levels are compared for Nordic sites in Figures 3.2–3.5. As seen in the plots the model performs well for ozone, both in terms of levels and seasonality.

At the majority of Nordic sites the IOA is between 0.8 and 0.9. Among the 24 sites, for which data were analyzed both in Gauss et al. (2019) and this year, the model performance as measured by IOA has improved at 22 sites and remained unchanged at 2 sites. While the biases usually tend to be positive, in 2018 there is no clear tendency. The relatively high IOA and the low biases may be related to the exceptionally dry and hot summer of 2018 in Northern Europe.

Eastern European sites

Measured and modelled maximum ozone levels for sites in the Eastern European region are shown in Figures 3.6 to 3.8. These sites are mostly typical continental sites with a clear summer maximum, reflecting local/regional ozone production in summer, and a winter minimum. In general the model performance is rather good, and largely in line with the performance in earlier years (Gauss et al. 2019, 2018).

Out of the 19 sites, for which data were analyzed both in (Gauss et al. 2019) and this year, the model performance, in terms of the index of agreement, has improved at 12 sites, got worse at 5 and remained unchange at 2 sites.

The index of agreement is larger than 0.8 at most stations, and below 0.7 only at one station (MK0007). In contrast to previous years, the bias is negative at most sites. Strong underestimations (>5 ppb) are seen at BG0053, HU0002, MK0007, and SK0002. Existing overestimations are small.

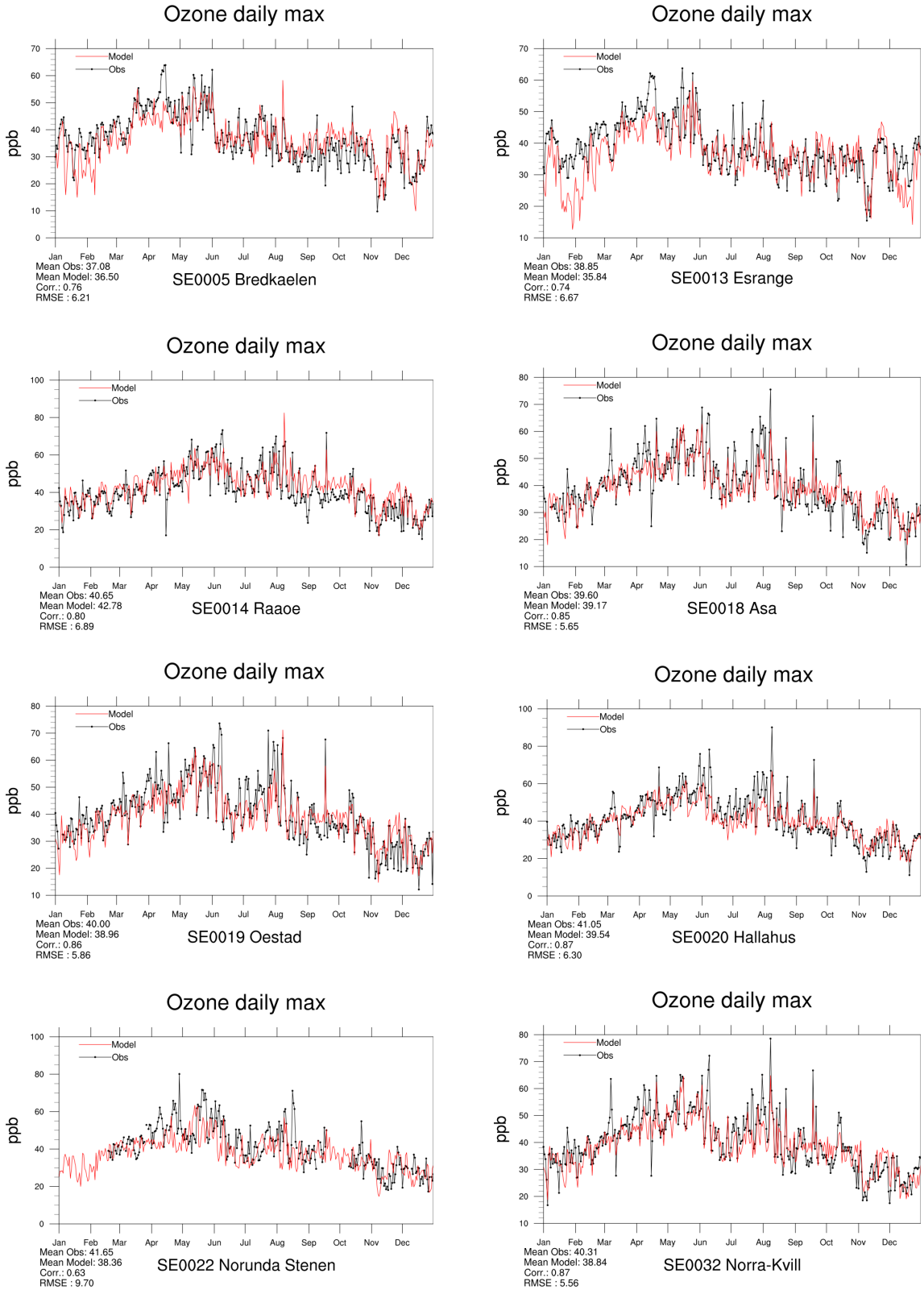

Figure 3.2: Modelled versus Observed Daily Maximum Ozone [ppb] at Swedish sites for 2018. *Note that in some plots the vertical axis does not start at zero.*

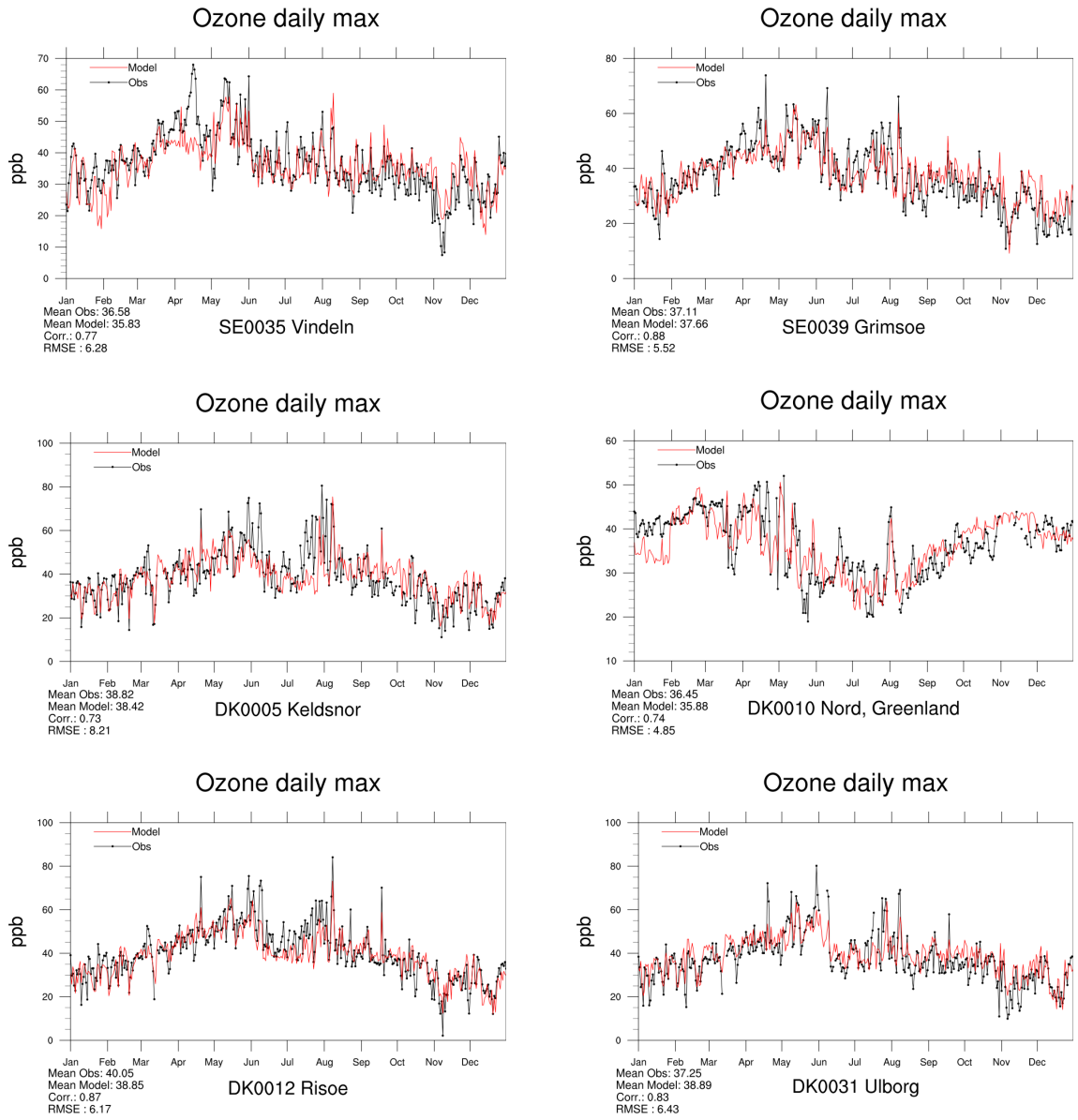

Figure 3.3: Modelled versus Observed Daily Maximum Ozone [ppb] at Swedish and Danish sites for 2018. *Note that in some plots the vertical axis does not start at zero.*

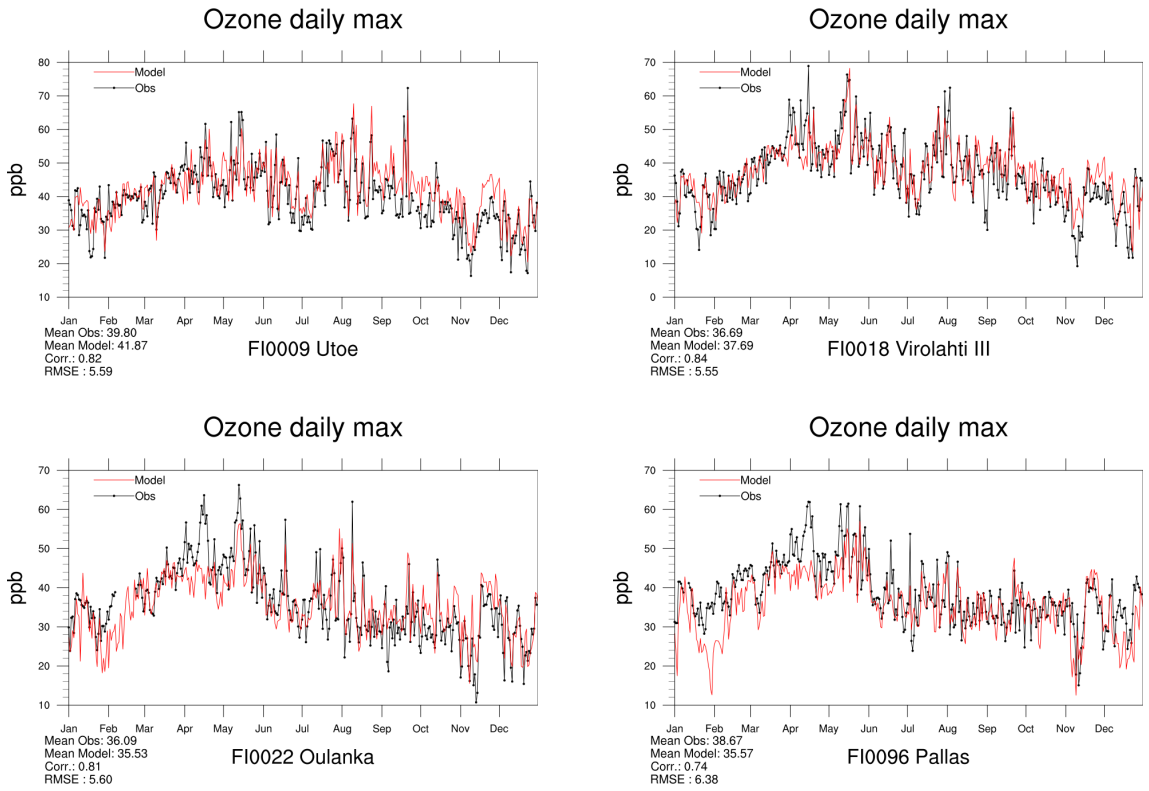

Figure 3.4: Modelled versus Observed Daily Maximum Ozone [ppb] at Finnish sites for 2018. *Note that in some plots the vertical axis does not start at zero.*

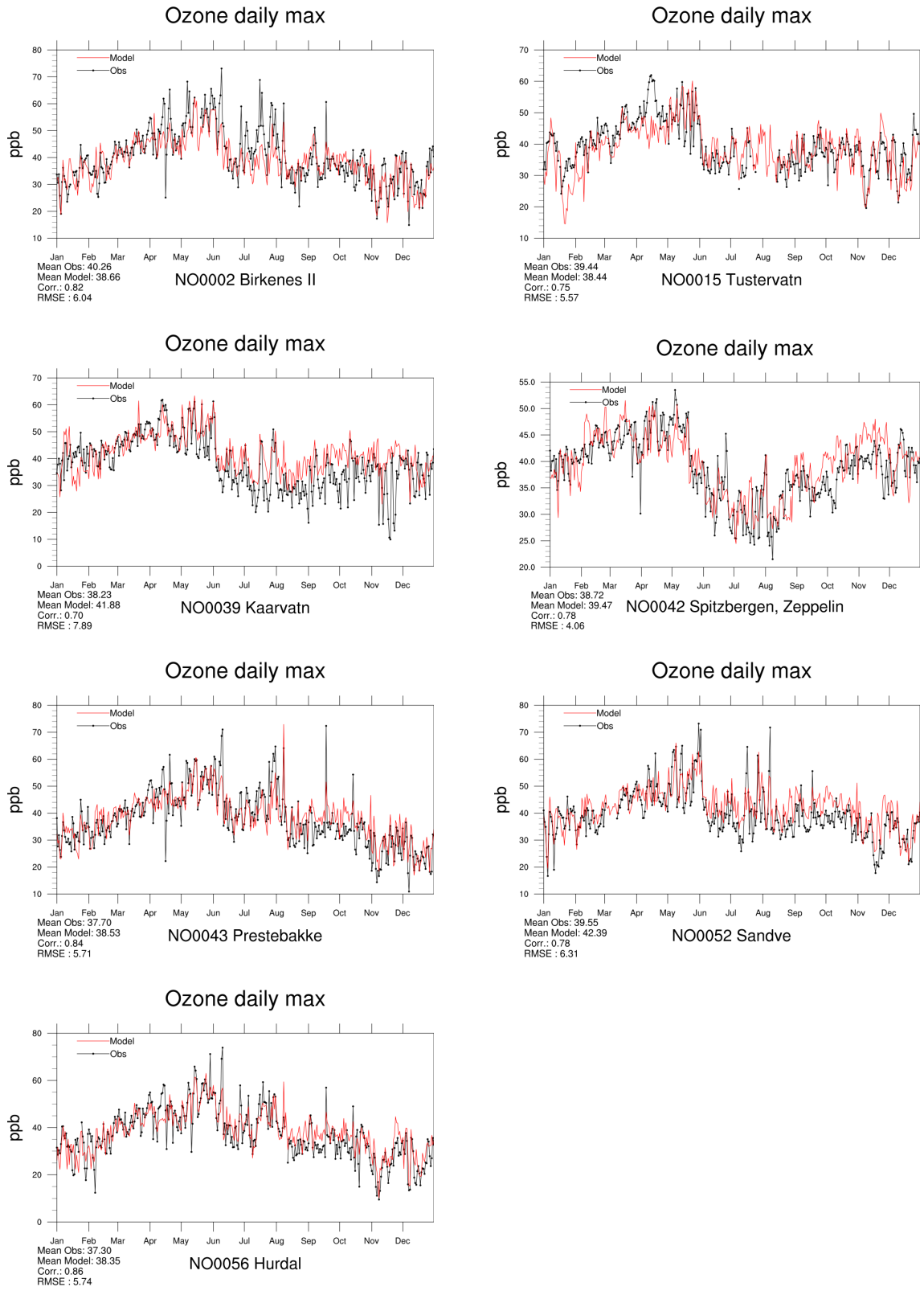

Figure 3.5: Modelled versus Observed Daily Maximum Ozone [ppb] at Norwegian sites for 2018. *Note that in some plots the vertical axis does not start at zero.*

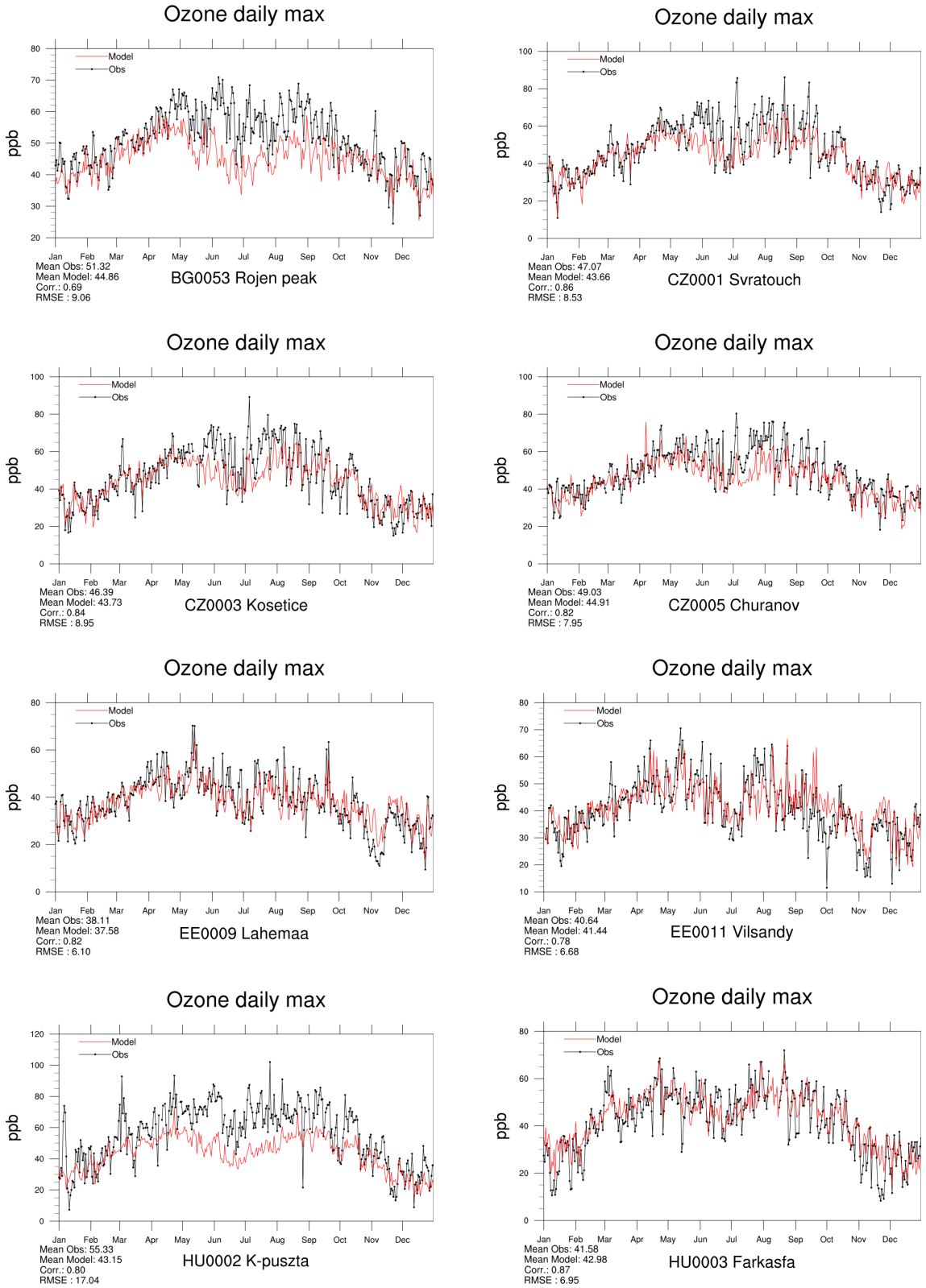

Figure 3.6: Modelled versus Observed Daily Maximum Ozone [ppb] at Eastern European sites for 2018. *Note that in some plots the vertical axis does not start at zero.*

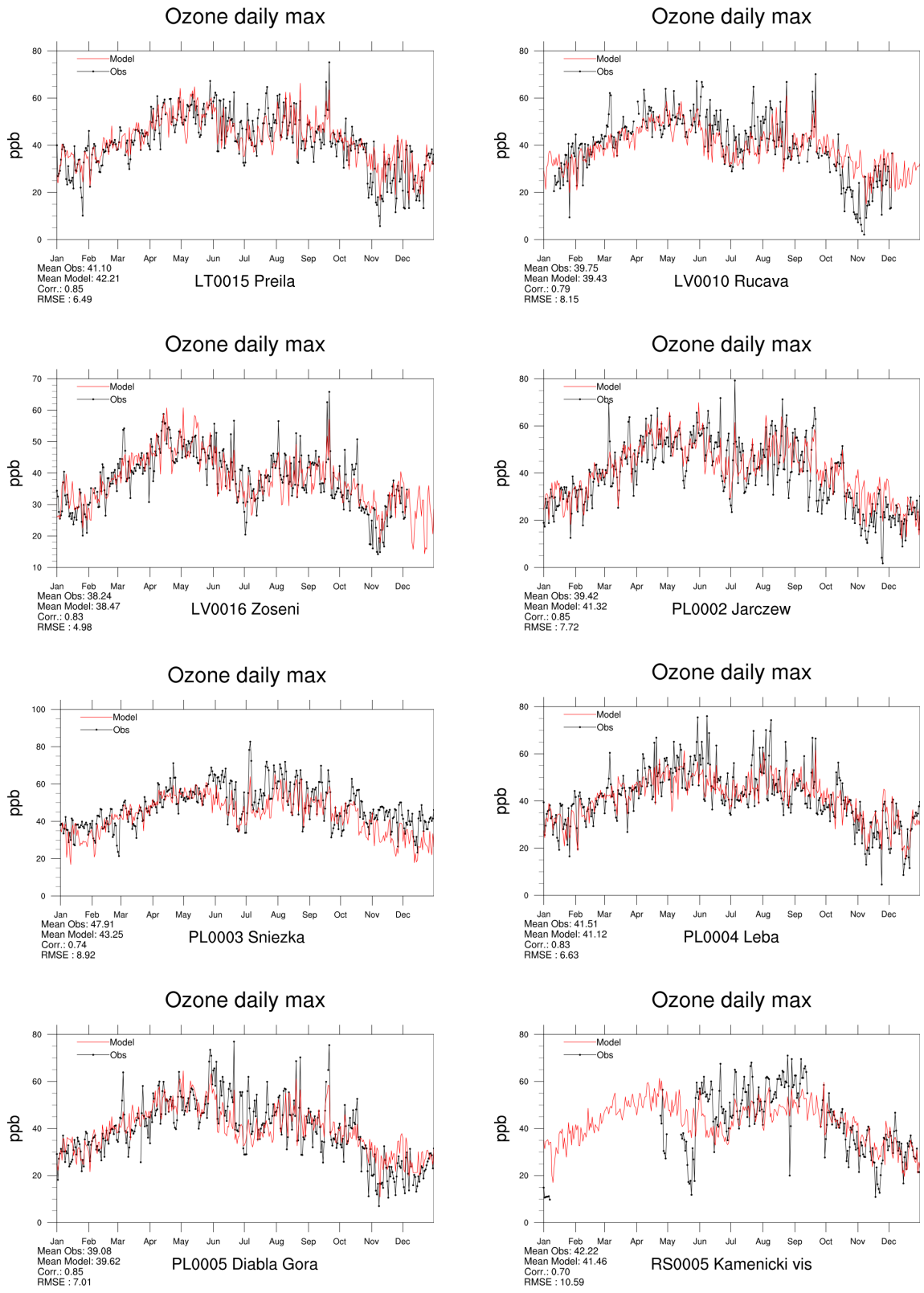

Figure 3.7: Modelled versus Observed Daily Maximum Ozone [ppb] at Eastern European sites for 2018. *Note that in some plots the vertical axis does not start at zero.*

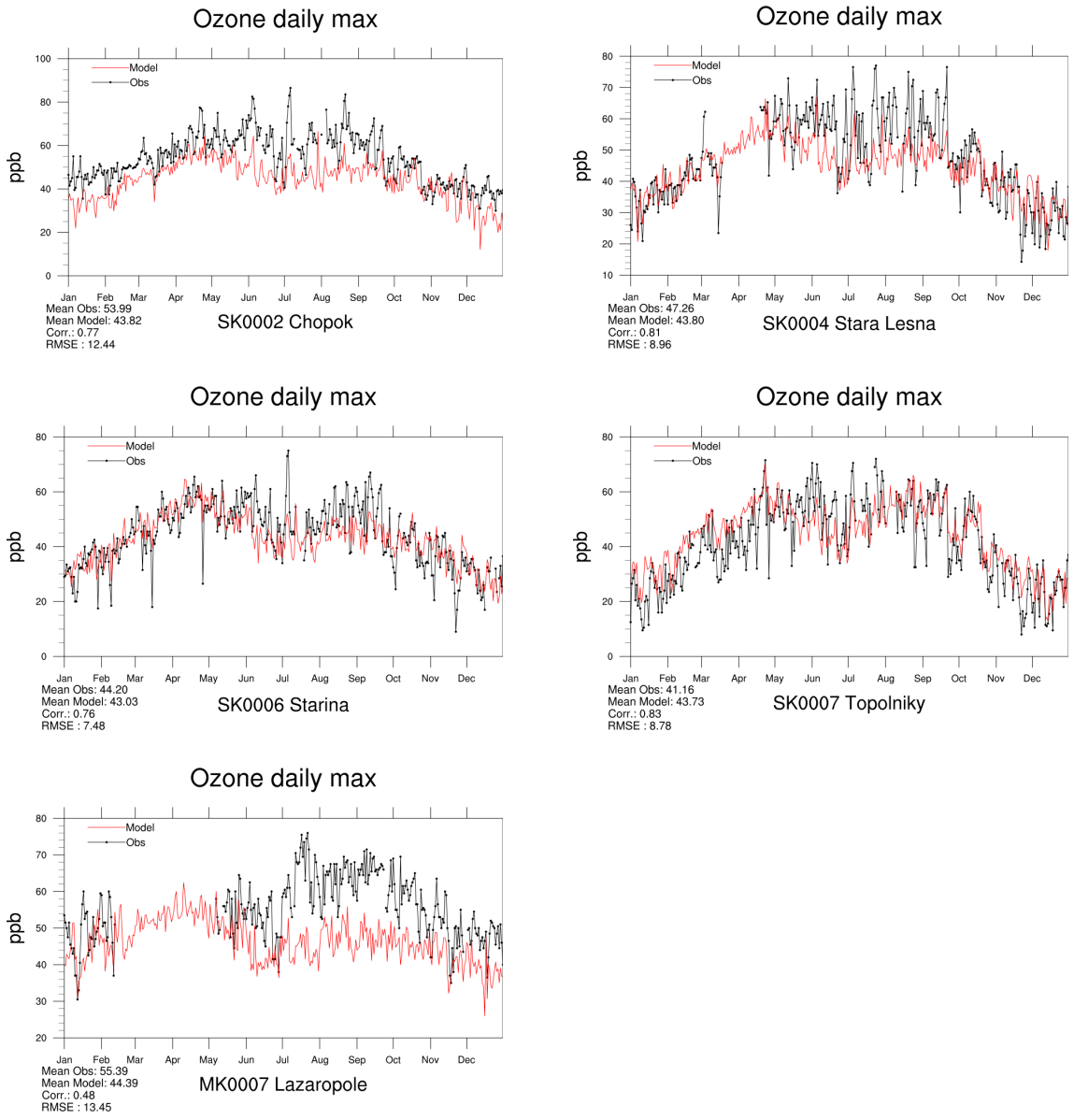

Figure 3.8: Modelled versus Observed Daily Maximum Ozone [ppb] at Eastern European sites for 2018. *Note that in some plots the vertical axis does not start at zero.*

Central and Northwestern European sites

Measured and modelled maximum ozone levels for selected sites in Central and Northwestern Europe are shown in Figures 3.9–3.18. These sites are mainly typical continental sites with a clear summer maximum, reflecting local/regional ozone production in summer, and a winter minimum. Concentrations at the site Mace Head in Ireland (IE0031) are partly used to specify background conditions for the EMEP model, so that good performance, at least for the seasonal cycle, is guaranteed.

The overall model performance is good in this area, and the index of agreement has increased with respect to last year (Gauss et al. 2019) at about half of the stations. Out of the 67 stations for which model performance has been analysed both last year and this year IOA has improved at 38 and decreased at 17 stations. At 12 stations it has remained the same.

As a proper way of comparing model data and measurement sites at very high elevations is not implemented yet, Jungfraujoch (CH0001) and Zugspitze-Schneeferner (DE0054) are not shown in this year's evaluation, although measurement data have been well received.

The reason for the very low measured value at station Sirta (FR000) towards the end of May has not been resolved yet, but could be an artefact.

Another measured peak of about 200 ug/m3 at Valentia (IE0001) on 11-12 March is not seen in the model, but could also be related to a technical problem.

In general the model tends to underestimate levels during summer at many stations in Central Europe, which could be related to too high dry deposition.

Mediterranean sites

Measured and modelled ozone levels for selected sites in the Mediterranean region are shown in Figures 3.19–3.21. The meteorological situation in and around the Mediterranean basin differs considerably from the rest of Europe. This region also receives more solar radiation resulting in conditions favourable for ozone production. Hence these sites have some of the highest ozone levels in Europe.

In general the model performance is good for most sites in this region, with IOA values between 0.7 and 0.9. Exceptions with IOA below 0.7 are ES0006, ES0011, ES0012, GR0002, IT0009 and IT0018 (i.e. the same stations as last year). Out of the 23 stations for which model performance has been analyzed both last year and this year, IOA has become better at 12 stations and worse at 10 stations. At one station it remained unchanged.

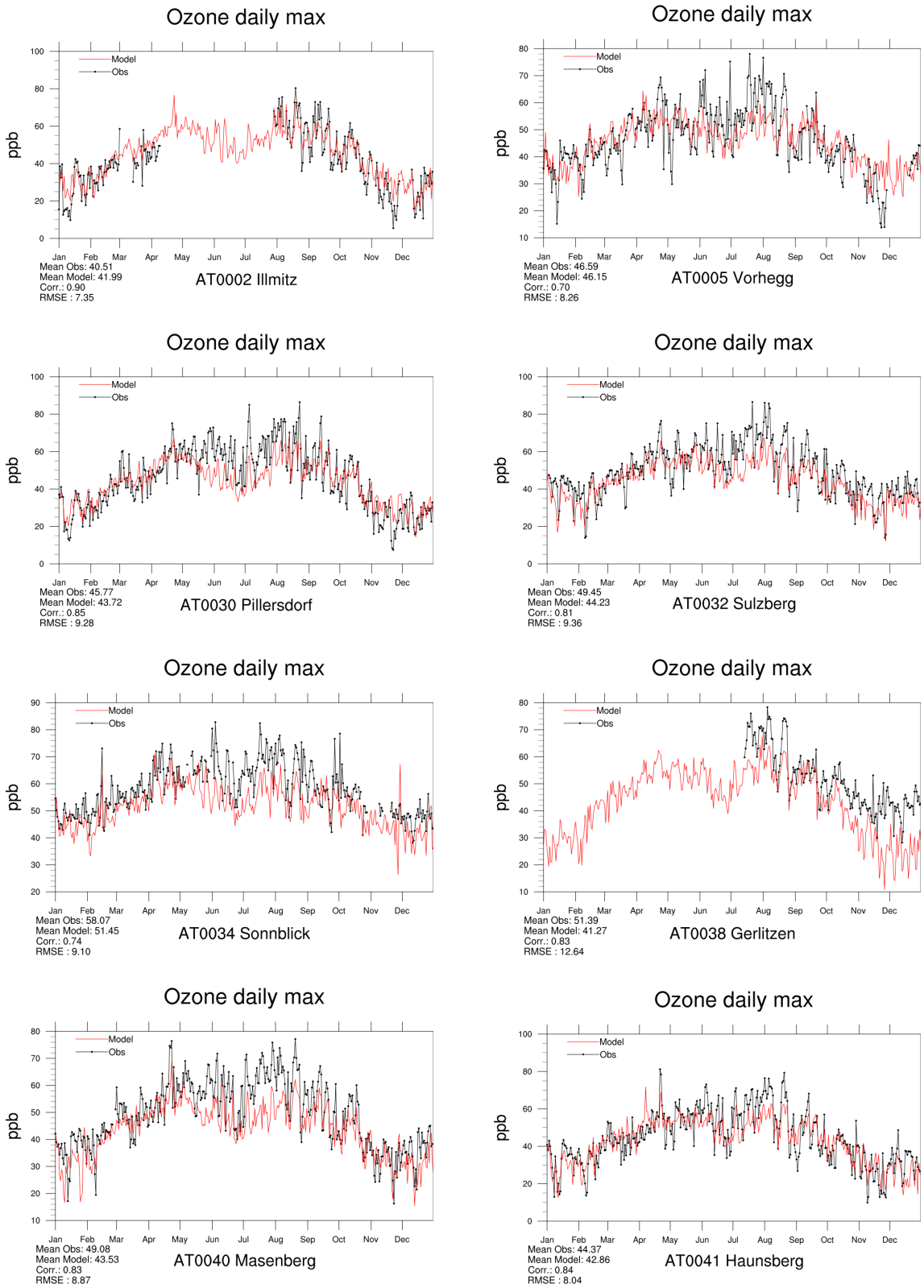

Figure 3.9: Modelled versus Observed Daily Maximum Ozone [ppb] at Austrian sites for 2018. *Note that in some plots the vertical axis does not start at zero.*

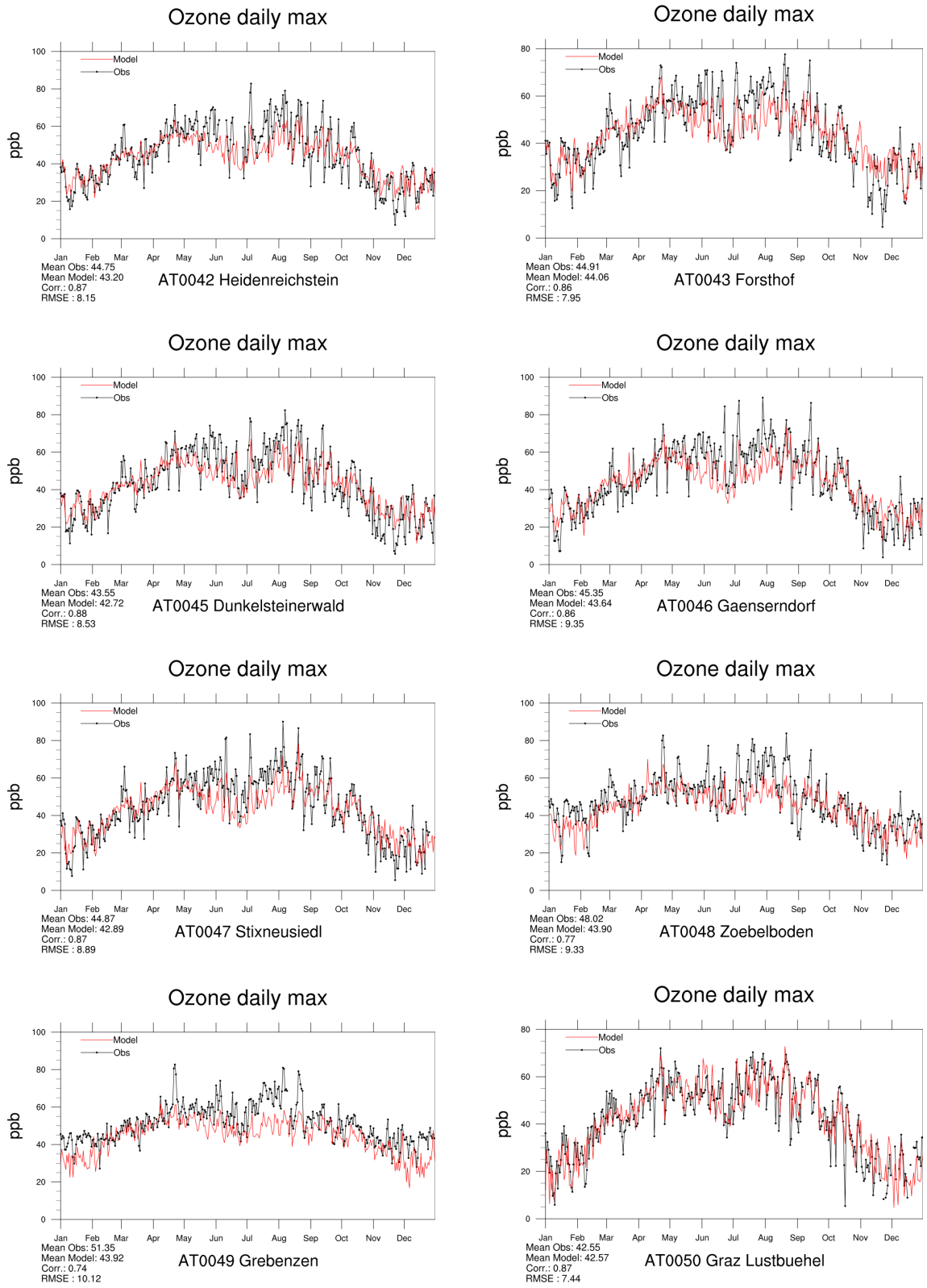

Figure 3.10: Modelled versus Observed Daily Maximum Ozone [ppb] at Austrian sites for 2018.

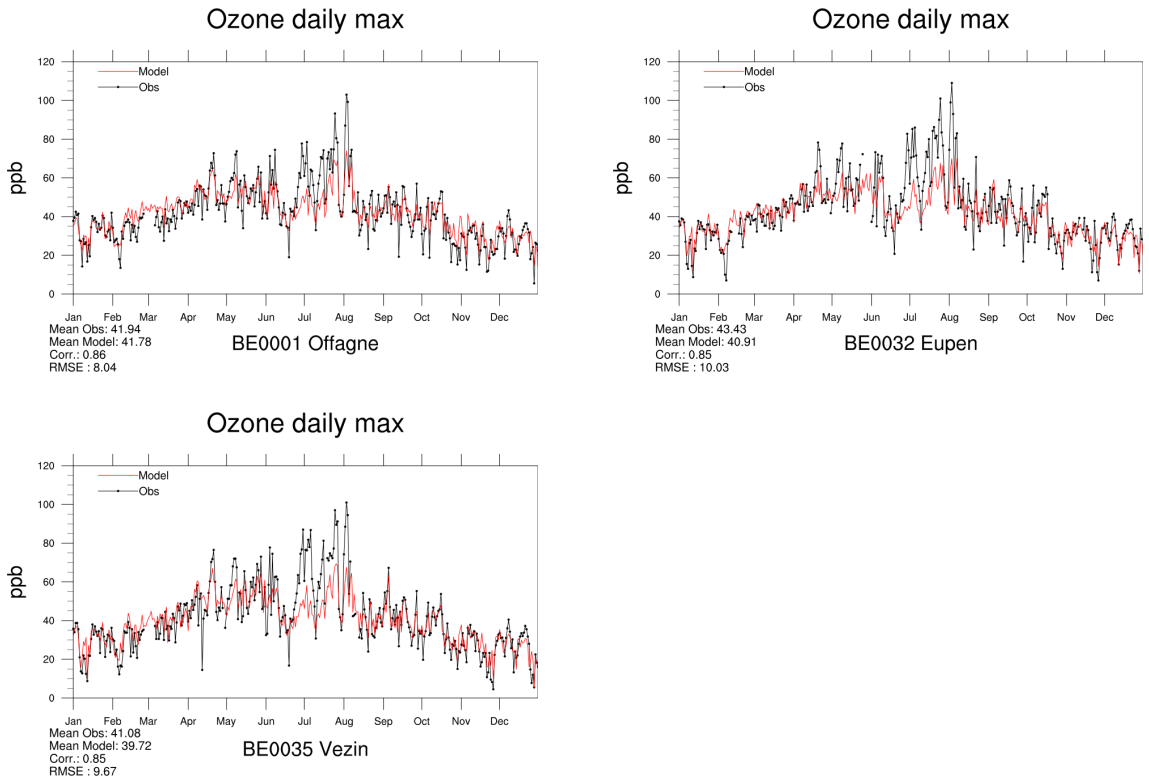

Figure 3.11: Modelled versus Observed Daily Maximum Ozone [ppb] at sites in Belgium for 2018. *Note that in some plots the vertical axis does not start at zero.*

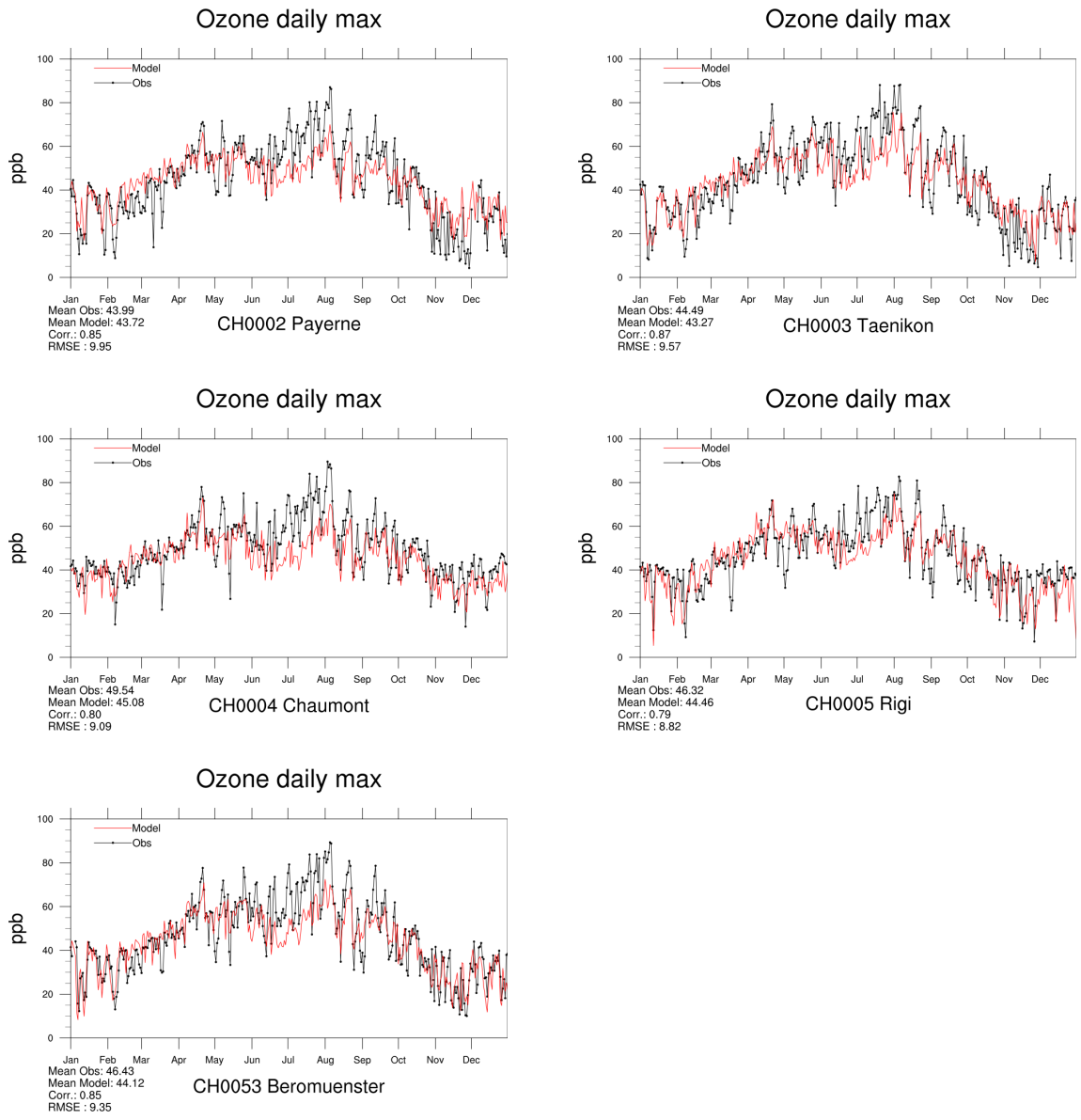

Figure 3.12: Modelled versus Observed Daily Maximum Ozone [ppb] at sites in Switzerland for 2018. *Note that in some plots the vertical axis does not start at zero.*

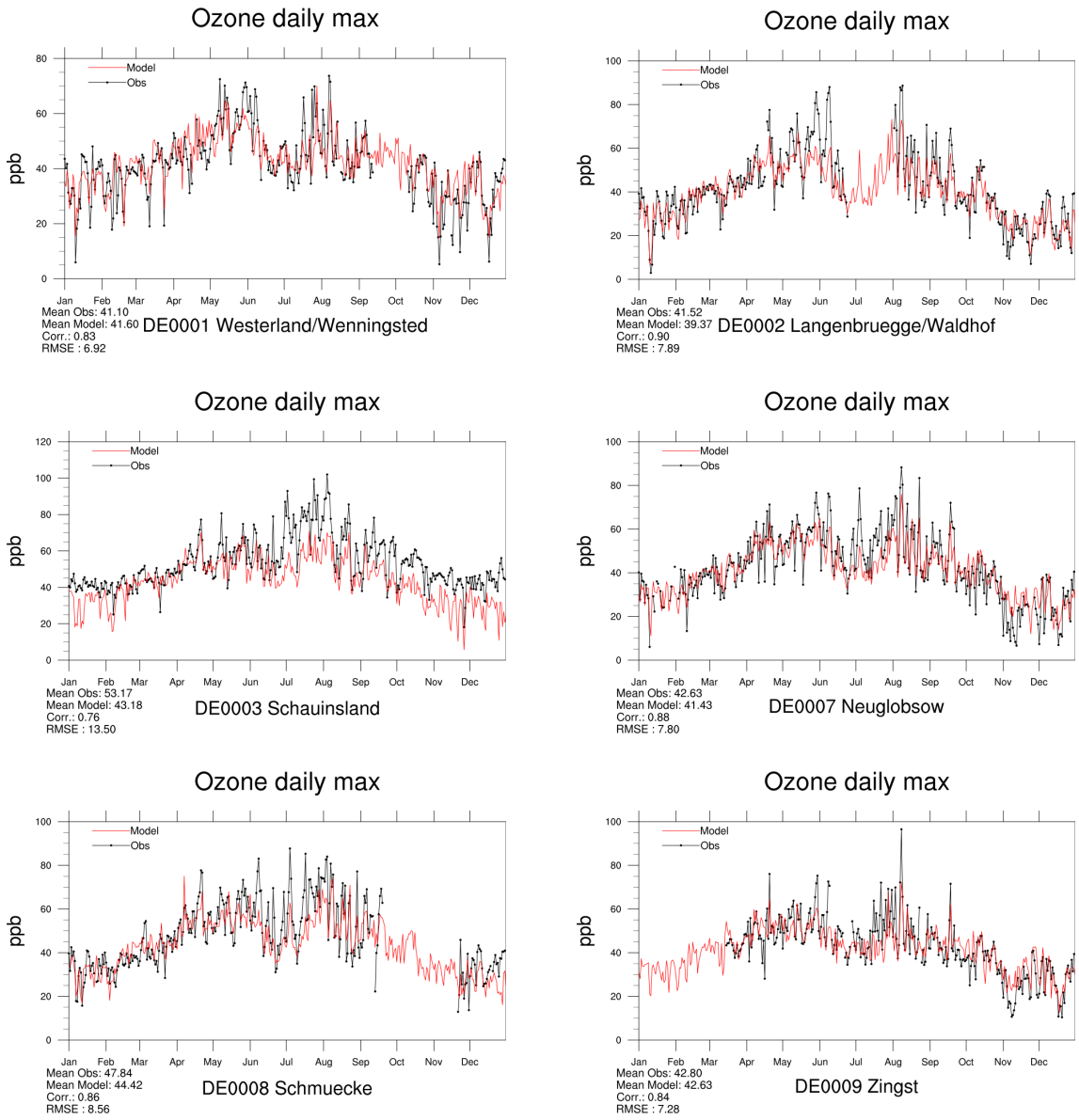

Figure 3.13: Modelled versus Observed Daily Maximum Ozone [ppb] at sites in Germany for 2018. *Note that in some plots the vertical axis does not start at zero.*

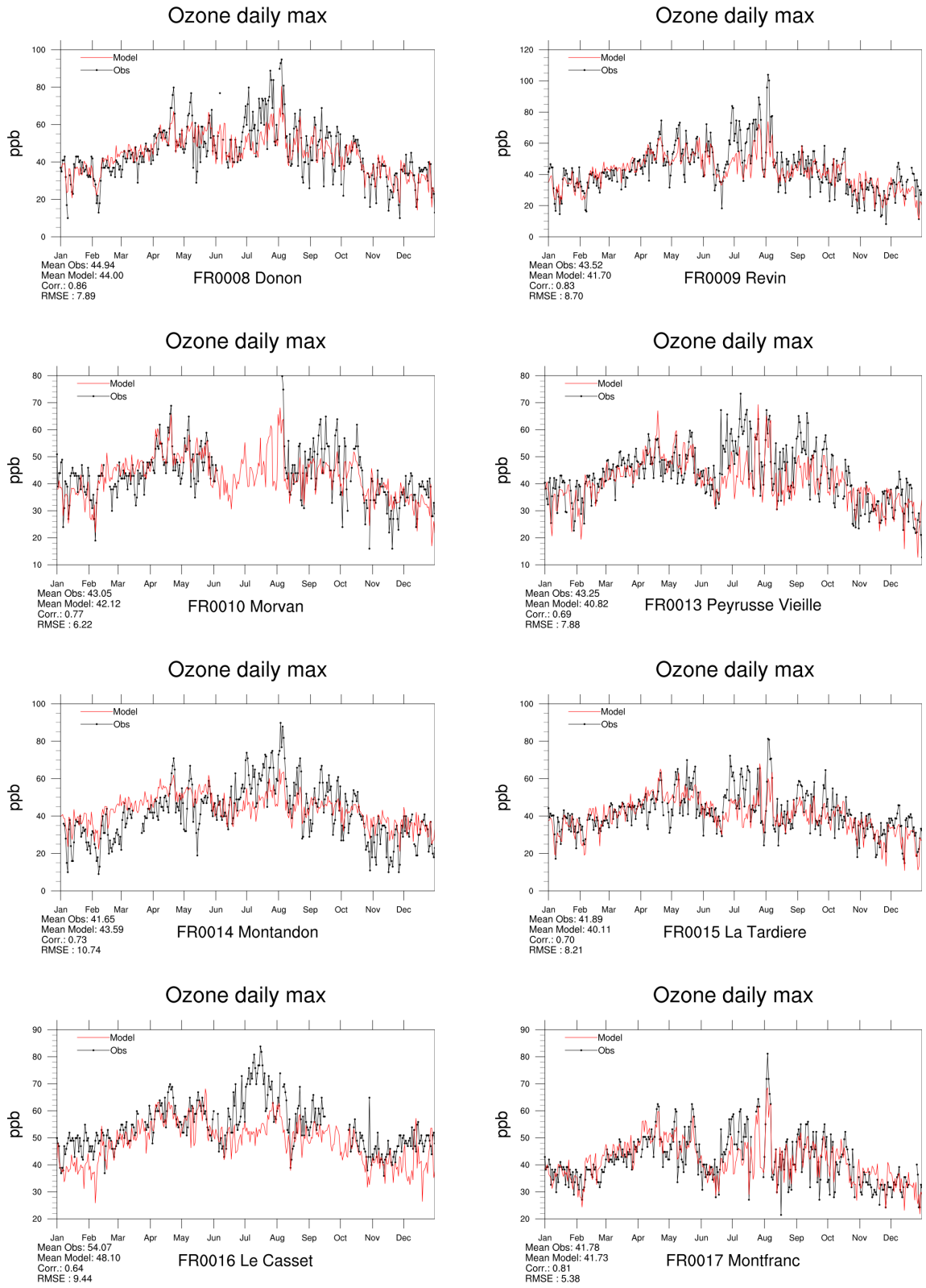

Figure 3.14: Modelled versus Observed Daily Maximum Ozone [ppb] at French sites for 2018. *Note that in some plots the vertical axis does not start at zero.*

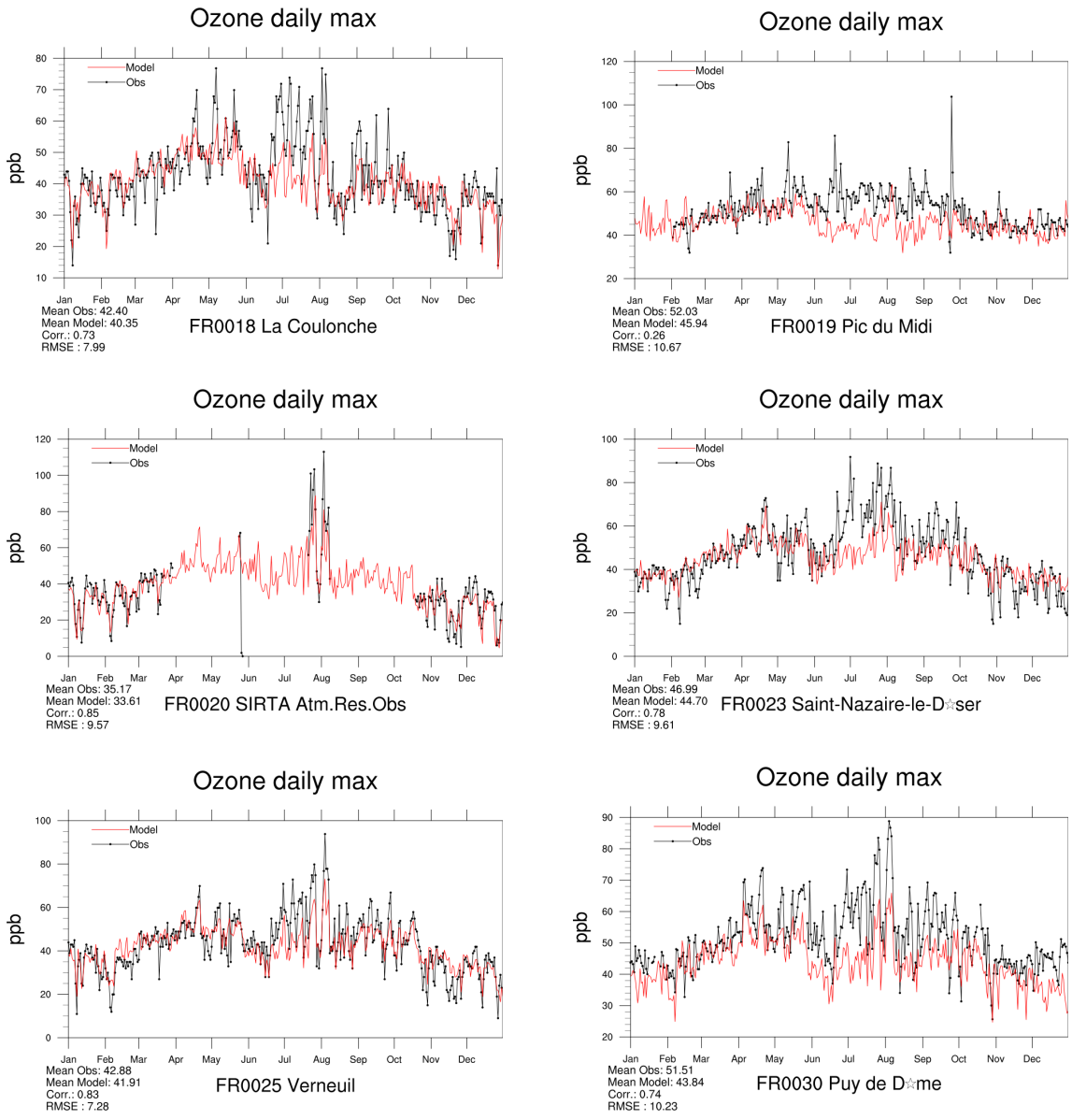

Figure 3.15: Modelled versus Observed Daily Maximum Ozone [ppb] at French sites for 2018. *Note that in some plots the vertical axis does not start at zero.*

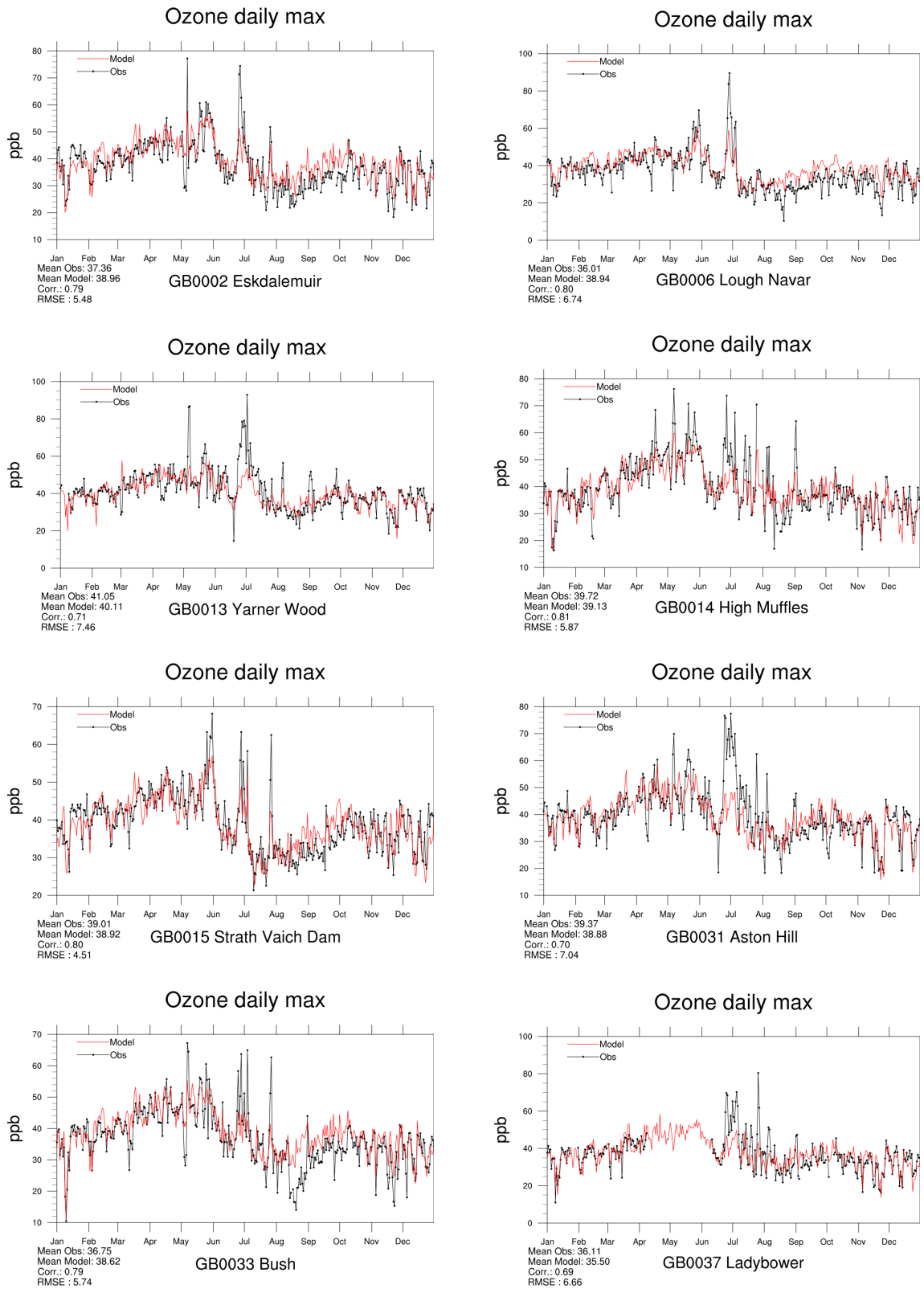

Figure 3.16: Modelled versus Observed Daily Maximum Ozone [ppb] at British sites for 2018. *Note that in some plots the vertical axis does not start at zero.*

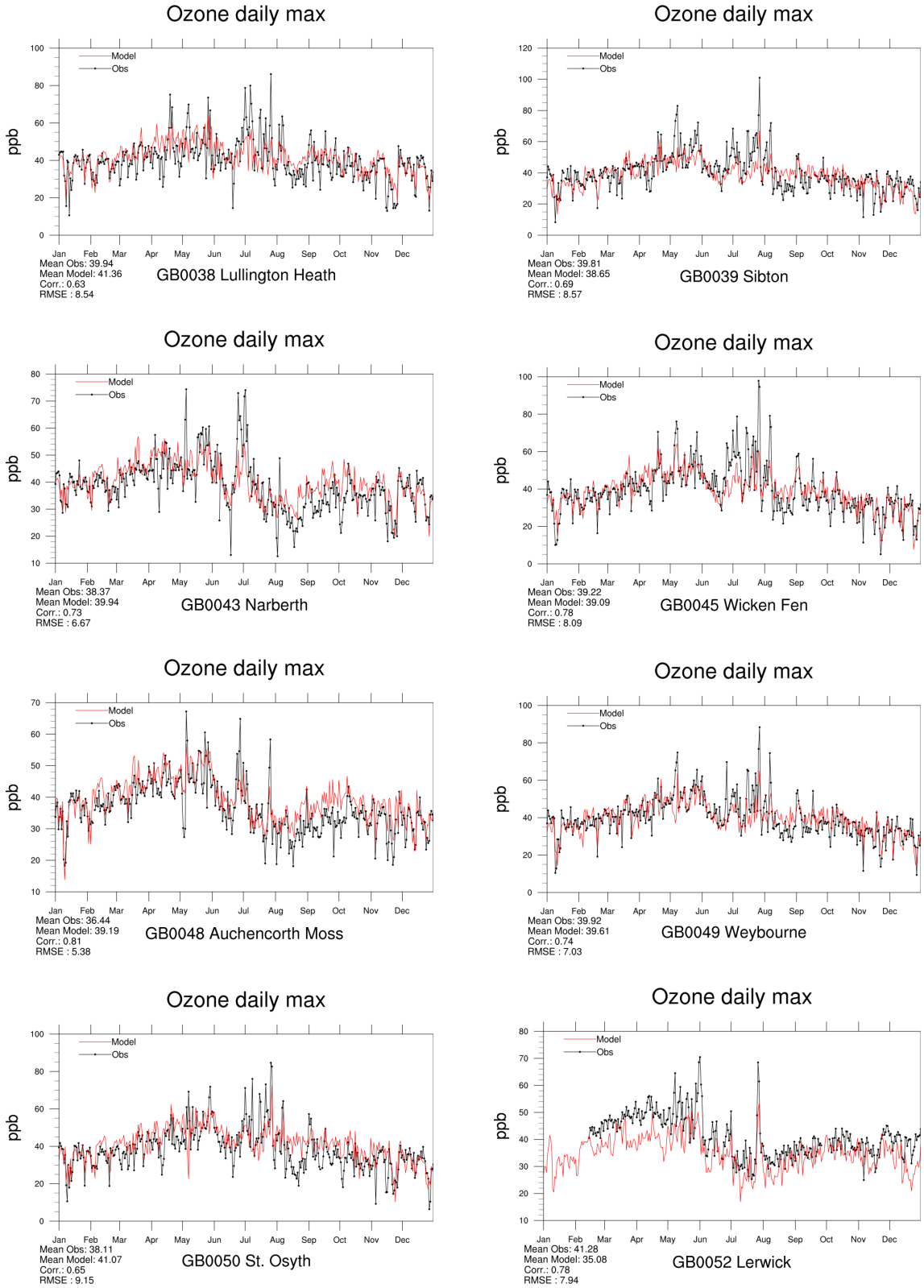

Figure 3.17: Modelled versus Observed Daily Maximum Ozone [ppb] at British sites for 2018. *Note that in some plots the vertical axis does not start at zero.*

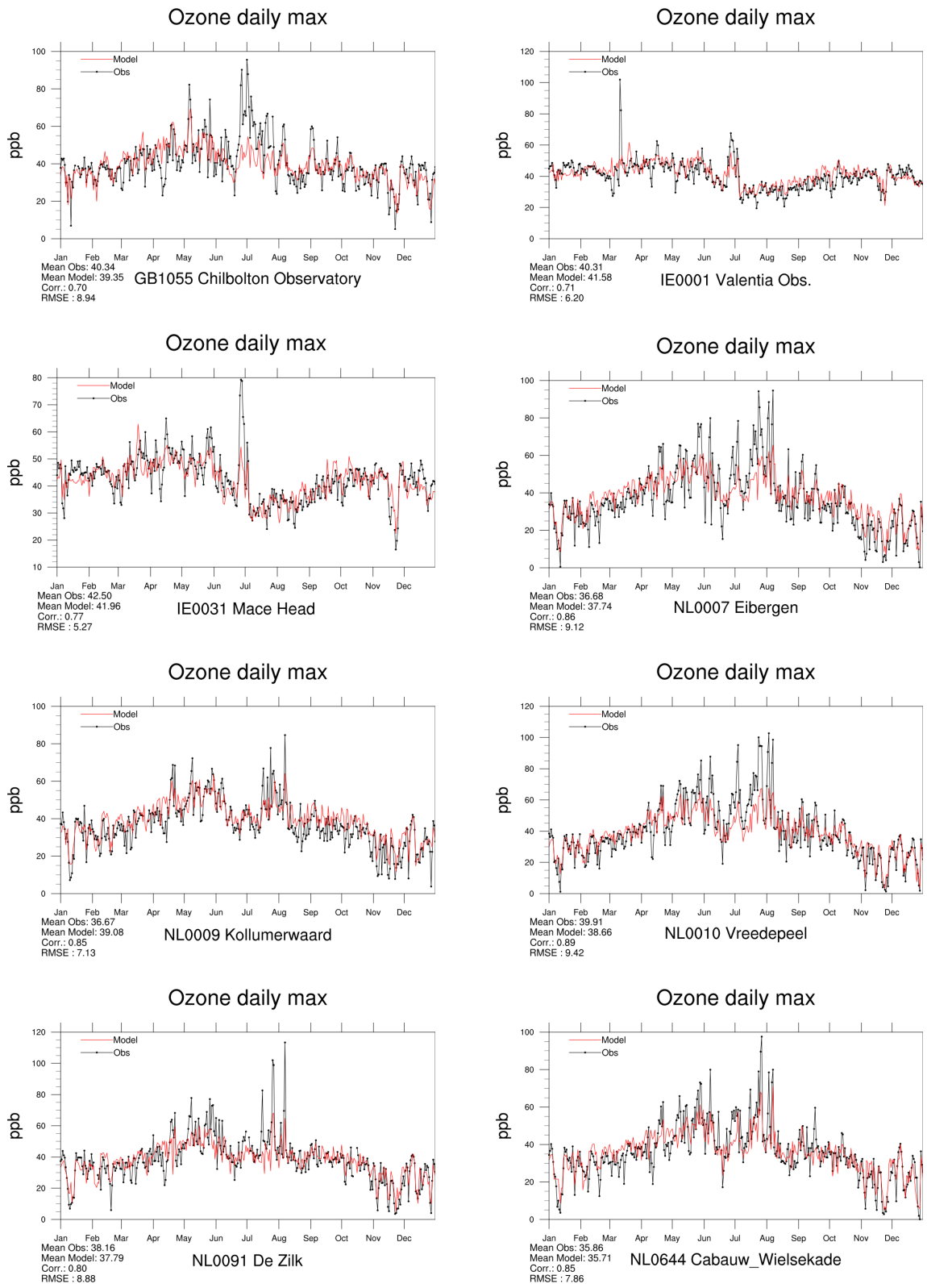

Figure 3.18: Modelled versus Observed Daily Maximum Ozone [ppb] at British, Irish and Dutch sites for 2018. *Note that in some plots the vertical axis does not start at zero.*

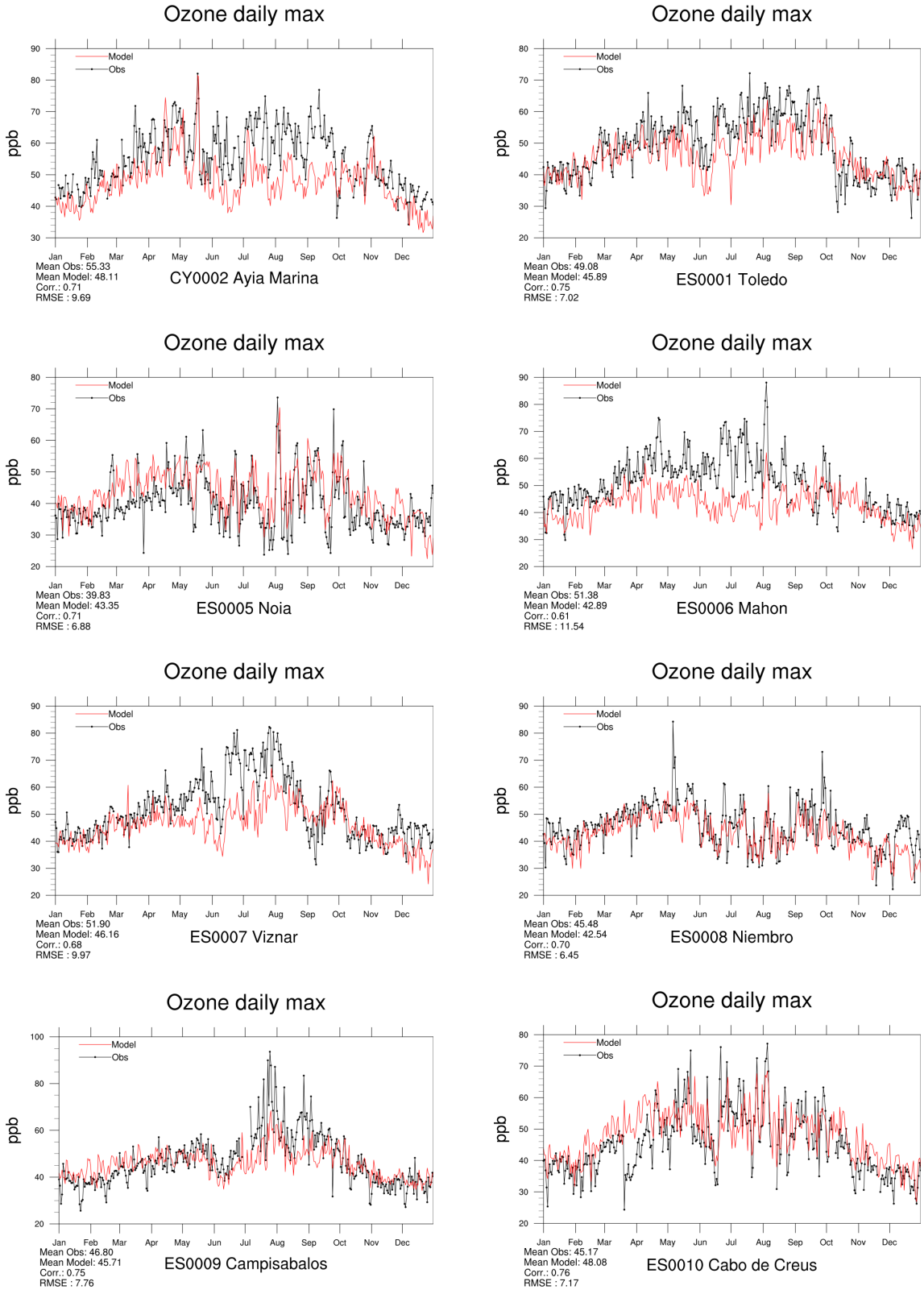

Figure 3.19: Modelled versus Observed Daily Maximum Ozone [ppb] at Mediterranean sites (Cyprus and Spain) for 2018. *Note that in some plots the vertical axis does not start at zero.*

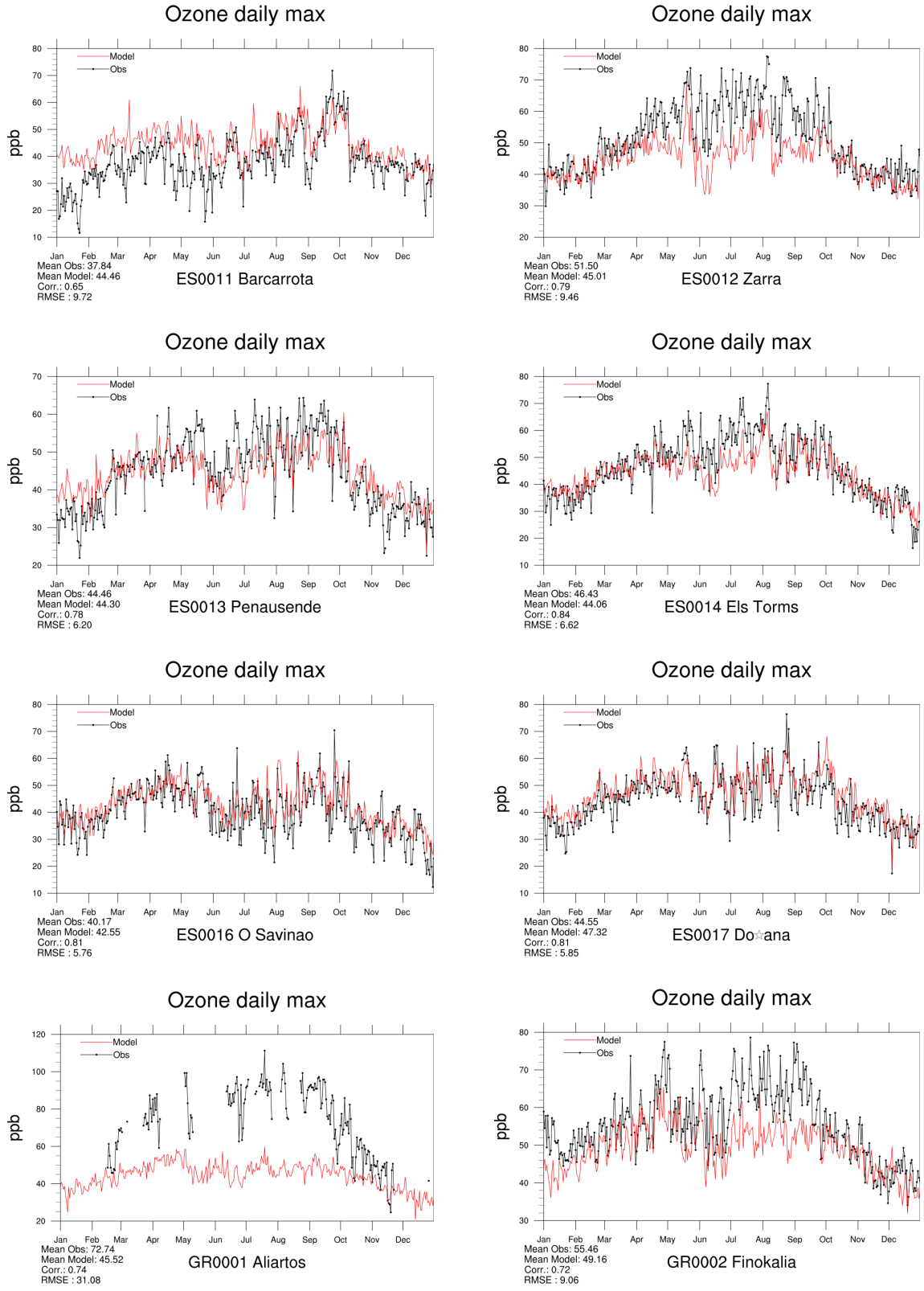

Figure 3.20: Modelled versus Observed Daily Maximum Ozone [ppb] at Mediterranean Sites (Spain and Greece) for 2018. *Note that in some plots the vertical axis does not start at zero.*

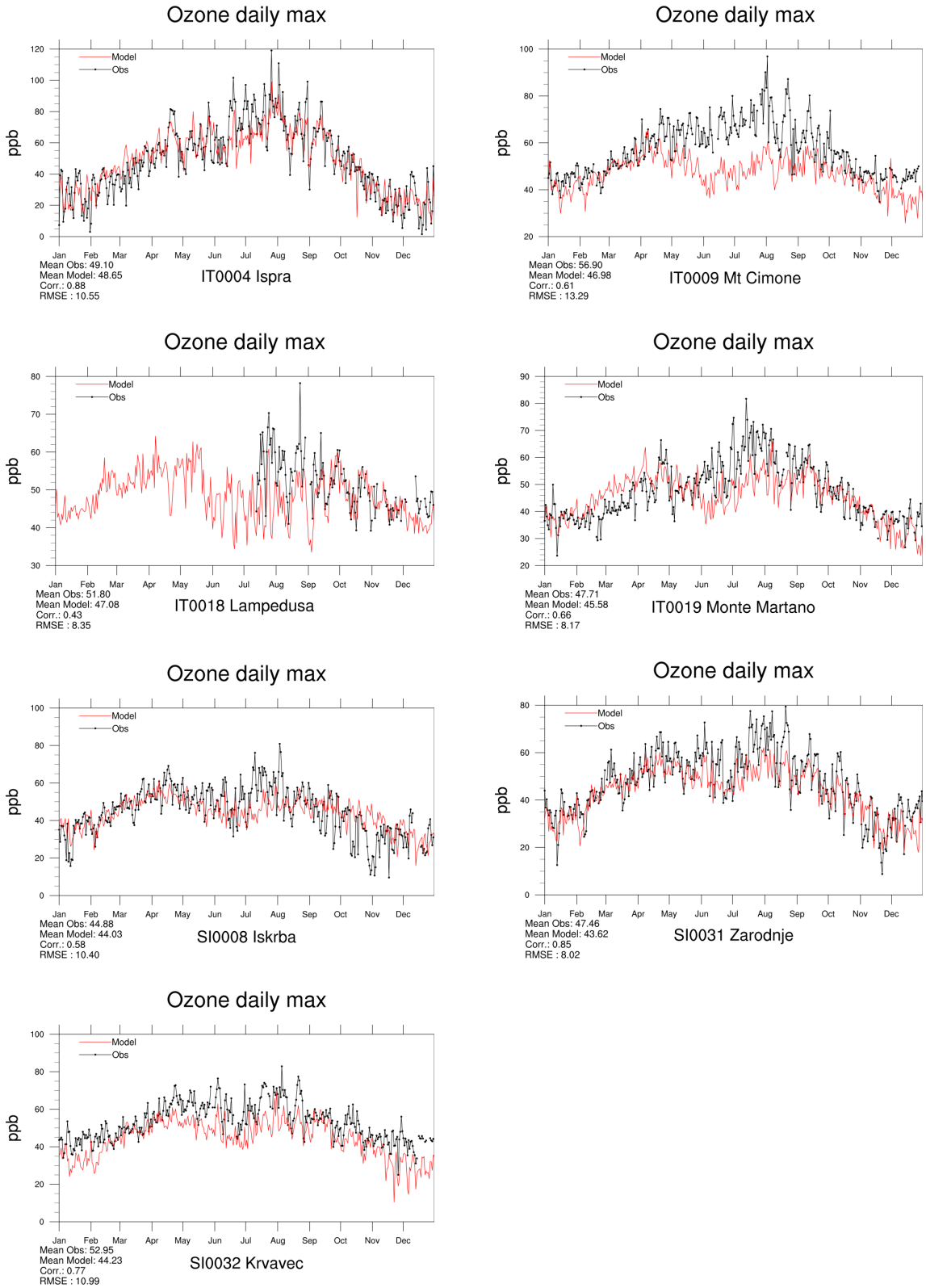

Figure 3.21: Modelled versus Observed Daily Maximum Ozone [ppb] at Mediterranean Sites for 2018.

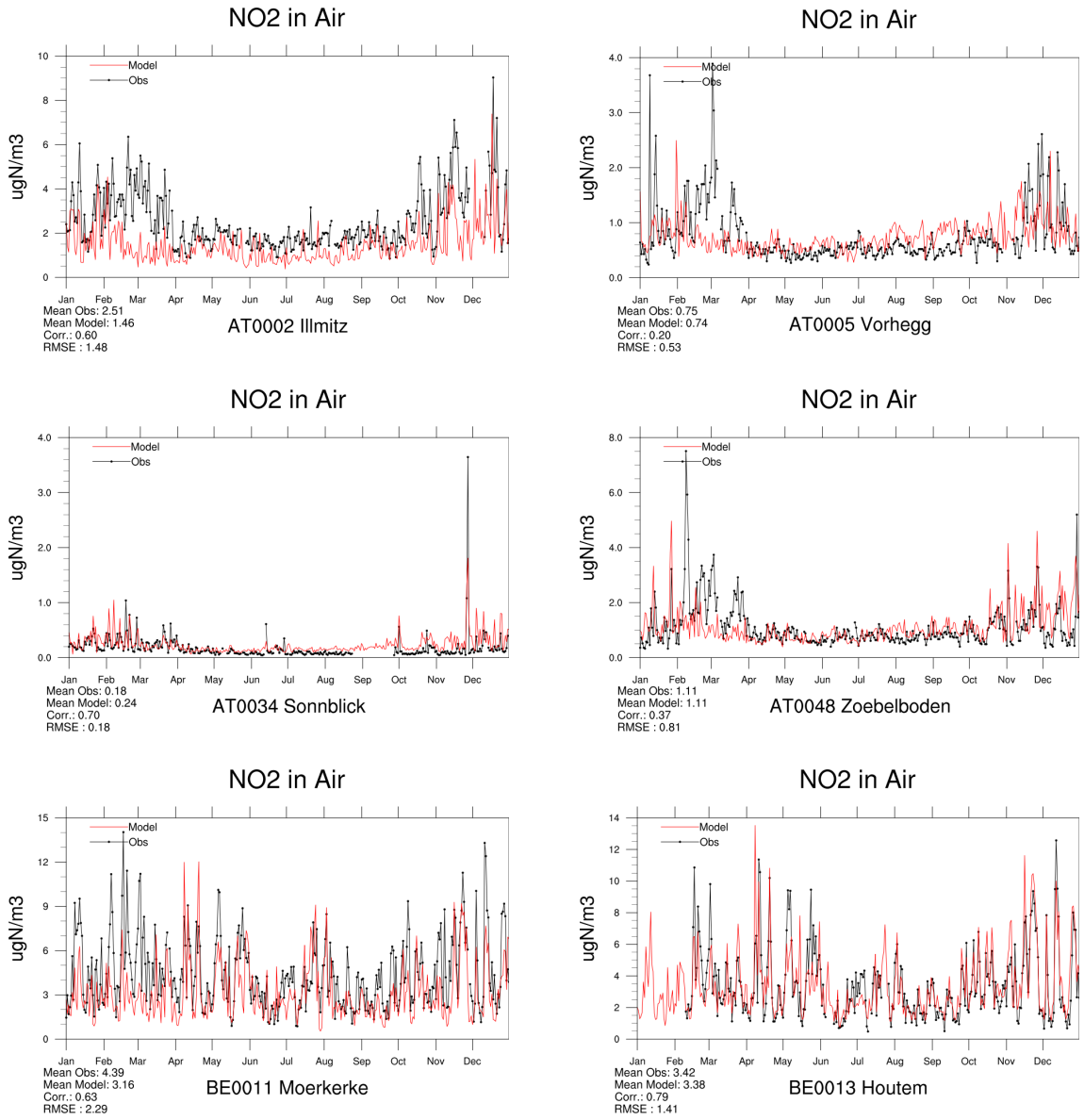

Figure 3.22: Modelled versus Observed Daily Mean NO_2 (μg(N) m^{-3}) for 2018.

3.3 Time series for nitrogen dioxide

In this section we present time series plots for a selection of stations that have supplied data on NO_2 levels to EMEP CCC for 2018. The plots show daily model results and measurements of NO_2, where available. The plots are arranged in alphabetical order by country code.

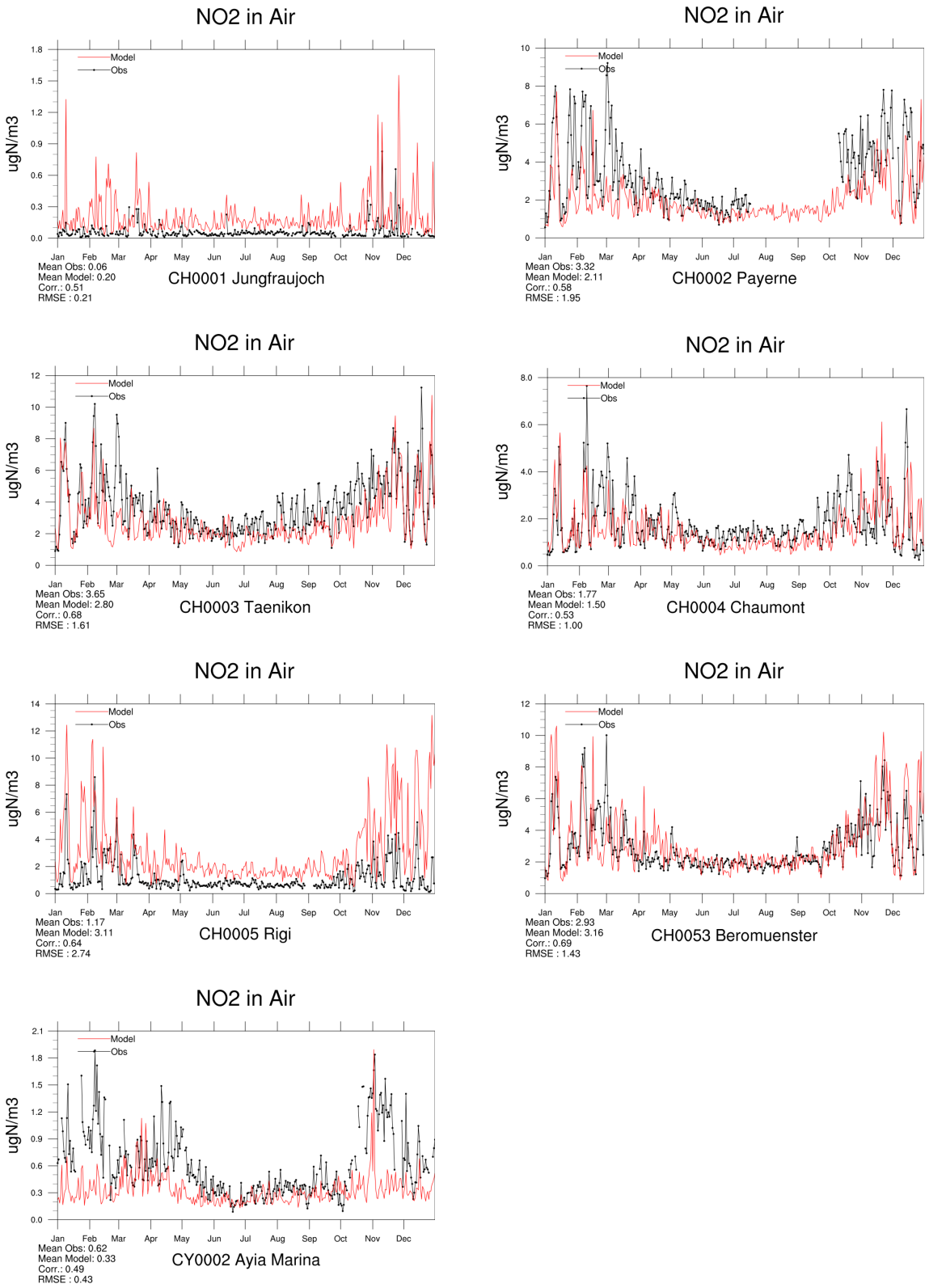

Figure 3.23: Modelled versus Observed Daily Mean NO_2 (μg(N) m^{-3}) for 2018.

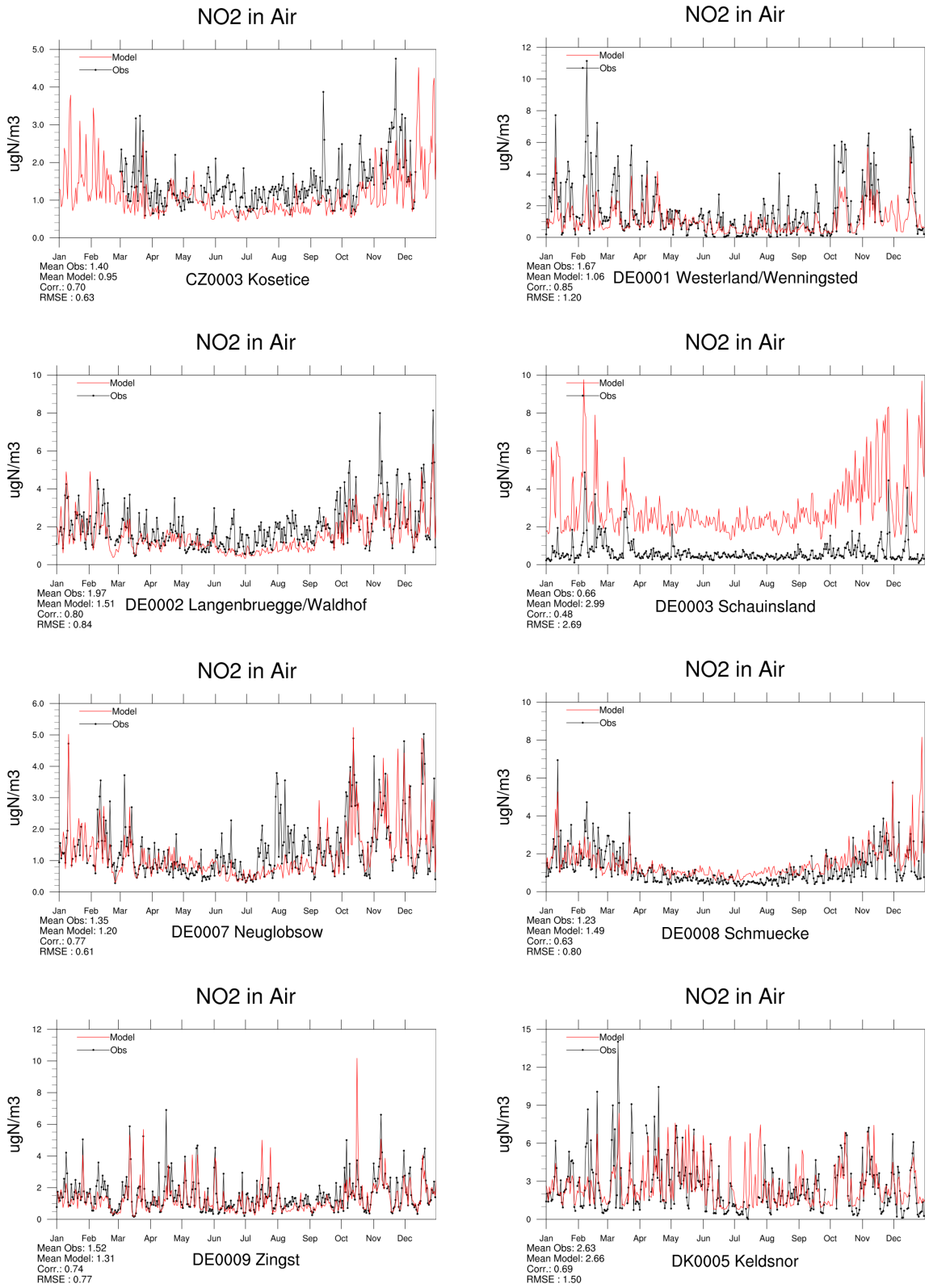

Figure 3.24: Modelled versus Observed Daily Mean NO_2 (μg(N) m^{-3}) for 2018.

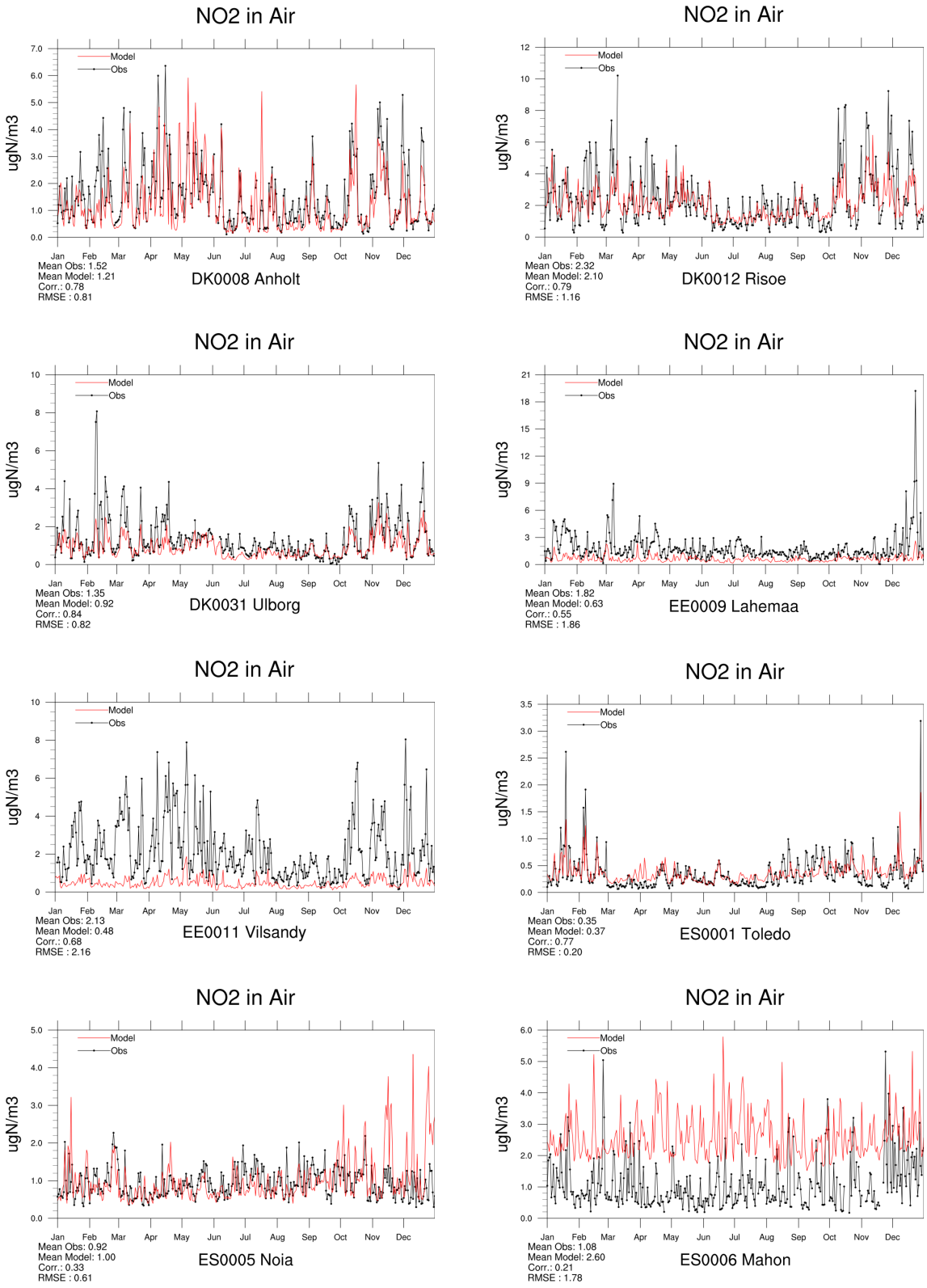

Figure 3.25: Modelled versus Observed Daily Mean NO_2 (μg(N) m^{-3}) for 2018.

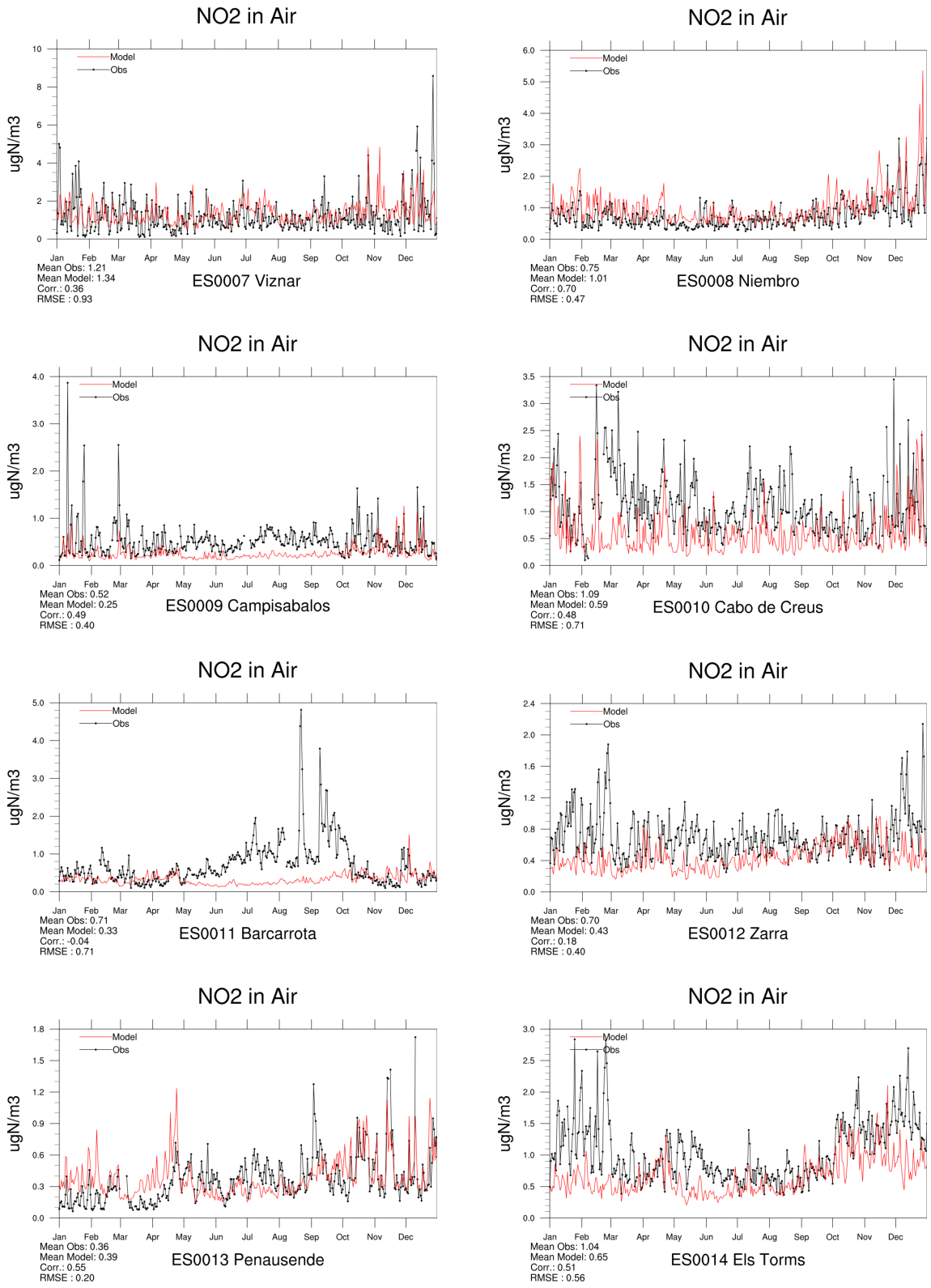

Figure 3.26: Modelled versus Observed Daily Mean NO_2 (μg(N) m^{-3}) for 2018.

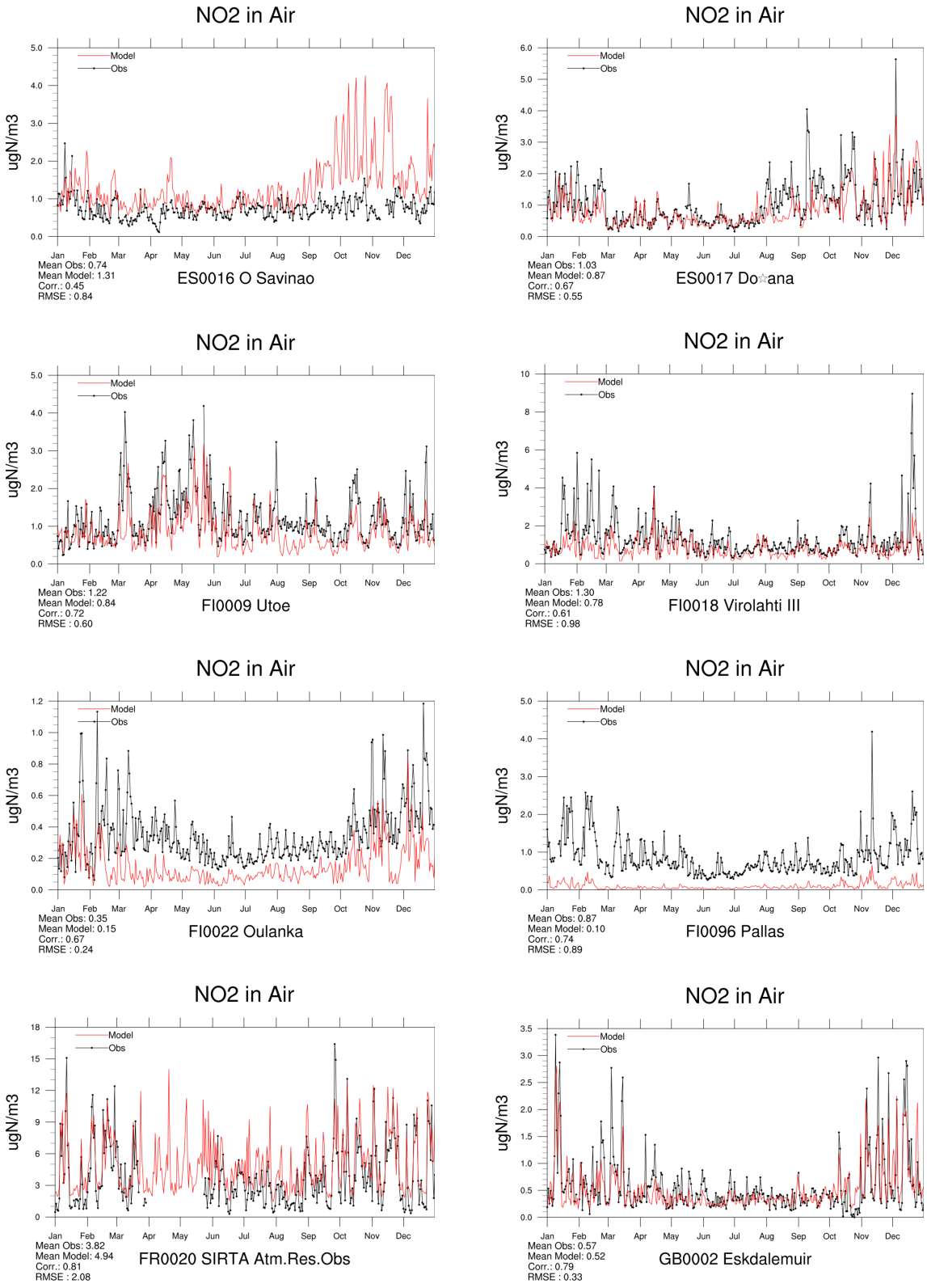

Figure 3.27: Modelled versus Observed Daily Mean NO_2 (μg(N) m^{-3}) for 2018.

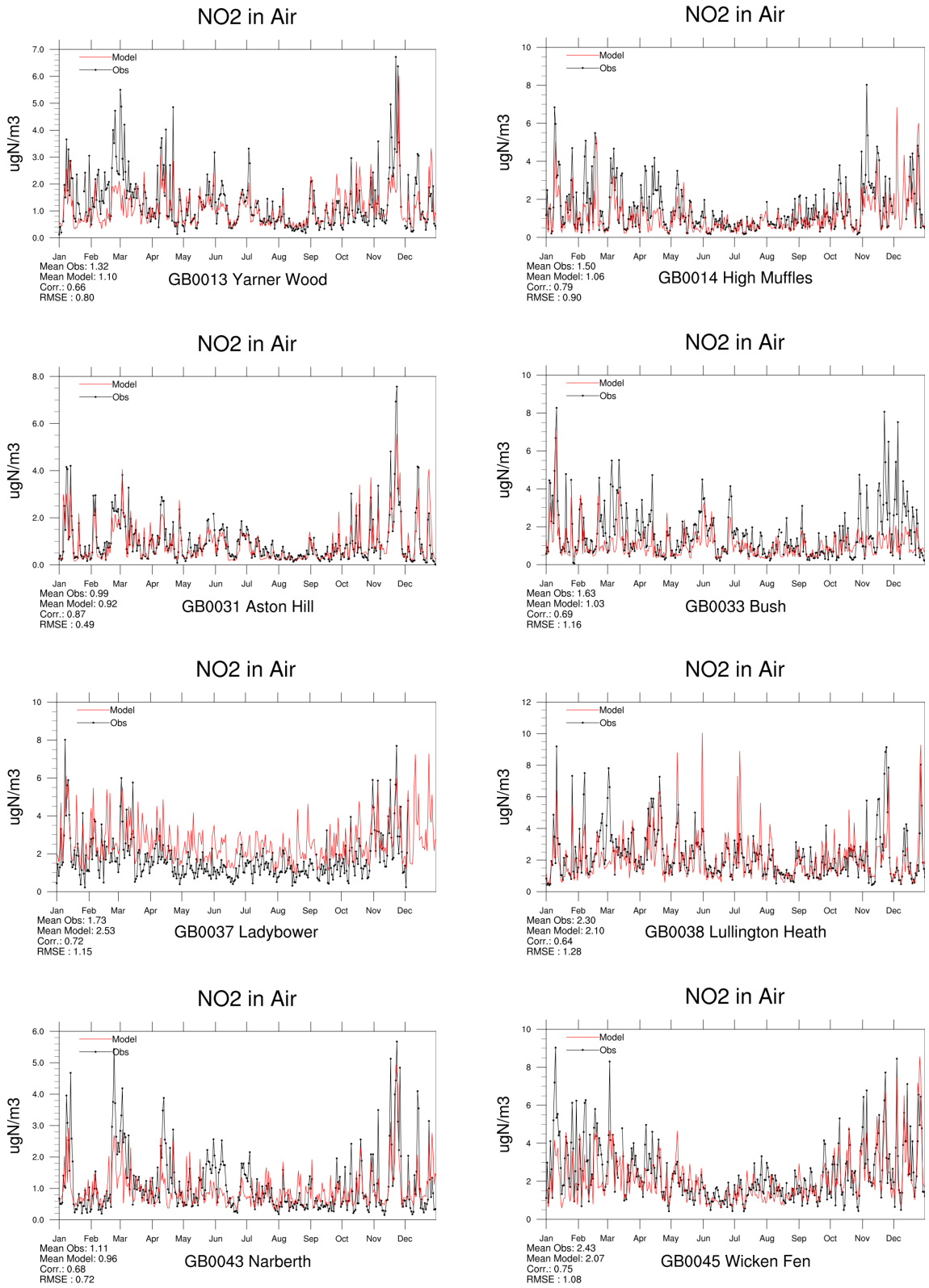

Figure 3.28: Modelled versus Observed Daily Mean NO_2 (μg(N) m^{-3}) for 2018.

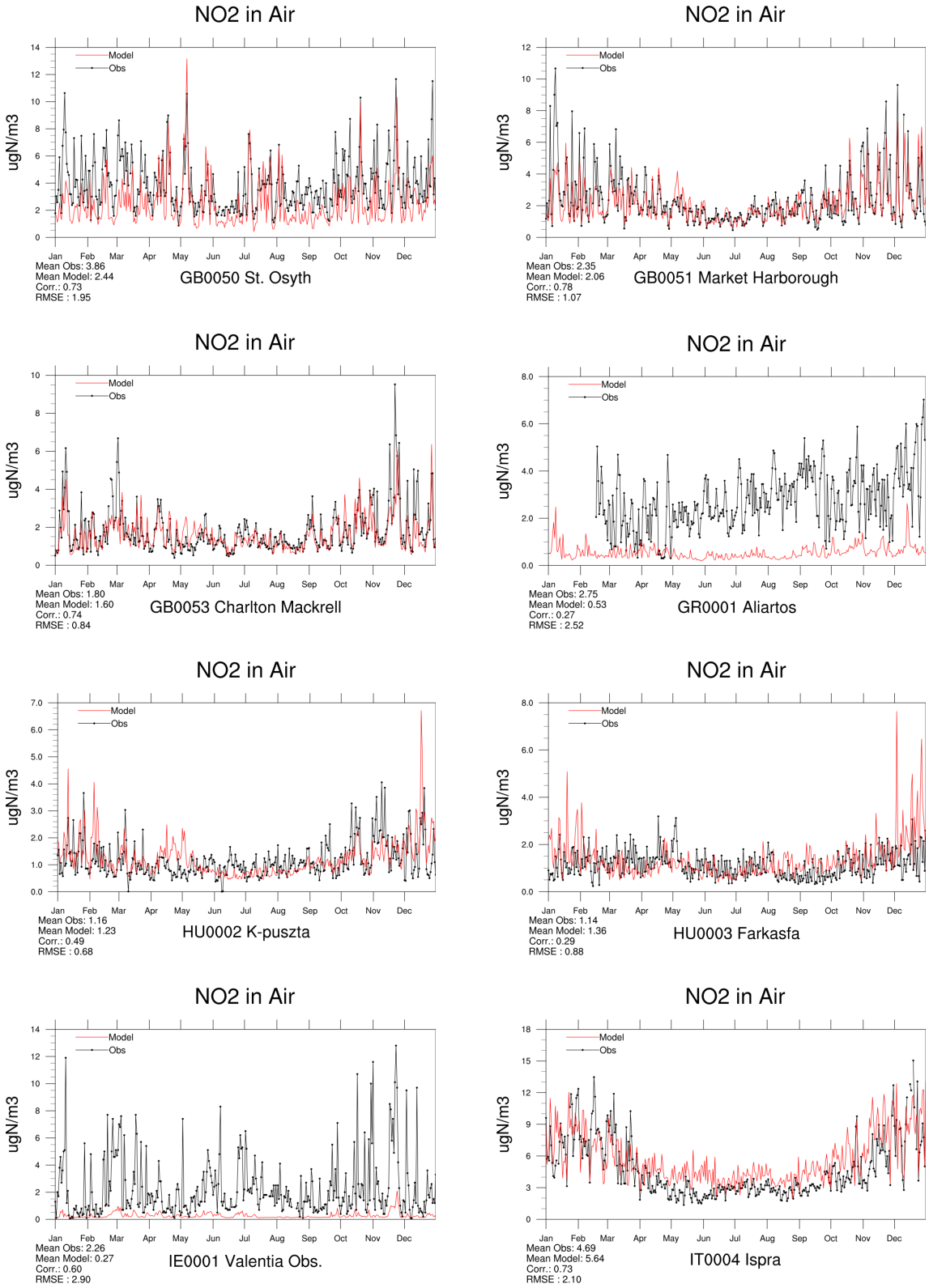

Figure 3.29: Modelled versus Observed Daily Mean NO_2 (μg(N) m^{-3}) for 2018.

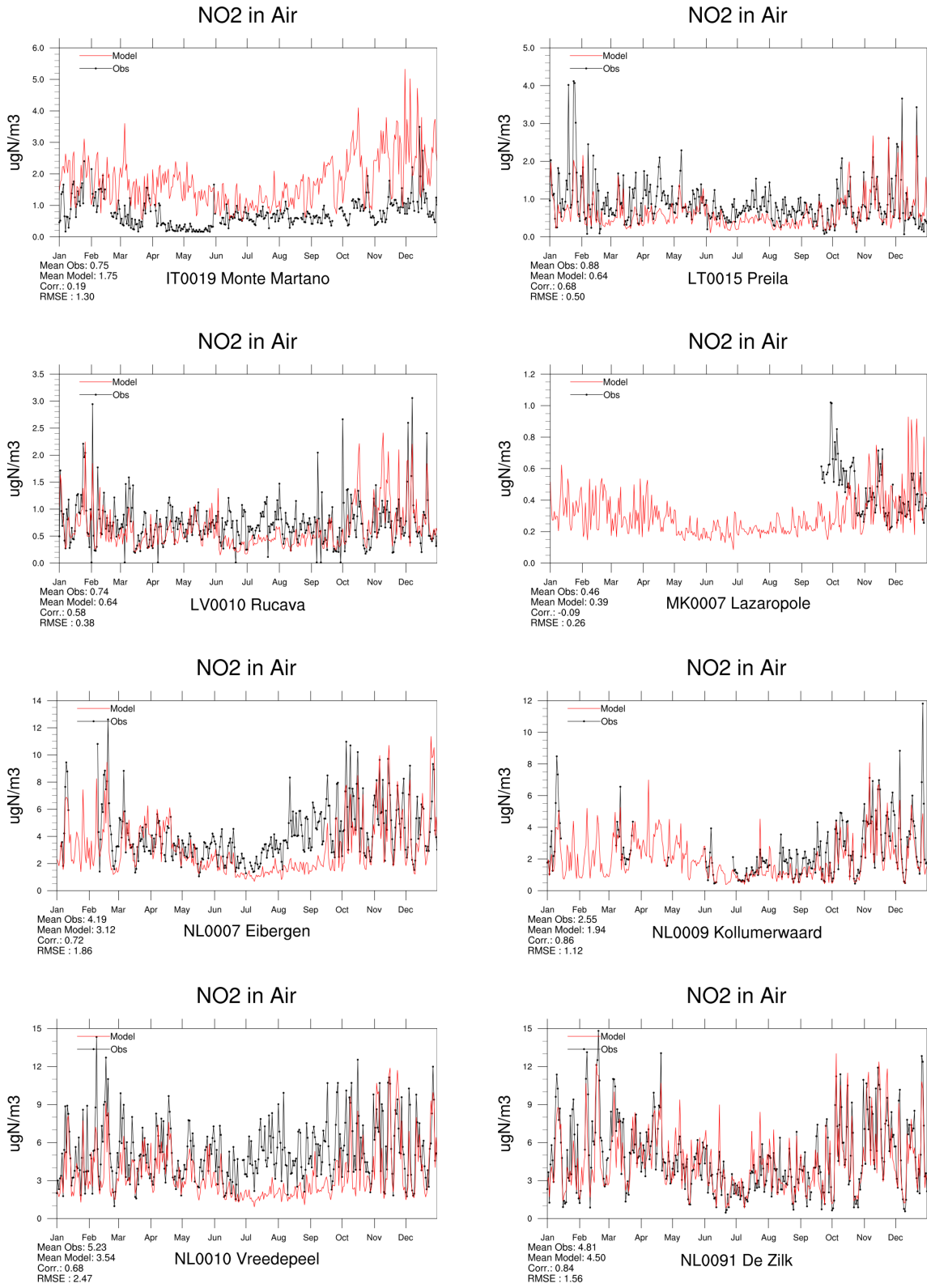

Figure 3.30: Modelled versus Observed Daily Mean NO_2 (μg(N) m^{-3}) for 2018.

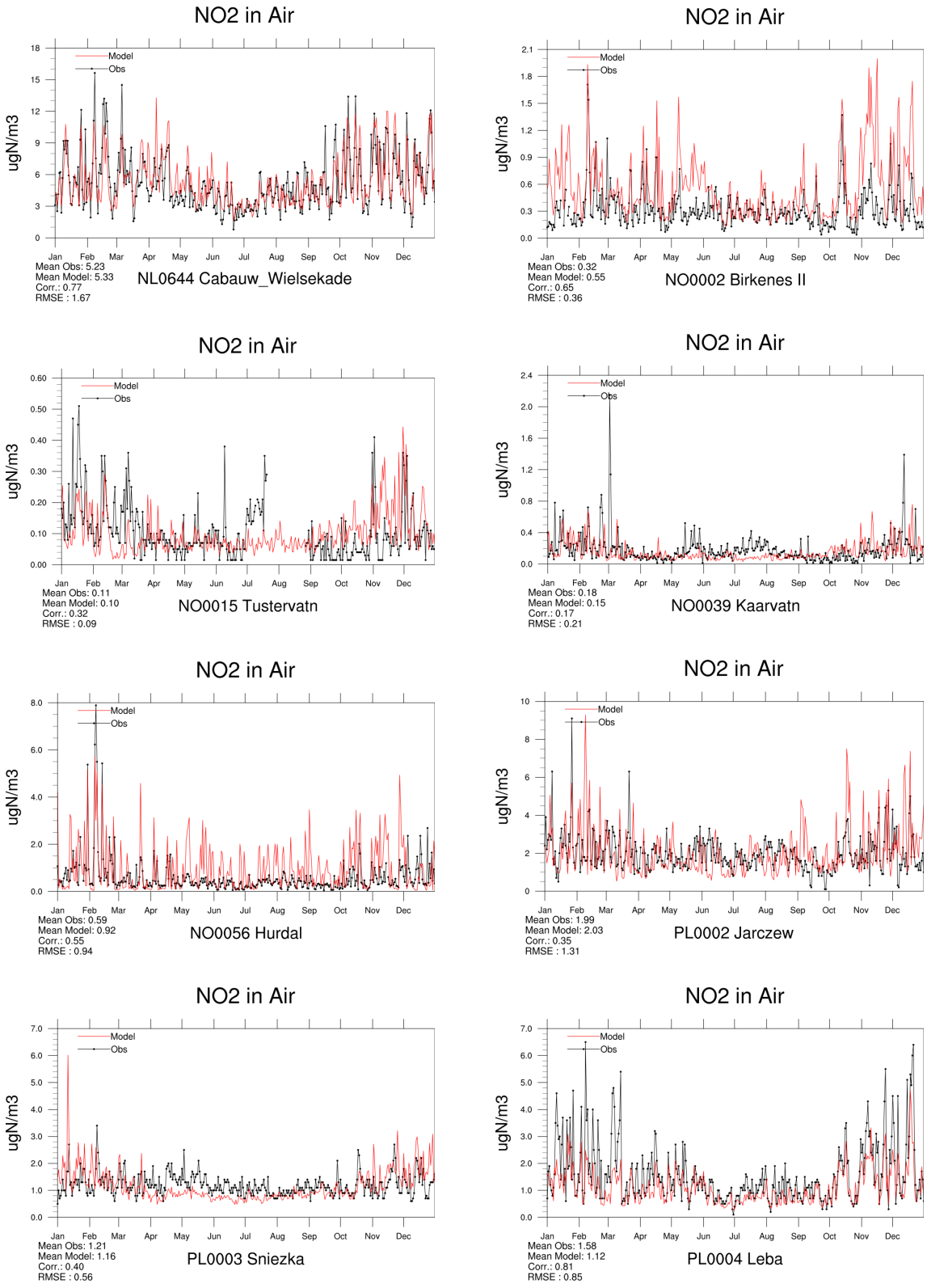

Figure 3.31: Modelled versus Observed Daily Mean NO_2 (μg(N) m^{-3}) for 2018.

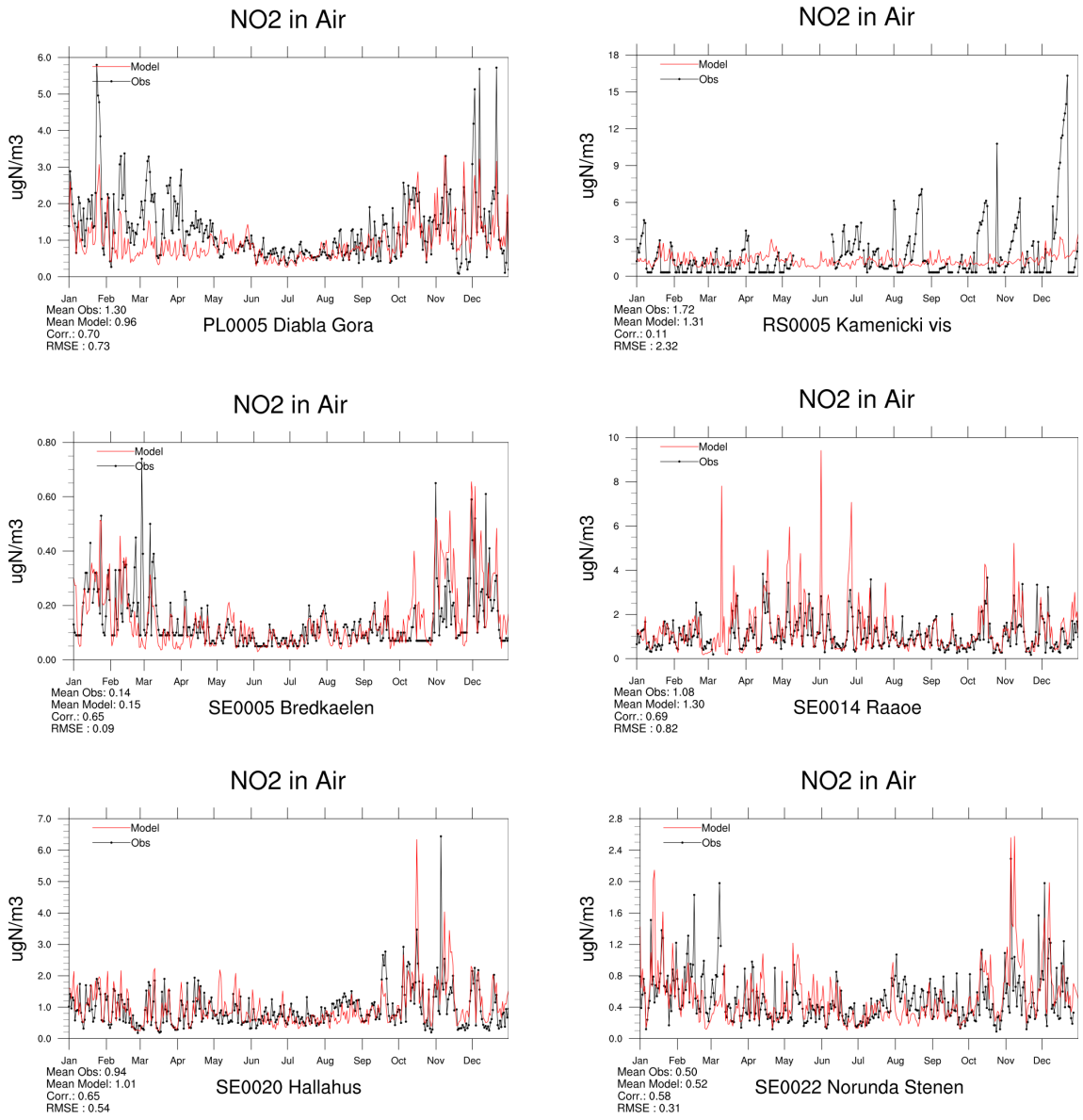

Figure 3.32: Modelled versus Observed Daily Mean NO_2 (μg(N) m^{-3}) for 2018.

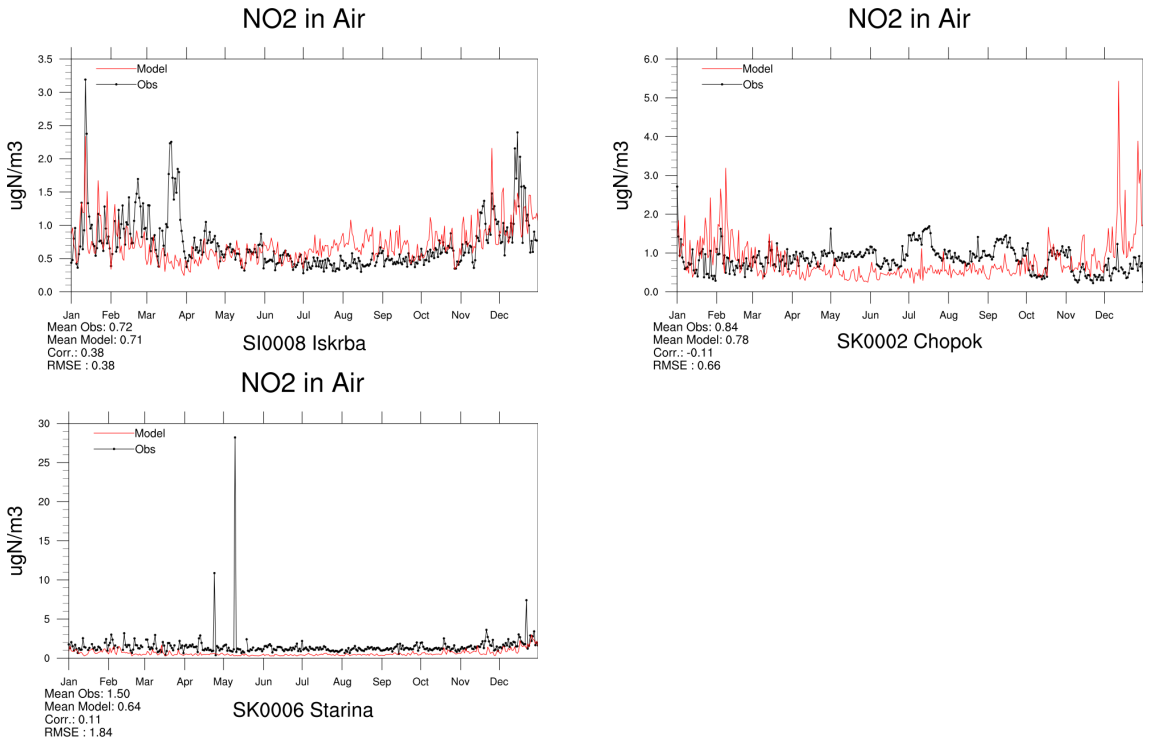

Figure 3.33: Modelled versus Observed Daily Mean NO_2 (μg(N) m^{-3}) for 2018.

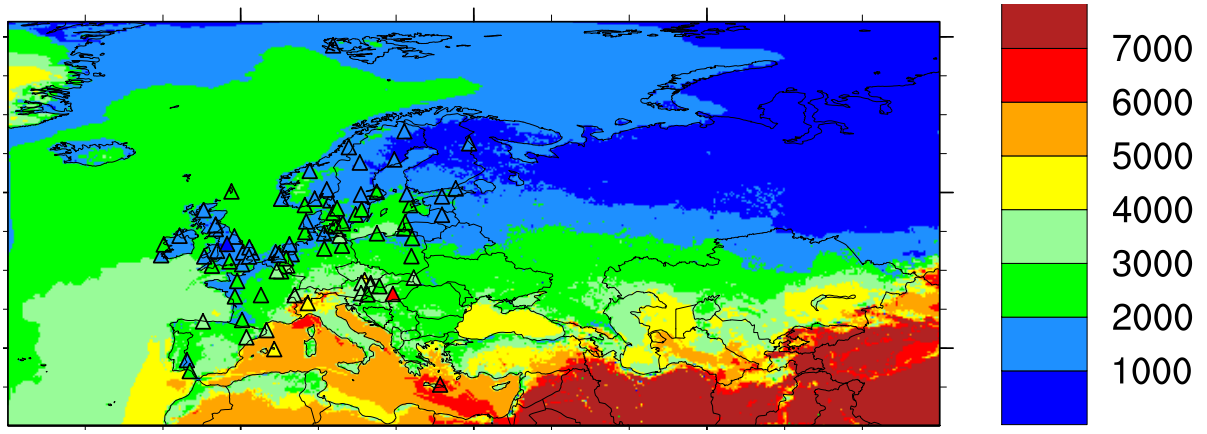

(a) SOMO35

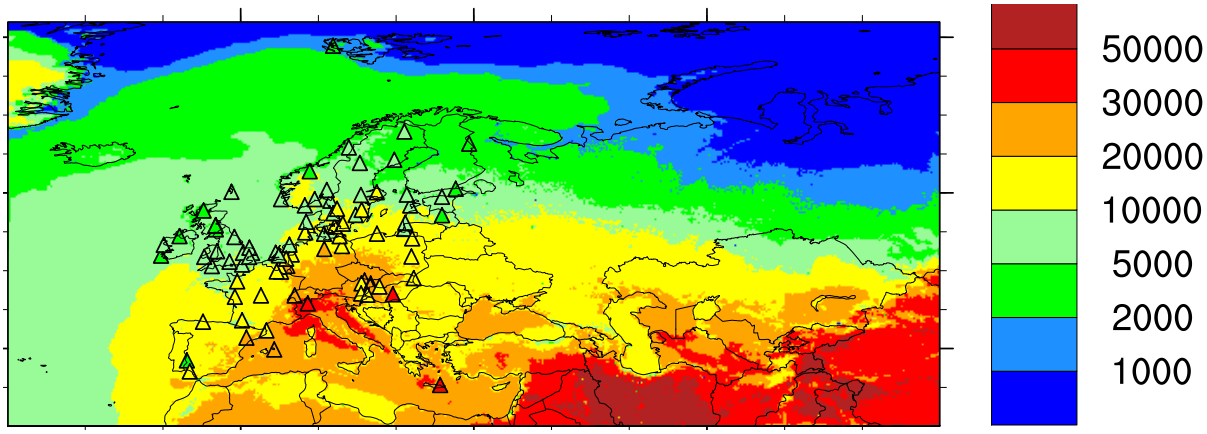

(b) AOT40

Figure 3.34: SOMO35 [ppb.days] and AOT40 [ppb.hours]. The maps show model results, with observations superimposed by triangles. The figure of daily maximum ozone covers the months of April to September only.

3.4 Combined maps of model results and observations

In Figure 3.34, maps of modeled SOMO35 and AOT40 are shown. Observations, taken from the EMEP network for 2018, are super-imposed with triangles. By and large, the plots show good agreement between model and observations also for this year.

References

M. Gauss, A.-G. Hjellbrekke, W. Aas, and S. Solberg. Ozone. Supplementary material to EMEP Status Report 1/2018, available online at www.emep.int, The Norwegian Meteorological Institute, Oslo, Norway, 2018.

M. Gauss, A.-G. Hjellbrekke, W. Aas, and S. Solberg. Ozone. Supplementary material to EMEP Status Report 1/2019, available online at www.emep.int, The Norwegian Meteorological Institute, Oslo, Norway, 2019.

CHAPTER 4

PM_{10}, $PM_{2.5}$ and individual aerosol components

This chapter presents an evaluation of the EMEP MSC-W model performance in terms of particulate matter. Tables of model skill are presented for the entire EMEP domain and timeseries plots are shown for individual EMEP measurement stations with daily PM measurements.

4.1 Scatter plots and tables

The yearly mean scatter plots in Figure 4.1 compares modelled PM with daily (upper panels) and hourly (lower panels) observations at EMEP stations that have provided data for 2018. The daily PM measurements were made with a gravimetric method, using high or low volume samplers and the sample weighing at 20°C and 50% relative humidity. Hourly PM concentrations were measured with automatic instruments (e.g. TEOM, beta gauge) using various approaches, but are generally corrected to comply with the gravimetric reference methods, in accordance to the European standard EN 16450:2017. The modelled $PM_{2.5}$ and PM_{10} concentrations include aerosol associated water at 20°C and 50% humidity and thus represent gravimetrically measured PM mass.

The lines on the scatter plots display deviations in the scatter of 30% ('30% line') and 50% ('50% line') relative bias, respectively. Relative bias is defined here as $\frac{Mod-Obs}{0.5\,(Mod+Obs)} \times 100\%$, where 'Mod' refers to yearly(hourly) averaged modelled concentrations, while 'Obs' refers to yearly(hourly) averaged measured concentrations.

Table 4.1 shows for PM and individual components:

- N_{stat} - the number of stations where daily measurements were available and data coverage criteria were satisfied
- Obs - measured yearly average over all stations
- Mod - modelled yearly average over all stations

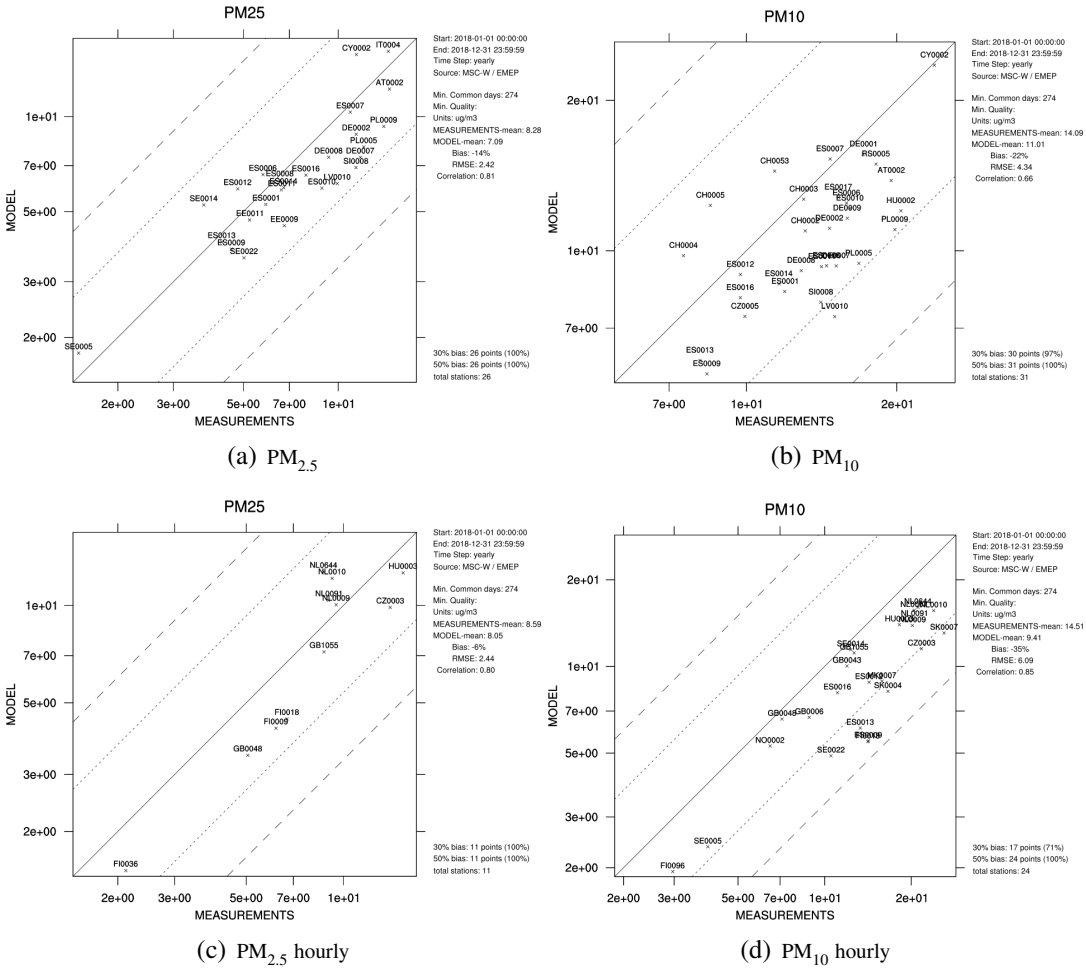

(a) $PM_{2.5}$ (b) PM_{10}

(c) $PM_{2.5}$ hourly (d) PM_{10} hourly

Figure 4.1: Scatter plots for 2018 of model results versus daily observations of a) $PM_{2.5}$ and b) PM_{10}, and hourly observations of c) $PM_{2.5}$ and d) PM_{10}. Unit: μg m^{-3} .

- Bias - relative bias in percent
- Corr - correlation between observation and model for station yearly averages
- RMSE - root mean square error
- IOA - index of agreement (as defined in Section 2.1).

On average, the model underestimates annual mean daily measured PM_{10} by 22% and $PM_{2.5}$ by 14% for 2018 (see also 4.1), while the biases were 22% and 19%, respectively, reported last year for 2017. The annual spatial correlations between model results and measurements are 0.66 for PM_{10} and 0.81 for $PM_{2.5}$ (0.76 and 0.81, respectively, reported last year for 2017). The differences in the model performance are partly due to model development, but also due to the different suites of monitoring sites with reported PM measurements, namely 31 and 26 in 2018 compared to 30 and 25 sites in 2017. Compared with hourly measurements, the model underestimates annual mean PM_{10} by 32% and $PM_{2.5}$ by 6%, and the spatial correlation between the model results and observed PM_{10} and $PM_{2.5}$ is 0.85 and 0.80 respectively.

Component	N_{stat}	Obs.	Mod.	Bias (%)	RMSE	Corr.	IOA
PM_{10} ($\mu g\ m^{-3}$)	31	14.09	11.01	-22	4.34	0.66	0.70
$PM_{2.5}$ ($\mu g\ m^{-3}$)	26	8.28	7.09	-14	2.42	0.81	0.87
SO_4^{2-}, including sea salt ($\mu g\ m^{-3}$)	33	1.41	0.86	-39	0.72	0.88	0.72
SO_4^{2-}, sea salt corrected ($\mu g\ m^{-3}$)	25	1.12	0.64	-42	0.70	0.85	0.69
SO_4^{2-} in PM_{10} ($\mu g\ m^{-3}$)	13	1.62	1.01	-37	0.70	0.91	0.85
NO_3^- ($\mu g\ m^{-3}$)	25	1.17	1.35	15	0.55	0.80	0.88
NO_3^- in PM_{10} ($\mu g\ m^{-3}$)	13	1.01	1.23	22	0.55	0.29	0.59
NO_3^- in $PM_{2.5}$ ($\mu g\ m^{-3}$) $\star$	7	1.87	2.06	11	0.546	0.91	0.93
NH_4^+ ($\mu g\ m^{-3}$)	26	0.65	0.55	-16	0.25	0.78	0.86
NH_4^+ in PM_{10} ($\mu g\ m^{-3}$) $\star$	3	1.37	1.45	6	0.22	0.79	0.49
NH_4^+ in $PM_{2.5}$ ($\mu g\ m^{-3}$) $\star$	7	1.12	0.90	-20	0.27	0.59	0.60
EC in PM_{10} (μg(C) m^{-3}) $\star$	3	0.36	0.39	8	0.09	0.48	0.66
EC in $PM_{2.5}$ (μg(C) m^{-3}) $\star$	12	0.35	0.44	24	0.17	0.89	0.84
OC in PM_{10} (μg(C) m^{-3}) $\star$	3	3.20	1.67	-48	1.84	-0.60	0.45
OC in $PM_{2.5}$ (μg(C) m^{-3}) $\star$	12	2.77	1.91	-31	1.53	0.26	0.53
Na+ ($\mu g\ m^{-3}$)	23	0.86	0.72	-16	0.64	0.85	0.87
Na+ in PM_{10} ($\mu g\ m^{-3}$)	6	0.42	0.25	-41	0.38	0.80	0.62
Na+ in $PM_{2.5}$ ($\mu g\ m^{-3}$) $\star$	8	0.11	0.15	41	0.12	0.80	0.70

Table 4.1: Comparison of model results and observations for 2018. Annual averages over all EMEP sites with measurements. N_{stat}= number of stations, wd=wet deposition, cp= concentration in precipitation, Corr. = spatial correlation coefficient, RMSE = root mean square error, IOA = index of agreement. The requirement for being included is that measurements be available for 75% of all days in 2018, except for the components marked with $\star$, where observational data covers the whole year of 2018, but with measurements 3-5 times a month.

The model performance statistics are overall better for $PM_{2.5}$ than for PM_{10}. This is because of a larger inaccuracy of simulation of the coarse fraction of the latter due to existing uncertainties in modelling natural PM components (e.g. sea salt and windblown mineral dust) and secondary aerosol formation of those, as well as due to some unaccounted for coarse PM (e.g. biogenic organic aerosol, agricultural and resuspension dust), whereas the contribution of natural particles in $PM_{2.5}$ is relatively smaller. Also, PPM emissions in the coarse fraction are likely more uncertain (fugitive dust, production processes, etc.).

On an annual basis, the model shows quite variable performance for the individual aerosol components. Calculated SO_4^{2-} is underestimated by 39% compared to observations. The model overestimates total NO_3^- by 15%, NO_3^- in PM_{10} by 5% (only 3 sites), and NO_3^- in $PM_{2.5}$ by 11% (note that the suites of sites are not the same).

NH_4^+, which in the model consists of fine aerosol, is understimated by 16% against total ammonium data (e.g. sampling without size cut-off). NH_4^+ in PM_{10} is overestimated by 6% (only 3 sites), and NH_4^+ in $PM_{2.5}$ is underestimated by 20% (also here the sites are not the same).

Modelled elemental carbon (EC) in $PM_{2.5}$ is overestimated by 24% on an annual basis, while organic carbon (OC) in $PM_{2.5}$ is underestimated by 31%. The corresponding values for EC and OC in PM_{10} are 8 and -48% respectively, but it has to be noted that these scores are based on only 3 stations.

Tables 4.2 to 4.7 show model performance for PM_{10} and $PM_{2.5}$ against daily, hourly and weekly observations at individual stations. The statistics reveal significant variability in the model ability to reproduce the observed concentrations at different locations. For most of the sites with daily observations, the bias varies between -30 and +30% (24 out of 36 for PM_{10} and 21 out of 32 for $PM_{2.5}$). The temporal correlation is mostly between 0.5 and 0.7 (at 21 sites for PM_{10} and 15 sites for $PM_{2.5}$). Compared with daily averages of PM_{10} hourly observations, the model underestimates by over 30% at relatively more sites.

It can also be noted that for both PM_{10} and $PM_{2.5}$ from hourly observations, the correlation is generally better than for daily observations. This, of course, can also be due to the fact that the sets of sites available for hourly and daily observations are different.

Table 4.2: Statistical analysis of model calculated PM_{10} against **daily** observations in 2018. Obs: measured mean, Mod: calculated mean, Bias: calculated as (Mod-Obs)/Obs x100%, R: temporal correlation coefficient, and RMSE: root mean square error.

Site	Name	Obs	Mod	Bias	R	RMSE	IOA
AT0002	Illmitz	19.49	13.82	-29.0	0.66	10.16	0.73
AT0005	Vorhegg	7.67	7.83	2.0	0.05	18.68	0.14
AT0048	Zoebelboden	8.35	8.52	2.0	0.29	7.93	0.58
CH0002	Payerne	13.12	10.96	-16.0	0.68	6.40	0.80
CH0003	Taenikon	13.02	12.68	-3.0	0.66	6.62	0.81
CH0004	Chaumont	7.48	9.78	31.0	0.52	6.55	0.69
CH0005	Rigi	8.47	12.32	45.0	0.53	8.83	0.65
CY0002	Ayia Marina	23.80	23.52	-1.0	0.44	22.85	0.62
CZ0005	Churanov	9.93	7.39	-26.0	0.48	6.82	0.65
DE0001	Westerland/Wenningsted	17.13	15.60	-9.0	0.63	8.36	0.78
DE0002	Langenbruegge/Waldhof	14.67	11.09	-24.0	0.62	7.85	0.74
DE0003	Schauinsland	11.55	9.29	-20.0	0.32	9.19	0.56
DE0007	Neuglobsow	15.13	9.32	-38.0	0.63	9.43	0.67
DE0008	Schmuecke	12.88	9.12	-29.0	0.33	9.18	0.56
DE0009	Zingst	15.92	11.61	-27.0	0.49	10.78	0.64
ES0001	Toledo	11.93	8.29	-31.0	0.68	10.78	0.79
ES0005	Noia	8.18	9.05	11.0	0.62	5.58	0.77
ES0006	Mahon	15.87	12.46	-21.0	0.48	9.12	0.60
ES0007	Viznar	14.71	15.26	4.0	0.70	13.28	0.78
ES0008	Niembro	14.47	9.33	-36.0	0.36	11.40	0.56
ES0009	Campisabalos	8.33	5.67	-32.0	0.67	7.17	0.79
ES0010	Cabo de Creus	16.13	12.16	-25.0	0.47	8.16	0.63
ES0011	Barcarrota	14.14	9.29	-34.0	0.66	10.19	0.77
ES0012	Zarra	9.73	8.96	-8.0	0.65	7.78	0.73
ES0013	Penausende	8.07	6.03	-25.0	0.68	6.76	0.80
ES0014	Els Torms	11.62	8.58	-26.0	0.58	7.19	0.72
ES0016	O Savinao	9.72	8.05	-17.0	0.67	5.27	0.80
ES0017	DoÃśana	15.29	12.79	-16.0	0.59	9.41	0.72
HR0002	Puntijarka	13.42	15.16	13.0	0.14	13.97	0.41
HU0002	K-puszta	20.39	12.02	-41.0	0.65	11.77	0.66
IT0019	Monte Martano	11.29	10.24	-9.0	0.29	9.01	0.55
LV0010	Rucava	15.03	7.38	-51.0	0.48	11.54	0.59
PL0005	Diabla Gora	16.80	9.43	-44.0	0.64	10.73	0.68
PL0009	Zielonka	19.83	11.02	-44.0	0.70	12.63	0.69
RS0005	Kamenicki vis	18.18	14.91	-18.0	0.49	9.33	0.67
SI0008	Iskrba	14.09	7.89	-44.0	0.48	9.48	0.59

Table 4.3: Statistical analysis of model calculated $PM_{2.5}$ against **daily** observations in 2018. Obs: measured mean, Mod: calculated mean, Bias: calculated as (Mod-Obs)/Obs x100%, R: temporal correlation coefficient, and RMSE: root mean square error.

Site	Name	Obs	Mod	Bias	R	RMSE	IOA
AT0002	Illmitz	14.53	12.23	-16.0	0.70	7.67	0.80
CH0002	Payerne	10.16	10.31	1.0	0.74	5.44	0.86
CH0005	Rigi	6.08	10.68	76.0	0.58	7.77	0.62
CY0002	Ayia Marina	11.42	15.73	38.0	0.54	10.02	0.63
DE0002	Langenbruegge/Waldhof	11.40	8.79	-23.0	0.68	6.57	0.79
DE0003	Schauinsland	9.53	7.98	-16.0	0.23	8.66	0.49
DE0007	Neuglobsow	11.76	7.43	-37.0	0.70	7.60	0.73
DE0008	Schmuecke	9.32	7.43	-20.0	0.44	6.68	0.65
EE0009	Lahemaa	6.75	4.52	-33.0	0.55	4.56	0.68
EE0011	Vilsandy	5.23	4.71	-10.0	0.62	4.20	0.78
ES0001	Toledo	5.89	5.27	-11.0	0.65	5.50	0.74
ES0006	Mahon	5.77	6.55	14.0	0.44	4.66	0.53
ES0007	Viznar	10.92	10.33	-5.0	0.69	7.52	0.82
ES0008	Niembro	6.53	6.30	-4.0	0.48	5.76	0.66
ES0009	Campisabalos	4.58	3.81	-17.0	0.56	3.87	0.72
ES0010	Cabo de Creus	8.88	5.93	-33.0	0.43	5.39	0.61
ES0011	Barcarrota	6.60	5.86	-11.0	0.58	5.55	0.73
ES0012	Zarra	4.80	5.91	23.0	0.72	4.28	0.71
ES0013	Penausende	4.27	4.01	-6.0	0.57	3.86	0.73
ES0014	Els Torms	6.71	5.96	-11.0	0.68	3.58	0.80
ES0016	O Savinao	7.90	6.53	-17.0	0.72	4.15	0.82
HR0002	Puntijarka	7.35	13.51	84.0	0.06	13.53	0.28
HU0002	K-puszta	11.83	9.82	-17.0	0.74	6.74	0.81
IT0004	Ispra	14.42	16.10	12.0	0.73	8.61	0.85
IT0019	Monte Martano	7.41	8.49	15.0	0.21	6.60	0.48
LV0010	Rucava	9.93	6.14	-38.0	0.66	6.93	0.72
PL0005	Diabla Gora	12.05	8.02	-33.0	0.72	7.26	0.77
PL0009	Zielonka	13.95	9.31	-33.0	0.71	8.22	0.77
SE0005	Bredkaelen	1.50	1.78	19.0	0.48	1.44	0.66
SE0014	Raaoe	3.75	5.25	40.0	0.46	4.70	0.62
SE0022	Norunda Stenen	5.02	3.57	-29.0	0.61	3.42	0.74
SI0008	Iskrba	11.38	6.90	-39.0	0.49	7.95	0.60

Table 4.4: Statistical analysis of model calculated PM_{10} against **hourly** observations in 2018. Obs: measured mean, Mod: calculated mean, Bias: calculated as (Mod-Obs)/Obs x100%, R: temporal correlation coefficient, and RMSE: root mean square error.

Site	Name	Obs	Mod	Bias	R	RMSE	IOA
CZ0003	Kosetice	22.63	11.52	-49.0	0.67	14.98	0.60
ES0009	Campisabalos	11.77	5.71	-51.0	0.72	9.72	0.76
ES0012	Zarra	12.67	8.91	-30.0	0.67	8.43	0.75
ES0013	Penausende	12.15	6.08	-50.0	0.68	9.66	0.73
ES0016	O Savinao	9.12	8.15	-11.0	0.68	4.73	0.80
FI0018	Virolahti III	13.87	5.47	-61.0	0.27	13.31	0.47
FI0096	Pallas	3.07	1.94	-37.0	0.24	3.27	0.47
GB0006	Lough Navar	7.58	6.59	-13.0	0.66	3.78	0.80
GB0043	Narberth	11.92	10.04	-16.0	0.55	5.75	0.72
GB0048	Auchencorth Moss	6.99	6.56	-6.0	0.48	4.72	0.69
GB1055	Chilbolton Observatory	12.27	11.09	-10.0	0.64	5.56	0.78
GR0001	Aliartos	25.40	10.40	-59.0	0.40	21.17	0.50
HU0003	Farkasfa	18.09	13.96	-23.0	0.52	10.50	0.68
MK0007	Lazaropole	12.29	8.80	-28.0	0.41	11.15	0.62
NL0007	Eibergen	18.76	15.62	-17.0	0.56	8.97	0.72
NL0009	Kollumerwaard	18.17	13.88	-24.0	0.71	8.38	0.79
NL0010	Vreedepeel	21.55	15.63	-27.0	0.55	11.07	0.68
NL0091	De Zilk	16.93	14.66	-13.0	0.65	7.10	0.78
NL0644	Cabauw Wielsekade	17.68	16.06	-9.0	0.65	7.40	0.79
NO0002	Birkenes II	5.55	5.28	-5.0	0.67	3.59	0.80
SE0005	Bredkaelen	3.87	2.36	-39.0	0.49	3.52	0.59
SE0014	Raaoe	12.57	11.59	-8.0	0.67	6.43	0.81
SE0022	Norunda Stenen	10.64	4.85	-54.0	0.39	7.93	0.53
SK0004	Stara Lesna	15.46	8.29	-46.0	0.44	10.43	0.56
SK0007	Topolniky	25.72	12.97	-50.0	0.74	15.50	0.63

Table 4.5: Statistical analysis of model calculated $PM_{2.5}$ against **hourly** observations in 2018. Obs: measured mean, Mod: calculated mean, Bias: calculated as (Mod-Obs)/Obs x100%, R: temporal correlation coefficient, and RMSE: root mean square error.

Site	Name	Obs	Mod	Bias	R	RMSE	IOA
CZ0003	Kosetice	14.57	9.87	-32.0	0.71	7.74	0.74
FI0009	Utoe	5.57	4.15	-25.0	0.69	3.46	0.80
FI0018	Virolahti III	6.50	4.45	-32.0	0.59	4.05	0.70
FI0036	Matorova	2.03	1.51	-26.0	0.44	2.29	0.55
GB0048	Auchencorth Moss	5.03	3.45	-31.0	0.61	3.61	0.73
GB1055	Chilbolton Observatory	8.66	7.22	-17.0	0.71	4.93	0.83
GR0001	Aliartos	12.20	7.28	-40.0	0.24	8.60	0.49
HU0003	Farkasfa	15.29	12.59	-18.0	0.52	9.57	0.69
NL0009	Kollumerwaard	9.89	10.04	2.0	0.77	5.81	0.87
NL0010	Vreedepeel	12.13	12.03	-1.0	0.71	6.17	0.84
NL0091	De Zilk	10.37	10.37	0.0	0.73	5.94	0.85
NL0644	Cabauw Wielsekade	11.18	12.66	13.0	0.74	6.18	0.85

Table 4.6: Statistical analysis of model calculated PM_{10} against **weekly** observations in 2018. Obs: measured mean, Mod: calculated mean, Bias: calculated as (Mod-Obs)/Obs x100%, R: temporal correlation coefficient, and RMSE: root mean square error.

Site	Name	Obs	Mod	Bias	R	RMSE	IOA
NO0002	Birkenes II	5.53	5.40	-2.0	0.20	4.21	0.47
NO0039	Kaarvatn	3.21	1.87	-42.0	0.67	2.56	0.63
NO0056	Hurdal	4.93	3.97	-19.0	0.66	2.44	0.77

Table 4.7: Statistical analysis of model calculated $PM_{2.5}$ against **weekly** observations in 2018. Obs: measured mean, Mod: calculated mean, Bias: calculated as (Mod-Obs)/Obs x100%, R: temporal correlation coefficient, and RMSE: root mean square error.

Site	Name	Obs	Mod	Bias	R	RMSE	IOA
NO0002	Birkenes II	3.05	3.32	9.0	0.17	2.76	0.50
NO0039	Kaarvatn	2.26	1.38	-39.0	0.68	2.09	0.59
NO0056	Hurdal	3.24	3.14	-3.0	0.75	1.43	0.85

4.2 Time series

In this section we present time series plots for a selection of stations that have supplied data on particulate matter to EMEP CCC for 2018. All the site reported PM observations for 2018 are shown here, disregarding the data coverage.

A comprehensive discussion of model performance at individual stations is not given here, but for reference, the following time series plots are shown:

The following time series plots, supplemented with the values of modelled and observed mean, correlation and RMSE, are shown:

- Figures 4.2–4.5: $PM_{2.5}$ daily measurements
- Figures 4.6–4.10: PM_{10} daily measurements

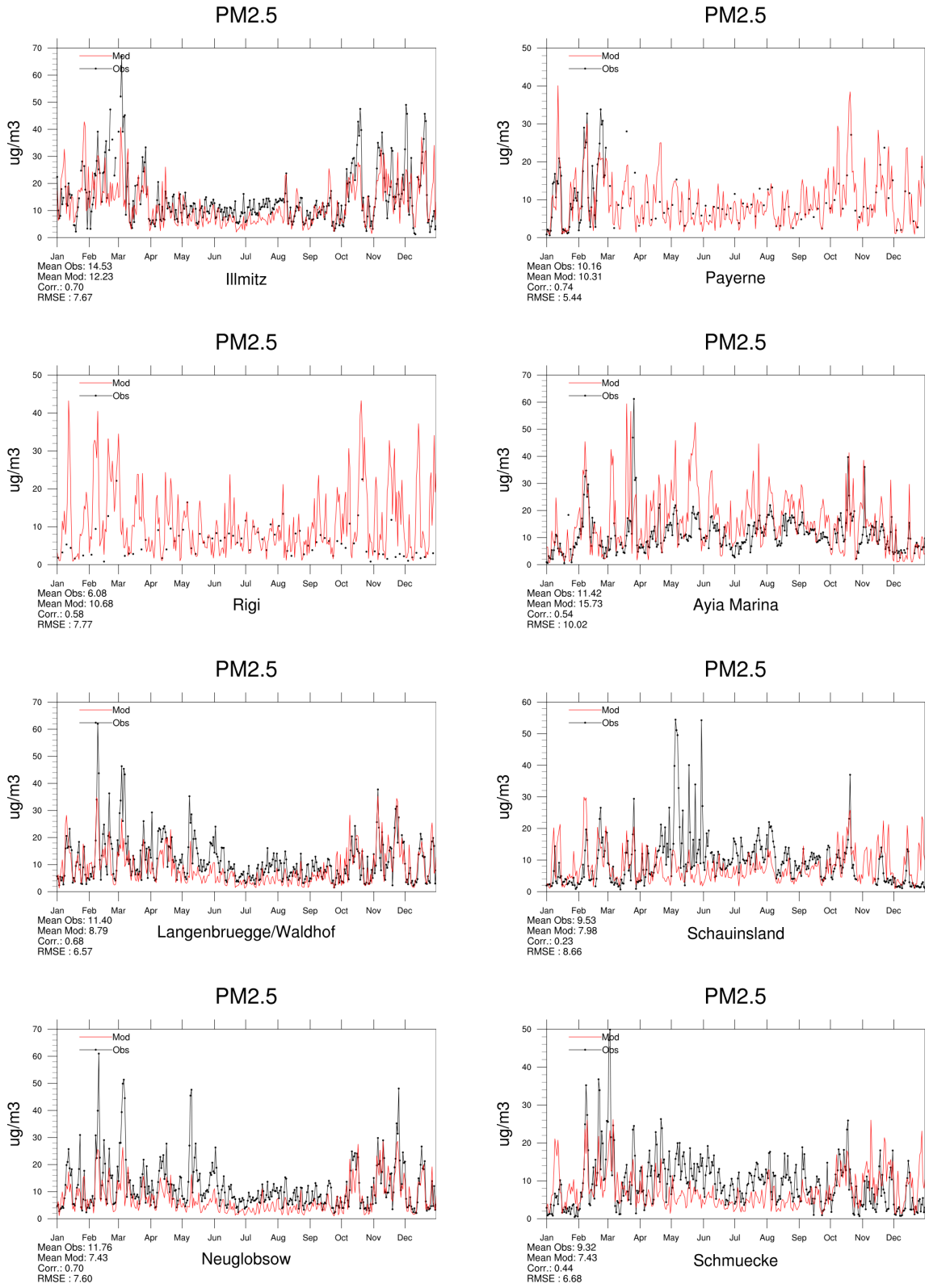

Figure 4.2: Modelled versus Observed Daily $PM_{2.5}$ [μg m^{-3}] in 2018.

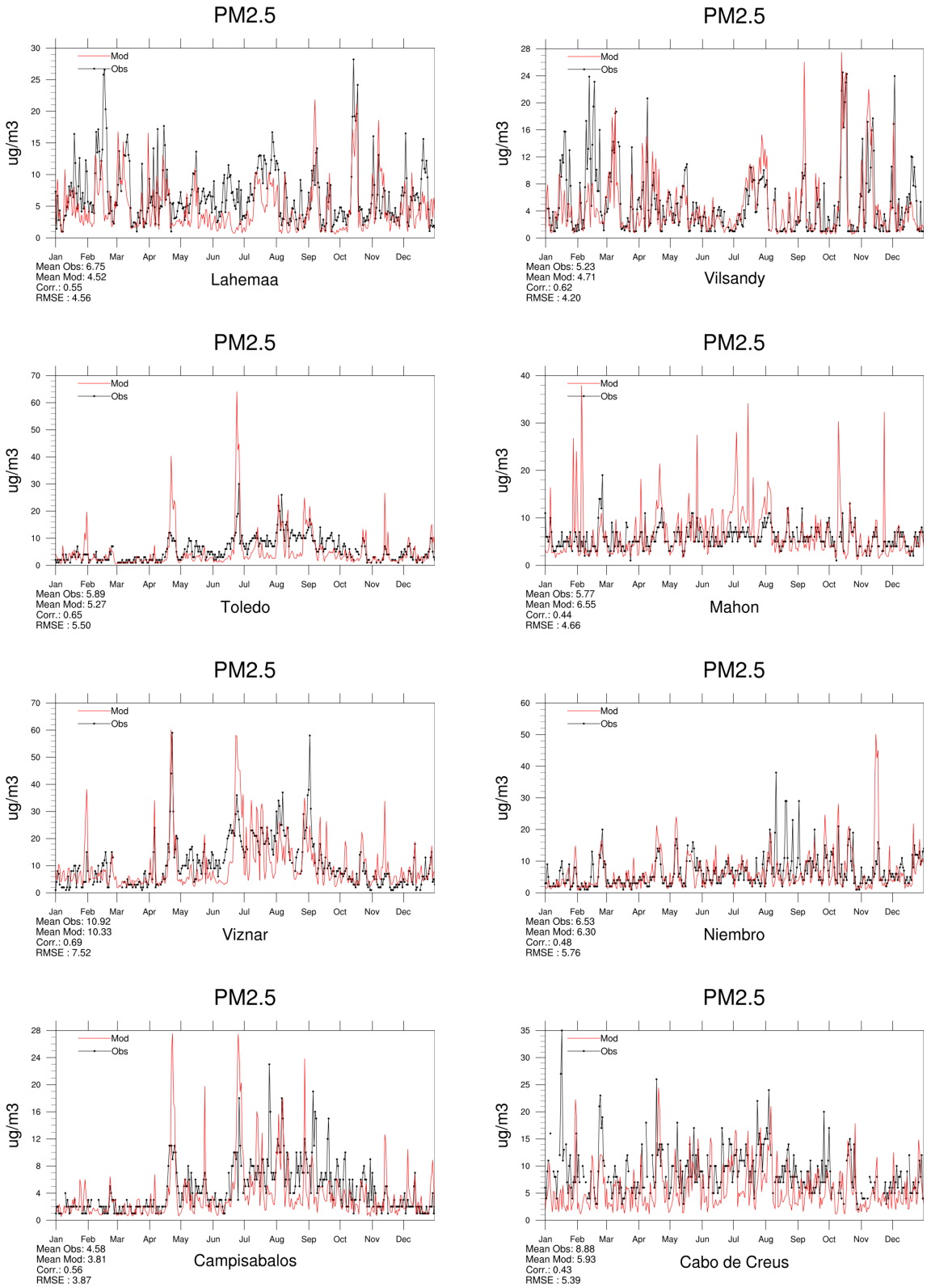

Figure 4.3: Modelled versus Observed Daily $PM_{2.5}$ [μg m^{-3}] in 2018.

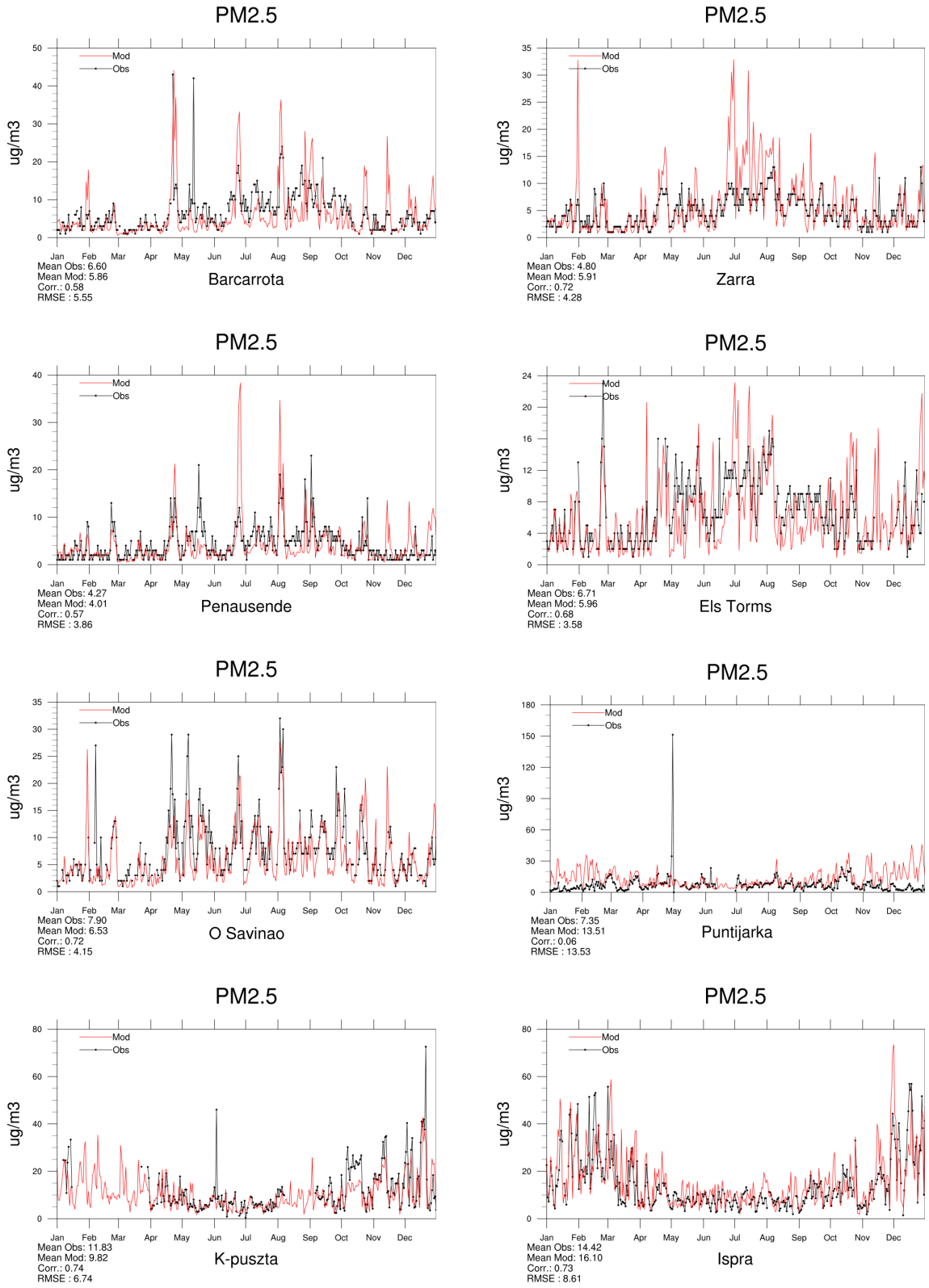

Figure 4.4: Modelled versus Observed Daily $PM_{2.5}$ [μg m^{-3}] in 2018.

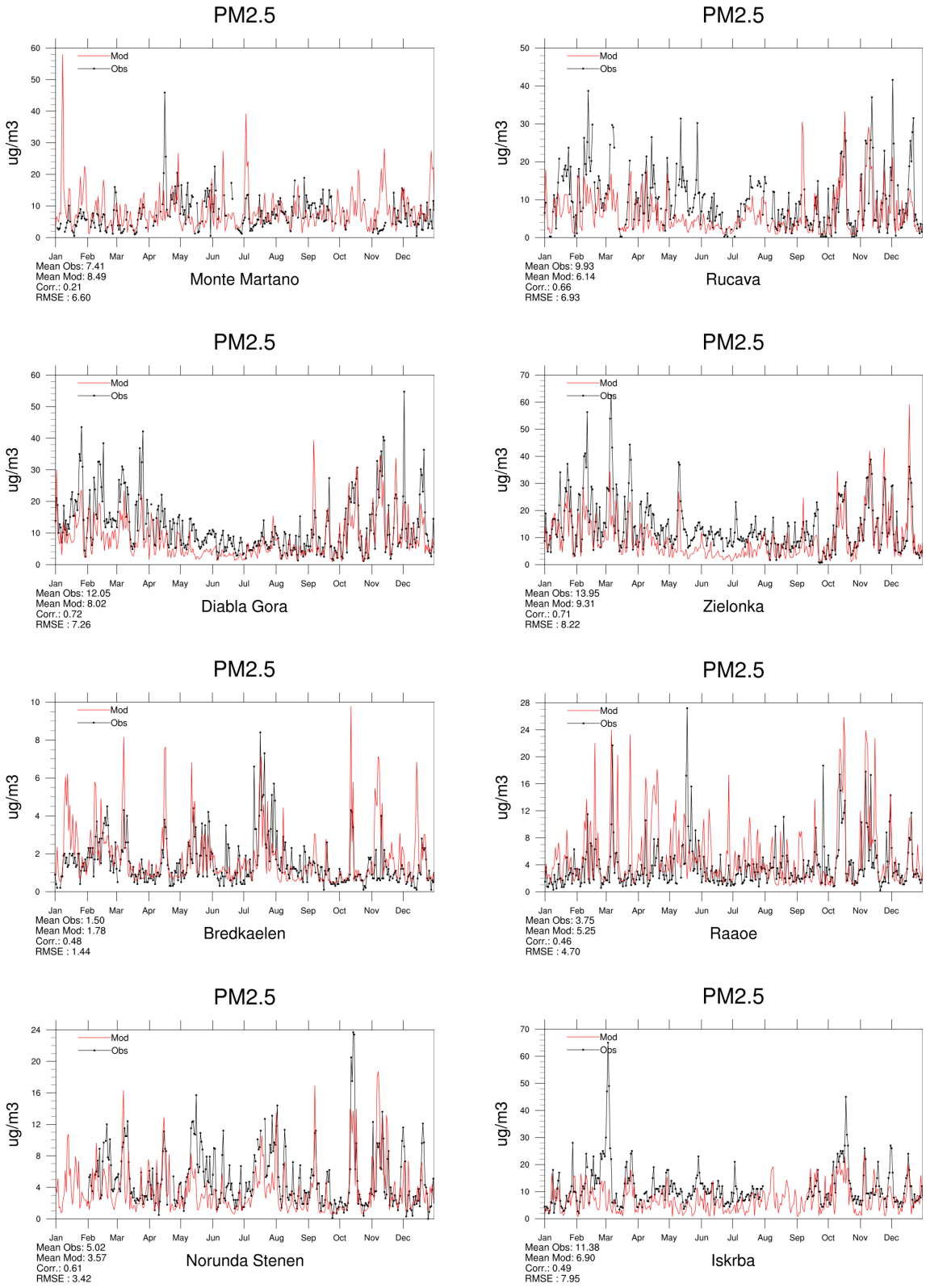

Figure 4.5: Modelled versus Observed Daily $PM_{2.5}$ [μg m^{-3}] in 2018.

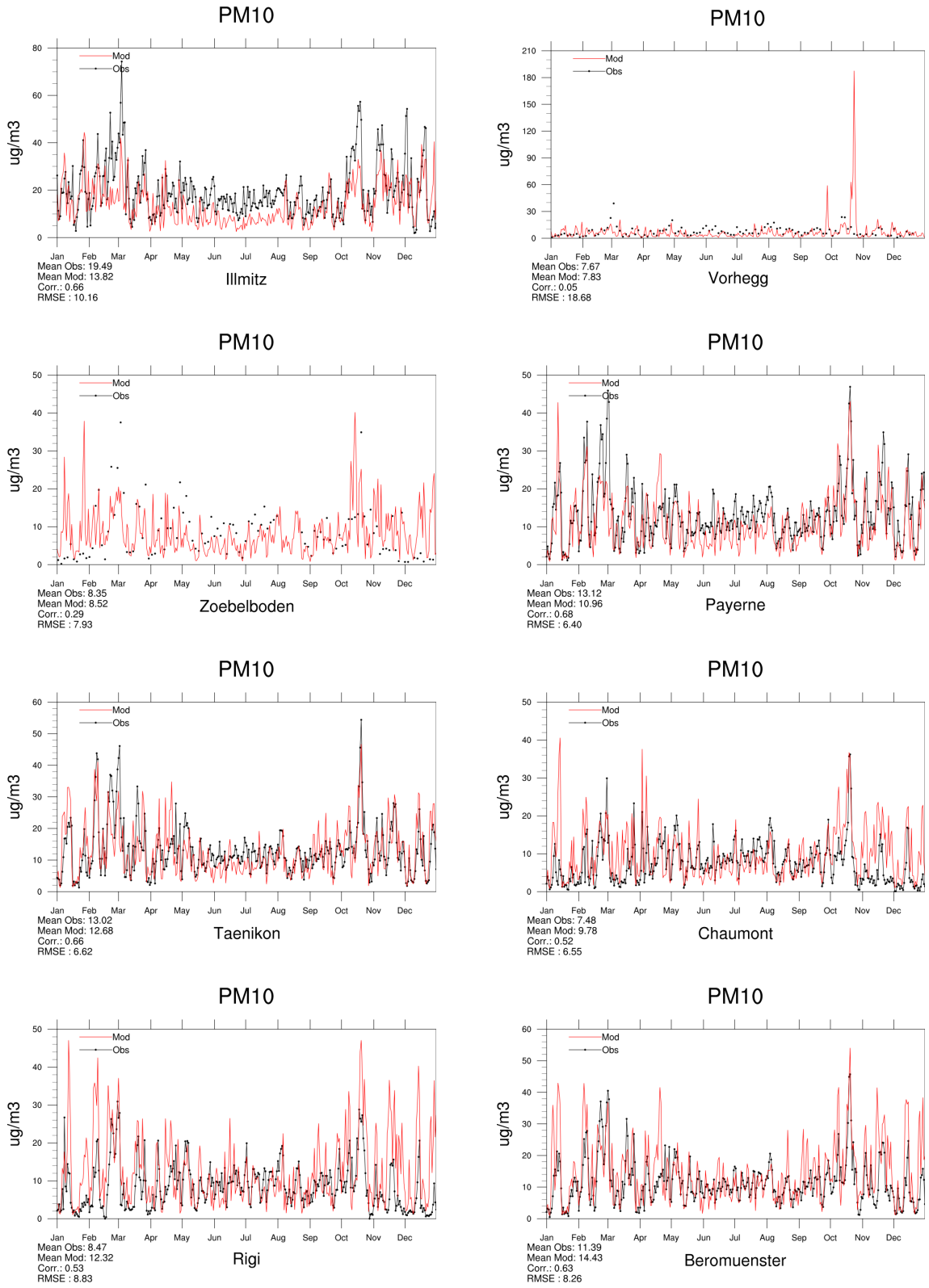

Figure 4.6: Modelled versus Observed Daily PM_{10} [μg m^{-3}] in 2018.

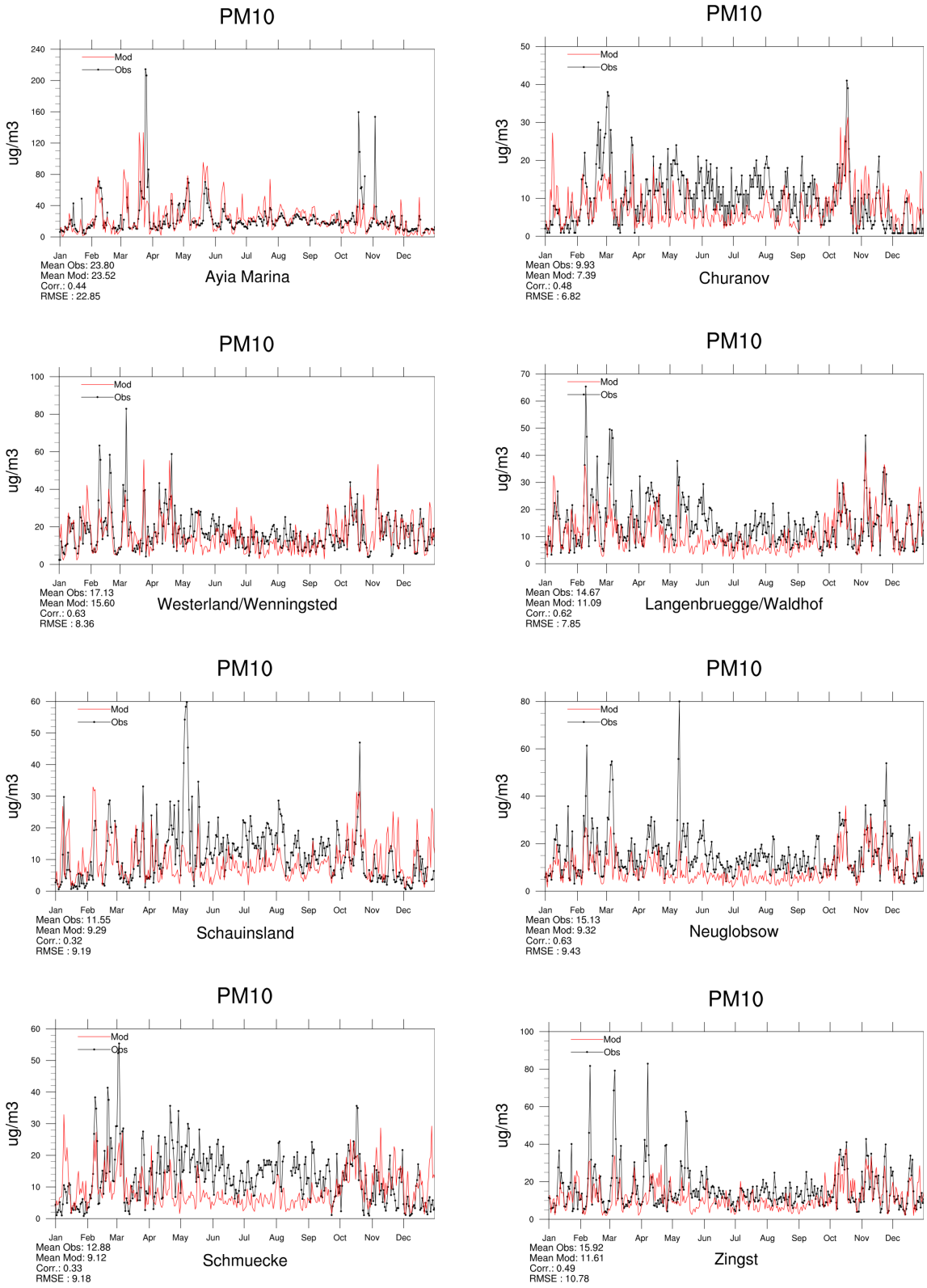

Figure 4.7: Modelled versus Observed Daily PM_{10} [μg m^{-3}] in 2018.

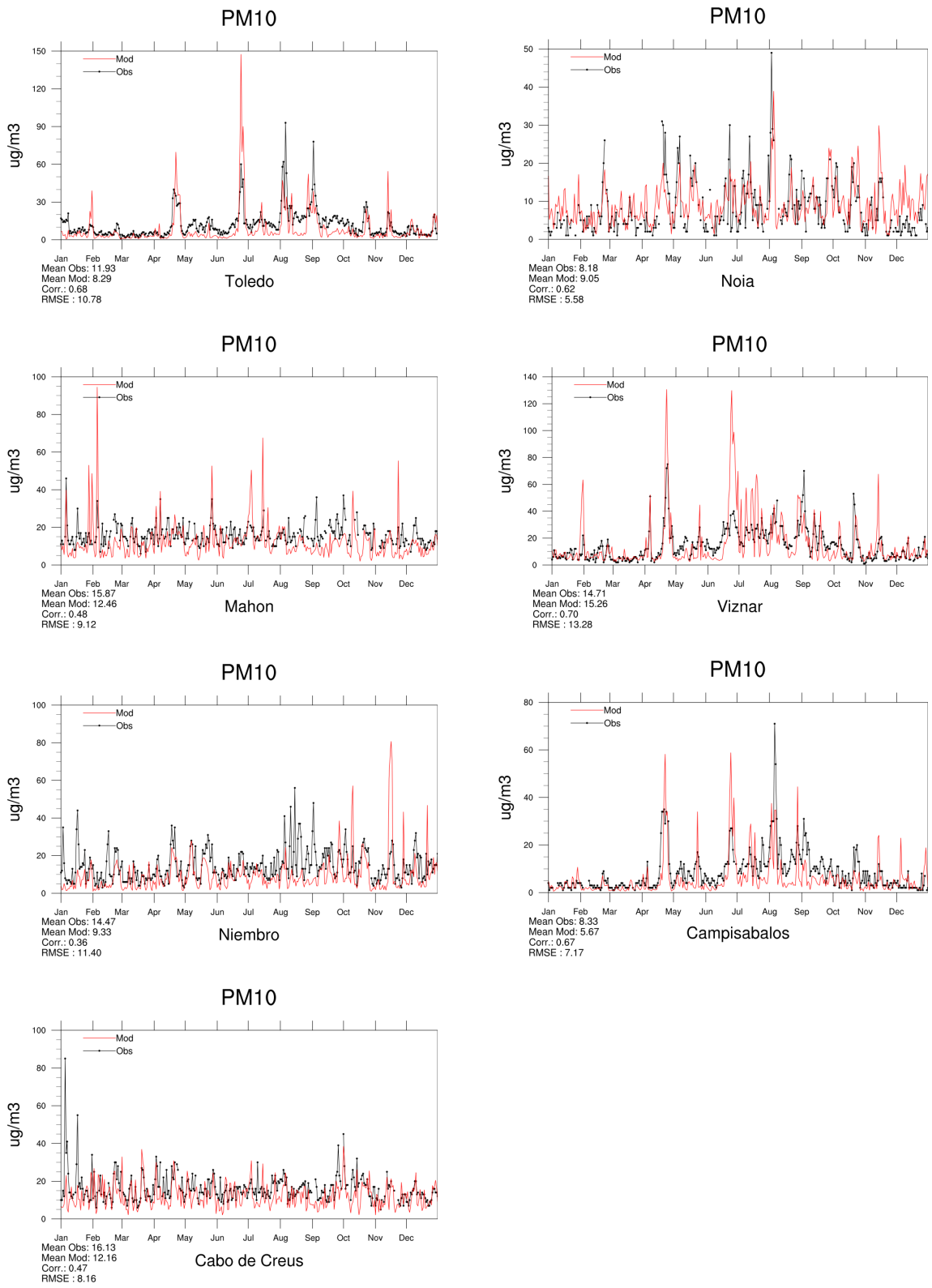

Figure 4.8: Modelled versus Observed Daily PM_{10} [μg m^{-3}] in 2018.

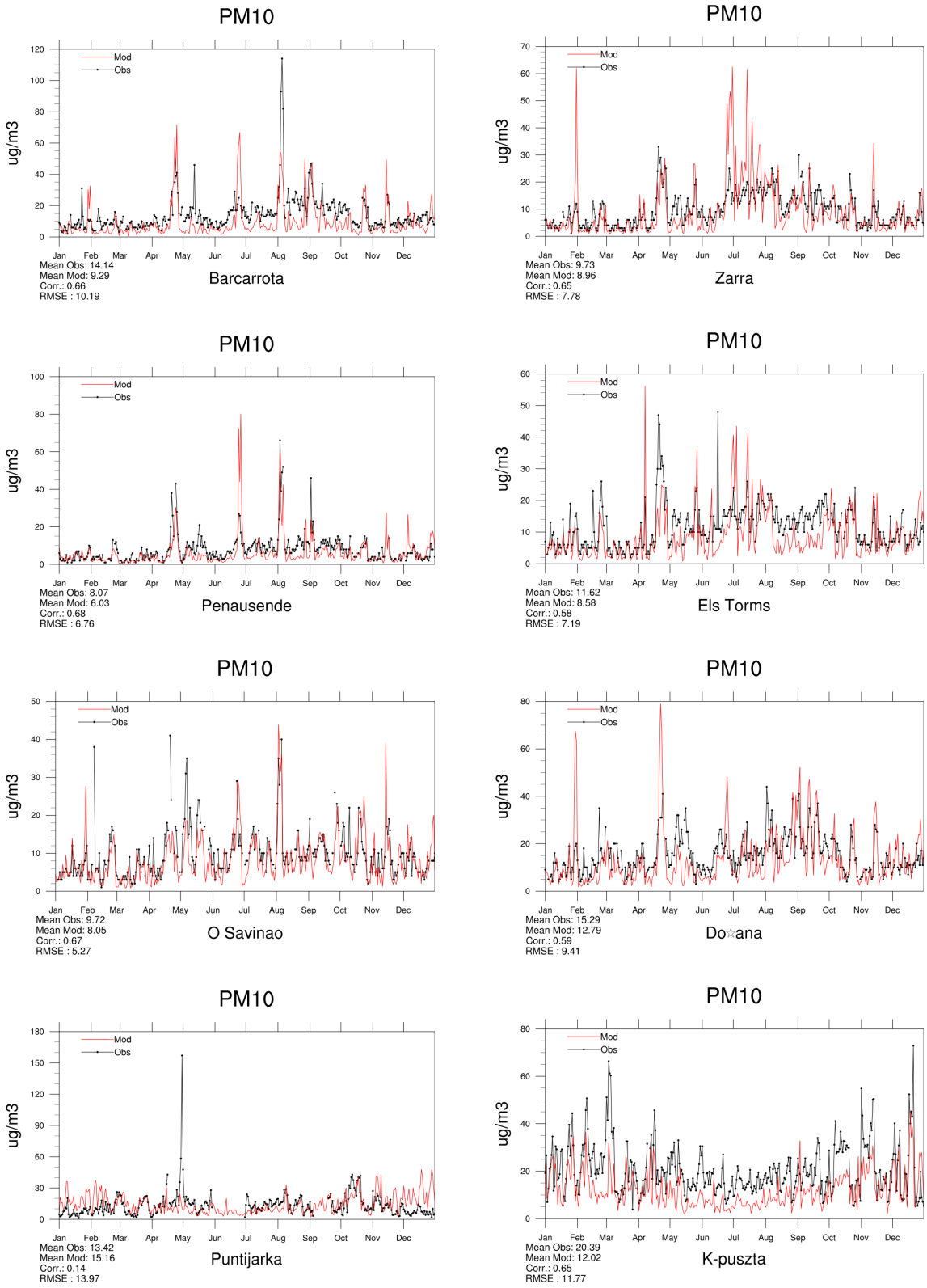

Figure 4.9: Modelled versus Observed Daily PM_{10} [μg m^{-3}] in 2018.

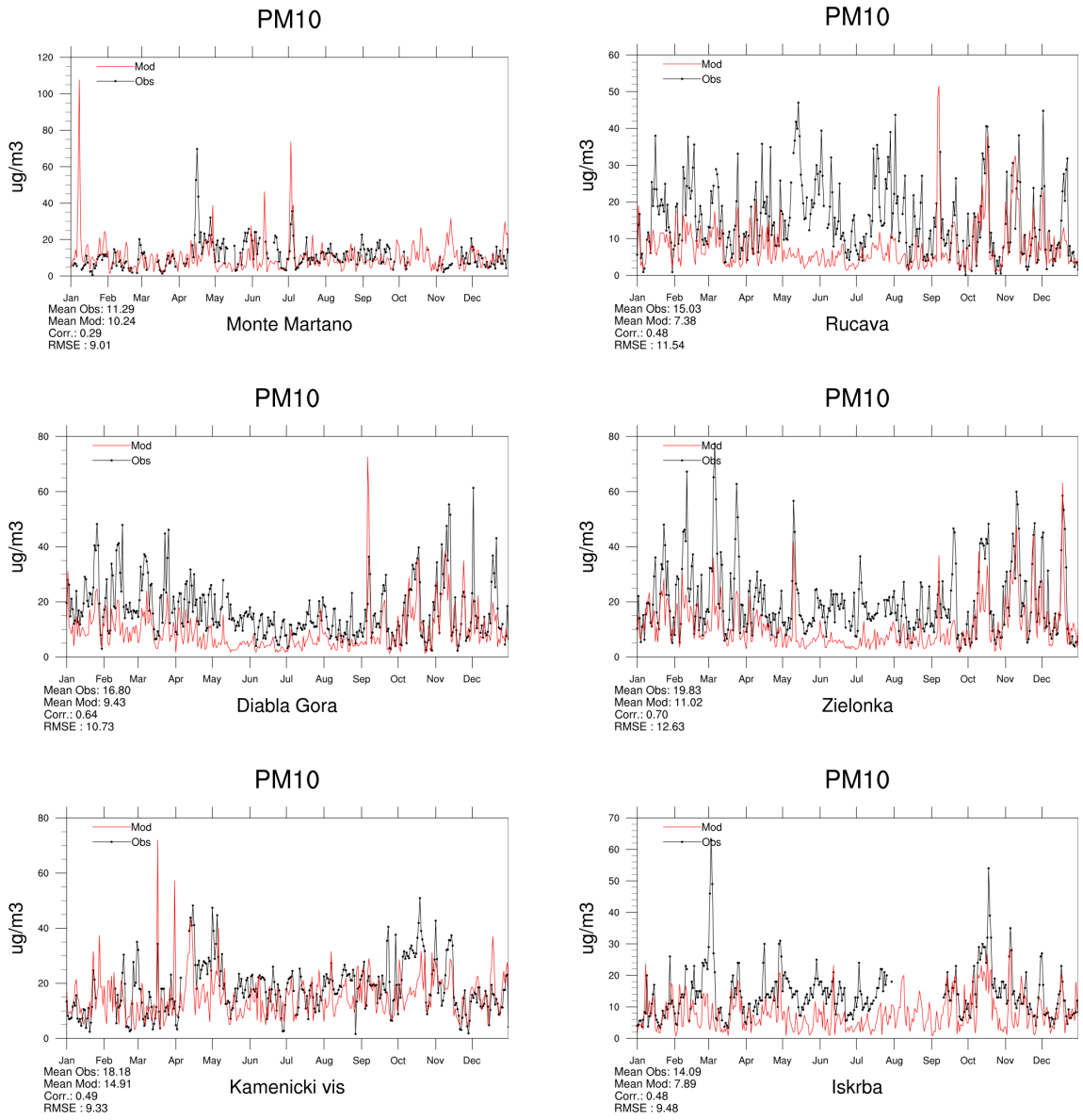

Figure 4.10: Modelled versus Observed Daily PM_{10} [μg m^{-3}] in 2018.

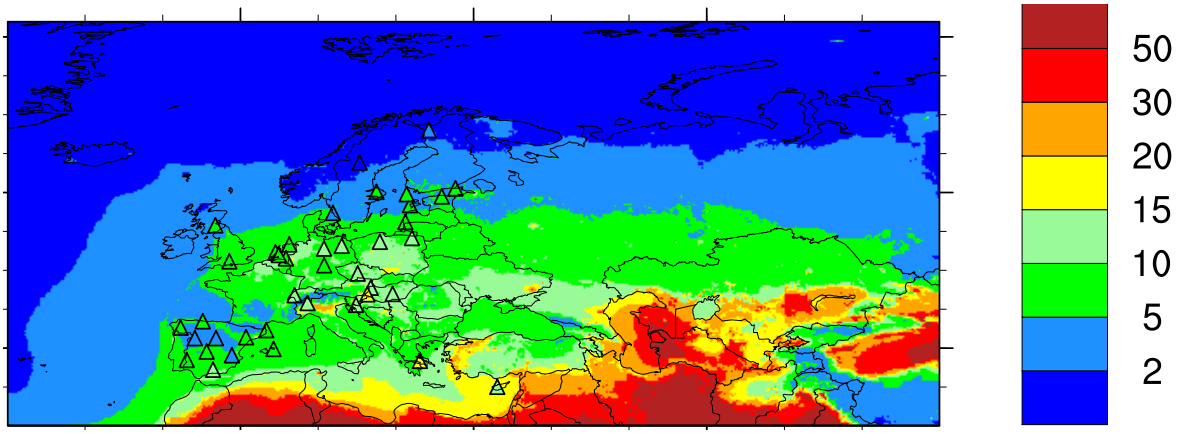

(a) PM2.5

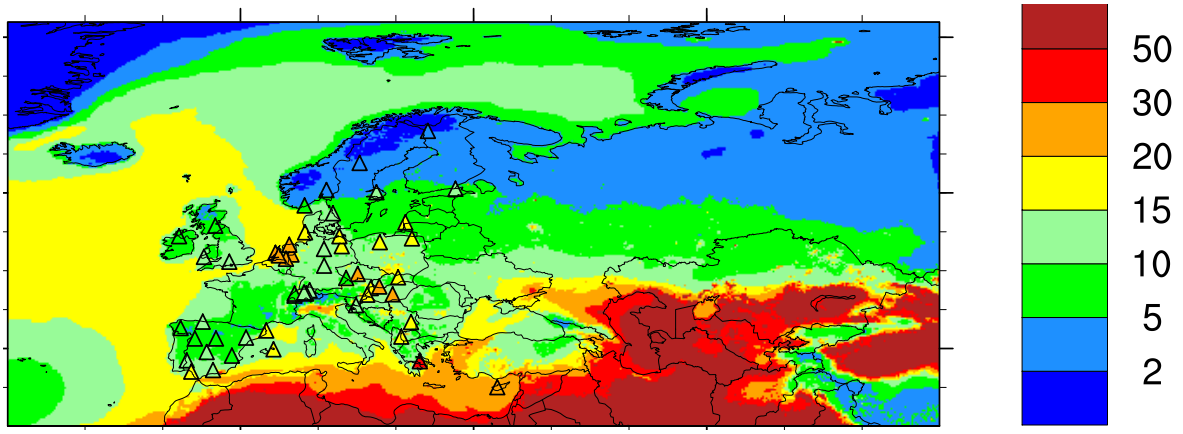

(b) PM10

Figure 4.11: Yearly $PM_{2.5}$ and PM_{10}, in 2018 [μg m^{-3}]. The maps show model results, with observations superimposed by triangles.

4.3 Combined maps of model results and observations

Combined maps of model results and observations have been produced for particulate matter $PM_{2.5}$ and PM_{10} (see Figure 4.11) and for exceedance days (see Figure 4.12).

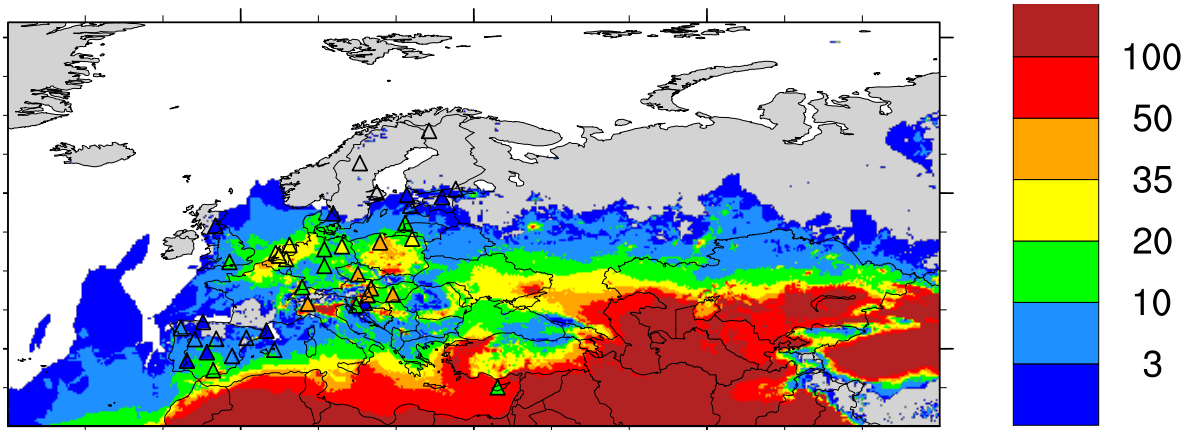

(a) PM2.5

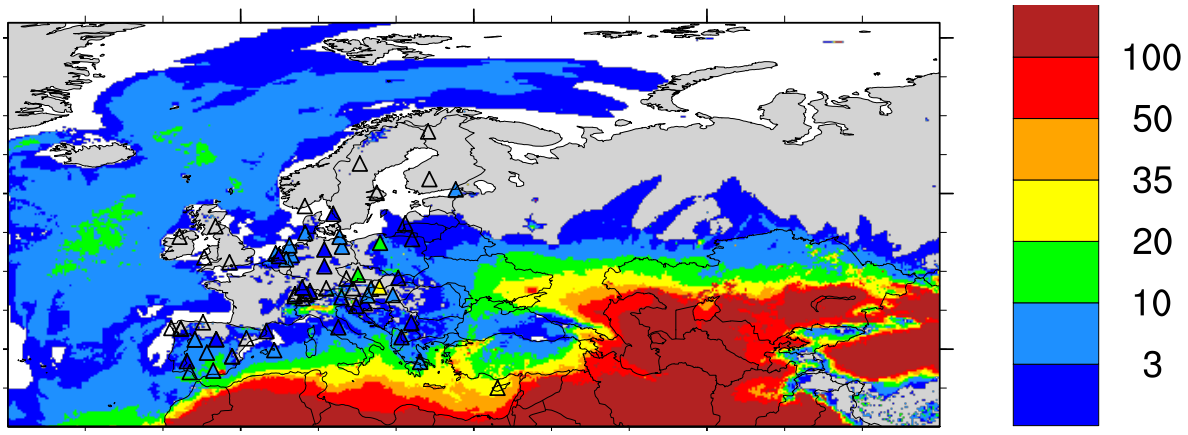

(b) PM10

Figure 4.12: Number of exceedance days in 2018 for $PM_{2.5}$ and PM_{10}. The maps show model results, with observations superimposed by triangles.